NUCLEAR POWER PLANT EQUIPMENT PROGNOSTICS AND HEALTH MANAGEMENT BASED ON DATA-DRIVEN METHODS

EDITED BY: Jun Wang, Xianping Zhong, Xingang Zhao, Joseph P. Yurko and Shripad T. Revankar

PUBLISHED IN: Frontiers in Energy Research

frontiers Research Topics

ISSN 1664-8714
ISBN 978-2-88971-299-1
DOI 10.3389/978-2-88971-299-1

About Frontiers

Frontiers is more than just an open-access publisher of scholarly articles: it is a pioneering approach to the world of academia, radically improving the way scholarly research is managed. The grand vision of Frontiers is a world where all people have an equal opportunity to seek, share and generate knowledge. Frontiers provides immediate and permanent online open access to all its publications, but this alone is not enough to realize our grand goals.

Frontiers Journal Series

The Frontiers Journal Series is a multi-tier and interdisciplinary set of open-access, online journals, promising a paradigm shift from the current review, selection and dissemination processes in academic publishing. All Frontiers journals are driven by researchers for researchers; therefore, they constitute a service to the scholarly community. At the same time, the Frontiers Journal Series operates on a revolutionary invention, the tiered publishing system, initially addressing specific communities of scholars, and gradually climbing up to broader public understanding, thus serving the interests of the lay society, too.

Dedication to Quality

Each Frontiers article is a landmark of the highest quality, thanks to genuinely collaborative interactions between authors and review editors, who include some of the world's best academicians. Research must be certified by peers before entering a stream of knowledge that may eventually reach the public - and shape society; therefore, Frontiers only applies the most rigorous and unbiased reviews.
Frontiers revolutionizes research publishing by freely delivering the most outstanding research, evaluated with no bias from both the academic and social point of view. By applying the most advanced information technologies, Frontiers is catapulting scholarly publishing into a new generation.

What are Frontiers Research Topics?

Frontiers Research Topics are very popular trademarks of the Frontiers Journals Series: they are collections of at least ten articles, all centered on a particular subject. With their unique mix of varied contributions from Original Research to Review Articles, Frontiers Research Topics unify the most influential researchers, the latest key findings and historical advances in a hot research area! Find out more on how to host your own Frontiers Research Topic or contribute to one as an author by contacting the Frontiers Editorial Office: frontiersin.org/about/contact

NUCLEAR POWER PLANT EQUIPMENT PROGNOSTICS AND HEALTH MANAGEMENT BASED ON DATA-DRIVEN METHODS

Topic Editors:
Jun Wang, University of Wisconsin-Madison, United States
Xianping Zhong, University of Pittsburgh, United States
Xingang Zhao, Oak Ridge National Laboratory (DOE), United States
Joseph P. Yurko, University of Pittsburgh, United States
Shripad T. Revankar, Purdue University West Lafayette, United States

Citation: Wang, J., Zhong, X., Zhao, X., Yurko, J. P., Revankar, S. T., eds. (2021). Nuclear Power Plant Equipment Prognostics and Health Management Based on Data-driven methods. Lausanne: Frontiers Media SA.
doi: 10.3389/978-2-88971-299-1

Table of Contents

frontiers in Energy Research

EDITORIAL
published: 12 July 2021
doi: 10.3389/fenrg.2021.719245

Editorial: Nuclear Power Plant Equipment Prognostics and Health Management Based on Data-Driven Methods

Jun Wang[1], Xianping Zhong[2], Xingang Zhao[3], Joseph P. Yurko[2] and Shripad T. Revankar[4]*

[1]University of Wisconsin-Madison, Madison, WI, United States, [2]University of Pittsburgh, Pittsburgh, PA, United States, [3]Oak Ridge National Laboratory (DOE), Oak Ridge, TN, United States, [4]Purdue University, West Lafayette, IN, United States

Keywords: advanced sensor, fault diagnosis, data-driven approach, condition monitoring, prognostics

OPEN ACCESS

Edited and reviewed by:
Uwe Schröder, Technische Universitat Braunschweig, Germany

***Correspondence:**
Xianping Zhong
xianping.zhong@pitt.edu

Specialty section:
This article was submitted to Nuclear Energy, a section of the journal Frontiers in Energy Research

Received: *02 June 2021*
Accepted: *28 June 2021*
Published: *12 July 2021*

Citation:
Wang J, Zhong X, Zhao X, Yurko JP and Revankar ST (2021) Editorial: Nuclear Power Plant Equipment Prognostics and Health Management Based on Data-Driven Methods. Front. Energy Res. 9:719245. doi: 10.3389/fenrg.2021.719245

Editorial on the Research Topic

Nuclear Power Plant Equipment Prognostics and Health Management Based on Data-Driven Methods

In response to the fierce competition in the energy market, nuclear power companies are considering operating nuclear power plants in a more economical, efficient, and safe manner. Besides, with the upgrading of nuclear power plants, systems and equipment are becoming more sophisticated and expensive (Kwon et al., 2018), which poses challenges to the timeliness, accuracy, and forward-looking of operation and maintenance (O&M) practices (Al Rashdan and St Germain, 2018; Liu and Wang, 2019). Traditional O&M practices with periodic maintenance as the core need to be further upgraded to meet these requirements. As a novel O&M strategy, data-driven health management of nuclear power plant equipment is gaining more and more attention (Patel and Shah, 2018). On the one hand, the digitization of nuclear power plants provides a rich source of data. On the other hand, the development of data science and technology, especially the development of big data technology and artificial intelligence technology represented by machine learning and deep learning, provides technical means for efficiently mining and learning laws and knowledge from data. This Research Topic explore's the application of the latest technical means such as big data, artificial intelligence, deep learning, etc. for the prognostics and health management (PHM) of crucial equipment of nuclear power plants. We include the advanced sensor technology. For example, Chu's work *Study on Measure Approach of Void Fraction in Narrow Channel Based on Fully Convolutional Neural Network* (Chu et al.). Besides, we have three articles about the data-driven approach in condition monitoring, which include Xu's work *Research on Time-Dependent Component Importance Measures Considering State Duration and Common Cause Failure* (Xu et al.), Huang's work *Data-Driven-Based Forecasting of Two-Phase Flow Parameters in Rectangular Channel* (Huang et al.), and Wang's work *A Method of Containment Leakage Rate Estimation Based on Convolution Neural Network* (Wang et al.).

For the data-drive approach in fault diagnosis, we collect four articles, they are Wu's *A Framework for Monitoring and Fault Diagnosis in Nuclear Power Plants Based on Signed Directed Graph Methods* (Wu et al.), Hu's *Data-Driven Machine Learning for Fault Detection and Diagnosis in Nuclear Power Plants: A Review* (Hu et al.), She's *Diagnosis and Prediction for Loss of Coolant Accidents in Nuclear Power Plants Using Deep Learning Methods* (She et al.), and Wu's *A Framework of Distributed Fault Diagnosis for Nuclear Power Plant* (Wu et al.). We also have one article for the data-driven approach in prognostics, it is Wang's *Remaining Useful Life Prediction Based on Improved Temporal Convolutional Network for Nuclear Power Plant Valves* (Wang et al.). Zhao's *Prognostics and health management in nuclear power plants: an updated method-centric review with special focus on data-driven methods* (Zhao et al.) provides a systematic overview of the full PHM spectrum and an in-depth survey of its modeling approaches, placing a strong emphasis on the state of the art of data-driven methods for PHM. Finally, Sun's *Development and Validation of Multiscale Coupled Thermal-Hydraulic Code Combining RELAP5 and Fluent Code* (Sun et al.) contributes to the simulation capability of computational tools for nuclear systems.

AUTHOR CONTRIBUTIONS

All authors listed have made a substantial, direct, and intellectual contribution to the work and approved it for publication.

REFERENCES

Al Rashdan, A. Y., and St Germain, S. W. (2018). *Automation of Data Collection Methods for Online Monitoring of Nuclear Power Plants*. Idaho Falls, ID (United States): Idaho National Lab.(INL). doi:10.2172/1475451

Kwon, S., Kim, B., An, K., Ryu, D., Mun, D., and Han, S. (2018). Standardized Exchange of Plant Equipment and Materials Data Based on ISO 15926 Methodology in Nuclear Power Plants. *Ann. Nucl. Energ.* 118, 185–198. doi:10.1016/j.anucene.2018.04.001

Liu, B.-Y., and Wang, M.-M. (2019). *Research and Application of Reliability Management Process in Nuclear Power Plants.* 2019 International Conference On Quality, Reliability, Risk, Maintenance, and Safety Engineering. QR2MSE, 224–229.

Patel, H. R., and Shah, V. A. (2018). Fault Detection and Diagnosis Methods in Power Generation Plants-The Indian Power Generation Sector Perspective: an Introductory Review. *PDPU J. Energ. Manag.* 2 (2), 31–49.

Conflict of Interest: The authors declare that the research was conducted in the absence of any commercial or financial relationships that could be construed as a potential conflict of interest.

frontiers in Energy Research

ORIGINAL RESEARCH
published: 06 November 2020
doi: 10.3389/fenrg.2020.584463

Remaining Useful Life Prediction Based on Improved Temporal Convolutional Network for Nuclear Power Plant Valves

Hang Wang, Minjun Peng, Renyi Xu, Abiodun Ayodeji and Hong Xia*

Key Subject Laboratory of Nuclear Safety and Simulation Technology, Harbin Engineering University, Harbin, China

Proper risk assessment and monitoring of critical component is crucial to the safe operation of Nuclear Power Plants. One of the ways to ensure real-time monitoring is the development of Prognostics and Health Management systems for safety-critical equipment. Recently, the remaining useful life prediction (RUL) has been found to be important in ensuring predictive maintenance and avoiding critical component failure. With the development of artificial intelligent techniques, deep learning algorithms are becoming popular for RUL prediction. Consequently, this paper presents RUL prediction techniques for nuclear plant electric gate valves with a temporal convolution network (TCN). The main advantage of using TCN is its ability to capture and process useful information in short-term sensor measurement changes. Moreover, the efficiency of the proposed TCN is enhanced by incorporating a convolution auto-encoder as a preprocessing layer in its structure, which greatly improved the residual convolution mode. The proposed method is verified on the electric gate valves experimental dataset that represents the real-world operation of the valve, and the result obtained is compared with other conventional data-driven approaches. The evaluation result shows impressive performance of the proposed model in predicting the remaining service life of the gate valves used in the nuclear reactor control system. Moreover, the generalization of the proposed model is evaluated on the turbofan engine benchmark dataset. The evaluation result also shows improved performance in the predicted RUL. Broader application of the proposed TCN is envisaged for critical components in other industries.

Keywords: remaining useful life prediction, electric gate valve, temporal convolutional network, residual convolution, nuclear power plant

OPEN ACCESS

Edited by:
Jun Wang,
University of Wisconsin-Madison,
United States

Reviewed by:
Khalil Ur Rahman,
Pakistan Nuclear Regulatory Authority,
Pakistan
Cheng Liu,
University of Wisconsin-Madison,
United States

****Correspondence:***
Hang Wang
wanghang1990312@126.com

Specialty section:
This article was submitted to Nuclear Energy, a section of the journal Frontiers in Energy Research

Received: *17 July 2020*
Accepted: *08 October 2020*
Published: *06 November 2020*

Citation:
Wang H, Peng M, Xu R, Ayodeji A and Xia H (2020) Remaining Useful Life Prediction Based on Improved Temporal Convolutional Network for Nuclear Power Plant Valves. 8:584463. doi: 10.3389/fenrg.2020.584463

INTRODUCTION

Concerns over energy security and global warming have risen during the past decade and those concerns have increased the NPPs share in the global energy mix due to its zero-carbon and sulfur compound emission. Efforts toward research and development of advanced, fail-safe nuclear reactors have also increased. Conversely, public concerns over the environmental impacts of a nuclear accident and potential risk of radioactive release (Coble et al., 2015) have also risen globally during the past decade and the same has delayed new nuclear projects. To ensure operational safety, relevant equipment in NPPs are designed to the highest standards. However, the probability of component failure may increase over time due to prolonged and uninterrupted operation and degradation in equipment (Lee et al., 2006). In such a diverse and highly radioactive environment, ensuring safe and reliable operation of equipment is a substantial challenge (Ayo-Imoru and Cilliers, 2018).

To address the safety and reliability issues, prognostics and health management (PHM) systems and programs are being developed (Gouriveau et al., 2016). In a PHM system, real-time data streams from plant sensors are preprocessed, extracted, compressed and packaged into standard formats. Standardization of data allows the system to accurately detect any abnormality through comparison with threshold values. In case of abnormality, PHM carries out system prognosis including the application of RUL prediction techniques. The prognostic result is usually presented as a set of potential issues and specific remedial actions such as component replacement or stoppage and maintenance of machinery before breakdown. PHM system can also initiate Condition-Based Maintenance (CBM) (Jardine et al., 2006). An overview of PHM research trends shows that three key areas of research are in focus at the moment. These are:

(1) Historic and representative data acquisition and processing: Nuclear power plant data are subject to export control, for security reasons. Hence, it is difficult to directly obtain operating data for various working conditions, different failure modes, aging and degradation modes. Without such historical data, it is difficult to develop deep learning models and accurately estimate the RUL of components. Hence, it is necessary to conduct accelerated aging and degradation experiments on key equipment to provide necessary data to support the development of RUL predictive models. This experiment is being aided by the advent of the Internet of Things (IoT) and edge computing that enable aging and failure data acquisition (Huang, 2020).
(2) Optimal arrangement and modification of sensors: Currently, sensor measurements and layout in the nuclear power plant are limited due to space constraints. Therefore, it is necessary to further optimize the sensor layout scheme for key components of the NPP.
(3) Intelligent RUL prediction: RUL is closely related to the aging mechanism, sensing and measurement, characteristic parameter analysis and other front-end factors. Currently, most industrial maintenance policy is corrective. Moreover, the maintenance cycle is generally scheduled and is based on experience. That is, even if the production equipment maintains a high level of reliability, there will still be downtime for maintenance. However, accurate RUL prediction could aid in discovering fault or component degradation trends before failure and support predictive maintenance. Therefore, it is necessary to optimize the available RUL predictive model, thus reducing the operation and maintenance costs (Vichare and Pecht, 2006; Pawar and Ganguli, 2007).

The first two identified issues are the recent bottleneck to the development of effective PHM technology for nuclear power plants, and the solution requires long-term effort. The need to make plant data available for researchers and to optimize sensor layout can be significantly justified by demonstrating the benefits of effective RUL prediction. Hence, this manuscript focuses on the development of an enhanced, accurate, and generalized RUL predictive model.

RUL prediction techniques are generally divided into three main categories: physical model-based, data-driven, and reliability-based methods. Each RUL prediction method has its advantages and disadvantages. Reliability-based RUL prediction uses methods such as probability theory and mathematical statistics to fit observation data without relying on any physical mechanism and has the most extensive applicability (Kundu et al., 2019; Peng et al., 2019; Wang et al., 2019). However, such methods need to assume prior probability and a life distribution such as a Gaussian or Weibull distribution with a linear relationship. However, for RUL prediction, the relationship between measurements is nonlinear, and the assumed probabilistic distribution contradicts the actual situation (Tang et al., 2019; Chiachío et al., 2020). Also, estimating the transfer probability matrix often require a large amount of training data (Papadopoulos et al., 2019). For physical model-based RUL prediction, the model development is a tedious and complicated process (Downey et al., 2019; Sato et al., 2019). Moreover, in a complex system such as the nuclear power plant, it is difficult to understand the degradation mechanism with physical models and this limits the application of the method (Mardar et al., 2019). Moreover, even if a physical model is successfully developed, some parameters in the model are related to material properties and stress levels which still need to be determined through specific experiments (Mishra et al., 2019).

The data-driven method is effective, without the bottlenecks identified in the other models (Lee and Kwon, 2019). Deep learning is a new branch of machine learning, developed by stacking layers of neurons to extract the deep and complex nonlinear relations in features and datasets (Lin et al., 2018). A deep neural network (DNN) has stronger pattern recognition ability than a shallow neural network and its accuracy is significantly higher when the volume of historical data is enough (Nguyen and Medjaher, 2019). DNNs have also been applied for RUL prediction. Chen et al. proposed an end-to-end RUL prediction method based on a recurrent neural network (RNN), which could improve long-term prediction accuracy (Chen et al., 2020). Zemouri and Gouriveau (2010) proposed a recurrent radial basis function network and used it to predict the mechanical RUL. Hinchi and Tkiouat (2018) proposed a convolutional long-short-term memory (LSTM) network to predict RUL of rolling bearings with FEMTO-ST ball bearing datasets. Wang et al. (2020a) proposed a new recurrent convolutional neural network that could integrate variational inference for giving a probabilistic RUL result. Xia et al. (2020) presented an ensemble framework with convolutional bi-directional LSTM for RUL prediction which could adaptively select trained base models for ensemble and further predicting RUL. An et al. (2020) utilized convolutional stacked

LSTM for RUL prediction of milling tools where time-domain and frequency-domain features were combined, encoded and denoised through unidirectional LSTM.

However, RNNs require large computational resources and training data. Moreover, although RNNs could theoretically remember remote historical information, the effect is not ideal in practical applications. Compared with RNN and other networks, a convolution neural network (CNN) has a natural advantage in large-scale parallel processing of data, especially in dealing with time series problems. On this basis, we propose an improved Temporal Convolution Network (TCN) for RUL prediction. The proposed TCN is a one-dimensional convolution network whose structure and associated hyperparameters were optimized and verified through actual experimental data. Previous application of TCN include pattern recognition tasks on the MNIST dataset, the wiki test-103, and comparison with other model shows improved accuracy and speed (Bai et al., 2018). Deng et al. (2019) also used TCN to predict temporal traffic flow and optimized the hyper-parameters in TCN through a random search strategy. To the best of the authors' knowledge, there are only a few research works that utilized TCN for RUL prediction. However, these research works did not evaluate their result on real-world representation inherent in the electric valve dataset used for this work. This paper takes electric gate valves as the case study and major contributions in this work are:

(1) Three critical issues of PHM that need to be addressed are identified and summarized.
(2) Convolutional autoencoder is integrated with TCN for effective feature extraction.
(3) Also, the residual convolution mode in TCN is optimized which enriches the features during RUL prediction.
(4) Comparative analysis of TCN hyper-parameters is carried out using real-world electric valve data. Further evaluation is also done with the turbofan benchmark dataset.

This paper is arranged as follows: The first section introduces the background and motivation; *Methodology* analyzes the theory of improved TCN network. The research objects and architecture of RUL prediction are introduced in *Experiment and System Architecture*. The simulation tests are carried out with different datasets and the proposed model is compared with other state-of-the-art models in *Simulation Analysis*. Finally, *Conclusion* contains the conclusion and limitation of the work.

METHODOLOGY

Sensors associated with equipment show specific trends over a protracted period. This relationship between sensor output and equipment degradation can be assessed by utilizing machine learning for precise RUL prediction. However, traditional methods assess instantaneous values and therefore, cannot learn features hidden in sequential time series. Bai et al. (2018) proposed the integration of TCN and causal convolution as a replacement of the RNN/LSTM network for sequential task analysis. Compared to the RNN network, it has the following advantages:

(1) For a given a sequence, the TCN could process the time-series information in parallel rather than sequentially as RNN.
(2) RNNs often have a diminishing or exploding gradient problem while TCN does not.
(3) RNNs retain the information at each step, which will occupy a large amount of computer memory. However, for TCN, the convolution kernel in each layer is shared so it is computationally less expensive.

Therefore, this paper adopts improved TCN to mine deep features and to predict the RUL. The proposed TCN is further condensed and optimized to deal with sequential tasks. For the RUL prediction problem, given a sequence of sensor measurements $x^0, x^1, x^2, ., x^T$, and the corresponding event labels $y^0, y^1, y^2, ., y^T$ at time T, the task is to predict the label y based on the previous sensor input before end of time T. For this task, the TCN performs better than ordinary CNN because of the causal relationship between the layers of TCN. That is, TCN only uses the historical sequence of information before T as shown in **Figure 1**. To consider such a historical sequence, the TCN layers need to be deep enough. Moreover, the availability of GPU parallel computing resources makes it easy to train such a large network.

The historical data captured by a simple causal convolution is only linearly related to the depth of the network, which is a great challenge for sequential tasks that need to consider longer sequential dependencies. Vanilla CNN has a small receptive field to cope with such sequences. To address this, Yu and Koltun (2015) applied the classical dilated convolution neural network to exponentially expand the convolution receptive field). Specifically, for inputs x^0, x^1, $x^2 \ldots$, x^T and filters f:{0, 1, $\ldots$,$k-1$}, the dilated convolution in sequential series s could be represented as:

$$F(s) = \sum_{i=0}^{k-1} f(i) \times x_{s-d(i)} \tag{1}$$

where d is the dilated factor and k is the size of filters, s-d(i) refers to the history. Dilated convolution is an effective strategy to increase the receptive field without increasing the kernel size or the number of parameters. When the dilation $d = 1$, the dilated convolution functions as a normal convolution. The larger the dilated factor is, the longer the input range. As a result, a better receptive field for the convolution network is achieved as shown in **Figure 1**. Consequently, the receptive field of the TCN can be freely enlarged by changing the dilation rate.

Despite the causal and dilated convolution used for the TCN, the model may sometimes encounter problems such as gradient disappearance. To address this issue, the TCN structure is made to be generic, motivated by the residual structure presented in ResNet (An et al., 2020). In this paper, the residual convolution takes X series of input, transforms them, and the results are concatenated with the input. Consequently, the output of the residual convolution is:

$$A = Activation(X + F(x)) \tag{2}$$

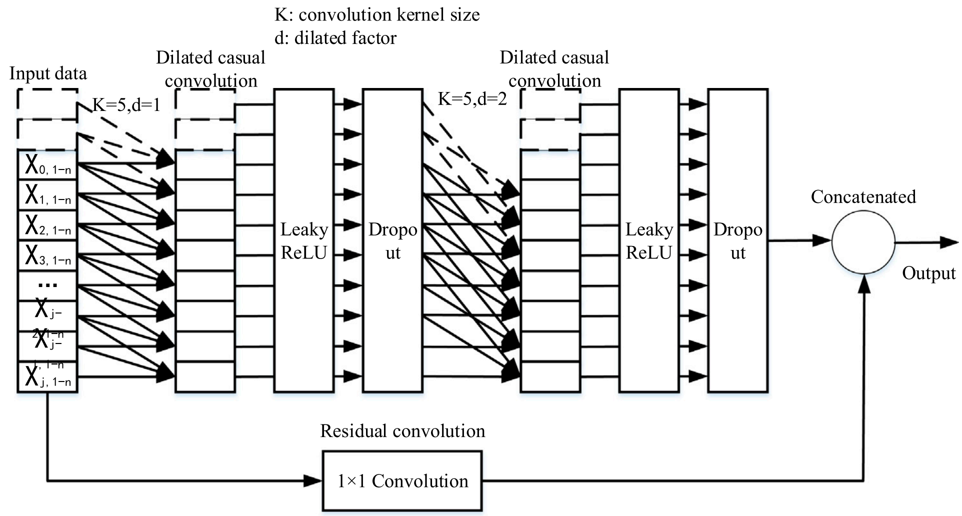

FIGURE 1 | Flowchart of TCN residual convolution.

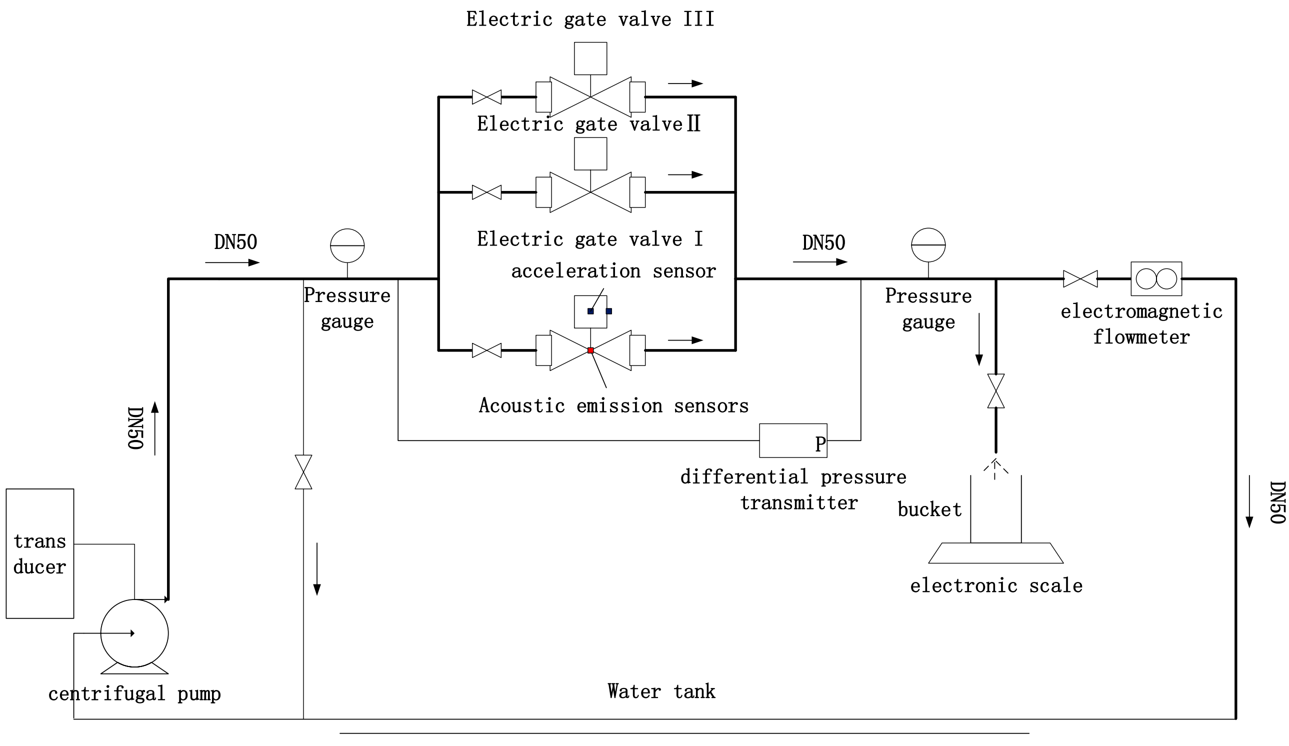

FIGURE 2 | Illustration of the electric gate valves experimental platform.

As shown in **Figure 1**, two layers of dilated causal convolution and activation function are included in a residual convolution. Moreover, dropout operation is used for regularization at each dilated convolutional layer. After that, 1 × 1 convolution is implemented for input X to ensure the same scale of tensors between inputs and outputs of residual convolution.

EXPERIMENT AND SYSTEM ARCHITECTURE

Research Object

NPPs are composed of different components. Since the method proposed in this paper has not been verified through an engineering application, we select electric gate valves to

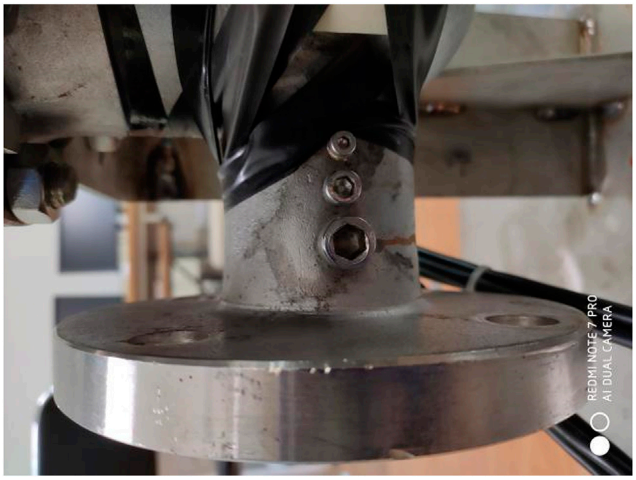

FIGURE 3 | The electric valve studied in the experiment to simulate degradation.

evaluate the RUL predictive model. In NPPs, the valve is one of the most important components, used for flow control and to adjust the working fluid pressure. Research shows that the proportion of nuclear power plant shutdown due to valve failure is 19%, which is mainly caused by assembly defects, human factors, and operating environment. Apart from scheduled maintenance, the valve is generally not allowed to stop for inspection and its condition could only be detected from the outside i.e. through a nondestructive test. Moreover, for nuclear safety-related valves, due to the limitation of installation space and cost, there are limited redundant provisions. Considering the importance of electric gate valve to the safe operation of light and heavy water reactors, the run to failure data of the gate valve is taken as the training dataset to verify the effectiveness of the proposed RUL predictive model.

As shown in **Figure 2**, the electric gate valve used for this experiment is the Z941h-25P straight screw gate valve, driven by squirrel cage coil motor. Also, the diameter of gate valve is 50 mm while the truncation mode is rigid single gate with nominal pressure of 2.5 MPa. The experimental gate valves' running conditions are configured to closely mimic what is obtainable in the real NPP operation.

In this paper, the external crack of the electric valve is selected as a typical fault mode. The main reasons for the crack are as follows: first, the uneven lattice of the valve plate or valve body leads to a material defect. Secondly, the uneven impact of the fluid or installation defects lead to uneven force on the valve plate or valve body. Thirdly, the fluid corrosion effect and the radioactive material irradiation lead to a corrosive hole that causes leakage. To preserve the valves for further experiments, and to ensure reproducibility and save cost, destructive cracks are not made on the valves during the experiment. Instead, certain reasonable assumptions and approximations are made to design the aging parts of the electric valve as shown in **Figure 3**. Three holes with 3, 5, and 10 mm are inserted and screwed on the valve body plate. During the experiment, the aging degrees are simulated by slowly adjusting the rotating screw.

For an accurate RUL prediction for electric valves, the selection of measurements to reflect the status of the electric valve is important. In this paper, the static pressure and pressure difference at the valve inlet and outlet is measured by static pressure and differential pressure gauge. The electromagnetic flowmeter is also used to measure the flow rate for analysis. To completely represents the aging state of the electric valves, other signal detection methods are used to measure the characteristic parameters. The acoustic emission methods use sensors to measure the transient stress waves on the surface of the valve body when cracks occur. When the valve runs normally, no acoustic emission occurs. After the valve show cracks or even leakage, fluid flow through the leakage produces jet turbulence,

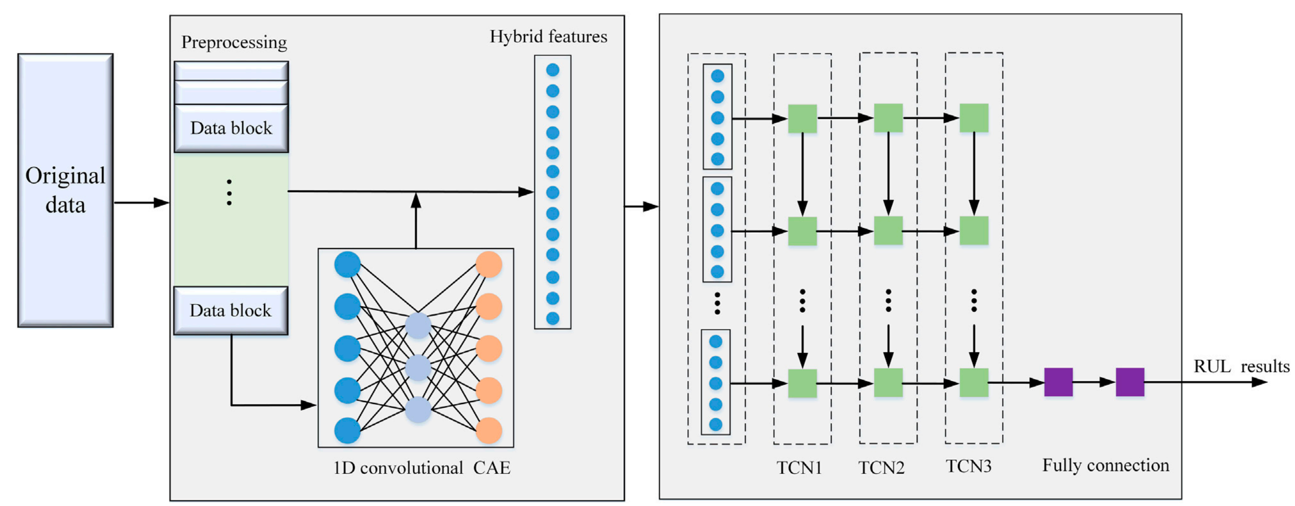

FIGURE 4 | The complete architecture of the RUL predictive model.

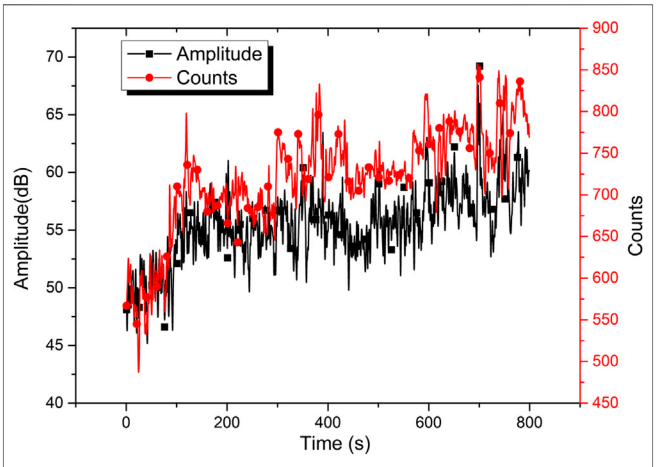

FIGURE 5 | The trends of parameters with PF = 30 Hz, VP = 35%.

which in turn produces a continuous mechanical stress wave. The sensor mounting surface is polished with sandpaper in advance to remove any impurities. Details of the mounted valves, components, the experiment procedure, and circuit configuration can be found in Wang et al. (2015).

Model Architecture and Implementation Flowchart

The architecture of the RUL predictive model based on improved TCN described in this paper is shown in **Figure 4**. The whole process is divided into the training and actual RUL prediction phase:

Step 1. Feature engineering is carried out on the acquired data from the experimental platform. Irrelevant features are removed to ensure an effective and compact model. The selected features are normalized and standardized.

Step 2. To enable the algorithms to fully take into account the sequential characteristics, the original 2*D* ($N * D$) data collected is preprocessed and reshaped to 3D stacked data block in the form $(n - num\_steps + 1) * num\_steps * D$, where N is the batch length, D is the features, and num_steps refers to sequence length of the time series. In this paper, the sliding window with length num_steps is adopted to the original 2D degradation data x. Since there is an overlap between slides of each window, the total input length is $(n - num\_steps + 1)$. In this way, the input data is not just a single data point but a sequence of time-series data, which better reflect the sequential characteristics of the degradation process.

Step 3. Unsupervised feature extraction by one-dimensional convolutional auto-encoder (CAE) is implemented. The theoretical analysis of CAE and its advantages can be found in reference (Wang et al., 2020c). The model is developed using the Tensorflow framework, where the encoding and decoding processes are implemented to form the deep feature representation.

Step 4. Results of the one-dimensional CAE are concatenated with the original data gathered from Step 2. By doing so, significant features in the aging data could be enriched to further develop an accurate RUL predictive model.

Step 5. The feature extraction results are transferred to the TCN network. On the Tensorflow framework, the TCN tuple

TABLE 1 | The architecture definition of ITCN.

Name	Definition	Default value
Network structure	CAE + ITCN	None
Sliding window size	Size of the sliding window for data preprocessing	40 (Wang et al., 2020b)
Normalization mode	Normalization of data	Z-score
Encoder of CAE	Layers of convolution kernel in the encoder	3
Decoder of CAE	Layers of convolution kernel in the decoder	3
CAE	Numbers of convolution kernel in encoder and decoder	64
CAE	Size of 1D convolution in encoder and decoder	3
CAE	1D pooling size of the encoder	2
CAE	1D upsampling size of the decoder	2
ITCN	Layers of ITCN units	4
ITCN	The dilated rate in each unit	1-2-4-8
ITCN	Number of 1D convolution in each TCN unit	64
ITCN	Layers of 1D convolution in each TCN unit	2
ITCN	Residual convolution mode in each TCN unit	Concatenated
ITCN	Size of 1D convolution kernel in each TCN unit	5 (Cui and Bai, 2019)
Keep_prob	Percentage retained in dropout operations	0.99
Init_learning_rate	Initial learning rate	0.001
Init_epoch	Iterations using the initial learning rate	5
Max_epoch	Total training times	100
Attenuation rate	Attenuation rate of the learning rate	0.99
Batch_size	The amount of data used in small batches	128
Loss function	None	RMSE
Optimization method	Optimization algorithms for backpropagation	Adams
Dropout coefficient	Dropout coefficient	0.5
Activation function	Coefficient *a* in Leaky ReLU	0.3

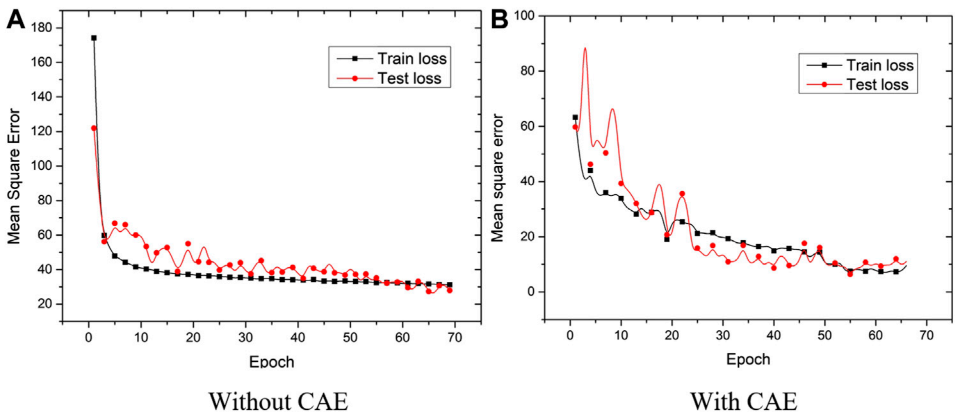

FIGURE 6 | Training and testing curves with or without CAE.

TABLE 2 | Metrics with or without CAE.

Network structure	Without CAE	With CAE	With CAE and original data
EVS	0.858	0.958	0.957
MAE	4.35	2.97	2.07
RMSE	32.03	12.33	8.47
R^2_score	0.845	0.924	0.957

model is first developed, which consists of 1D causal convolution with many layers. For each causal convolutional layer, the dilated function is used after each TCN to increase the model receptive field.

Step 6. The residual convolution described in *Research Object* is improved by concatenating the results of the convolution filter. Moreover, the leaky ReLU activation function and sparse dropout operation are also used instead of ReLU or Sigmoid activation function based on the previous impressive performance of the Leaky ReLU activation function on non-linear sequential datasets (Wang et al., 2020b).

Step 7. When the TCN tuple unit is developed, the stack function is adopted to construct the entire TCN network.

Step 8. During CAE and TCN training, the processed data is randomly shuffled to avoid overfitting and then input into CAE and TCN models.

Step 9. The loss function in this paper is the root mean squared error (RMSE). Adam optimizer is used as the training algorithm. During backpropagation processes, the learning rate at the first 5 iterations is set to 0.001 without attenuation. Then the attenuation rate of each subsequent iteration is set to 0.99. With increasing training epochs, the training errors decreases until it stabilized.

Step 10. When the off-line training process is completed, the randomly selected test data is normalized as shown in step 1 and step 2. Then, the optimized TCN models are used to predict the RUL of the electric gate valves. The model evaluation metrics are the explained variance score, mean absolute error, mean squared error, and R^2 score.

TABLE 3 | Average test loss with different layers and neurons of CAE.

Numbers of causal layers	2	3	4	5
Dilated factors	1–8	1-4-4	1-2-4-8	1-2-4-8-16
EVS	0.917	0.933	0.957	0.949
MAE	4.58	2.42	2.07	3.78
RMSE	30.68	10.44	8.47	20.60
R^2 score	0.806	0.932	0.957	0.867

TABLE 4 | Average test losses of different RUL prediction models.

RUL model	FCN	CNN	LSTM	CAE + LSTM	Improved TCN
EVS	0.342	0.68	0.67	0.902	0.957
MAE	9.84	8.151	4.74	2.94	2.07
RMSE	137.18	34.68	27.43	13.55	8.47
R^2 score	−0.43	0.64	0.66	0.90	0.957

SIMULATION ANALYSIS

Data Acquisition

The degradation of the electric-valves is measured in the experiment. First, the water tank is filled as shown in **Figure 2**, and an electric valve loop is fully opened. The inverter for the pump is set to 15 kHz and its corresponding pump speed is about 870 r/min. The pipeline is filled with water after some time. Then, the driving pressure of the pipeline is 0.26 MPa, the valve is in normal operation, the pressure difference across the valve is 6 KPa and the total flow in the pipeline is 3 m^3/h. Also, relevant parameters of acoustic emission cards are set as: sampling frequency-5,000 kHz, digital filter band-15~70 kHz, the interval of parameters-500 μs, hangover time-1,000 μs, peak interval-300 μs, locking time-1,000 μs, single-channel waveform threshold-40 dB, and single-channel parameter threshold 40 dB.

In the experiment, the crack simulating screw is slowly adjusted under a certain pump frequency and the electric valve position (opening degree) to gradually increase the

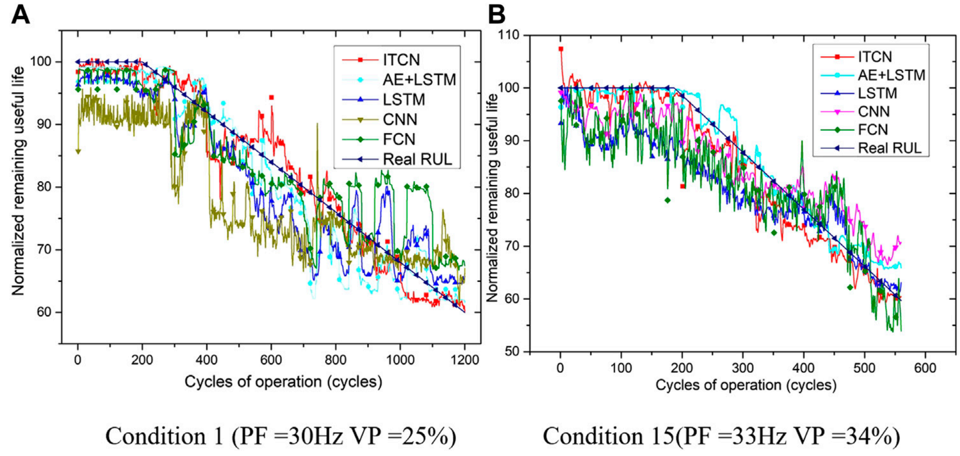

FIGURE 7 | RUL results with different algorithms.

leakage. Different pump frequencies and opening degrees represent different operating conditions of the electric-valves. In this paper, a total of five different circulating pump frequencies (PF) and eight valve openings (VP) are set during the experiment with a total of 40 operating conditions. Under each operating condition, 30 groups of experiments are carried out with various levels of screw tightness. In each group of the experiment, the measured variables are the frequency of the circulating pump, opening degree of the electric-valve, pressure difference between the front and rear of the electric-valve, and the fluid flow rate through the valve. For acoustic emission signals acquisition, computer software is used to automatically calculate the amplitude, ringing count, rising time, energy, root mean square (RMS), average signal level (ASL), and other parameters.

Moreover, the length of time for each group varies from 2 to 3 h to provide adequate aging data. **Figure 5** shows different variations of some selected conditions under which the acoustic emission sensors measurements were obtained. From the figure, the amplitude of acoustic emission parameters and ringing count all show approximately the same trend as the leakage volume increases under a certain pump frequency and valve opening position. When the leakage is less than a certain value, the relevant characteristic parameter has no significant deviation. However, when the leakage exceeds a threshold, the parameter presents an obvious change in trend. When the leakage further increases to a certain critical value, the parameter remains constant again. This is because when the leakage is tiny, the leakage has little effect on the flow in the pipeline. But, when the leakage becomes too large, the pipeline flow is no longer under turbulent states.

Comparison of Different Model Structures and Hyper-Parameters

For pattern recognition with deep learning, many trainable parameters directly influence the model performance. However, there are no generic hyperparameter selection criteria. Hence, it is necessary to analyze and compare different hyperparameters to obtain an optimal model for the RUL prediction.

Optimizable hyperparameters in TCN include the learning rate, learning rate delay factor, maximum iterations, batch number, selection of training algorithm, and dropout coefficient, among others. From the authors' experience, the fine-tuning of these hyperparameters has little impact on the overall results. Therefore, the hyperparameters selected in this work is motivated by the performance recorded in recent literature. The default structure and hyperparameters of the proposed ITCN are shown in **Table 1**.

In addition to the above hyperparameters, we analyzed the effect of the CAE preprocessing layer and different dilation rates on the predictive performance of TCN. Finally, explained variance score (EVS), mean absolute error (MAE), RMSE, and R^2 score metrics are obtained to evaluate the performance of the RUL predictive model.

With or Without Convolutional Auto-Encoder

First, an experiment is performed by adding the CAE layer without changing the structure of the proposed TCN, and the effect of the CAE layer is analyzed. **Figure 6** shows the training and test curve for the specified epochs. It is seen that the network neither underfit nor overfit.

Metrics are calculated for further analysis, as shown in **Table 2**. From the table, the metric for the model with CAE is better than that without CAE, which means CAE has a positive effect on feature

TABLE 5 | Average test losses of different RUL prediction models.

RUL model	FCN	CNN	CAE + LSTM	Improved TCN
EVS	0.901	0.951	0.967	0.968
MAE	22.92	16.88	3.13	2.38
RMSE	29.15	20.37	17.48	9.09
R^2 score	0.896	0.932	0.963	0.965

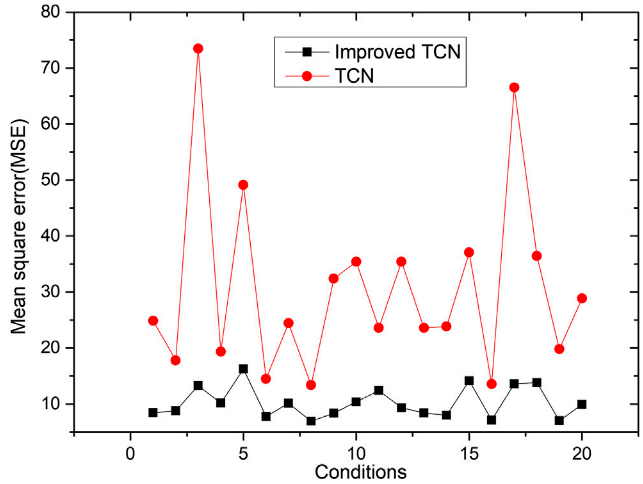

FIGURE 8 | RMSE results of ITCN vs, vanilla TCN under different operating conditions.

extraction. Furthermore, after combining the feature extraction results of CAE with the original data, the explained variance score, RMSE, and R^2 score are better than those without the parallel structure. This is mainly because after adopting the parallel structure of CAE and the original data, the dimension of the feature map expanded from the original 9 dimensions to 18 dimensions, which is equivalent to enhancing the feature performance. Therefore, the CAE layer has a significant effect on the improved TCN network for RUL prediction.

Receptive Field With Different Layers and Dilated Factors

After evaluating the effect of the CAE layer, we compared a different number of causal convolution layers and the dilated factors for TCN optimization. As shown in **Figure 1**, two layers of dilated causal convolution and activation function are included in each causal convolution layer. **Table 3** shows the comparison result. It is seen that the best metric for the predictive model is obtained when there is four causal convolutional layer and dilated factor is set to 1, 2, 4, 8. Therefore, it is concluded that this structure optimizes the RUL predictive model.

Comparison of the Proposed Method With Conventional Algorithms

To verify the performance of the proposed improved TCN model, a fully connected network (FCN), Convolutional Neural Network (CNN), LSTM model, and its variation were implemented and compared for the same dataset. For FCN, it adopts the full connection of neurons between different layers, which is different from the TCN network during the training process. Therefore, by comparing with FCN, the advantage of DNNs is demonstrated. Also, to show that the improved TCN method is better than other DNNs, this paper compared the results of CNN, LSTM, and TCN. The relevant comparison results are shown in **Table 4**. From the results, it is seen that the accuracy and performance of TCN are better than other networks on the task of predicting the RUL of electric gate valves. Moreover, two operating conditions are selected at random, and the predicted RUL curves obtained from different

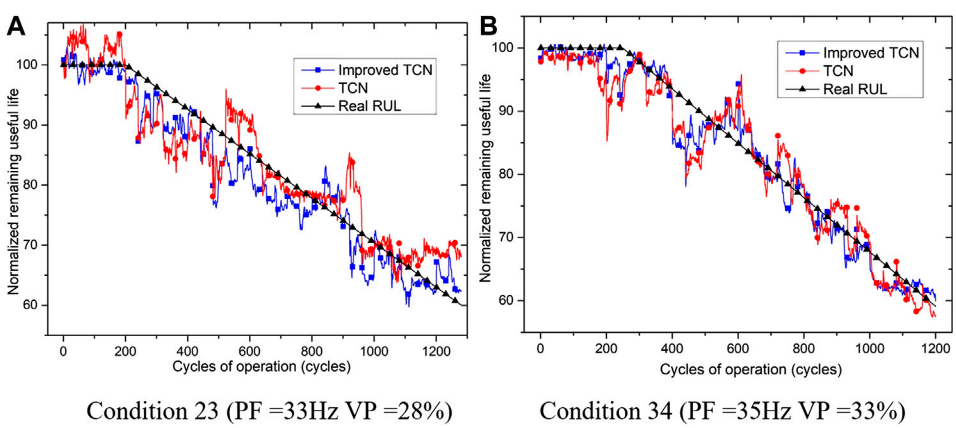

FIGURE 9 | Results of RUL prediction under different operating conditions.

models are shown in **Figure 7**. The RUL prediction trend for the improved TCN is the closest to the real RUL, which shows that the best prediction is obtained from the improved TCN model. This result is also consistent with the metric shown in **Table 4**.

To further verify the predictive performance and demonstrate the generalization capability of the proposed improved TCN model, we also applied it to predict RULs for the turbofan engines in the NASA C-MAPSS benchmark datasets. The C-MAPSS dataset contains the degradation history of aero-propulsion engines operating under different fault modes. The dataset has four subsets composed of multi-variate temporal data obtained from 21 sensors. Detailed information on the composition of the dataset can be found in reference (Ramasso, 2014). Due to space constraints, we evaluated the proposed method only on the FD001 subset of the C-MAPSS dataset.

Similarly, the different methods mentioned in this section are compared. The relevant comparison results are shown in **Table 5**. It is seen that the improved TCN network still has the highest accuracy for FD001 data and all TCN evaluation metrics are better than other networks.

Remaining Useful Life Prediction Results

This section presents the RUL prediction results under different aging conditions. As shown in **Figure 8**, the average RMSE of the improved TCN and the original TCN under different operating conditions are presented. It is seen that there is an impressive increase in accuracy of improved TCN compared with that of the original (vanilla) TCN under different operating conditions.

Moreover, **Figure 9** is the results of the RUL prediction curve after randomly selecting different operating conditions. It is seen that the RMSE in **Figure 8** is consistent with the RUL prediction curve of the improved TCN, which is significantly better than the original TCN. Moreover, it can be seen that before and at the beginning of the equipment degradation, the errors between the predicted curves and the real curve is large, which is mainly caused by the sensor measurement error and noise during normal operation. With the gradual development of degradation, the improved TCN could better track the real RUL. As the equipment approaches the end of life, there is a minor deviation between predicted and real RUL but within the acceptable range.

CONCLUSION

This work proposes an improved TCN (ITCN) model for nuclear power plant electric gate valve remaining useful life estimation. Multi-variate training datasets that represent the degradation history of the valve are acquired from an experimental platform. The dataset is subsequently preprocessed and normalized. High-performing convolution auto-encoder layers are also integrated into the ITCN model to improve model performance. Moreover, we experimented with different model hyperparameters and convolution dilation factors to determine the best parameters for the model. The research result and evaluation metric show the impressive performance of the ITCN model. To further verify the generalization capability of the proposed method, the model is evaluated on NASA's C-MAPSS dataset, to predict RUL for aero-propulsion engines. Evaluation results show similar impressive performance on the benchmark dataset. The results also show that the work can be further extended to other mechanical components and devices. Other advantages of the proposed method are its ability to solve the problem of large computing resources and memory requirements that is common to LSTM and other RNNs. The originality of this study is summarized below:

(1) We present and analyze major issues that constraint the implementation of PHM for nuclear power systems
(2) We propose an improved TCN predictive model, based on CAE and improved residual convolution. The parallel structure of the TCN is augmented to enhance feature processing for accurate RUL prediction.
(3) The proposed method is extensively evaluated using aging characteristics of electric gate valves and other benchmark datasets. The RUL prediction result and the comparative analysis of other state-of-the-art models show an impressive performance of the proposed method.

The results also show that the proposed method can be applied to critical components and devices in other industries. It could also enable predictive maintenance which reduces maintenance downtime and part replacement cost, and improves productivity. Nevertheless, we observed some limitations of the research. First, the data acquisition procedure presented in this work needs to be optimized. Aging and degradation modes in experiments also need to be extended to completely reflect the real degradation process. Further, the proposed method needs to be verified using real degradation information from operating NPPs. Moreover, the hyper-parameters and layer numbers of the proposed ITCN are selected manually which is time-consuming. The application of heuristic optimization algorithms and auto-tuners could further optimize the predictive model performance. These limitations will be addressed in our future work.

DATA AVAILABILITY STATEMENT

The raw data supporting the conclusions of this article will be made available by the authors, without undue reservation.

AUTHOR CONTRIBUTIONS

HW: writing and tested RUL prediction algorithms. MP: designed the whole architecture. RX: experiment and acquiring data. HX: comparison with other typical methods. HS: writing and English grammar problem revision.

FUNDING

This work was supported by the Foundation project of nuclear power technology innovation center of science, technology and industry under Grant HDLCXZX-2019-ZH-036.

REFERENCES

An, Q., Tao, Z., Xu, X., El Mansori, M., and Chen, M. (2020). A data-driven model for milling tool remaining useful life prediction with convolutional and stacked LSTM network. *Measurement.* 154, 107461. doi:10.1016/j.measurement.2019.107461

Ayo-Imoru, R. M., and Cilliers, A. C. (2018). A survey of the state of condition-based maintenance (CBM) in the nuclear power industry. *Ann. Nucl. Energy.* 112, 177–188. doi:10.1016/j.anucene.2017.10.010

Bai, S., Kolter, J. Z., and Koltun, V. (2018). An empirical evaluation of generic convolutional and recurrent networks for sequence modeling. [Preprint]. arXiv :1803.01271v2 [cs.LG].

Chen, L. T., Xu, G. H., Zhang, S. C., Yan, W. Q., and Wu, Q. Q. (2020). Health indicator construction of machinery based on end-to-end trainable convolution recurrent neural networks. *J. Manuf. Syst.* 54, 1–12. doi:10.1016/j.jmsy.2019.11.008

Chiachío, J., Jalón, M. L., Chiachío, M., and Kolios, A. (2020). A Markov chains prognostics framework for complex degradation processes. *Reliab. Eng. Syst. Saf.* 195, 106621. doi:10.1016/j.ress.2019.106621

Coble, J., Ramuhalli, P., Bond, L. J., Hines, J. W., and UIpadhyaya, B. R. (2015). A review of prognostics and health management applications in nuclear power plants. *Intl. J. Progn. Health Manag.* 16, 2153–2648.

Cui, H., and Bai, J. (2019). A new hyperparameters optimization method for convolutional neural networks. *Pattern Recogn. Lett.* 125, 828–834. doi:10.1016/j.patrec.2019.02.009

Deng, S. J., Jia, S. Y., and Chen, J. (2019). Exploring spatial–temporal relations via deep convolutional neural networks for traffic flow prediction with incomplete data. *Appl. Soft. Comput.* 78, 712–721. doi:10.1016/j.asoc.2018.09.040

Downey, A., Liu, Y. H., Hu, C., Laflamme, S., and Hu, H. (2019). Physics-based prognostics of lithium-ion battery using non-linear least squares with dynamic bounds. *Reliab. Eng. Syst. Saf.* 182, 1–12. doi:10.1016/j.ress.2018.09.018

Gouriveau, R., Medjaher, K., and Zerhouni, N. (2016). *From prognostics and health systems management to predictive maintenance 1: monitoring and prognostics*. Editor A. EL Hami (London, UK: John Wiley & Sons), 15–26.

Hinchi, A. Z., and Tkiouat, M. (2018). Rolling element bearing remaining useful life estimation based on a convolutional long-short-term memory network. *Procedia Comput. Sci.* 127, 123–132. doi:10.1016/j.procs.2018.01.106

Huang, X. M. (2020). Intelligent remote monitoring and manufacturing system of production line based on industrial Internet of Things. *Comput. Commun.* 150, 421–428. doi:10.1016/j.comcom.2019.12.011

Jardine, A. K. S., Lin, D., and Banjevic, D. (2006). A review on machinery diagnostics and prognostics implementing condition-based maintenance. *Mech. Syst. Signal Process.* 20 (7), 1483–1510. doi:10.1016/j.ymssp.2005.09.012

Kundu, P., Darpe, A. K., and Kulkarni, M. S. (2019). Weibull accelerated failure time regression model for remaining useful life prediction of bearing working under multiple operating conditions. *Mech. Syst. Signal Process.* 134, 106302. doi:10.1016/j.ymssp.2019.106302

Lee, C. Y., and Kwon, D. (2019). A similarity based prognostics approach for real time health management of electronics using impedance analysis and SVM regression. *Microelectron Reliab.* 83, 77–83. doi:10.1016/j.microrel.2018.02.014

Lee, J., Ni, J., Djurdjanovic, D., Qiu, H., and Liao, H. T. (2006). Intelligent prognostics tools and e-maintenance. *Comput. Ind.* 57 (6), 476–489. doi:10.1016/j.compind.2006.02.014

Lin, Y. H., Li, X. D., and Hu, Y. (2018). Deep diagnostics and prognostics: an integrated hierarchical learning framework in PHM applications. *Appl. Soft. Comput.* 72, 555–564. doi:10.1016/j.asoc.2018.01.036

Mardar, E., Klei, R., and Bortman, J. (2019). Contribution of dynamic modeling to prognostics of rotating machinery. *Mech. Syst. Signal Process.* 123, 496–512. doi:10.1016/j.ymssp.2019.01.003

Mishra, M., Martinsson, J., Rantatalo, M., and Goebel, K. (2019). Bayesian hierarchical model-based prognostics for lithium-ion batteries. *Reliab. Eng. Syst. Saf.* 172, 25–35. doi:10.1016/j.ress.2017.11.020

Nguyen, K., and Medjaher, K. (2019). A new dynamic predictive maintenance framework using deep learning for failure prognostics. *Reliab. Eng. Syst. Saf.* 188, 251–262. doi:10.1016/j.ress.2019.03.018

Papadopoulos, C. T., Li, J. S., and O'Kelly, M. (2019). A classification and review of timed Markov models of manufacturing systems. *Comput. Ind. Eng.* 128, 219–244. doi:10.1016/j.cie.2018.12.019

Pawar, P., and Ganguli, R. (2007). Fuzzy-logic-based health monitoring and residual-life prediction for composite helicopter rotor. *J. Aircr.* 44 (3), 981–995. doi:10.2514/1.26495

Peng, K. X., Jiao, R. H., Dong, J., and Pi, Y. T. (2019). A deep belief network based health indicator construction and remaining useful life prediction using improved particle filter [J]. *Neurocomputing.* 361, 19–28. doi:10.1016/j.neucom.2019.07.075

Ramasso, E. (2014). Investigating computational geometry for failure prognostics. *Int. J. Progn. Health Manag.* 5 (1), 1–18.

Sato, M., Moura, L. S., Galvis, A. F., Albuquerque, E. L., and Sollero, P. (2019). Analysis of two-dimensional fatigue crack propagation in thin aluminum plates using the Paris law modified by a closure concept. *Eng. Anal. Bound. Elem.* 106, 513–527. doi:10.1016/j.enganabound.2019.06.008

Tang, D. Y., Cao, J. R., and Yu, J. S. (2019). Remaining useful life prediction for engineering systems under dynamic operational conditions: a semi-Markov decision process-based approach. *Chinese J. Aeronaut.* 32 (3), 627–638. doi:10.1016/j.cja.2018.08.015

Vichare, N. M., and Pecht, M. G. (2006). Prognostics and health management of electronics. *IEEE T Comp. Pack. Man.* 29 (1), 222–229. doi:10.1109/tcapt.2006.870387

Wang, B., Lei, Y. G., Yan, T., Li, N., and Guo, L. (2020a). Recurrent convolutional neural network: a new framework for remaining useful life prediction of machinery. *Neurocomputing.* 379, 117–129. doi:10.1016/j.neucom.2019.10.064

Wang, H., Peng, M. J., Miao, Z., Liu, Y. K., and Ayodeji, A. (Forthcoming 2020b). Remaining useful life prediction techniques of electric valves based on CAE and LSTM. *ISA Trans.* doi:10.1016/j.isatra.2020.08.031

Wang, S. X., Chen, H. W., Wu, L., and Wang, J. F. (2020c). A novel smart meter data compression method via stacked convolutional sparse auto-encoder. *Int. J. Elec. Power.* 118, 105761. doi:10.1016/j.ijepes.2019.105761

Wang, H., Ma, X. B., and Zhao, Y. (2019). An improved Wiener process model with adaptive drift and diffusion for online remaining useful life prediction. *Mech. Syst. Signal Process.* 127, 380–387. doi:10.1016/j.ymssp.2019.03.019

Wang, Y. F., Xue, C., Jia, X. H., and Peng, X. Y. (2015). Fault diagnosis of reciprocating compressor valve with the method integrating acoustic emission signal and simulated valve motion. *Mech. Syst. Signal Process.* 56–57, 197–212. doi:10.1016/j.ymssp.2014.11.002

Xia, T., Song, Y., Zheng, Y., Pan, E., and Xi, L. (2020). An ensemble framework based on convolutional bi-directional LSTM with multiple time windows for remaining useful life estimation. *Comput. Ind.* 115, 103182. doi:10.1016/j.compind.2019.103182

Yu, F., and Koltun, V. (2015). Multi-scale context aggregation by dilated convolutions. [Preprint]. arXiv:1511.07122v3 [cs.CV].

Zemouri, R., and Gouriveau, R. (2010). "Towards accurate and reproducible predictions for prognostic: an approach combining a RRBF network and an autoregressive model. *IFAC Proc. Volumes* 43 (3), 140–145. doi:10.3182/20100701-2-PT-4012.00025

Conflict of Interest: The authors declare that the research was conducted in the absence of any commercial or financial relationships that could be construed as a potential conflict of interest.

frontiers in Energy Research

ORIGINAL RESEARCH
published: 27 November 2020
doi: 10.3389/fenrg.2020.584750

Research on Time-Dependent Component Importance Measures Considering State Duration and Common Cause Failure

Anqi Xu[1], Zhijian Zhang[1], Huazhi Zhang[1], He Wang[1], Min Zhang[2], Sijuan Chen[1], Yingfei Ma[1] and Xiaomeng Dong[3]*

[1]Fundamental Science on Nuclear Safety and Simulation Technology Laboratory, Harbin Engineering University, Heilongjiang, China, [2]China Nuclear Power Engineering Co., LTD., Beijing, China, [3]Shenzhen University, Guangdong, China

OPEN ACCESS

Edited by:
Jun Wang,
University of Wisconsin-Madison,
United States

Reviewed by:
Guohua Wu,
Harbin Institute of Technology, China
Muhammad Zubair,
University of Sharjah,
United Arab Emirates
Ming Yang,
South China University of Technology,
China

***Correspondence:**
Zhijian Zhang
zhangzhijian_heu@hrbeu.edu.cn

Specialty section:
This article was submitted to
Nuclear Energy,
a section of the journal
Frontiers in Energy Research

Received: 18 July 2020
Accepted: 15 September 2020
Published: 27 November 2020

Citation:
Xu A, Zhang Z, Zhang H, Wang H, Zhang M, Chen S, Ma Y and Dong X (2020) Research on Time-Dependent Component Importance Measures Considering State Duration and Common Cause Failure. Front. Energy Res. 8:584750. doi: 10.3389/fenrg.2020.584750

Unlike the current risk monitors, Real-time Online Risk Monitoring and Management Technology is characterized by time-dependent modeling on the state duration of components. Given the real-time plant configuration, it eventually provides the time-dependent risk level and importance measures for operation and maintenance management. This paper focuses on the assessment method of time-dependent importance measures and its risk-informed applications in real-time online risk monitoring and management technology, including Fussell-Vesely (FV), risk achievement worth (RAW), and risk reduction worth (RRW). In this study, the values of component importance have been investigated with a time-dependent risk quantification model, as well as the common cause failure treatment model. Here three options of common cause failure treatment have been developed, assuming that the unavailability of a component could be due to an independent factor (Option 1), a common cause factor (Option 2), or an unconfirmed cause (Option 3). In the special case of "what if a component is out-of-service" of the RAW numerator, a hybrid method for the RAW evaluation is presented resulting in a balanced and reasonable RAW value. A simple case study was demonstrated. The results showed that the absolute values and ranking order of time-dependent importance not only reflected the effect of the cumulative state duration of component on risk, but also comprehensively accounted for all possible situations of component unavailability. Moreover, time-dependent importance measures improved and provided novel insights for online configuration management, 1) ranking SSCs/events/

Abbreviations: ACT, allowed configuration time; BE, basic event; CCDP, conditional core damage probability; CCF, common cause failure; CCCG, common cause-component group; CDF, core damage frequency; ET, event tree; FT, fault tree; FV, Fussell-Vesely; ICDP, incremental core damage probability; IE, initiating event; IM, importance measure; IRORM, integrated platform for nuclear power plant real-time online risk monitoring and management; LPSA, living-PSA; MCS, minimal cut set; NPP, nuclear power plant; PRA, probabilistic risk assessment; RAW, risk achievement worth; RECAS, reliability data online collection, analysis, and storage system; RM, risk monitor; RORM, real-time online risk monitoring and management system; RORMT, real-time online risk monitoring and management technology; RRW, risk reduction worth; SAPHIRE, systems analysis programs for hands-on integrated reliability evaluations; SMF, state monitoring and fault diagnostics system; SSC, system, structure, and component; TS, technical specification.

human actions for controlling increased risk and optimizing near–term plans; and 2) exempting or limiting temporary configurations during online operation.

Keywords: component importance measure, time-dependent, real-time online risk monitoring, common cause failure, risk-informed operation and maintenance, configuration risk assessment

INTRODUCTION

Time-Dependent Characteristics of Real-Time Online Risk Monitoring and Management Technology

The safety and reliability of nuclear power plants (NPP) depend on the inherent safety of reactor design, as well as the operational safety under different operating conditions. The systems, structures, and components (SSC) of NPP would experience state changes due to random failures, maintenance, or permanent design modifications. And the unavailability of components may increase with operational time, which imposes on the risk level during accident scenarios. Thus, it is a fundamental requirement for online operation and maintenance management to be kept informed of the current risk level and importance measures (IMs) of NPP.

Real-time online risk monitoring and management technology (RORMT) is based on a time-dependent living-PSA model and an updated method of NPP (Zhang et al., 2015b). "Time-dependent" refers to the impact of state duration on the reliability of components. "Configuration" means the alignment of the system, component state, environmental conditions, and NPP scenarios. All of them affect the logical values of events (normal, true, false) or reliability parameters (such as failure rate/failure probability of component, frequency of initiating event (IE)) in the time-dependent living-PSA model, named as "RORM model".

An integrated platform for nuclear power plant real-time online risk monitoring and management (IRORM) was developed as a generic tool for risk-informed operation, online maintenance, and risk-informed management. It consists of four interactive subsystems. The architecture of IRORM was established as shown in **Figure 1**.

- The state monitoring and fault diagnostics system(SMF) was developed to online monitor and identify the operational states of systems and equipment with running time. So it identifies the real-time configuration of NPP via access to the digital I&C system in NPP.
- The reliability data online collection, analysis, and storage system (RECAS) (Zubair and Zhang, 2011; Ma and Zhang, 2015) was developed to record state changes and failure times of components. It can automatically update the failure probability of components in time, and provide the reliability parameters to the RORM model. In the long run, it can provide long-term restoration of reliability data for multi-units.
- The living-probabilistic safety assessment (LPSA) system is used for modeling and updating an LPSA model. In case of plant configuration changes or after a fixed period, it can automatically be triggered to update the time-dependent LPSA model in time. After that, a parallel computing engine of IRORM would calculate minimal cut sets (MCS) and risk metrics.
- A real-time online risk monitoring and management system (RORM) is a risk monitor (RM) which is used for displaying and evaluating time-dependent risk measures and other related information.

PRA Importance Measures and Challenges of Real-Time Online Risk Monitoring and Management Technology

A variety of IMs were evaluated to identify the risk-significant contributors (Gunnar and Jan, 1994; Kalpesh and Kirtee, 2017) in PRA analysis, for instance, Fussell-Vesely (FV), risk achievement worth (RAW), risk reduction worth (RRW), and Birnbaum importance (Birnbaum, 1969). Among them, FV and RAW have been commonly accepted in engineering practice for SSC categorization (NRC, 2004). The computation of IMs is performed at the level of reliability parameter, individual basic event, event group, as well as component. The IMs of basic events (BE) or components are ranked relatively (Kafka, 1997). In terms of component importance, new measures were introduced to reflect the risk fluctuation due to any events/parameters related to a component, such as the differential importance measure (DIM) (Borgonovo and Apostolakis, 2001), and the component DIM (CPDIM) (Wang et al. 2008). And another treatment for complex components uses a set of minterms (Dutuit and Rauzy, 2015). In the previous literature, several methods for component RAW importance were discussed. For instance, the south Texas project (STP) method (NRC, 2001a) and maximum method (NRC, 2001b) would overestimate the component RAW, while the NEI 00-04 Rev.C method (NEI, 2002) and NEI 00-04 Rev.D method (NEI, 2003) significantly underestimates it. Here three previous methods with respect to the RAW evaluation of components are briefly reviewed including their limitations.

(1) The "direct method" was used for evaluating RAW directly based on MCSs. For an event group $\{Z_1, Z_2, ..., Z_k\}$ of a component, the unavailability of failure mode events in the group were set as one. However, it was not appropriate to extend the component RAW in this way (Kuo and Zhu, 2012). First, the event group excludes the CCF events of the component. Second, after the treatment of the direct method, the cut sets should be minimalized again with the Boolean laws of reduction.
(2) To improve the direct method, Check et al. (1998b) suggested that all BE in the event group be replaced with the same indicator, then the Boolean operation was performed to remove the possible non-MCSs. This approach has been widely applied in most risk monitors. However, it only

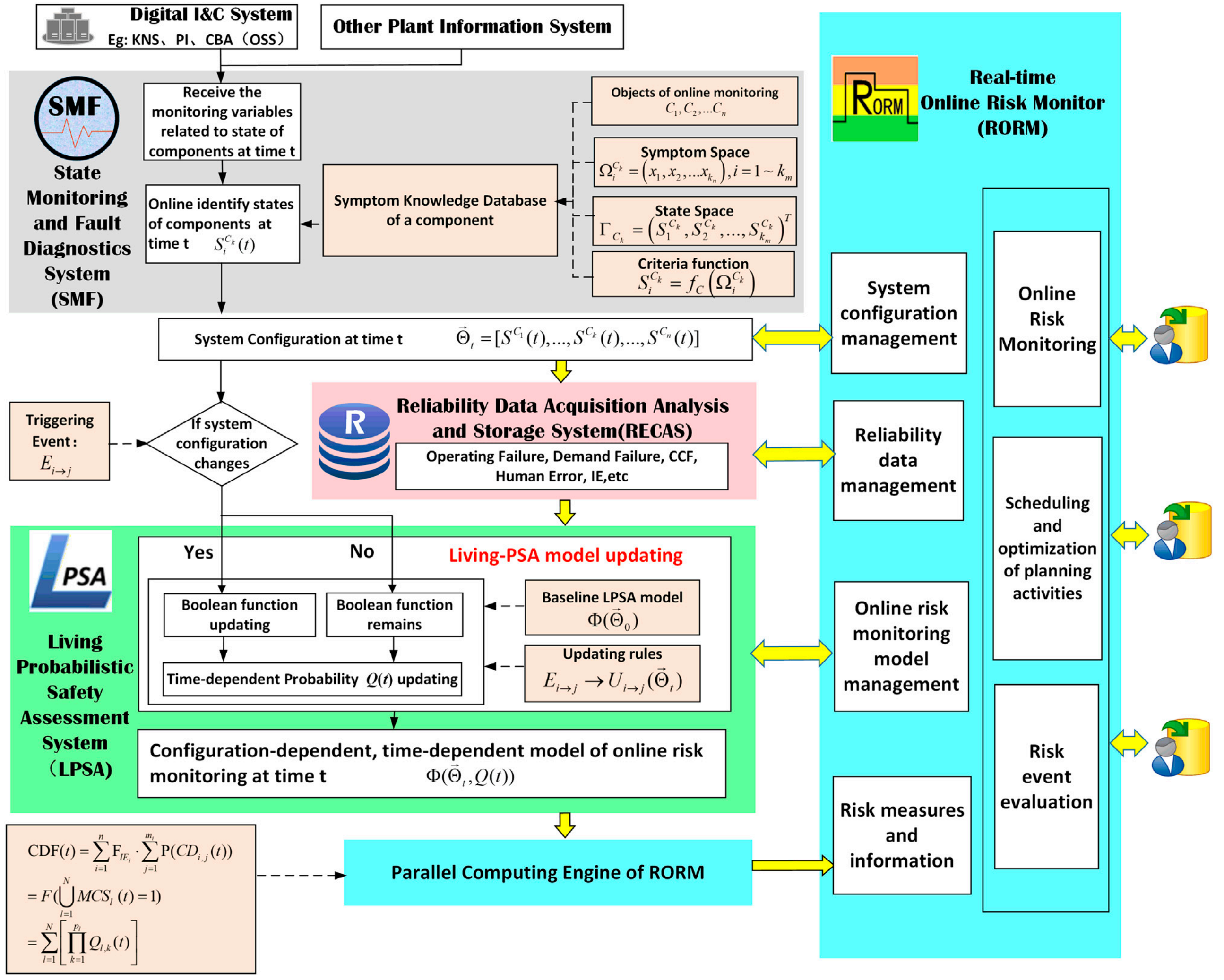

FIGURE 1 | Architecture of an integrated platform for nuclear power plant real-time online risk monitoring and management (IRORM).

concerned situations when the SSC-related BE can be grouped as one module in fault trees (FT). It also believed that the unavailability of components must be due to independent reasons, and ignored the unavailability situations arising from common cause factors.

(3) The balancing method (BM) (Kim et al., 2005) considering CCF events was proposed to calculate the RAW importance of components based on Martorell et al. (1996), as expressed in **Eq. 1**.

$$\mathrm{RAW} = 1 + \frac{\mathrm{FV}(1-p)}{p} \tag{1}$$

Here $p = \sum_{w=1}^{k} Q_w = p_{\text{independent events}} + p_{\text{CCF events}}$ indicates the sum of probabilities of all events related to a component, including independent failure basic events and CCF events k is the number of events. $\mathrm{FV} = \mathrm{FV}_{\text{independent events}} + \mathrm{FV}_{\text{CCF events}}$.

But the BM had certain limitations. First, **Eq. 1** is derived on the basis that the FV importance of a component is additive. But the basis is insufficient under some circumstances as mentioned in *Discussion*. Second, the BM is not conservative when the event group of a component consists of more than one basic event. In a word, the methods above were not fully applicable to RORMT.

The time-dependent IMs of components depend on the component lifetime distribution (Borgonovo et al., 2016). They could be evaluated at any time and the ranking order of them may vary with time. To give support for online operation and maintenance, the time-dependent IMs of components should be evaluated and updated in the RORM system whenever the real-time configuration changes. However, some technical challenges still exist in the importance analysis of RORM.

(1) It is necessary to investigate the evaluation method and potential benefits of time-dependent IMs, which is influenced by the time-dependent LPSA model.
(2) It is controversial to extend the importance of a basic event to the level of multiple BE/components (Vaurio, 2011).

(3) It still lacks consensus on updating the CCF model in the case of "what if a component is out-of-service," such as the numerator of RAW.

In this paper, we agree that both of the independent failure events and CCF events should be considered. Since the unavailability of components is possibly an independent failure, common cause failure, or failure due to an unconfirmed cause, the treatment for unavailability has to balance each assumption. When adjusting the probability of CCF events, it is crucial to account for each unavailability and specific plant configuration.

To solve the problems above, this paper is organized as follows. First, since the time-dependent IMs are affected by both the time-dependent risk and CCF updates, the two mathematical models of risk quantification and CCF treatment are introduced in *Mathematical Model of Real-Time Online Risk Monitoring and Management Technology*. The time-dependent IMs are presented in *Time-Dependent Importance Measures*, including FV, RAW, and RRW. The IMs of an individual event are developed to the level of basic event groups/components. A hybrid method for RAW evaluation is proposed by using the three options of CCF treatment in *Mathematical Model of Real-Time Online Risk Monitoring and Management Technology*. In *Case Study*, a simple case study is given for demonstration. *Time-Dependent Importance Measure for Risk-Informed Decision Making* illustrates what the time-dependent IMs contribute to risk-informed decision making, especially for configuration risk management.

MATHEMATICAL MODEL OF REAL-TIME ONLINE RISK MONITORING AND MANAGEMENT TECHNOLOGY

Risk Quantification in Real-Time Online Risk Monitoring and Management System

The RORM model is a time-dependent LPSA model used for online risk monitoring, which is established by event trees (ET) and FT. Here the concept of time-dependence is explained in Appendix A. Compared with other generic risk monitor models, there are two main enhancements of the RORM model. First, the unavailability of a component changes with its state and running time in the RORM model (as illustrated in Appendix B) while other RMs generally consider the unavailability of components with a fixed mission time or fixed probability. Second, the CCF modeling and updating methods are improved in the RORM model. The CCF updating method on the alpha model (Zubair and Amjad, 2016; Zhang et al., 2017) considered that the failure causes (independent failure, common cause failure, and uncertain cause failure) would influence the reduction of common cause component group (CCCG) order and CCF event probability.

Under any of the following three situations, the RORM model is triggered to update and calculate, according to the modeling and updating rules described (Zhang et al., 2015a; Chen et al., 2020).

(1) Updating due to configuration changes: The structural function $\Phi(\mathrm{Z})$ of the RORM model would be updated. $\Phi(\mathbf{Z})$ can be expressed in the form of minimal cut sets (MCS).

$$\Phi(\mathbf{Z}) = \bigcup_{l=1}^{N} MCS_l = \bigcup_{l=1}^{N} \bigcap_{k=1}^{p_l} Z_{l,k} \tag{2}$$

where N is the total number of MCSs ($l = 1,2,3,\ldots N$). $Z_{l,k} \in MCS_l$ is the kth event of MCS_l, $MCS_l = \{Z_{l,1}, Z_{l,2}, \ldots Z_{l,p_l}\}$ is the lth MCS. p_l is the number of BE under MCS_l (k = 1,2,3,...p_l).

Besides, the state of equipment and state duration T_s are updated if the configuration changes, and the probability of BE at time t $Q_{l,k}(t)$ (refers to Q(t) mentioned in **Table A2** of Appendix B) is automatically calculated in time for quantifying the RORM model.

(2) Regularly updating: The structural function $\Phi(\mathrm{Z})$ does not change. Even if no configuration changes, the RORM system automatically updates the state duration T_s, and then performs a risk calculation every few hours (generally whenever operators change shifts).

(3) Reliability parameter updating: The structural function $\Phi(\mathrm{Z})$ does not change in this case. The reliability parameters (such as running failure rates and demand probability) are not updated whenever the risk calculation is performed. The classical estimation method and Bayesian estimation method in updating reliability parameters (Atwood, 2003; Zubair et al., 2011) are also utilized in RECAS. In addition, based on the long-term restoration of failure data, RECAS could fit a life distribution of components by a maximum estimation method and a goodness-of-fit test. The results of updated parameters are used in calculating the probability of BE.

Assume that: 1) all events (including independent failure events and CCF events) in the RORM model are mutually exclusive, i.e., $Z_m \cap Z_n = \phi$ ($m \neq n$). 2) after the Boolean operation, MCSs obtained are mutually disjoint.

Within the scope of level 1 PRA, the instantaneous risk metric of NPP refers to the core damage frequency (CDF, per unit year). If any possible IE occurs at the current moment t, CDF(t) estimates the frequency of core damage given the real-time plant configuration after a predefined mission time T_m. Based on **Eq. 2**, the time-dependent risk measure CDF(t) can be quantified using rare event approximation which is mathematically expressed as

$$\begin{aligned} \mathrm{CDF}(t) &= \sum_{i=1}^{n} \mathrm{F}_{IE_i} \cdot \sum_{j=1}^{m_i} \mathrm{P}\left(CD_{i,j}(t)\right) \\ &= F\left(\bigcup_{l=1}^{N} MCS_l(t) = 1\right) \\ &= \sum_{l=1}^{N} \left[\prod_{k=1}^{p_l} \mathrm{Q}_{l,k}(t)\right] \end{aligned} \tag{3}$$

where $\mathrm{F}(\cdot)$ is frequency and $\mathrm{P}(\cdot)$ refers to probability. F_{IE_i} is the occurrence frequency of IE_i. n is the number of IEs, (i = 1,2,3,...n). $CD_{i,j}$ is the core damage sequence j in the event tree of IE_i. m_i is the number of CD sequences under IE_i (j = 1,2,3,...,m_i). $MCS_l = \{Z_{l,1}, Z_{l,2}, \ldots Z_{l,k}, \ldots, Z_{l,p_l}\}$ indicates the lth MCS and p_l is the number of events under MCS_l (k = 1,2,3,...p_l).

Note that: MCS_l is composed of IE and failure events of equipment. So $F(MCS_l(t) = 1)$ means the occurrence frequency of MCS_l, which is the product of all events in MCS_l.

If $Z_{l,k}$ is IE, then $Q_{l,k}(t) = F_{IE}(t)$. If $Z_{l,k}$ is a failure event of equipment, $Q_{l,k}(t)$ refers to the probability of a basic event at time t (refer to $Q(t)$ mentioned in **Table A2** of Appendix B).

A set of BEs with similar attributes would constitute a BE group, such as BE related to a component, system, or safety function. For instance, a BE group $\{Z_1, Z_2, ..., Z_k\}$ of component C. Then BEs of the same component would not appear in one MCS simultaneously after the Boolean operation. For example, a CCCG consists of failure events of three redundant components A, B, and C. The independent failure event of A (denoted as A_I) and CCF events of B and C (denoted as C_{BC}) may occur in the same MCS, but C_I, C_{AC}, C_{BC}, and C_{ABC} of component C would not appear in the same MCS. Likewise, a basic event may occur in multiple accident sequences, but it only appears in an accident sequence at most once.

For an event group $\{Z_1, Z_2, ..., Z_k\}$ of a component C, the risk metric CDF(t) would be expressed by a linear function as **Eq. 4**.

$$\mathrm{CDF}(t) = \sum_{w=1}^{k} A_w(t) Q_w(t) + B(t) \tag{4}$$

where $Z_w\ (w = 1, 2, ...k)$ is an event related to C. If any Z_w is within a CCCG, then the BE group includes both the independent failure events and CCF events which consist of multiple BE. $Q_w(t)$ is the time-dependent probability of Z_w at time t. Here $Q_w(t)$ is the same as $Q(t)$ mentioned above.

$$\sum_{w=1}^{k} A_w(t) Q_w(t) = \sum_{w=1}^{k} \mathrm{F}\Big(\bigcup_{Z_w \in MCS_l} MCS_l(t) = 1\Big)$$
$$= \sum_{w=1}^{k} \sum_{Z_w \in MCS_l} F(MCS_l(t) = 1)) \tag{5}$$

Note that the first term refers to the sum of frequencies of MCSs containing any event in the event group. The second term $B(t)$ is the probability of other MCSs. $A_w(t)$ indicates that the occurrence probability of MCSs containing Z_w in the case of $Q_w(t) = 1$.

Common Cause Failure Treatment of Unavailability

In this section, three options of what if treatment of unavailability are derived by solving the RORM model with adjusted CCF probability, reflecting the knowledge that a component is out of service. They provide a new idea considering CCF to quantify the what if risk of RAW numerator and RRW denominator.

For an n-order CCCG, the probability of k component failures and total failure probability are expressed in **Eqs 6**, **7**. (1≤k≤n)

$$Q_k^{(n)} = Q_{k0}^{(n)} + \sum_{j=1}^{l} Q_{kR_j}^{(n)} = (p_0)^k (1 - p_0)^{n-k} + \sum_{j=1}^{l} \eta_k^{R_j} P(R_j) \tag{6}$$

$$Q_t^{(n)} = \sum_{k=1}^{n} C_{n-1}^{k-1} Q_k^{(n)} \tag{7}$$

where $Q_k^{(n)}$ is the probability of k component failures of n-order CCCG. $Q_t^{(n)}$ is the total failure probability of a component in CCCG. $Q_{k0}^{(n)} = (p_0)^k (1 - p_0)^{n-k}$ is the probability of k component independent failures of n-order CCCG.

$Q_{kR_j}^{(n)} = \eta_k^{R_j} P(R_j)$ is the probability of k component failures of n-order CCCG due to common cause factor $R_j\ (j = 1, 2, ...l)$. $\eta_k^{R_j}$ is the coupling factor of k specific components due to common cause $R_j\ (j = 1, 2, ...l)$, especially R_0 is the independent failure factor. $P(R_j)$ is the probability of common cause $R_j\ (j = 1, 2, ...l)$. p_0 refers to the independent failure probability.

Option 1: what if unavailability of SSC due to independent factor

The independent factor refers to independent failure, or other preventive maintenance, or tests. When i specific components are identified to be unavailable, the probability of CCF events essentially remains, but they are reorganized to a new CCF event group.

$$\begin{aligned} Q_t^{(n-i)} &= Q_t^{(n)} \\ Q_k^{(n-i)} &= \sum_{m=0}^{i} C_i^m Q_{k+m}^{(n)} \end{aligned}, \quad \begin{aligned} i &= 1, 2, ..., n-1; \\ k &= 1, 2, ..., n-i \end{aligned} \tag{8}$$

where $Q_t^{(n-i)}$ is the failure probability of a component in CCCG, given the fact that i independent failures have occurred. $Q_k^{(n-i)}$ is the probability of k component failures of n-order CCCG, given the fact that i independent failures have occurred.

Thus, it is required to regenerate CCF events and update their probabilities, without updating CCF parameters in this case.

Option 2: what if unavailability of SSC due to common cause factor

Suppose that a certain common cause factor $R_p\ (p = 1, 2, ...l)$ is known to happen, then $P(R_p) = 1$.

$$\widetilde{Q_{kR_p}^{(n)}} = \frac{Q_{kR_p}^{(n)}}{P(R_p)} \tag{9}$$

From **Eq. 9**, when a known common cause factor $R_p\ (p = 1, 2, ...l)$ happens and it leads to failures of i components ($i \le n$), the probability of other remaining CCF events becomes a conditional probability, given the fact that i components failed due to R_p.

$$\widetilde{Q_k^{(n)}}\Big|_{R_p} = Q_{k0}^{(n)} + \sum_{j=1}^{l} \widetilde{Q_{kR_p}^{(n)}} = (p_0)^k (1 - p_0)^{n-k} + \sum_{j=1, j \ne p}^{l} \eta_k^{R_j} P(R_j) + \eta_k^{R_p} \tag{10}$$

For i failures of n-order CCCG due to R_p, the new failure parameters are written as **Eqs 11**, **12**. $i = 1, 2, ..., n-1; k = 1, 2, ..., n-i$.

$$\widetilde{Q_k^{(n-i)}}\Big|_{R_p} = \sum_{m=0}^{i} C_i^m \widetilde{Q_{k+m}^{(n)}}\Big|_{R_p} = \sum_{m=0}^{i} C_i^m \Big[Q_{(k+m)0}^{(n)} + \sum_{j=1}^{l} \widetilde{Q_{(k+m)R_j}^{(n)}}\Big|_{R_p}\Big]$$
$$= \sum_{m=0}^{i} C_i^m \Big[Q_{(k+m)}^{(n)} + Q_{(k+m)R_p}^{(n)} \Big(\frac{1 - P(R_p)}{P(R_p)}\Big)\Big] \tag{11}$$

$$\widetilde{Q_t^{(n-i)}} = Q_t^{(n)} + \sum_{k=1}^{n} C_{n-1}^{k-1} Q_{kR_p}^{(n)} \frac{1 - P_{R_p}}{P_{R_p}} \tag{12}$$

where $\widetilde{Q_k^{(n-i)}}|_{R_P}$ is the conditional probability of k component failures of n-order CCCG with the fact that i failures occurred, because of the common cause factor $R_P\,(p = 1, 2, \ldots l)$.

From **Eqs 11**, **12**, the probability of a CCF event due to a common cause factor is higher than that of an independent factor, that is, $\widetilde{Q_t^{(n-i)}} > Q_t^{(n-i)}$ and $\widetilde{Q_k^{(n-i)}} > Q_k^{(n-i)}$. So Option 2 is more conservative than Option 1.

Option 3: what if unavailability of SSC due to unconfirmed cause

During the online operation of NPP, it is often impossible to detect the reasons why a component is unavailable (except for some voluntary planned activities such as preventive maintenance and periodic testing). Thus, it is suggested to estimate the probability of CCF events due to unconfirmed causes using the expected value of Option 1 and Option 2.

Given that i components have become unavailable ($i = 1, 2, \ldots, n-1$), the conditional probability of $R_j\,(j = 0, 1, 2, \ldots l)$ which lead to the unavailability is written as

$$P\left(R_j|i\right) = \frac{P\left(R_j\right)P\left(i|R_j\right)}{P(i)} = \frac{Q_{iR_j}^{(n)}}{Q_i^{(n)}} = \begin{cases} \dfrac{(p_0)^i(1-p_0)^{n-i}}{(p_0)^i(1-p_0)^{n-i} + \sum_{j=1}^{l}\eta_i^{R_j}P\left(R_j\right)} & j = 0 \\[2ex] \dfrac{\eta_i^{R_j}P\left(R_j\right)}{(p_0)^i(1-p_0)^{n-i} + \sum_{j=1}^{l}\eta_i^{R_j}P\left(R_j\right)} & j = 1, 2, \ldots, l \end{cases} \tag{13}$$

where $\eta_i^{R_j}$ is the coupling factor of i components due to cause $R_j\,(j = 0, 2, \ldots l)$, especially R_0 is the independent failure factor.

From **Eq. 13**, we can obtain the expected probability value of events as **Eqs 14**, **15**.

$$E(Q_k^{(n-i)}) = \sum_{j=0}^{l} P(R_j|i)Q_{kR_j}^{(n-i)} = \frac{(p_0)^i(1-p_0)^{n-i}\sum_{m=0}^{i}C_i^m Q_{k+m}^{(n)} + \sum_{j=1}^{l}\sum_{m=0}^{i}\eta_i^{R_j}P(R_j)C_i^m\left[Q_{k+m}^{(n)} + \frac{1-P(R_j)}{P(R_j)}Q_{(k+m)R_j}^{(n)}\right]}{(p_0)^i(1-p_0)^{n-i} + \sum_{j=1}^{l}\eta_i^{R_j}P(R_j)} \tag{14}$$

$$\begin{aligned} E(Q_t^{(n-i)}) &= \sum_{j=0}^{l} P(R_j|i)Q_t^{(n-i)} \\ &= \frac{(p_0)^i(1-p_0)^{n-i}}{(p_0)^i(1-p_0)^{n-i} + \sum_{j=1}^{l}\eta_i^{R_j}P(R_j)}Q_t^{(n)} \\ &\quad + \frac{\sum_{j=1}^{l}\eta_i^{R_j}P(R_j)\left[1 + \dfrac{\left[1-P(R_j)\right]\sum_{k=1}^{n}C_{n-1}^{k-1}\eta_k^{R_j}}{Q_t^{(n)}}\right]Q_t^{(n)}}{(p_0)^i(1-p_0)^{n-i} + \sum_{j=1}^{l}\eta_i^{R_j}P(R_j)} \\ &= Q_t^{(n)}\cdot\left\{1 + \frac{\sum_{j=1}^{l}\eta_i^{R_j}P(R_j)\dfrac{\left[1-P(R_j)\right]\sum_{k=1}^{n}C_{n-1}^{k-1}\eta_k^{R_j}}{Q_t^{(n)}}}{(p_0)^i(1-p_0)^{n-i} + \sum_{j=1}^{l}\eta_i^{R_j}P(R_j)}\right\} \end{aligned} \tag{15}$$

Based on three basic parameter models for CCF analysis (Mosleh et al., 1998), Option 3 is further developed as follows:

(1) For a β-factor model, if i components are known to have failed, the reason for i failures must be due to an independent factor. So the CCF event probability of the (n-i) remaining components does not change.

$$\begin{cases} Q_1^{(n-i)} = (1-\beta)Q_t \\ Q_{n-i}^{(n-i)} = \beta Q_t \\ Q_t^{(n-i)} = Q_t^{(n)} \end{cases} \quad i = 1, 2, \ldots n-1 \tag{16}$$

(1) For an α-factor model (non-staggered testing scheme):

$$E(Q_k^{(n-i)}) = \frac{(p_0)^i(1-p_0)^{n-i}Q_{k0}^{(n-i)} + \sum_{m=0}^{i}\eta_i^{R_j}P(R_j)C_i^m\left[\frac{n}{C_n^{k+m}}\frac{\alpha_{k+m}}{\alpha_t}Q_t + \frac{1-P(R_j)}{P(R_j)}Q_{(k+m)R_j}^{(n)}\right]}{(p_0)^i(1-p_0)^{n-i} + \sum_{j=1}^{l}\eta_i^{R_j}P(R_j)} \tag{17}$$

For an α-factor model (staggered testing scheme):

$$E(Q_k^{(n-i)}) = \frac{(p_0)^i(1-p_0)^{n-i}Q_{k0}^{(n-i)} + \sum_{m=0}^{i}\eta_i^{R_j}P(R_j)C_i^m\left[\frac{\alpha_{k+m}}{C_{n-1}^{k+m-1}}Q_t + \frac{1-P(R_j)}{P(R_j)}Q_{(k+m)R_j}^{(n)}\right]}{(p_0)^i(1-p_0)^{n-i} + \sum_{j=1}^{l}\eta_i^{R_j}P(R_j)} \tag{18}$$

(1) For an MGL model:

$$E(Q_k^{(n-i)}) = \frac{(p_0)^i(1-p_0)^{n-i}\sum_{m=0}^{i}C_i^m Q_{k+m}^{(n)} + \sum_{j=1}^{l}\sum_{m=0}^{i}\eta_i^{R_j}P_{R_j}C_i^m\left[\frac{1}{C_{m-1}^{k-1}}\left(\prod_{i=1}^{k+m}\rho_i\right)(1-\rho_{k+m+1})Q_t + \frac{1-P_{R_j}}{P_{R_j}}Q_{(k+m)R_j}^{(n)}\right]}{(p_0)^i(1-p_0)^{n-i} + \sum_{j=1}^{l}\eta_i^{R_j}P_{R_j}} \tag{19}$$

where $\rho_i = \begin{cases} 1 & i = 1 \\ \dfrac{\sum_{k=i}^{m}C_{m-1}^{k-1}Q_k}{\sum_{k=i-1}^{m}C_{m-1}^{k-1}Q_k} & i = 2, 3, \ldots, m, \\ 0 & i > m \end{cases}$ that is, $\rho_1 = 1, \rho_2 = \beta, \rho_3 = \gamma, \rho_4 = \delta, \ldots, \rho_{m+1} = 0$

For practical considerations, U.S. NRC has proposed methods for CCF treatment. For instance, Appendix E.3 of NUREG/CR-5485 (Mosleh et al., 1998) discussed about the condition that one of the components in the CCCG has failed or is under preventive maintenance. But there are two main deficiencies. First, the manner of CCF modeling for a three-order group in the report is "a single common cause basic event (C_{ABC}) and three BE (A_I, B_I, C_I)". This is different from what is currently used in NPP CCF analysis. Second, the approximations of **Eqs E.11**, **E.12** of NUREG/CR-5485 in the report are not valid.

The Risk Assessment of Operational Events handbook (NRC, 2017) had eight CCF treatment cases based on the SAPHIRE software (NRC, 2011). In RASP, given an observed failure of a component in the CCCG, the general consideration is to set the BE of a failed component to TRUE and apply the conditional CCF probability using the original CCF parameter without updating (e.g., $\alpha 2$ for CCCG = 2, α_3 for CCCG = 3). That is not appropriate, no matter that the observed failure is because of an independent factor, or a common cause factor.

We have known that the output of RORM might change significantly due to CCF. However, the critical CCF data are hard to obtain. Thus, the following two CCF engineering treatments are applied to the development of IRORM.

- CCF engineering treatment #1: Given a detected random failure of a component

In most cases, it is difficult to quickly determine the failure mode of a failed component online, especially to identify whether it is due to independent failure or CCF. Thus, a tradeoff approach is proposed as follows: for the failed component, set the intermediate event of component "A fails" to be true. For the other components B and C of the same CCCG, the probabilities of certain CCF events (such as C_{AC}, C_{AB}, C_{ABC}) are divided by the unavailability $Q(t)$.

- CCF engineering treatment #2: Given preventive maintenance/periodic testing which will lead component A to be unavailable.

In this case, the equipment is unavailable due to independent reasons, but not due to failure. So the basic event "unavailability due to test or maintenance" of A is set to true while the probabilities of CCF events stay the same.

Another possible solution of CCF treatment #2 is to quantify the Boolean function of the RORM model. First, delete all possible BE of component A, and regenerate new CCF trees of comparable components in CCCG. Then update the CCF event probabilities as Option 1 is introduced.

TIME-DEPENDENT IMPORTANCE MEASURES

The time-dependent IMs are influenced by the RORM model at time t, but also the CCF treatment, as shown in **Figure 2**. The importance analysis in PRA is mostly performed based on individual BE or parameters, such as FV (Fussell and Vesely, 1972; Fussell, 1975), RAW, and RRW (Vesely et al. 1986). But for risk-informed applications, the IMs are evaluated to identify the risk-significant SSCs. Thus, in the next section, the time-dependent IMs are defined and evaluated at different levels (basic event, basic event group, and component).

Time-Dependent Fussell-Vesely Importance

The time-dependent FV importance of a basic event Z_w is defined as the proportion of the probabilities of all MCSs containing Z_w to the time-dependent risk metric, expressed by **Eq. 20**.

$$\mathrm{FV}_{Z_w}(t) = \frac{\mathrm{P}\left(\underset{Z_w \in MCS_l}{\cup} MCS_l\right)}{\mathrm{P}\left(\cup_{l=1}^{N} MCS_l\right)} = 1 - \frac{R_w^-(t)}{R(t)} \tag{20}$$

where $\underset{Z_w \in MCS_l}{\cup} MCS_l$ is the union of MCSs containing Z_w. N is the total number of MCSs. $R(t)$ is the time-dependent risk metric of real-time configuration.

$R_w^-(t)$ is the real-time risk level when the Boolean variable of Z_w is set to false, or the failure probability of Z_w is set to zero.

For an event group $\{Z_1, Z_2, ..., Z_k\}$ of component C, it is expressed as **Eq. 21**.

$$\mathrm{FV}_c(t) = \mathrm{FV}\left(\bigcup_{w=1}^{k} Z_w\right) = \frac{\sum_{w=1}^{k} A_w(t) Q_w(t)}{\mathrm{CDF}(t)} \tag{21}$$

where $A_w(t)$ indicates the occurrence probability of MCSs which includes Z_w in the case of Q_w(t) = 1.

In consideration of engineering practice, FV importance of an individual event which is related to the same component are ranked together, including failure mode events and CCF events. If the FV importance of component C ranks high among components for the current configuration, its preventive maintenance should be preferentially implemented. The operators should be reminded to pay special attention to the components with top FV ranking orders.

Time-Dependent Risk Achievement Worth Importance

The time-dependent $\mathrm{RAW}_{Z_w}(t)$ is expressed as the ratio of $R(\mathrm{T}|Q_w(t) = 1)$ to the time-dependent risk level, as shown in **Eq. 22**.

$$\mathrm{RAW}_{Z_w}(t) = \frac{R(\mathrm{T}|Q_w(t) = 1)}{R(t)} \tag{22}$$

where T is the top event of system failure. Q_w(t) is the failure probability of Z_w.

$R(\mathrm{T}|Q_w(t) = 1)$ is the real-time risk level what if Z_w does not exist in FT. That is, the Boolean variable of Z_w is set to true, or Q_w(t) is set to one.

Note that when calculating $R(\mathrm{T}|Q_w(t) = 1)$, other BEs which have interdependencies with Z_w are possibly influenced. For example, if Z_w indicates the CCF failure of component A and B, then the other events of CCCG should be updated.

For an event group $\{Z_1, Z_2, ..., Z_k\}$ of component C, $\mathrm{RAW}_C(t)$ is independent of Q_w(t), as indicated in **Eq. 23**.

$$\mathrm{RAW}_C(t) = \frac{\mathrm{CDF}(t)^{C^+}}{\mathrm{CDF}(t)} = \frac{\sum_{w=1}^{k} A_w(t) + B(t)}{\mathrm{CDF}(t)} \tag{23}$$

where $A_w(t)$ indicates that the occurrence probability of MCSs including Z_w in the case of Q_w(t) = 1. $B(t)$ is the sum of frequencies of MCSs that does not contain any event in the event group.

In consideration of engineering practice, $\mathrm{RAW}_C(t)$ is quantified based on the MCS results of real-time configuration, but the manner of quantification is different under the following two situations.

(1) To avoid certain failures of components: $\mathrm{RAW}_C(t)$ refers to the situation what if C failed. Thus, the individual BE of C are

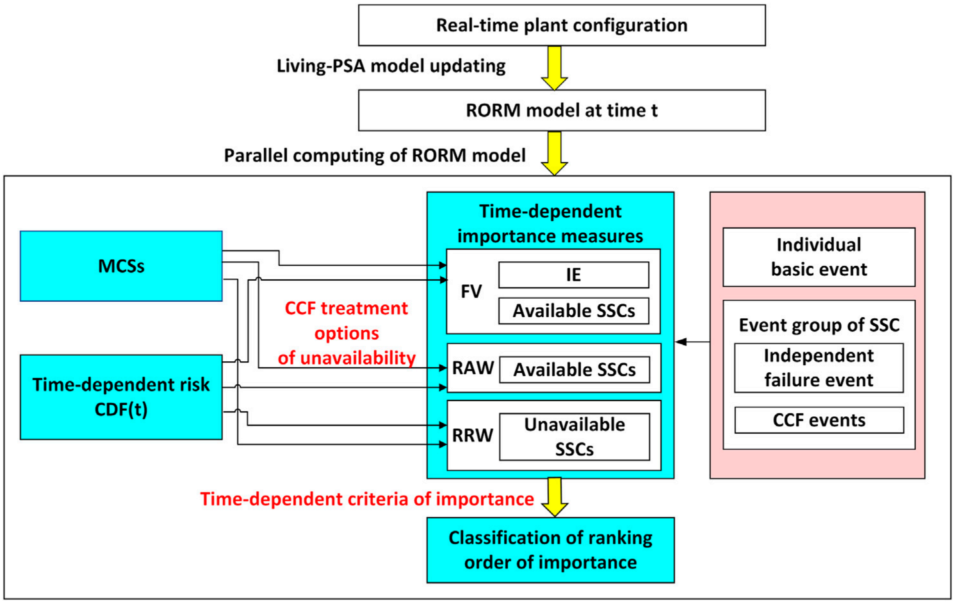

FIGURE 2 | The evaluation process of time-dependent importance measures.

updated according to **Table A2** of Appendix B. And the CCF events related to *C* would follow the CCF engineering treatment #1 in *Common Cause Failure Treatment of Unavailability*.

(2) To prioritize the near-term planned activities of components: $\mathrm{RAW}_C(t)$ refers to the situation if component C was in maintenance/testing. Thus, the individual BE should be updated according to **Table A2** of Appendix B. And the CCF events related to C would follow the CCF engineering treatment #2 in *Common Cause Failure Treatment of Unavailability*.

Time-Dependent Risk Reduction Worth Importance

The time-dependent $\mathrm{RRW}_{Z_w}(t)$ is expressed as a ratio of the time-dependent risk level to $R(\mathrm{T}|Q_w(t)=0)$, as shown in **Eq. 24**.

$$\mathrm{RRW}_{Z_w}(t) = \frac{R(t)}{R(\mathrm{T}|Q_w(t)=0)} \tag{24}$$

where $R(\mathrm{T}|Q_w(t)=0)$ is the risk level assuming that Z_w is perfect, i.e., Z_w= False or $Q_w(t)=0$.

For an event group $\{Z_1, Z_2, \ldots, Z_k\}$ of component *C*, we can see that $\mathrm{RRW}_C(t)$ is independent of Q_w(t), as shown in **Eq. 25**.

$$\mathrm{RRW}_C(t) = \frac{\mathrm{CDF}(t)}{\mathrm{CDF}(t)^{c-}} = \frac{\mathrm{CDF}(t)}{B(t)} \tag{25}$$

where $B(t)$ is the sum of MCSs that does not contain any event in the group.

The RRW importance of unavailable components answers what would happen if it is perfect. Thus, the ranking of RRW can be used to prioritize the maintenance actions.

Since the failure events of unavailable components no longer exist in MCSs, RRW importance of an unavailable component is quantified using MCSs "zero-repair configuration," in order to find out the missing MCSs. Here "zero-repair configuration" is a virtual configuration with all equipment available, it is predefined by PRA analysts and safety engineers.

The procedures of quantifying $\mathrm{RRW}_C(t)$ are as follows:

Step 1 Obtain the MCS analysis results of the zero-repair configuration.

Step 2 Except for *C*, the states of other components are set to their real-time states, in order to generate new MCSs in case component *C* becomes available again. The logical value of its BE should be consistent with its state, as listed in **Table A2** of Appendix B.

Step 3 For component C, its state duration T_s is reset to zero, while the state duration of other components remains unchanged. Update the unavailability of failure events of *C*.

Step 4 Calculate $B(t)$ with new MCSs.

Step 5 Determine the RRW of an unavailable component by using the ratio of $\mathrm{CDF}(t)$ and $B(t)$.

DISCUSSION

If an IM of the union of an event group is the sum of the IMs of the individual BE, then the IM is "additive," as expressed in **Eq. 26**.

$$\mathrm{IM}\left(\bigcup_{w=1}^{k} Z_w\right) = \sum_{w=1}^{k} \mathrm{IM}(Z_w) \tag{26}$$

For a general event group $G = \cup_{w=1}^{k} Z_w$, the importance of G is quantified depending on how these events are modeled in FT.

(1) When $Z_1, Z_2, ..., Z_k$ are connected by an OR gate, FV importance of G is the sum of all individual event FVs, that is, FV is additive in this case.

$$\mathrm{FV}_G(t) = \sum_{w=1}^{k} \mathrm{FV}_{Z_w}(t) \tag{27}$$

(2) When $Z_1, Z_2, ..., Z_k$ are connected by an AND gate, FV importance of G is equivalent to the FV of any individual event.

$$\mathrm{FV}_G(t) = \mathrm{FV}_{Z_1}(t) = \mathrm{FV}_{Z_2}(t) = ...\mathrm{FV}_{Z_w}(t) = ... = \mathrm{FV}_{Z_k}(t) \tag{28}$$

(3) In general, if multiple BE are not modeled in a modular FT, there is no certain connection between the FV importance of G and those of individual BE.

$$\mathrm{FV}_G(t) \neq \sum_{w=1}^{k} \mathrm{FV}_{Z_w}(t) \tag{29}$$

It is observed that in the latter two cases, the time-dependent FV importance of G cannot directly sum up the importance of individual BE. Specifically, in most cases, BEs of a component are inputs of OR gate in the RORM model. Thus **Eq. 27** is generally used for the FV of a component.

For any of the three situations, neither of the RAW and RRW for an event group are additive, as expressed in **Eqs. 30**, **31**.

$$\begin{aligned} &\forall w = 1, 2, 3, ...k,\ \mathrm{RAW}_G(t) > \mathrm{RAW}_{Z_w}(t) \\ &\text{and } \mathrm{RAW}_G(t) \neq \sum_{w=1}^{k} \mathrm{RAW}_{Z_w}(t) \end{aligned} \tag{30}$$

$$\begin{aligned} &\forall w = 1, 2, 3, ...k,\ \mathrm{RRW}_G(t) > \mathrm{RRW}_{Z_w}(t) \\ &\text{and } \mathrm{RRW}_G(t) \neq \sum_{w=1}^{k} \mathrm{RRW}_{Z_w}(t) \end{aligned} \tag{31}$$

HYBRID METHOD FOR TIME-DEPENDENT RISK ACHIEVEMENT WORTH EVALUATION

The $\mathrm{RAW}_C(t)$ of available components should be both configuration-dependent and time-dependent. The quantification of the time-dependent RAW importance of a component focuses on how to calculate the "what if risk" level as the numerator of $\mathrm{RAW}_C(t)$

· The treatment of "A component is unavailable" for the numerator of RAW does not mean that "the component does not exist or is removed from the PRA model." Because "a component is out of service" gives a conditional CCF probability for the remaining components changed according to what type a basic event is. When a component is just out of service with an unconfirmed cause, the component could be out of service due to a common cause factor or due to an independent cause (such as independent random failure, preventive maintenance, or a periodic test).

How to deal with the CCF issue in "what if" is a controversial and tough problem. For a given event group or a component, it should include all related BE and CCF events. But when the logical value of a CCF event is true, it means that two or more components have failed due to a common cause. The probability of other CCF events may become a conditional probability given the known failures in the CCCG. For example, if one of the CCCG elements (such as component C in a three-order CCCG) has been just out of service, the probability of a CCF event which associates C with other components (such as C_{BC}, C_{AC}, *and* C_{ABC}) will increase.

Thus, the reasons for the unavailability of SSC C in CCCG include: 1) a what if independent cause; 2) a common cause factor; and 3) an unconfirmed cause.

Considering the "what if" assumptions of CCF events, a hybrid method to deal with independent failure events and CCF events is proposed to quantify the RAW importance of SSC. The procedures of the hybrid method are shown in **Figure 3**.

Step 1: Update the RORM model according to the real-time plant configuration at time t. The updating rules are concerned with the Boolean function updating of system failure. Qualify the MCSs based on the updated Boolean function of the system.

Step 2The reliability data from the RECAS system are given to quantify the failure probability of failure mode events (refer to **Table A2** of Appendix B), CCF events, and IEs, etc. As a result, the risk measures such as CDF(t) are quantified.

Step 3For SSC C, identify all the events $Z_w\,(w = 1, 2, 3..., k)$ associated with SSC C. Here Z_w consists of failure mode events Z_w^B and CCF events Z_w^C.

Step 4Update the probability of MCSs under the assumption of "C is out of service." For CCF events Z_w^C, there are three options of what if treatment considering CCF. It requires an update in the failure probability of Z_w^C as introduced in *Common Cause Failure Treatment of Unavailability*. For failure mode events Z_w^B, the failure probability is set to 1. If the failure mode events of SSC C is negated within MCSs, then its failure probability is set to 0.

$$A_w(t) = \frac{P\left(\bigcup_{Z_w^B \in \mathrm{MCS}_l} \mathrm{MCS}_l\right)}{Q_w(t)} \tag{32}$$

Step 5Calculate $\mathrm{CDF}(t)^{C^+}$ based on the updated MCS and new failure probabilities of all events, as the numerator of $\mathrm{RAW}_C(t)$.

$$\mathrm{CDF}(t)^{C^+} = \sum_{w=1}^{k} A_w(t) + B(t) \tag{33}$$

Step 6The final result $\mathrm{RAW}_C(\mathrm{t})$ is calculated.

$$\mathrm{RAW}_C(\mathrm{t}) = \mathrm{CDF}(t)^{C^+}/\mathrm{CDF}(t) \tag{34}$$

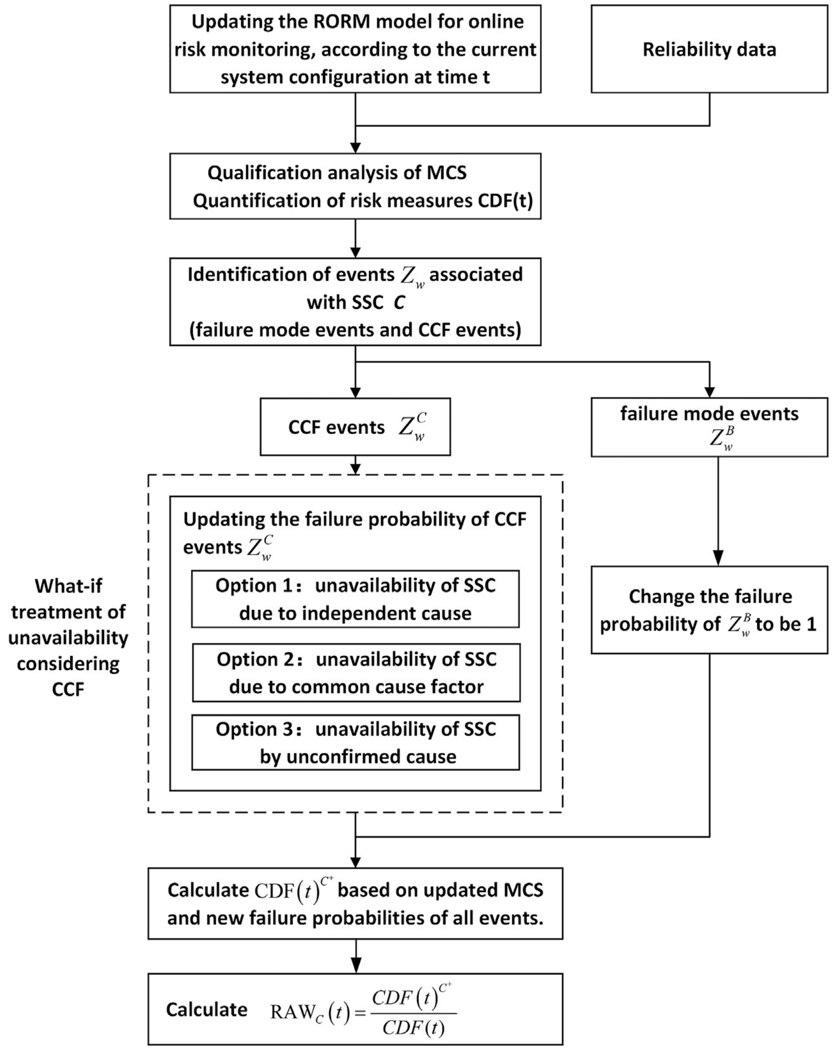

FIGURE 3 | Procedures of the RAW importance calculation of SSC *C*.

CASE STUDY

Description

A typical fluid system (**Figures 4A**) consists of three redundant pump trains. Each train has a 100% pump and its related valve. In normal conditions, at least one pump train of the system supplies water to other systems. P_1, P_2, and P_3 are three redundant and identical electric pumps. The running state of an electrical pump is continuously monitored online, but its standby state cannot be monitored. V_1, V_2, and V_3 are check valves to control the fluid of each pump train. All valves are non-online monitored equipment. When a pump is running/standby, the related valve of the train is open/closed. When the pump is tested/repaired, then the whole pump train (including the related valve) will be out of service for test/maintenance. When the pump happens to fail, the related valve will be automatically triggered to close. The operating pump train normally switches every 30 days-45 days.

Assumptions and Simplifications:

(1) If the equipment is not online monitored, the last moment to confirm availability is the moment of on-demand action or the end moment of periodic testing/preventive maintenance.
(2) No failure occurs when switching the operating pump train, and no demand failure occurs when a valve transfers its state.
(3) All equipment is available and perfect at t = 0. The pump train #1 is restored to operation. The other two pump trains are in standby.
(4) The mission time of all equipment T_m = 24 h. In this case, the time-dependent risk of the system is a conditional failure probability of the system after the future mission time T_m based on the real-time plant configuration.
(5) The top event of the FT model is "all the pump trains of the system fail to supply water to other systems."
(6) Only the CCCG of "pump operating failure" is considered in the FT model.

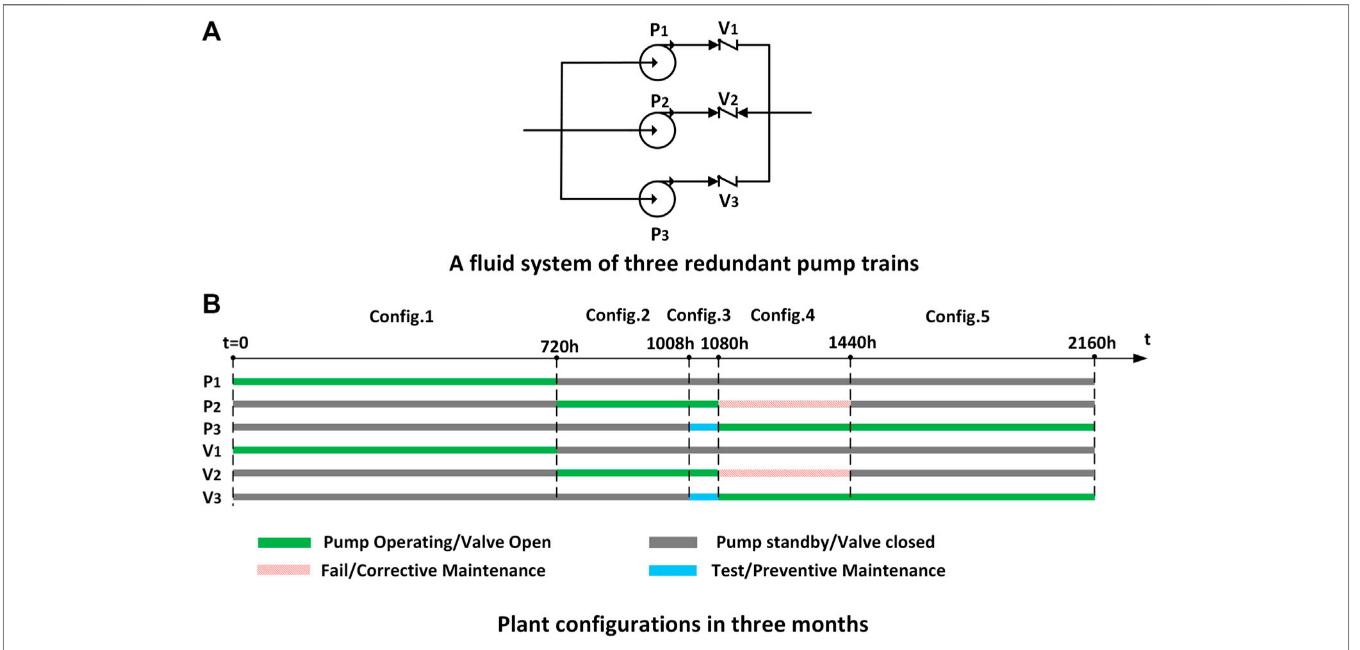

FIGURE 4 | Description of fluid system. **(A)** A fluid system of three redundant pump trains. **(B)** Plant configurations in three months.

(7) The risk calculation of the system is triggered whenever the configuration changes, and it is regularly calculated every 120 h if the configuration stays the same.

During a 3-month (2,160 h) operation, the system experienced multiple configuration changes as shown in **Figures 4B**. Train 1 is running, trains 2 and 3 are in standby from t = 0. At t = 720 h, train 1 switches to standby, and train 2 begins to operate. At the same time, V1 becomes closed and V2 becomes open. At t = 1,008 h, the standby pump train 3 starts to carry out a periodic test. At t = 1,080 h, P2 fails randomly. Train 3 changes from standby to operation. Then train 2 enters into online maintenance. At t = 1,440 h, P2 returns to standby, and pump train 3 continues to run.

RESULTS AND DISCUSSION

Time-Dependent Risk Evaluation

To demonstrate the time-dependent probabilistic model, the Weibull and exponential distributions of components are used as two examples. If the life distribution of the equipment is exponential, the failure rate is constant. If the life distribution of the equipment follows other continuous distributions such as Weibull distribution, the failure rate varies with time. The reliability parameters of the two examples are listed in **Table 1A**.

The insights of risk are inaccurate in current RMs. First, PRA data used by RMs are based on the assumption that the "time to failure" of continuous operating equipment is exponentially distributed, that is, the estimated value of failure rate $\lambda(t)$ is constant. Second, for a predefined mission time of the system, the risk level is only dependent on the plant configuration regardless of state duration, so the risk is constant under the same configuration. From the black lines of **Figures 5A, B**, we found out that no matter what distribution the life of equipment is, the risk levels of different configurations are almost the same as long as the combination of available equipment is the same, such as Config.1, Config.2, and Config.5. Based on the above risk information of RM, we can infer that the operating equipment is allowed to operate continuously, with no requirements of periodic testing/preventive maintenance or regularly switching between redundant units. That is obviously in contrast with the engineering experience of NPP.

The system risk of RORM varies with plant configuration and equipment unavailability. It is a sort of saw-tooth type. Take the blue line of **Figures 5A** as an example. For Config.1 (train 1 is running, train 2 and 3 are standby), the risk rises rapidly from baseline risk 1.860e-18 to 2.430e-13. At t = 720 h, train 1 switches to standby, and train 2 begins to operate. At the same time V_1 turns to closed and V_2 turns to open. For configuration 2, firstly the risk drops to 2.019e-18, which is quite close to the baseline risk, then it increases to 1.751e-14. At t = 1,008 h, the standby pump train 3 starts to carry out a periodic test. For Config.3, the redundancy of the system is reduced, so the risk suddenly increases to 6.794e-10. During the test, the risk rises until the end of test. After the test of train 3, the state durations of P_3 and V_3 are both reset. At t = 1,080 h, P_2 fails randomly. The standby train 3 is put into operation. Then train 2 enters into online maintenance. After the maintenance of train 2, the state durations of P_2 and V_2 are both reset. For Config.4, the risk drops to 8.954e-14 due to P_2 failure, then it increases to 1.3980e-9 with the continuous operation of train 3. At t = 1,440 h, P_2 returns to

TABLE 1A | Reliability parameters of failure events.

Component	Failure mode	Example 1		Example 2		
		Distribution	Parameter	Distribution	λ (h^{-1})	P_d
P_1, P_2, P_3	FO	Weibull	a = 3,000,b = 4	Exponential	3.0e-5	— —
	FD	— —	2.10e-5	— —	— —	2.10e-5
	FB	Weibull	a = 12,500, b = 4	Exponential	2.00e-5	— —
V_1, V_2, V_3	RPO	Weibull	a = 50,000, b = 3	Exponential	1.00e-5	— —
	RPC	Weibull	a = 50,000, b = 3	Exponential	1.00e-5	— —

Notes.
1) For pumps, FO—failure during operation; FB—standby failure; FD—failure on demand
2) For valves, RPO—not keep position at open; RPC—not keep position at closed
3)Two-parameter Weibull distribution

$$f(x;a,b)=\begin{cases}\frac{b}{a}\left(\frac{x}{a}\right)^{b-1}e^{-\left(\frac{x}{a}\right)^{b}} & , \quad x\geq 0\\ 0 & , \quad x<0\end{cases}$$

where a is the scale parameter and b is the shape parameter.
So the probability of a basic event under Weibull distribution is written as

$$F(t)=1-\exp\left(-\frac{(T_S+T_A+T_m)^b-T_S^b}{a^b}\right)$$

The failure probabilities of the same event in different configurations increase with the state duration of the equipment.
4) λ: failure rate; P_d: the probability of failure on the demand of pumps

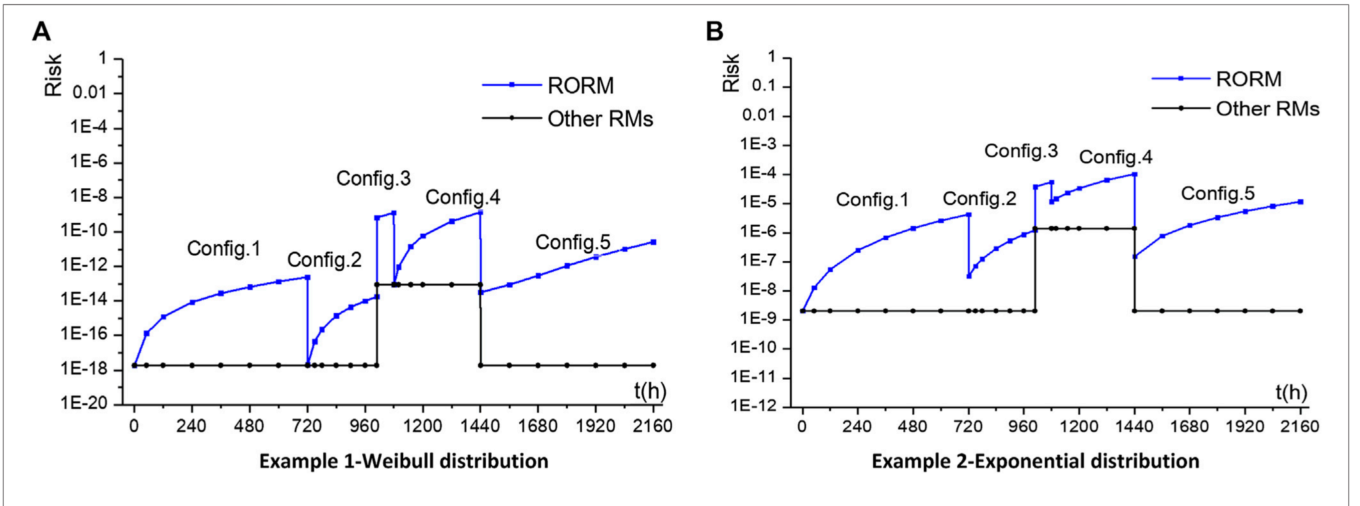

FIGURE 5 | Comparison of risk profile between RORM and other RMs. **(A)** Example 1-Weibull distribution. **(B)** Example 2-Exponential distribution.

standby, and train 3 continues to run. For Config.5, the risk steps down to 3.1510e-14, and then gradually climbs to 2.633e-11.

The RORM model brings novel risk insights based on the effect of cumulative state duration. Even if the plant configuration remains, the risk also increases with the system running time. By comparison of Config.1, 2, and 5, it is clear that even if the combination of available equipment is the same, the risk levels of different configurations vary from each other. Thus, it is necessary to carry out periodic testing, inspection, maintenance, and switching regularly in order to keep the risk level within an acceptable range.

As mentioned in *Time-Dependent Fussell-Vesely Importance*, the FV importance values of equipment for Config.1 and 2 are calculated according to the parameters in Example 1, as shown in **Figure 6**. We can see that the characteristics of time-dependence greatly affect the absolute value of FV. More importantly, the relative rankings of them also change with time. Note that in Config.1, $FV_{P2}(t) = FV_{P3}(t)$,$FV_{V2}(t) = FV_{V3}(t)$.

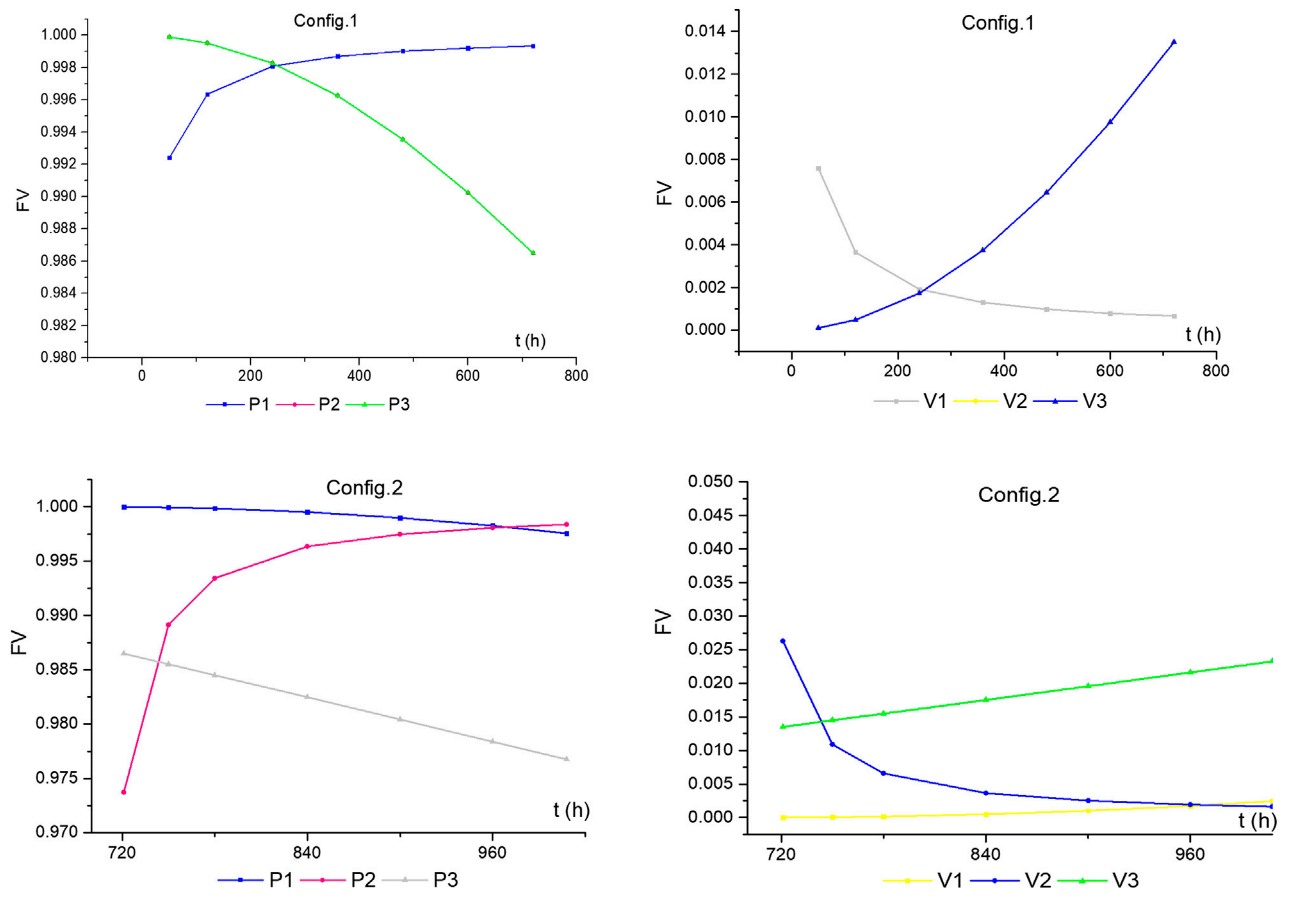

FIGURE 6 | FV importance of component (Config.1 and 2).

For the RRW calculation, since the components in the same pump train are in series, the RRW values of these unavailable components are equal. For instance, RRW(P_3) = RRW(V_3)≈1 for the Config.3.

Common Cause Failure Treatment Options Imposed on Risk Achievement Worth

Example 1 (Weibull distribution) is used in this section for the validation of CCF treatment options. The BE P_1-FO, P_2-FO, and P_3-FO make up a CCCG (CCCG3_FO). The size of CCCG $n = 3$ with common cause factors $l = 2$. **Table 1B** gives the parameters of CCCG at several different time points. The total failure probability $Q_t^{(n)}$ corresponds to the time-dependent probabilistic model of BE in **Table A2** of Appendix B.

Note that the CCF model and parameters in the current PRA model are based on statistical failure data and symmetrical assumptions. But in the RORM model, the failure probabilities of three components in the CCCG would be asymmetrical due to different state duration. In this case, to simplify CCF consideration, $Q_t^{(3)}$ is assumed to be the biggest value of the three conservatively.

$$Q_t^{(3)}(t) = \max\{Q_{\mathrm{P1-FO}}(\mathrm{t}), Q_{\mathrm{P2-FO}}(\mathrm{t}), Q_{\mathrm{P3-FO}}(\mathrm{t})\} \tag{35}$$

The coupling mechanism in CCCG might be location-related, operational-related, maintenance-related, and manufacturer-related, etc. The CCF coupling factors $\eta_k^{R_j}$, independent failure probability p_0, and the conditional probability of common cause factor $P(R_j)$ might depend on state duration. In this case, $\eta_k^{R_j}$ is assumed to be manufacturer-related, which does not vary with time.

If A, B, and C are BE P_1-FO, P_2-FO, and P_3-FO respectively, the probability of failure event is expressed as

$$Q_1^{(3)} = P(A) = P(B) = P(C) = (p_0)(1-p_0)^2 + \sum_{j=1}^{2}\eta_1^{R_j}P(R_j) \tag{36}$$

$$Q_2^{(3)} = P(AB) = P(AC) = P(BC) = P(BD) = P(CD)$$
$$= (p_0)^2(1-p_0) + \sum_{j=1}^{2}\eta_2^{R_j}P(R_j) \tag{37}$$

$$Q_3^{(3)} = P(ABC) = (p_0)^3 + \sum_{j=1}^{2}\eta_3^{R_j}P(R_j) \tag{38}$$

TABLE 1B | Parameters of CCCG (P_1-FO,P_2-FO,P_3-FO).

t/h	0	120	240	360	480	600	720
$Q_t^{(3)}$	4.096e-9	2.748e-6	1.901E-5	6.107e-5	1.412e-4	2.717e-4	4.649e-4
P_0	1.451e-9	2.722e-6	1.897E-5	6.102e-5	1.411e-4	2.716e-4	4.647e-4
$P(R_1)$	8.000e-5	4.000e-4	6.000E-4	8.000e-4	1.200e-3	1.600e-3	2.000e-3
$P(R_2)$	2.000e-5	1.000e-4	1.500E-4	2.000e-4	3.000e-4	4.000e-4	5.000e-4
$\eta_1^{R_1}$	5.000e-5	5.000e-5	5.000e-5	5.000e-5	5.000e-5	5.000e-5	5.000e-5
$\eta_2^{R_1}$	4.500e-6	4.500e-6	4.500e-6	4.500e-6	4.500e-6	4.500e-6	4.500e-6
$\eta_3^{R_1}$	2.500e-6	2.500e-6	2.500e-6	2.500e-6	2.500e-6	2.500e-6	2.500e-6
$\eta_1^{R_2}$	1.200e-5	1.200e-5	1.200e-5	1.200e-5	1.200e-5	1.200e-5	1.200e-5
$\eta_2^{R_2}$	2.500e-6	2.500e-6	2.500e-6	2.500e-6	2.500e-6	2.500e-6	2.500e-6
$\eta_3^{R_2}$	1.500e-6	1.500e-6	1.500e-6	1.500e-6	1.500e-6	1.500e-6	1.500e-6

$$Q_t^{(3)} = Q_t(A) = Q_t(B) = Q_t(C) = Q_1^{(3)} + 2Q_2^{(3)} + Q_3^{(3)} \quad (39)$$

where $Q_t^{(3)}$ is the total failure probability, $Q_i^{(3)}\,(i = 1, 2, 3)$ indicates the probability of the failure event of specific component(s) due to either independent failure factors or common cause factors.

The results of three CCF treatment options are shown in **Table 2** if one of components in CCCG is unavailable ($i = 1$) at t = 120 h. As for the updated probabilities of CCF events in CCCG, Option 2 and Option 3 are greatly larger than those of Option 1, because the conditional probability of a CCF event would rise due to the occurrence of a common cause factor. So it is proven that the engineering practice of Option 1 is not conservative.

In RORMT, the numerator of the RAW importance of a component is mainly influenced by what if treatment considering CCF. That is different from other risk monitors. The results of different methods are compared in **Tables 3A–C** at different time points. Here NUREG/CR-5485 refers to Appendix E3.1 without approximation in this report. RASP refers to the CCF treatment case 1 (when observed failure with the loss of function of one component in the CCCG). By comparing the results in **Tables 3A–C**, it can be seen that:

(1) For components out of CCCG, RAWs of all methods are almost the same. But for a component in the CCCG, RAW importance values of different methods vary greatly. The direct method only treats with the failure mode events of the component, whose result is not accurate as discussed in *PRA Importance Measures and Challenges of Real-Time Online Risk Monitoring and Management Technology*. The other methods consider both CCF events and failure mode events.

(2) If a basic event of a component is within a CCCG, such as P1-FO, P2-FO, and P3-FO, the RAW values of that component calculated by the BM and the NUREG/CR-5485 method, are at least two orders of magnitude higher than the other methods. The RAW result obtained by NUREG/CR-5485 is very large, because it does not distinguish the failure cause of the component. The probabilities of all CCF events in CCCG are divided by the total failure probability of the component. And the basic event probability (such as P2-FB) is set to 1. Thus, the components within CCCG are always at the top of the RAW ranking list. However, these results may mislead the operator actions.

(3) Since the CCF treatment of the RASP method and Option 1 are similar, the RAW results of the two methods are quite similar. They both set the failure mode basic event of that component to TRUE and adjust the CCF event probability. The difference is that RASP updates the CCF parameters based on the reduced size of the CCCG, while Option 1 updates the CCF event probability by grouping the time-dependent events into a new CCCG.

(4) For Option 2, the conditional probability of CCF events given a specified common cause factor contributes to the high RAW value. Option 3 in the hybrid method results in the expected value of Option 1 and Option 2. Besides, it is difficult to identify the real cause of failure (independent cause or common cause) as soon as failure happens. It requires more maintenance and inspection work to detect the failure cause. Thus, Option 3 makes sense for online applications of RORMT.

(5) Comparing the results at different times in Config.1, it is found that the absolute values and ranking order of component RAW would change with time for a certain configuration.

TIME-DEPENDENT IMPORTANCE MEASURE FOR RISK-INFORMED DECISION MAKING

Based on the current plant configuration, the time-dependent IMs of RORM would provide risk insights in the following three groups of activities: 1) ranking SSC activities and human actions for prioritizing maintenance or tests and 2) exempting or limiting

TABLE 2 | Results of three CCF treatment options if a component is unavailable ($i = 1$, $t = 120$ h).

	Option 1 Independent factor	Option 2 Common cause factor		Option 3 Unconfirmed cause
		R_1	R_2	
$Q_1^{(2)}$	2.745e-6	5.722e-5	1.724e-5	3.149e-6
$Q_2^{(2)}$	3.207e-9	7.000e-6	4.003e-6	5.597e-8
$Q_t(2)$	2.748e-6	6.422e-5	2.125e-5	3.205e-6

TABLE 3A | RAW importance results of different methods (t = 120 h).

RAW	Direct Method	Balancing method	NUREG/CR-5485	RASP	Hybrid method (What if treatment of unavailability)			
					Option 1	Option 2		Option 3
						R1	R2	
P_1	3.28	42,092.05	363,846.43	3.88	3.28	6,092.08	3,481.66	49.12
P_2	6.54	42,092.05	363,836.01	3.44	2.85	6,090.65	3,480.96	48.74
P_3	6.54	42,092.05	363,836.01	3.44	2.85	6,090.65	3,480.96	48.74
V_1	3.28	3.28	3.28	3.28	3.28	3.28	3.28	3.28
V_2	2.85	2.85	2.85	2.85	2.85	2.85	2.85	2.85
V_3	2.85	2.85	2.85	2.85	2.85	2.85	2.85	2.85

TABLE 3B | RAW importance results of different methods (t = 360 h).

RAW	DirectMethod	Balancing method	NUREG/CR-5485	RASP	Hybrid method(What if treatment of unavailability)			
					Option 1	Option 2		Option 3
						R1	R2	
P_1	7.34	12,154.05	16,373.68	7.32	7.34	3,050.38	1745.43	8.85
P_2	17.75	12,154.05	16,382.91	6.56	6.58	3,049.13	1744.54	8.64
P_3	17.75	12,154.05	16,382.91	6.56	6.58	3,049.13	1744.54	8.64
V_1	7.34	7.34	7.34	7.34	7.34	7.34	7.34	7.34
V_2	6.58	6.58	6.58	6.58	6.58	6.58	6.58	6.58
V_3	6.58	6.58	6.58	6.58	6.58	6.58	6.58	6.58

TABLE 3C | RAW importance results of different methods (t = 720 h).

RAW	DirectMethod	Balancing method	NUREG/CR-5485	RASP	Hybrid method(What if treatment of unavailability)			
					Option 1	Option 2		Option 3
						R1	R2	
P_1	74.71	2051.56	2,151.07	73.91	74.71	1,194.93	712.99	73.41
P_2	216.96	2051.57	2,291.58	72.17	72.96	1,193.00	711.19	73.21
P_3	216.96	2051.57	2,291.58	72.17	72.96	1,193.00	711.19	73.21
V_1	74.74	74.74	74.74	74.74	74.74	74.74	74.74	74.74
V_2	73.00	73.00	73.00	73.00	73.00	73.00	73.00	73.00
V_3	73.00	73.00	73.00	73.00	73.00	73.00	73.00	73.00

temporary configurations beyond limiting conditions for operation (LCOs) of technical specification (TS) with allowed configuration times.

Time-Dependent Criteria of Systems, Structures, and Components Importance

The current risk-informed SSC categorization method for NPP was proposed in 10CFR 50.69 (NRC, 2004). The screening criteria of risk significant SSCs are FV and RAW importance of components based on the average PRA model of NPP. The average PRA model is established in a predefined condition which usually assumes all equipment is in an available state.

However, the 10CFR 50.69 method is offline and static, and not appropriate for SSC importance evaluation in the RORM model. First, the 10CFR50.69 method would not support when some SSCs are out of service. Second, the risk IMs, and risk significance in RORM are strongly dependent on the scenario conditions of NPP, real-time operational state, and state duration of a component. The same equipment will have different importance values under different plant configurations.

To better utilize the ranking order of IMs for online operation, we derive a type of time-dependent criteria of SSC importance from the operational safety criteria (OSC) of NPP. The classification of the instantaneous risk adopted by OSC is usually three-zone or four-zone. Take the three zones (unacceptable risk, high risk, and low risk) of CDF for example. The risk thresholds of CDF are predetermined by a nuclear safety supervisory authority, i.e., threshold between low and high risk ($\overline{CDF_1}$), between high and unacceptable risk ($\overline{CDF_2}$). Here $\overline{CDF_1}$ is set to be several times the baseline risk CDF_0. NUMARC93-01 (NEI, 2011) recommends that the lower limit of unacceptable risk $\overline{CDF_2}$ = 1.0e-3/yr.

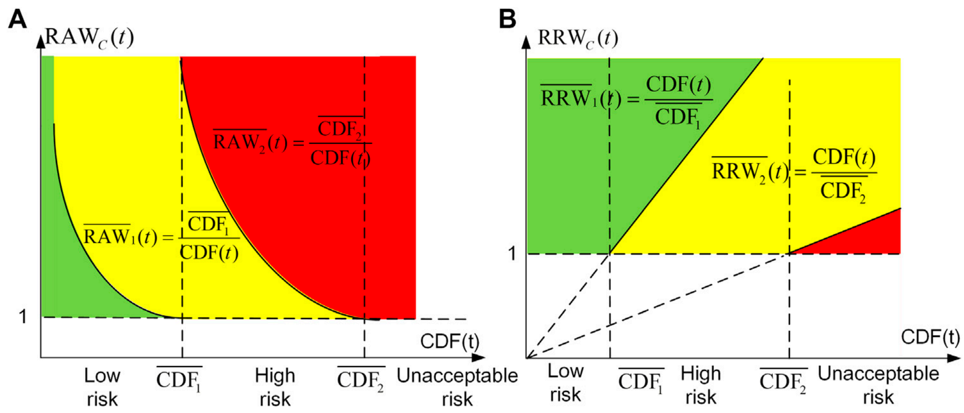

FIGURE 7 | Time-dependent criteria of SSC importance. **(A)** RAW. **(B)** RRW

TABLE 4A | Implications and actions of time-dependent criteria of $\mathrm{RAW}_C(t)$

CDF(t)	RAW_C (t)		Implications and actions
$\mathrm{CDF}(t) < \overline{\mathrm{CDF}_1}$	$\mathrm{RAW}_C(t) < \overline{\mathrm{RAW}_1}(t)$	G	Normal operation under TS. Normal maintenance work of C
	$\mathrm{RAW}_C(t) > \overline{\mathrm{RAW}_1}(t)$	Y	Planned testing or maintenance of C is allowed under current
$\mathrm{CDF}(t) < \overline{\mathrm{CDF}_2}$	$\mathrm{RAW}_C(t) < \overline{\mathrm{RAW}_2}(t)$ and $\mathrm{RAW}_C(t) > \overline{\mathrm{RAW}_1}(t)$	Y	configuration. Risk management actions should be prepared
	$\mathrm{RAW}_C(t) > \overline{\mathrm{RAW}_2}(t)$	R	Planned test or maintenance of C is not allowed under current configuration
$\mathrm{CDF}(t) > \overline{\mathrm{CDF}_2}$	– –	R	Risk management actions should be implemented immediately to reduce risk, such as reactor shutdown under control

Range: G—Green; Y—Yellow; and R—Red

TABLE 4B | Implications and actions of time-dependent criteria of $\mathrm{RRW}_C(t)$

CDF(t)	RRW_C (t)		Priority of restoring unavailable C
$\mathrm{CDF}(t) < \overline{\mathrm{CDF}_1}$	$\mathrm{RRW}_C(t) > \overline{\mathrm{RRW}_1}(t)$	G	High
$\mathrm{CDF}(t) > \overline{\mathrm{CDF}_1}$	$\mathrm{RRW}_C(t) > \overline{\mathrm{RRW}_1}(t)$	G	High
	$\mathrm{RRW}_C(t) < \overline{\mathrm{RRW}_1}(t)$ and $\mathrm{RRW}_C(t) > \overline{\mathrm{RRW}_2}(t)$	Y	Medium
	$\mathrm{RRW}_C(t) < \overline{\mathrm{RRW}_2}(t)$	R	Low

Range: G—Green; Y—Yellow; and R—Red

TABLE 5 | Risk-informed insights for online operation and maintenance using relative rankings of IMs.

IM	Item	Risk-informed insights
FV ranking	Available SSCs	Confirm the current availability of SSCs in redundant trains that compensate for the newly failed component(s)
	IE	Prevent certain accidents
	Human action	Avoid the occurrence of human error events before IE.
	MCS	Avoid the failure events of low-order MCSs
	Accident sequence	Avoid accident sequences with high frequency
RAW Ranking	Available SSCs	Priorities of components with greater RAW importance which would participate in near-term planned activities Avoid certain failures of components
RRW Ranking	Unavailable SSCs	Determine near-term real-time priorities for restoration of newly failed components

The threshold of FV, denoted as $\overline{\mathrm{FV}} = C$, is predetermined based on the risk contribution of SSC, such as the top 20 in the FV ranking. The time-dependent thresholds of RAW, and RRW for an SSC are defined in **Eqs. 40**, **41**. They are dependent on plant configuration and state duration. As a result, these importance thresholds should be updated with risk calculation.

$$\overline{\mathrm{RAW}}_{\mathrm{i}}(t) = \overline{\mathrm{CDF}_{\mathrm{i}}} \Big/ \mathrm{CDF}(t), i = 1, 2, .., s - 1 \tag{40}$$

$$\overline{\mathrm{RRW}}_{i}(t) = \mathrm{CDF}(t) \Big/ \overline{\mathrm{CDF}_{i}}, i = 1, 2.., s - 1 \tag{41}$$

where s is the number of risk zones.

Figures 7A indicates the time-dependent criteria of $\mathrm{RAW}_C(t)$ for available SSCs. In this way, the ranking order of RAW is further graded, and it is easy for operators and maintenance personnel to understand and execute risk management actions, as shown in **Table 4A**. No matter what the instantaneous risk level CDF(t) and importance measure $\mathrm{RAW}_C(t)$ is, the out of service time of equipment should be controlled based on cumulative risk ICDP(t) and allowed configuration time (ACT) of the current configuration as introduced in the risk-informed technical specification (RMTS) (NEI, 2006). **Figures 7B** indicates the time-dependent criteria of RRW of SSC. They give the priorities of restoring unavailable SSCs as **Table 4B**.

Risk-Informed Insights for Configuration Risk Management

Although the concepts "risk significance" and "safety significance" are often conflated in risk-informed applications, FV importance is generally regarded as a measure of risk significance, while RAW is that of safety significance (Cheok et al, 1998a; Cheok et al 1998b; NRC, 2019). But they are evaluated based on an average PRA model over different configurations and diverse accident sequences (Vesely, 1998). Youngblood clarified the two concepts and proposed a different measure: the "prevention worth" (Youngblood, 2001) of safety significance. The prevention worth was used in top event prevention analysis (Youngblood and Worrell, 1995; Blanchard et al. 2005).

Online risk evaluation requires quantifying the RORM model given a specific configuration change, or given planned sequential configuration changes. This action is to determine whether planned or temporary plant reconfigurations are sufficiently safe, especially when a planned configuration is overlapped with several unplanned events. In this case, the calculation of risk is mainly affected by time-dependent unavailability and CCF consideration.

Since temporary or emergency events might occur in the real-time configuration, it is necessary to consider the operational configuration changes and provide configuration-specific risk insights by the relative rankings of IMs, such as identifying risk-significant SSC/accident sequences/IEs/human actions. The relative rankings of IMs are utilized as shown in **Table 5**. In addition, other IMs such as Birnbaum importance (Birnbaum, 1969) and critical importance (Lambert, 1975) could also be evaluated based on real-time plant configuration and state duration.

It is worth noting that the uncertainty of relative ranking order of importance (Modarres and Agarwal, 1996; Aven and Nokland, 2010) would be affected by three main factors 1) the distribution of reliability data used, 2) the scope and quality of the RORM model, and 3) the truncation limit of risk calculation.

For maintenance plan scheduling and plan risk assessment, the time-dependent risk measures are also utilized in the real-time online risk monitoring and management method (Xu et al. 2018). If the calculated instantaneous risk or the cumulative risk for a planned sequence of configuration changes is unacceptable, equipment outages should be shortened and re-arranged. Also, the ranking order of IMs of SSCs is used to prepare risk management actions beforehand, so to strictly control the outage duration of equipment maintenance, protecting other risk-significant equipment, and administration control, etc.

CONCLUSION

RORMT is characterized by time-dependent modeling and updating for online risk monitoring of NPP. It is dependent on the real-time plant configuration and state duration of equipment. This paper discussed the risk-informed assessment and application of time-dependent IMs in RORMT. The time-dependent FV, RAW, and RRW defined for individual BE and event groups of a component. They are not only influenced by the time-dependent risk, but also the CCF treatment. Since the RAW of a component is particularly affected by updating the CCF model in the case "what if a component is out of service," three CCF treatment options for component unavailability are assumed: 1) Option 1 - independent cause; 2) Option 2 - common cause factor; 3) Option 3 - unconfirmed cause. The updating of CCF order and CCF event probability are discussed for the three options. Accordingly, a hybrid method for RAW evaluation has been proposed based on the three options. Using the hybrid method not only comprehensively accounts for all possible unavailable causes, but also reduces the conventional misunderstanding of component importance. A simple case study is demonstrated through examples of exponential distribution and Weibull distribution.

From the case study, it is found that since the time-dependent risk of the same configuration would increase with the state duration of the equipment, the absolute values and relative rankings of IMs may vary with time. Thus, if the real-time configuration changes or the state duration of a component increases, it is necessary to re-quantify the time-dependent IMs. Moreover, for the updated probabilities of CCF events in CCCG, the results of Option 2 and Option 3 are much larger than those of Option 1. The hybrid method with Option 3 generates a reasonable value for component RAW, and it is more suitable for RORMT.

The time-dependent IMs considering state duration and CCF would provide novel insights for online configuration risk management: 1) ranking SSCs/events/human actions for controlling the increased risk and optimizing near–term plans and 2) exempting or limiting temporary configurations beyond technical specifications with allowed configuration times. Besides, the time-dependent criteria of SSC IMs are established in this paper to further classify the ranking order of RAW and RRW. For practical engineering applications of the proposed methods, the future research will focus on: 1) verifying the time-dependent LPSA modeling with long-term operating data and 2) further study on the CCF failure mechanism to obtain the critical CCF data.

DATA AVAILABILITY STATEMENT

All datasets presented in this study are included in the article/supplementary material.

AUTHOR CONTRIBUTIONS

ZZ instructed and proposed the methodology of the RORM technology. AX conceptualized and implemented this study, and wrote the original draft. HZ dedicated his time to the development of the IRORM program, and validated the method. HW was the project administrator and provided the required resources. MZ provided the basic information about common cause failure modeling. SC and YM assisted in the conceptualization, investigation, and data curation. XD reviewed and verified the results.

FUNDING

This research is currently funded by the National Key R&D Program of China" titled "Research on Real-time Risk Monitoring, Evaluation and Management Technology of Nuclear Power Plant" (grant no. 2019YFB1900803). Besides, the earlier study was supported by Harbin Engineering University, the National Science and Technology Major Project of China titled "Research on Living PSA and On-line Risk Monitor and Management of Nuclear Power Plant" (grant no. 2014ZX06004-003), and the National High-tech R&D Program of China titled "Research on Online Risk Monitor and Management of Nuclear Power Plant" (grant no. 2012AA050904).

ACKNOWLEDGMENTS

The authors express gratitude to our former teammates, Wang Yan, Deng Yunli, Li Songfa, and Guo Biao. Besides, the whole team would give thanks to the Beijing Appsoft (Shen Zhou Pu Hui) Technology Co., Ltd. and the Shanghai Yaspeed Information Technology Co., Ltd. for their dedication.

REFERENCES

Atwood, C. L., LaChance, J. L., Martz, H. F., Anderson, D. L., Englehardte, M., Whitehead, D., and Wheeler, T. (2003). *Handbook of parameter estimation for probabilistic risk assessment*. Rockville, MD: Nuclear Regulatory Commission, NUREG/CR-6823.

Aven, T., and Nokland, T. E. (2010). On the use of uncertainty importance measures in reliability and risk analysis. *Reliab. Eng. Syst. Safety.*, 95, 127–133. doi:10.1016/j.ress.2009.09.002

Birnbaum, Z. W. (1969). *On the importance of different components in a multi-component system*. New York, US: Academic Press, 581–592.

Blanchard, D., Worrell, R. B., and Varnado, B. (2005). Risk-informed physical security; dynamic allocation of resources. in Proceeding of the ANS International Topical meeting on Probabilistic Safety Analysis (PSA 2005). San Francisco: American Nuclear Society.

Borgonovo, E., Aliee, H., Glaßb, M., and Teich, J. (2016). A new time-independent reliability importance measure. *Eur. J. Oper. Res.* 254, 427–442. doi:10.1016/j.ejor.2016.03.054

Borgonovo, E., and Apostolakis, G. E. (2001). A new Importance measure for risk-informed decision making. *Reliab. Eng. Syst. Safety.* 72, 193–212. doi:10.1016/s0951-8320(00)00108-3

Chen, S. J., Zhang, Z. J., Zhang, H. Z., Zhang, M., Wang, H., Ma, Y. F., et al. (2020). Research on living PSA method based on time-dependent MFT for real-time online risk monitoring. *Ann. Nucl. Energy.* 143, 107406. doi:10.1016/j.anucene.2020.107406

Cheok, M. C., Parry, G. W., and Sherry, R. R. (1998a). Response to 'Supplemental viewpoints on the use of importance measures in risk-informed regulatory applications'. *Reliab. Eng. Syst. Safety.* 60, 261. doi:10.1016/s0951-8320(97)00146-4

Cheok, M. C., Parry, G. W., and Sherry, R. R. (1998b). Use of importance measures in risk-informed regulatory applications. *Reliab. Eng. Syst. Safety.* 60, 213–226. doi:10.1016/s0951-8320(97)00144-0

Dutuit, Y., and Rauzy, A. (2015). On the extension of importance measures to complex components. *Reliab. Eng. Syst. Saf.* 142, 161–168. doi:10.1016/j.ress.2015.04.016

Fussell, J. B. (1975). How to hand-calculate system reliability and safety characteristics. *IEEE T. Reliab.* 24, 169–174. doi:10.1109/tr.1975.5215142

Fussell, J. B., and Vesely, W. E. (1972). A new methodology for obtaining cut sets for fault trees. *Trans. Am. Nucl. Soc.* 15, 262–263.

Gunnar, J., and Jan, H. (Editors) (1994). *Safety evaluation by living probabilistic safety assessment. Procedures and applications for planning of operational activities and analysis of operating experience*. Stockholm, Sweden: Swedish Nuclear Power Inspectorate, SKI Technical Report 94: No. NKS/SIK 1, 16.

Kafka, P. (1997). Living PSA-risk monitoring—current use and developments. *Nucl. Eng. Des.* 175, 197–204. doi:10.1016/s0029-5493(97)00037-x

Kalpesh, P. A., and Kirtee, K. K. (2017). An overview of various importance measures of reliability system. *Inter. J.Math., Eng.Management Sci.* 2, 150–171. doi:10.33889/IJMEMS.2017.2.3-014

Kim, K., Kang, D. I., and Yang, J. E. (2005). On the use of the balancing for calculation component RAW involving CCFs in SSC categorization. *Reliab. Eng. Syst. Safety.* 87, 233–242. doi:10.1016/j.ress.2004.04.017

Kuo, W., and Zhu, X. Y. (2012). *Importance measures in reliability risk and optimization: principles and applications*. New York, U.S.: John Wiley & Sons.

Lambert, H. E. (1975). "Measure of importance of events and cut sets in fault trees," in *Proceedings of conference on reliability and fault tree analysis*. Editors R.E. Barlow, J.B. Fussell, and N. D. Singpurwalla (Philadelphia, PA: Society for Industrial and Applied Mathematics), 77–100.

Ma, Y. F., and Zhang, Z. J. (2015). Development of reliability data analysis system in nuclear power plant. *Int. J. Nucl. Safety and Simul.* 6, 30–36.

Martorell, S., Serrade, V., and Verdu, G. (1996). Safety-related equipment prioritization for reliability centered maintenance purposes based on a plant specific level I PSA. *Reliab. Eng. Syst. Safety.* 27, 35–44. doi:10.1016/0951-8320(95)00122-0

Modarres, M., and Agarwal, M. (1996). "Consideration of probabilistic uncertainty in risk-based importance ranking," in Proceeding of international topical meeting on probabilistic safety assessment. Park City, UT, September 29–3 October, 1996 (La Grange Park, IL: American Nuclear Society).

Mosleh, A ., Rasmuson, D. M., and Marshall, F. M. (1998). *Guidelines on modeling common-cause failures in probabilistic risk assessment*. Washington, DC: Safety Programs Division, Office for Analysis and Evaluation of Operational Data, U.S. Nuclear Regulatory Commission, Vol. 5485.

NEI (2002). *10 CFR 50.69 SSC categorization guideline.* 1 NEI 00-04[Draft-Revision C].

NEI (2003). *10 CFR 50.69 SSC categorization guideline*. NEI 00-04[Draft-Revision D].

NEI (2011). *Industry guideline for monitoring the effectiveness of maintenance at Nuclear power plants*. NUMARC 93-01 Revision 4A.

NEI (2006). Risk-informed technical specifications initiative 4b. Risk-managed technical specifications (RMTS) guidelines. NEI 06-09(Revision 0)-A.

NRC (2004). *Risk-informed categorization and treatment of structures, systems and components for nuclear power reactors*. 10CFR50.69.

NRC (2019). NRC glossary. Available at: https://www.nrc.gov/reading-rm/basic-ref/glossary/full-text.html (Accessed March 11, 2020)

NRC (2001a). *STP nuclear operating company exemption requests: proof-of-concept for risk informed 10 CFR Part 50 Option 2, safety evaluation*. SECY-01-0103.

NRC (2001b). *Official transcript of proceedings of ACRS plant operations and PRA subcommittee.*, South Texas Project Exemption Requests.

NRC (2017). Risk assessment of operational events handbook-volume 1 internal events. *Rev.* 2

NRC (2011). Systems analysis programs for hands-on integrated reliability evaluations (SAPHIRE) version 8. NUREG/CR-7039 Vol.2.

Vaurio, J. K. (2011). Importance measures in risk-informed decision making: ranking, optimisation and configuration control. *Reliab. Eng. Syst. Safety.* 96, 1426–1436. doi:10.1016/j.ress.2011.06.012

Vesely, W. E., Davis, T. C., Denning, R. S., and Saltos, N. (1986). *Measures of risk importance and their applications*. NUREG/CR-3385.

Vesely, W. E. (1998). Supplemental viewpoints on the use of importance measures in risk-informed regulatory applications. *Reliab. Eng. Syst. Safety.* 60, 257–259. doi:10.1016/s0951-8320(97)00145-2

Wang et al. (2008). FDS team. Study on the algorithm of the calculation of the components' importance measures in a risk monitor. *Chinese Journal of Nuclear Science and Engineering.* 28, 61–65. doi:10.3321/j.issn:0258-0918.2008.01.012

Xu, A. Q., Zhang, Z. J., Zhang, H. Z., Zhang, M., Wang, H., Ma, Y. F., Chen, et al. (2018). "Real-time online risk monitoring and management method for maintenance optimization in nuclear power plant," in Proceedings of the 2018 26th international conference on nuclear engineering (ICONE 26). London, UK: American Society of Mechanical Engineers.

Youngblood, R. W. (2001). Risk significance and safety significance. *Reliab. Eng. Syst. Saf.* 73, 121–136. doi:10.1016/s0951-8320(01)00056-4

Youngblood, R. W., and Worrell, R. B. (1995). "Top event prevention in complex systems," in Proceedings of the 1995 joint ASME/JSME pressure vessels and piping conference. *PVP*-Vol. 296, SERA-Vol.3. Honolulu, Hawaii: American Society of Mechanical Engineers.

Zhang, M., Zhang, Z. J., Chen, S. J., and Zhang, H. Z. (2015a). Living PSA modeling and updating for online risk monitoring. *International Journal of Nuclear Safety and Simulation.* 6, 20–29.

Zhang, M., Zhang, Z. J., Mosleh, A., and Chen, S. J. (2017). Common cause failure model updating for risk monitoring in nuclear power plants based on alpha factor model. *J. Risk and Reliability.* 231, 209–220. doi:10.1177/1748006x16689542

Zhang, Z. J., Wang, H., and Li, S. F. (2015b). General design of online risk monitor for Nuclear Power Plant. *Int. J. Nucl. Safety and Simulation.* 6, 13–19.

Zubair, M., and Amjad, Q. M. N. (2016). Calculation and updating of Common Cause Failure unavailability by using alpha factor model. *Ann. Nucl. Energy.* 90, 106–114. doi:10.1016/j.anucene.2015.12.004

Zubair, M., Zhang, Z. J., and Khan, S. (2011). Calculation and updating of reliability parameters in probabilistic safety assessment. *J. Fusion Energ.* 30, 13–15. doi:10.1007/s10894-010-9325-8

Zubair, M., and Zhang, Z. J. (2011). Reliability data update method for emergency diesel generator of Daya Bay Nuclear Power Plant. *Ann. Nucl. Energy.* 38, 2575–2580. doi:10.1016/j.anucene.2011.07.020

Conflict of Interest: Author MZ was employed by China Nuclear Power Engineering Co., LTD.

The remaining authors declare that the research was conducted in the absence of any commercial or financial relationships that could be construed as a potential conflict of interest.

APPENDIX A: THE CONCEPT OF TIME-DEPENDENCE

During the online operation of NPP, the plant configuration changes because of random failures of a component, switching between running and standby trains, environment changes, and other activities such as repair work, periodic testing, inspection, and planned maintenance.

In RORMT, the state of equipment (such as valve open and closed, electric pump operation and standby) is either identified as "known" by the state monitoring and fault diagnostics system timely, or manually set by the operational maintenance personnel (after a possible time delay).

Let the state of a component at time t be $S(t) = \begin{cases} 0, \text{ available state} \\ 1, \text{ unavailable state} \end{cases}$. The state of the equipment is classified and listed in **Table A1**. Following the general practice of NPP, the maintenance/test (MT) and failed (FA) states are considered as "unavailable", and other states are "available". Thus, if $S(t) = 1$, then the unavailability of a component is known to be 1. If$S(t) = 0$, the component will remain in that state until the next time its state changes. The time-dependent unavailability function applied in RORMT would change with the duration of the available state.

The failure of a component in FT is often represented by multiple BE (also called failure events). The failure modes of equipment are defined in different manners among nuclear power units. In order to establish a generalized modeling method and updating rules, the specific failure modes of equipment are roughly grouped into three generalized failure mode categories, i.e., failure on demand (FD), standby failure (SB), and failure during operation (FO), as illustrated in **Table A1**.

To better illustrate time-dependent unavailability in RORMT, the concept of time-dependence is introduced as shown in the timeline plot of **Figure A1**. Here time-dependence refers to the real-time state duration of SSC, which is denoted as T_s.

t: the moment of risk for calculation. For real-time online risk monitoring, t is the current moment.

t_1: the completion moment of the last corrective/preventive maintenance of a component.

t_2: the moment when a particular available state of a component first appeared after t_1. For real-time online risk monitoring, t_2 refers to the real-time state of a component.

t_3: the last moment to confirm that the component is in an available state after t_1. Particularly, for continually monitored components, their states are transferred by sensors or the monitoring unit of the components to RORM at a very high frequency, so t_3 and t can be regarded as the same moment for the calculation, $t_3 \approx t$. For unmonitored components, there is a time delay between t_3 and t, since t_3 is manually recorded by the last periodic test, on-site inspection, etc.

T_A: the period when the availability of the real-time state is not fully confirmed. $T_A = t\text{-}t_3$. For the continually monitored components, $T_A \approx 0$. For other unmonitored components, T_A is not longer than a test/maintenance period.

t_{IE}: assuming moment when IE occurs. $t_{IE} = t$.

T_m: mission time.

T_s: the real-time state duration. It is the cumulative time interval of a specific state during the period from t_1 to t_3. Note that some components may experience multiple state transitions, thus $T_s \le (t_3\text{-}t_2)$.

APPENDIX B: TIME-DEPENDENT UNAVAILABILITY IN RORMT

The assumptions of the RORM model are as follows:

- When a component is in any available state, the real-time state at the current time t is the same as that of t_3. Its unavailability is time-dependent on state duration.

Table A1 | Classification of equipment state and failure events in RORMT.

Available states		Unavailable states	
RN	Operating state	MT	In maintenance/testing
SB	Standby state	FA	Failed state
OP	Valve open state	—	—
CL	Valve closed state	—	—
ON	Switch on state	—	—
OF	Switch off state	—	—
Failure mode (generalized)			
FD	Failure on demand	FO	Failure during operation
FB	Standby failure	—	—

Note:
1). For rotating equipment (such as pumps, fans, and motors, etc.), its state could be RN, SB, MT, or FA. The failure modes FD, FO, and FB are all involved.
2). For switch-type equipment (such as valves, switches, and breakers, etc.), its possible states are OP/ON, CL/OF, MT, or FA. The failure modes related to switching operation belong to FD while other failure modes are grouped into FO.
According to the relationship between failure mode and equipment state, FO is further subdivided into two groups, i.e., certain state-related (CS) and any state-related (AS).
Certain state-related (CS): some failure modes of FO only occur when the component is in a certain available state. For instance, not keeping a position when open, spurious action to close can only occur when an isolation valve is open.
Any state-related (AS): some failure modes of FO may occur in any available state, such as block/rupture/leakage of valve, short circuit of breaker.
For other SSCs (such as water tanks, heat exchangers, etc.), its possible states consist of RN, MT, or FA. All the failure modes are grouped into FO.

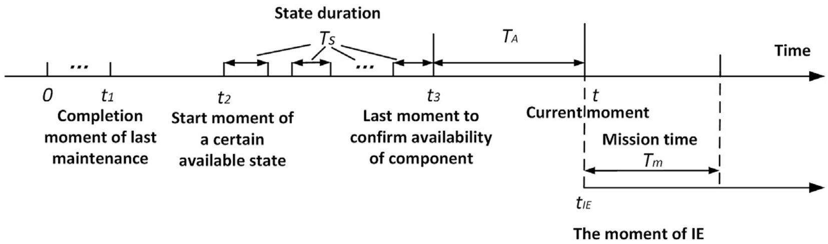

FIGURE A1 | Schematic diagram of time-dependent concept.

- When a component is in any unavailable state, conservatively, its unavailability is assumed to be 1.
- The occurrence time of any IE in the RORM model is assumed at the current moment, $t_{IE} = t$.
- The failure events of a component in a certain state are mutually independent. The failure events of the same component in different operating states are also independent.
- For the online repairable equipment, the completion of repair and recovery operation can be immediately reported. For the equipment which cannot be repaired online, it must be repaired during the refueling overhaul.
- No maintenance will be continued or carried out after IE.
- If the unavailable equipment has not been recovered and is not in service at the current moment, then it cannot be used for accident mitigation after IE occurs.
- The component/system can be considered "as good as new" after the completion of maintenance or testing. To put it simply, the reliability of equipment is 1.
- The state duration T_s is updated depending on its previous operating history.

The time-dependent probability of a basic event of a component at the current moment $Q(t)$is determined by its failure modes, real-time state, and state duration of the component, as summarized in **Table A2**. Specifically, $Q(t) = Q\{\mathrm{t} + \mathrm{T_m} | \mathrm{S}(\mathrm{t_3}) = 0\}$ means the estimated conditional failure probability of equipment during the future period$[T_s, (T_s + T_A + T_m)]$, if the last moment to confirm its available state is time point t_3 and the equipment has been available for a period of time T_s.

TABLE A2 | Time-dependent probability of failure events in the RORM model.

Failure events Component state	Failure on demand (FD) event Standby failure (FB) event	Failure during operation (FO) event	Maintenance/test (UT) event	
Operating state (OP)	Set FD to be false Set FB to be false (a-1)	$Q_{FO,OP}(t) = Q_{FO,OP}(t+T_m \mid S(t_3)=0) = \int_0^{T_m} f_{FO}(u+T_{RN})du = 1-\exp(-\int_{T_{RN}}^{T_{RN}+T_A+T_m} \lambda_R(u)du)$ (a-2)	Set UT to be false (a-5)	
Standby state(SB)	$Q_{FD,SB}(t) = q(t) = Q_0^{SB}$ $Q_{FB,SB}(t) = Q_{SB}(t+T_m \mid S(t_3)=0) = \int_0^{T_A+T_m} f_{SB}(s+T_{SB})ds = 1-\exp(-\int_{T_{SB}}^{T_{SB}+T_A+T_m} \lambda_S(u)du)$ (a-3)	$Q_{FO,SB}(t) = Q_{FO,SB}(t+T_m \mid S(t_3)=0) = \int_0^{T_m} f_{FO}(u)du = 1-\exp(-\int_0^{T_m} \lambda_R(u)du)$ (a-4)		
Open (OP)/Switch Off (OF) state. Closed (CL)/Switch on (ON) state	$Q_{FD,OP/OF/CL/ON}(t) = q(t) = Q_0^{OP/OF/CL/ON}$ (a-6)	$Q^{CS}_{FO,OP/OF/CL/ON}(t) = Q^{CS}_{FO}(t+T_m \mid S(t_3)=0) = 1-\exp(-\int_{(T_{OP}\text{ or }T_{CL})}^{(T_{OP}\text{ or }T_{CL})+T_A+T_m} \lambda_{CS}(u)du)$ (a-7) $Q^{AS}_{FO,OP/OF/CL/ON}(t) = Q^{AS}_{FO}(t+T_m \mid S(t_3)=0) = 1-\exp(-\int_{T_{OP}+T_{CL}}^{(T_{OP}+T_{CL})+T_A+T_m} \lambda_{AS}(u)du)$ (a-8)	Set UT to be false (a-9)	—
In maintenance/Test (MT) state	Set FD to be false (a-10)	Set T_s of any available state of this component to be 0 Set FO to be false (a-11)	Set UT to be true (a-12)	—
Failed state (FA)	Set FD to be true (a-13)	Set FO to be true (a-14)	Set UT to be false (a-15)	—

Note:

$\lambda_R(t)$: running failure rate. $\lambda_S(t)$: standby failure rate. For cold standby components, $\lambda_S(t) \equiv 0$. For hot standby components, $\lambda_S(t) \neq 0$.

$\lambda_{CS}(t)$: failure rate of CS events for valves, switches, etc. $\lambda_{AS}(t)$: failure rate of AS events for valves or switches, etc.

$f(t) = \lambda(t)\exp(-\int_0^t \lambda(u)du)$: probability density function for failure.

Q_0: the demand failure probability of switching from a standby to operating state, or switching between an open and closed state, such as refusing to open/close, stuck in position. It is considered as a constant.

frontiers in Energy Research

ORIGINAL RESEARCH
published: 29 January 2021
doi: 10.3389/fenrg.2021.636813

Study on Measure Approach of Void Fraction in Narrow Channel Based on Fully Convolutional Neural Network

*Wenjun Chu, Yang Liu, Liqiang Pan, Hongye Zhu and Xingtuan Yang**

Institute of Nuclear and New Energy Technology, Collaborative Innovation Center of Advanced Nuclear Energy Technology, Key Laboratory of Advanced Nuclear Reactor Engineering and Safety of Ministry of Education, Tsinghua University, Beijing, China

Void fraction is one of the key parameters for gas-liquid study and detection of nuclear power system state. Based on fully convolutional neural network (FCN) and high-speed photography, an indirect void fraction measure approach for flow boiling condition in narrow channels is developed in this paper. Deep learning technique is applied to extract image features and can better realize the identification of gas and liquid phase in channels of complicated flow pattern and high void fraction, and can obtain the instantaneous value of void fraction for analyzing and monitoring. This paper verified the FCN method with visual boiling experiment data. Compared with the time-averaged experimental results calculated by the energy conservation method and the empirical formula, the relative deviations are within 11%, which verifies the reliability of this method. Moreover, the recognition results show that the FCN method has promising improvement in the scope of application compared with the traditional morphological method, and meanwhile saves the design cost. In the future, it can be applied to void fraction measurement and flow state monitoring of narrow channels under complex working conditions.

Keywords: boiling two-phase flow, narrow channel, void fraction measurement, deep learning, convolutional neural network

OPEN ACCESS

Edited by:
Xingang Zhao,
Massachusetts Institute of Technology, United States

Reviewed by:
Guanyi Wang,
Argonne National Laboratory (DOE), United States
Sichao Tan,
Harbin Engineering University, China

****Correspondence:***
Xingtuan Yang
yangxt@tsinghua.edu.cn

Specialty section:
This article was submitted to Nuclear Energy, a section of the journal Frontiers in Energy Research

Received: *02 December 2020*
Accepted: *04 January 2021*
Published: *29 January 2021*

Citation:
Chu W, Liu Y, Pan L, Zhu H and Yang X (2021) Study on Measure Approach of Void Fraction in Narrow Channel Based on Fully Convolutional Neural Network. Front. Energy Res. 9:636813. doi: 10.3389/fenrg.2021.636813

INTRODUCTION

Gas-liquid two-phase flow reserves value for the research in fields of nuclear energy, petrochemical industry, erospace and various industrial applications (Triplett et al., 1999). In the two-phase flow study and engineering application, the cross sectional void fraction (or frequently abbreviated to void fraction) which functions as one of the key parameters, has important significance for determining the flow pattern, calculating the two-phase pressure drop and analyzing heat transfer characteristics (Winkler et al., 2012). For conventional pipeline conditions, some common methods in experiments include quick-closing valves (Srisomba et al., 2014), X-ray/γ-ray absorption (Zhao Y et al., 2016; Jahangir et al., 2019), differential pressure (Jia et al., 2015) and capacitive method (Jaworek et al., 2014). However, the data obtained by these common methods are mostly single-point values or time-averaged results, and the instantaneous void fraction distribution of the full flow region can hardly be obtained (Hong et al., 2011).

In recent years, an increasing number of mini-channel systems are applied for industrial systems such as nuclear power plant heat exchangers and refrigerators due to large surface area/volume ratio and high transfer efficiency of heat and mass (Kawahara et al., 2002). The narrow rectangular channel is an important structure of these systems. The flow boiling phenomenon tends to be more complicated in narrow channels than in normal pipelines, and direct measurement of void fraction is limited because of the geometry size of the flow channel. Therefore, non-contact measurement like high-speed photography can be applied and combined with digital technology. Compared with other methods, the high-speed photography method can observe the detailed behavior of bubbles without disturbing the flow, and also be able to process multiple images and extract the instantaneous void fraction information in a short time (Fu and Liu, 2016; Zahid et al., 2020).

Many image-processing algorithms for flow field photography have been proposed to figure out the characteristics of the gas-liquid interface and obtain the two-phase distribution. Some examples include edge detection, region filling and morphological operation. Bröder and Sommerfeld (2007) use an edge detecting Sobel filter and spline interpolation technique to determine the contour of in-focus bubbles in rectangular channels, and the bubble velocity is obtained by applying particle tracking velocimetry (PTV). Lau et al. (2013) handle the overlapping/clustering bubbles in bubbly flow with large void fractions by the watershedding algorithm, and segment the groups into individual bubble areas for analyzing. Karn et al. (2015) introduce a multi-level image analysis approach for highly turbulent bubbly flows, which uses H-Minima transform to binarize the image and successfully extract the bubble information by morphological operations. Pan et al. (2018) propose the two-step morphological method and the combined use of morphological opening and closing operations solves the problem of bubble boundary recognition, which improves the accuracy of void fraction measurement. However, these traditional algorithms depend on the extraction process and features designed by manual experience, which have certain influence on the recognition rate and accuracy of the void fraction. In addition, existing research mainly focuses on unheated test sections, while in actual boiling conditions bubbles grow and polymerize fiercely in the flow channel, therefore the gas-liquid interface tends to be hardly recognized. At the same time, in operating conditions with high heating power, the void fraction increases and the phase distribution changes drastically, which brings difficulties for the traditional image processing methods based on edge detection and mathematical morphology to achieve expected results.

The Convolutional Neural Network (CNN) algorithm is based on data extraction and supervised learning. Compared to traditional image recognition algorithms using artificially designed features, the multi-layer network structure of CNN can automatically extract different levels of features from massive training data, which avoiding errors caused by subjectivity and improving classification accuracy. In 2015, Jonathan Long et al. proposed a new structure of CNN—Fully Convolutional Network (FCN) (Long et al., 2015) applied for image segmentation. FCN model changes the last layer of the original CNN to a convolutional layer and adds upsampling layers to achieve any size of input images and classify the image pixel by pixel. In addition, FCN utilizes a variety of mature network structures which have been trained well in huge data set to initialize its network parameters, and reduces its design costs. For the last several years, fully convolutional networks have been widely used in various image segmentation tasks, such as autonomous driving (Wu et al., 2017), medical image (Ronneberger et al., 2015) and remote sensing (Maggiori et al., 2016). In this paper, based on the visualized experiment of two-phase boiling conditions in a narrow rectangular channel, a measurement approach of void fraction in narrow channels is proposed by setting up a fully convolutional neural network to process images of high-speed photography, and the measure results are verified with the experimental data calculated by the energy conservation method.

EXPERIMENTAL DEVICES AND PROCEDURES

In order to study the heat transfer characteristics of two-phase flow in narrow channels and the influence of different parameters on flow stability, the visualized flow boiling experiment system is designed and shown in **Figure 1**. The main part is composed of the test section, main pump, preheater, regulating valve, gas-water separator, flowmeter, etc. The experimental medium is purified deionized water. After preheating, the deionized water flows out of the main pump and is heated by the preheater to reach a preset degree of subcooling. Then it passes into the vertical test section and bypass to start boiling. The upwards two-phase mixture goes through the steam-water separator and returns to the main pump which forms a closed loop. ADMAG AXF electromagnetic flowmeters are adopted for flow measurement and the measuring error is ±0.4%. The temperature measuring applies T-type thermocouples with class I accuracy of ±0.5°C. The test data is collected by NI PXI equipment and the sampling frequency is 10 Hz. The range of critical parameters in the experiments is listed in **Table 1**.

The schematic diagram of the test section is shown in **Figure 2**. The narrow channel with a rectangular cross-section is composed of two pieces of glass. The cross-sectional size is 30×1.5 mm, and the length of the rectangular flow channel is 650 mm. A transparent heating film is evenly coated on the outside of each glass and the heating length is 550 mm. The test section is insulated by a transparent plexiglass barrel arranged outside, and the low-pressure nitrogen is filled into the gap between the barrel and the test section before power on. The image acquisition system beside the transparent test section applies an AOS X-MOTION high-speed camera. The photo-frequency is set to 1,000 frames per second. The resolution of the captured image is $1,280 \times 300$.

IMAGE PROCESSING METHOD BASED ON FULLY CONVOLUTIONAL NETWORK

Summary of the Algorithm

Figure 3 presents original experiment image samples of the flow channel in boiling conditions. Its characteristics include: 1) The gas phase occupies a large proportion of the flow channel, and on occasion the bubbles can fill the cross section of the flow channel; 2) The flow pattern is mostly slug flow or churn flow, and the boundary between gas and liquid phase is blurred at high flow

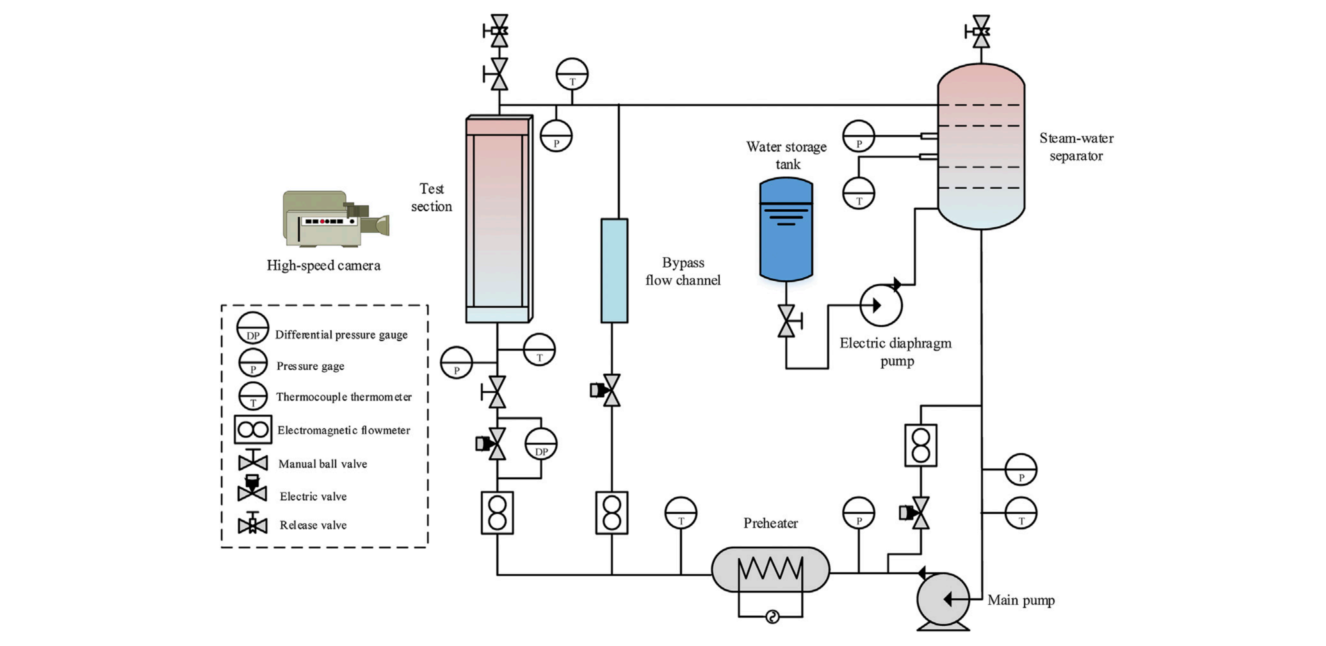

FIGURE 1 | Schematic diagram of the test loop.

TABLE 1 | The range of primary experimental parameters.

Parameters	Units	Experimental range
Inlet subcooling	°C	4–17
Inlet mass flow rate	kg/(s·m^2)	160–432
Heat flux density	kW/m^2	6–18.2
Outlet vapor quantity	%	0–1.8

velocity; 3) The void fraction changes drastically and the sizes of bubbles/slugs in different working conditions and different time are quite different. The above characteristics, which mean the unevenness of the gas phase distribution in space and time, are mainly caused by the narrow channel structure and heating conditions. As a result, it is difficult for most traditional recognition methods based on single scales or features (such as edges, pixel thresholds and morphological structures) to obtain stable and efficient results. In order to solve these problems, this paper proposes a new image segmentation algorithm of FCN method based on deep learning technology. It can extract information from pixel level to abstract semantic concepts through multi-layer convolution operations. It also uses up-sampling layers and multi-scale fusion technology to further optimize the results and achieve higher segmentation accuracy. At the same time, we enhance the adaptability of the FCN algorithm by automatically learning various features from a large amount of data at different times, which makes it suitable for identifying complex gas-liquid images in narrow channels.

In this paper, FCN algorithm is utilized to extract the gas phase part in **Figure 3**, and realize the segmentation of gas and liquid. The flow channel part of the original captured image (the input of the FCN network) can be defined as $\boldsymbol{C}$:

$$\boldsymbol{C}_{\boldsymbol{W}\times\boldsymbol{H}} = \{\boldsymbol{C}^{(1)}, \boldsymbol{C}^{(2)}, \boldsymbol{C}^{(3)}, \cdots, \boldsymbol{C}^{(i)}\}, \boldsymbol{i} = \boldsymbol{K} \tag{1}$$

Where $\boldsymbol{K}$ is the number of the experimental image set, and $\boldsymbol{C}^{(i)}$ is the $\boldsymbol{i}^{\boldsymbol{th}}$ single-frame image (RGB) of size $\boldsymbol{W}\times\boldsymbol{H}$. The output pixel-level segmentation results are defined as $\boldsymbol{G}$:

$$\boldsymbol{G}_{\boldsymbol{W}\times\boldsymbol{H}} = \{\boldsymbol{G}^{(1)}, \boldsymbol{G}^{(2)}, \boldsymbol{G}^{(3)}, \ldots, \boldsymbol{G}^{(i)}\}, \boldsymbol{i} = \boldsymbol{K} \tag{2}$$

The output of the FCN are binary images of the same size $\boldsymbol{W}\times\boldsymbol{H}$, in which pixels value of one mean to gas phase and value of 0 mean to liquid phase. Then the results are applied for calculating the void fraction of the narrow channel. The flowchart of the image-processing algorithm is shown in **Figure 4**.

TABLE 2 | Typical experiment conditions.

Condition number	Flow rate [L·h-1]	Heat flux [kW·m-2]	Inlet subcooling [°C]	Inlet resistance [kPa]
1	52.78	18.33	7	2.5
2	56.24	15.03	6.2	14.9
3	56.24	15.09	5	18.4

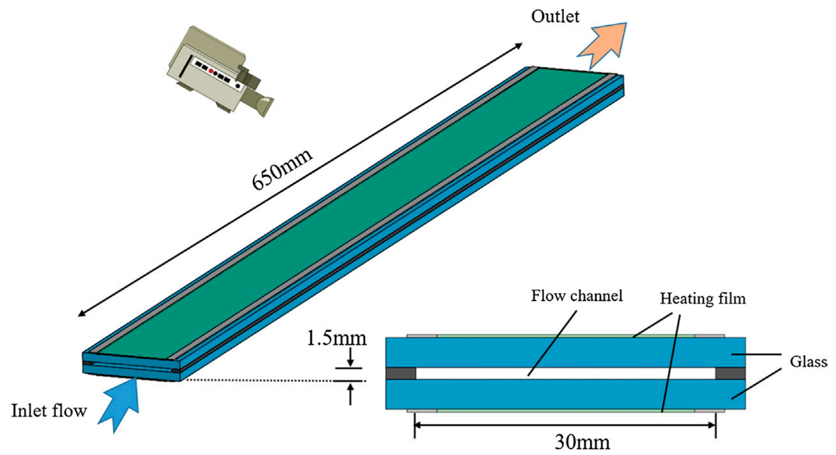

FIGURE 2 | Schematic diagram of the test section.

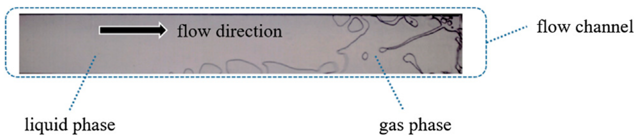

FIGURE 3 | Samples of original high-speed photography images.

Methods of the Fully Convolutional Network Model

Figure 5 is an overall schematic diagram of the structure of FCN model established in this paper. As shown in the figure, the FCN model is mainly composed of two parts. The left part in the box is called convolution (downsampling) part, which is mainly composed of convolutional layers and pooling layers to extract various features of the input image. The right box is called deconvolution (upsampling) part, which is mainly composed of deconvolution layers and a classification layer. It is used to restore the original image size from the high-dimensional feature map and identify each pixel. The methods used in these two parts are introduced below.

Convolution (Downsampling) Part

This paper applies VGG-Net 16 (Simonyan and Zisserman, 2014) as the basic neural network for extracting features, and sets up a new model on this basis to save training and calculation costs. The first half of the established FCN model retains the structure and initial parameters of the original VGG network before the fully connected (fc) layer. Five groups of 13 convolutional layers of increasing size is applied to extract different scales of the features by training 3 × 3 convolution kernels and performing convolution operations:

$$\boldsymbol{c}(\boldsymbol{i},\boldsymbol{j}) = (\mathrm{X} \cdot \mathrm{W})_{(i,j)} = \sum_{\boldsymbol{m}}\sum_{\boldsymbol{n}} \boldsymbol{x}(\boldsymbol{i}+\boldsymbol{m},\boldsymbol{j}+\boldsymbol{n})\boldsymbol{w}(\boldsymbol{m},\boldsymbol{n}) \tag{3}$$

Among them, $\boldsymbol{X}$ represents the input image transferred into two-dimensional matrix, $\boldsymbol{W}$ represents the convolution kernel, which

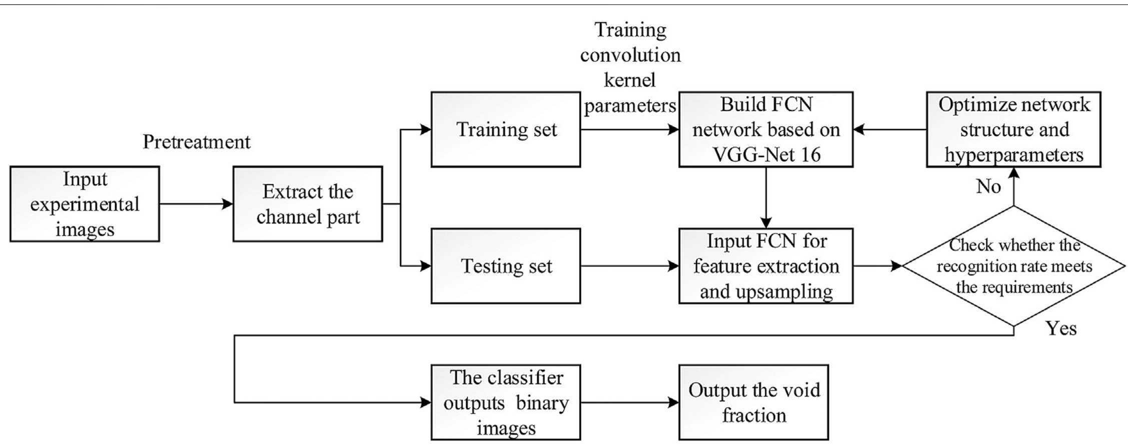

FIGURE 4 | Flowchart of the image-processing algorithm.

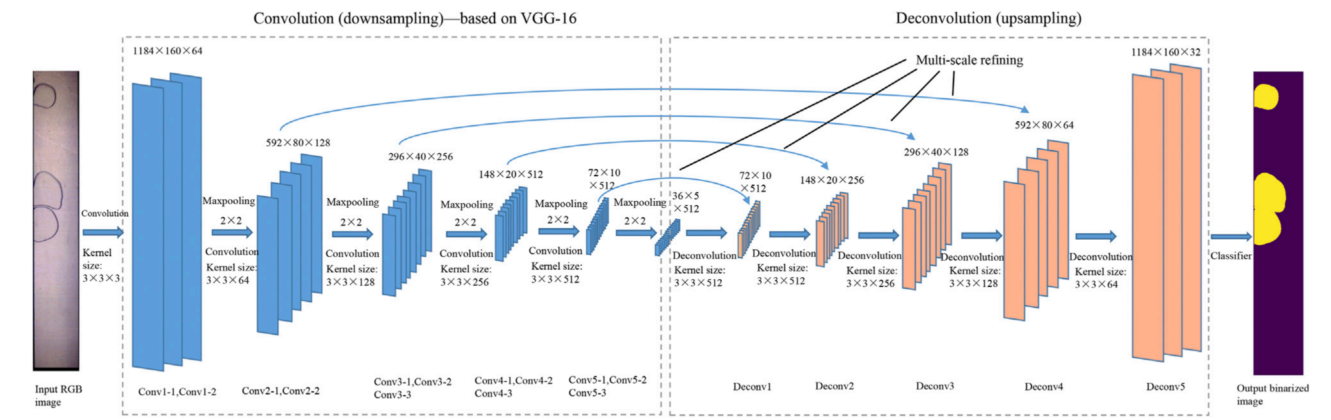

FIGURE 5 | Schematic diagram of the network structure in this paper.

is the core parameter of the training and learning of the convolution network; $c(i,j)$ is the output of the convolution operation at the position (i,j) of the image matrix, also known as feature mapping. m, n are sizes of the convolution kernel and in this paper $m = n = 3$. After extracting features through each convolutional layer, a non-linear output is achieved via a layer of RELU activation function.

VGG-Net 16 has a large number of convolutional kernels, and after the convolution operation the output data is large and the dimensionality is high. Therefore, a pooling layer (downsampling) is added after each group of convolution-activation layers to compress the image and reduce the difficulty of the subsequent calculation. Pooling layer can also extract the spatial details of the features to realize the spatial invariance (such as translation and rotation) and stability of image recognition. In this work, 2 × 2 maximum pooling layers are applied as:

$$f(i,j) = max\begin{pmatrix} c_{2i-1,2j-1} & c_{2i-1,2j} \\ c_{2i,2j-1} & c_{2i,2j} \end{pmatrix} \tag{4}$$

Where $f(i,j)$ is the output of the pooling operation at the position (i,j) of the image matrix, and c is the output matrix of the convolution-activation layer.

Deconvolution (Upsampling) Part

Due to pooling operations, the output image matrix (high-dimensional feature map) sampled by the convolution network is 1/32 of the original image size. To resize the classification results to the original, the three fully connected layers of VGG-Net are removed and five upsampling (deconvolution) layers are added after the convolution layers. Upsampling is the transpose of convolving and the specific process of upsampling in the model is shown in **Figure 6** and compared with convolution and pooling. The output size can be calculated by the formula:

$$O_{out} = (O_{in} - 1) \times s - 2p + k + O_p \tag{5}$$

where O_{out} and O_{in} are the size of input and output, s is the moving step size (stride) of the convolution kernel, p is the padding size of filling the surroundings while convolving, k is the size of the convolution kernel and O_p is the number of edge expansion rows for upsampling result to adjust its size.

The result of upsampling directly from the high-dimensional feature map to the original image size only contains the overall information and reveals too rough. Therefore, this paper also utilizes a multi-scale refining structure (Cen and Jung, 2018) commonly used in existing research, which is to add the output of the first 4 pooling layers to the upsampling layers in sequence in order to integrate local information with the overall spatial architecture. **Figure 7** shows that by adding the features at different scales from the downsampling layers, the output images tend to have more details and the recognition accuracy is improved.

In practical training, odd-sized images are fairly common. The convolution and pooling operation of odd-sized images in program will round down and the upsampling process cannot guarantee that the final output size is strictly consistent with the original. Most existing research solve this problem by resizing the input image to constant even size or dividing into parts and importing by batches, which may affect the subsequent calculation accuracy of void fraction in this paper. To solve this problem, an additional judging operation for input size is added before each upsampling layer, and padding (edge expansion) operation is added for odd-sized pictures to ensure the invariance of the input size. After upsampling, the classification of the image is completed through the classifier layer.

Network Training Settings

In this paper, the neural network training adopts the traditional back propagation algorithm, and its core idea is to obtain the partial derivative of the loss function of the samples, so as to adjust the weight and bias of the network operation layers (convolutional and upsampling layers in FCN model) along the gradient descent direction to minimize the loss function.

Loss function. Since it is a binary classification problem (gas and water), the cross entropy formula is used for the loss function:

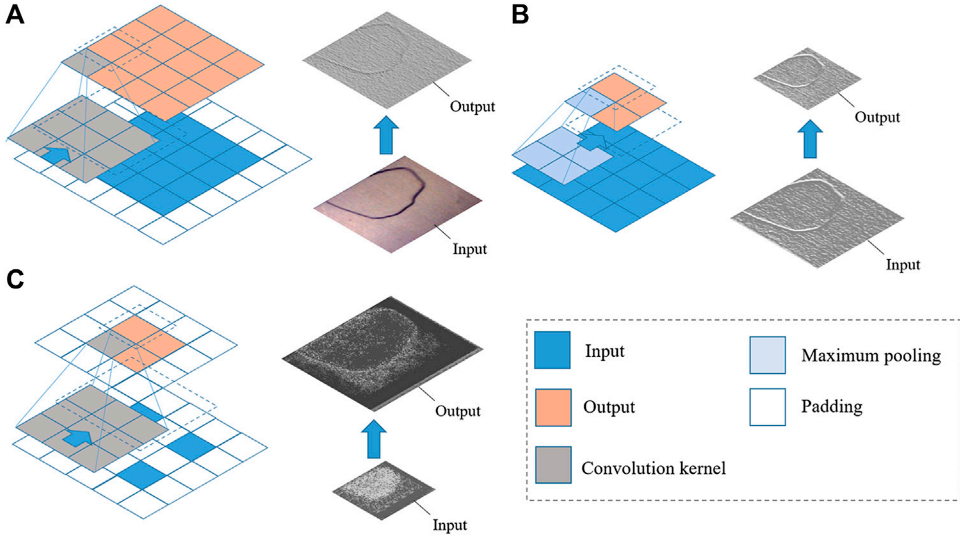

FIGURE 6 | Schematic diagram and visualization samples of three basic operation in FCN network of this paper. **(A)** Convolution. **(B)** Maximum pooling. **(C)** Upsampling (deconvolution).

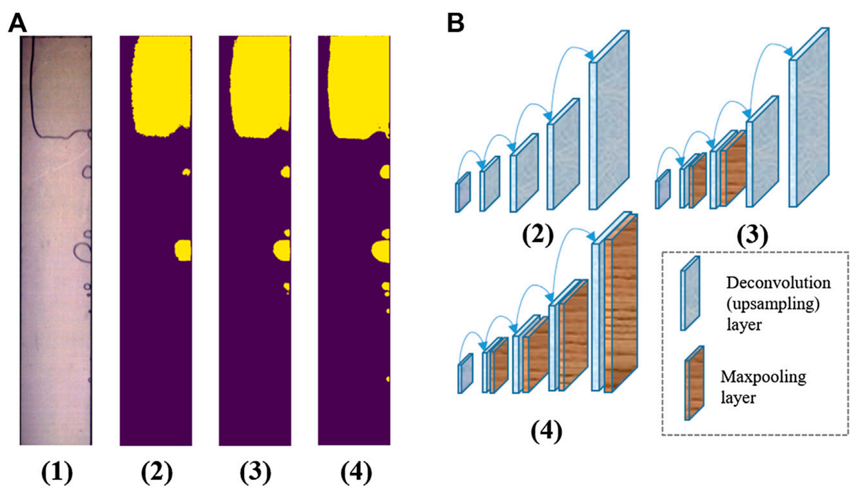

FIGURE 7 | The visualization and comparison of upsampling layers' results after refining of different scales. **(A)** Visualized results: (1)The original input image; (2) upsampling result directly from the high-dimensional feature map; (3) upsampling result adding features of pooling layers 3 and 4; (4) upsampling result adding features of pooling layers 1–4. **(B)** Schematic diagram of multi-scale refining structure. The yellow part in the image represents the recognition result of gas phase.

$$L(R,G) = -\frac{1}{N}\sum_{i=1}^{N}\left[g_i \cdot \log\left(\overline{g_i}\right) + \left(1-g_i\right)\cdot \log\left(1-\overline{g_i}\right)\right] \tag{6}$$

where R and G are respectively the training input samples and labels (ideal segmentation results), N is the total number of input pixels, g_i and $\overline{g_i}$ are the label result values and their occurrence probabilities (calculated by the network layers).

Training optimizer. In training process, the FCN model applies the VGG-16 network pre-training value as the initial value, and optimizing the network by the Stochastic Gradient Descent (SGD) optimizer with momentum. SGD optimizer can quickly find the direction of gradient descent and converge to the global minimum through multiple iterations. Momentum can make convergence faster to avoid staying in the local extreme value area for a long time, and suppress the oscillation to increase the calculation stability. Calculation formula can be written as:

$$v_t = \gamma \cdot v_{t-1} + \nabla f(w_t),\ w_{t+1} = w_t - \alpha v_t \tag{7}$$

where w is the network's weight of layers, $\nabla f(w)$ is the gradient of the loss function, v represents first order momentum, α is the learning rate (lr) which affects the rate of convergence, γ is the momentum factor to control the influence of the momentum which the $t-1$ moment has on t moment.

Performance evaluation. In performance evaluation of the FCN model, we use pixel accuracy (PA) and mean intersection of union (MIoU) of foreground to measure segmentation accuracy. PA means the proportion of correctly marked pixels to total pixels. MIoU calculates the mean ratio of intersection between segmentation result and ground truth mask to the union of them. In the binary classification problem in this article, PA and MIoU can be calculated with the following formula:

$$PA = \frac{G_{1,1}}{G} = \frac{G_{1,1}}{G_{0,0} + G_{0,1} + G_{1,1} + G_{1,0}}$$
$$MIoU = \frac{1}{2}\left(\frac{G_{1,1}}{G_{0,1} + G_{1,1} + G_{1,0}} + \frac{G_{0,0}}{G_{0,1} + G_{0,0} + G_{1,0}}\right) \tag{8}$$

where $G_{i,j}$ means the number of pixels that belong to class i and are predicted to be class j. Class 0 refers to liquid phase (background) and class 1 refers to gas phase. As defined, the values of PA and MIoU are between 0 and 1. The closer the value is up to one means the recognition effect is closer to the ground truth, and the accuracy of the model is higher. **Establishment of training set.** The training set used in the training network mainly adopts the method of Pan et al. (2018), which is based on the traditional image method of two-step morphology to process the experimental images of narrow channels, and then manually selects 1,500 binarized images with clear bubble morphology and high accuracy as training samples. We partition the samples into training set (85%) and test set (15%). Considering the training cost and accuracy, the images are cut and the flow channel part are selected. To avoid overfitting and increase the stability of the model, further strategy like data augmentation is used in the training, images receive both horizontal and vertical flip and added to the training set.

Training environment and configuration. This paper employs the deep learning framework Pytorch for network construction and training. The experimental hardware environment is AMD 4800H CPU, 16 GB memory, NVIDIA RTX2060 graphics card for GPU acceleration.

CALCULATION RESULTS AND VERIFICATION

Experimental Data Set

The data set used in the experiment in this paper comes from the images collected by the visual narrow channel flow boiling experiment system of Tsinghua University. Each working condition point records 13,800 pictures (1,000 frames per second and the acquisition time is 13.8 s). Three typical conditions are chosen and the operating parameters are shown in **Table 2**.

Results and Analysis

Figure 8 shows the train loss of the network and MIoU of the test set under different learning rates and momentum factors. From the picture, we can see the learning rate less affects the training process, while higher momentum can effectively improve computing stability. By comparing the results, we choose learning rate = 0.01 and momentum factor = 0.9. After 33,500 iterations, the train loss basically converges, and the average PA and MIoU of the test set reach 0.991 (99.1%) and 0.982 (98.2%) respectively, which can meet the requirements for convergence speed and training accuracy, and reduce computational oscillation. Then the FCN model established in this paper is applied for the experimental data set and part of the processing results are shown in **Figure 9**, achieving recognition of the gas phase in the image under the conditions of different void fraction and different flow patterns. It can be seen that the method has basically identified the gas phase's morphology, especially in the slug flow (**Figure 9** a1 and a2) and churn flow (**Figure 9** a3 and a4) of high void fraction. This verifies the portability and reliability of this method for different working conditions and flow patterns in boiling experiments.

As shown in **Figure 10**, the method in this paper is compared the traditional edge detection/filling algorithm and the two-step morphological method of Pan et al. (2018). It can be seen that in working condition A of low void fraction, the results of FCN method and the traditional algorithm are not much different, and both can identify bubbles with clear boundaries and regular shapes. The FCN method has a relatively better recognition effect on small bubbles. In working condition B and C where the void fraction is high, the traditional algorithm will overfill the gap between the bubble and the vapor slug, resulting in the unrecognizable gas phase areas and may detect an excessively high void fraction value. The designed morphological method can better extract the characteristics of local irregular bubbles, but it requires manual setting of parameters. When the pixel value of the picture changes greatly and the threshold parameters cannot be matched, a large block of recognition defects may occur like **Figure 10C**. The method in this paper also has some local recognition defects inside and between the bubbles, but it basically realizes the recognition of bubble shape. It also has better applicability for different flow patterns to improve the overall recognition accuracy, and does not require manual adjustment of parameters, which saves design costs.

The void fraction at the outlet of the flow channel is of significance to the calculation of the two-phase model and determining the flow pattern. After the gas-liquid recognition results are obtained by the method in this paper, the numerical matrix $H(i,j)$ (size = $M \times N$) near the outlet is extracted from the output binary image. The following formula is for calculating the void fraction of the outlet in narrow channels:

$$\alpha = \frac{\sum_{i-1}^{M} \sum_{j-1}^{N} H(i,j)}{M \times N} \tag{9}$$

The time-dependent change of the void fraction (0–2.5 s) obtained by the method in this paper is shown in **Figure 11**. It can be seen that due to the small size of the narrow channel, the bubble develops more rapidly after its generation, which cause the outlet void fraction extremely fluctuates with time. In condition 1, the flow channel is mainly dominated by annular flow, a large section of gas column is accompanied by intermittent liquid film

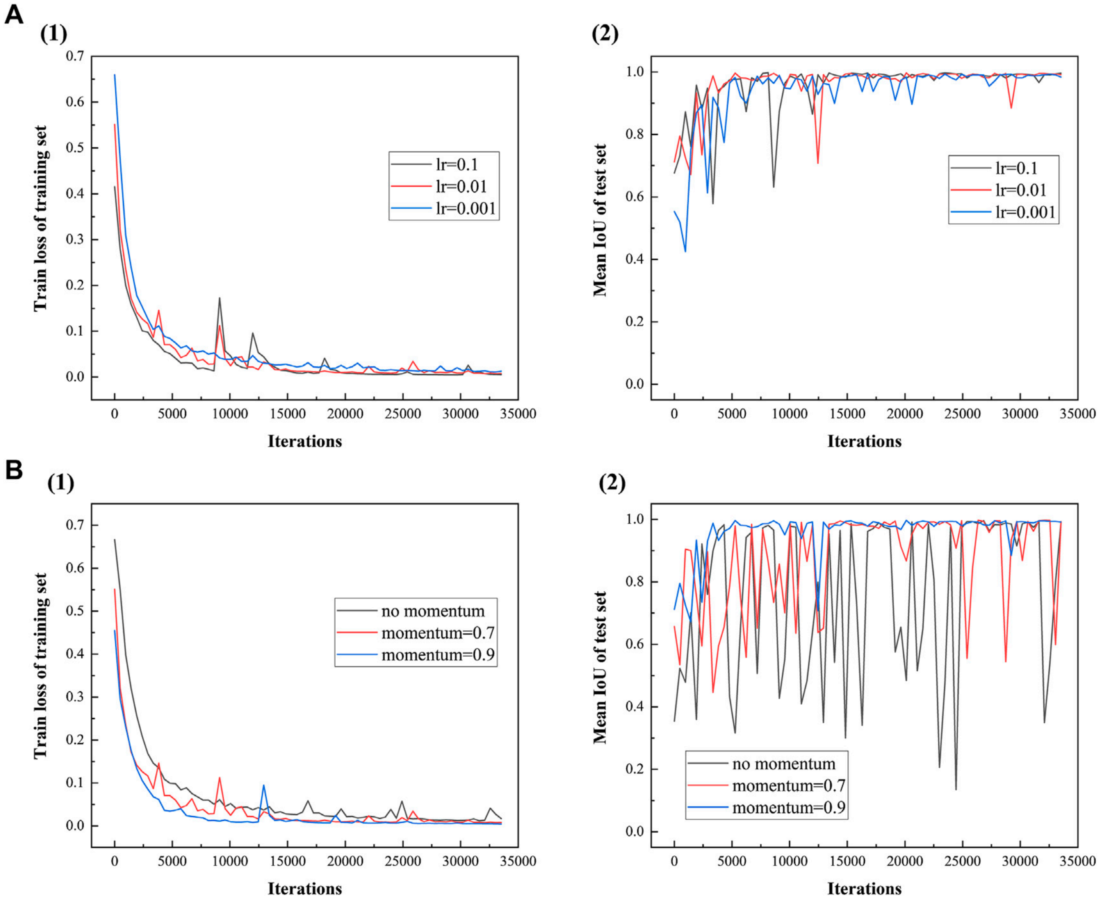

FIGURE 8 | The influence of training parameters on the training process and test set accuracy. **(A)** Different learning rate (momentum factor = 0.9). **(B)** Different momentum factor (learning rate = 0.01): (1) Changes of the train loss. (2) Changes of the mean iou of the test set.

oscillation, and the proportion of outlet void fraction alternately changes with a period of about 0.2s. Operating condition two and three have lower heat flux density than condition 1, and are dominated mainly by slug flow and churn flow. So we can observe from **Figure 11** that intermittent steam generation phenomenon occurs, resulting in a rapid and regular decrease and rise of the void fraction.., which is consistent with the high speed photography images at the corresponding time.

For further verifying the accuracy of the neural network recognition results, we use the theoretical method to calculate the time-averaged void fraction under experimental conditions and compare it with the average value obtained by the method in this paper. The formula of energy conservation method for calculating the mass quality of the gas at the outlet of the narrow channel is shown in the following:

$$\boldsymbol{x} = \frac{\frac{P(1-k)}{M} - \boldsymbol{h}_{l,out} + \boldsymbol{h}_{l,in}}{\boldsymbol{h}_{v,out} - \boldsymbol{h}_{l,out}} \tag{10}$$

where $\boldsymbol{x}$ is the mass quality of the gas, $\boldsymbol{P}$ is the heating power, $\boldsymbol{k}$ is the heat loss ratio, $\boldsymbol{M}$ is the mass flow rate, $\boldsymbol{h}$ is the enthalpy value, the subscript l indicates the liquid phase, v indicates the gas phase, the subscript *in* means the inlet of the test section while the *out* means the outlet. In calculating the heat loss ratio $\boldsymbol{k}$, the influence of the parameters is analyzed and it is found that the mass flow causes less change, indicating that the internal flow has little effect on the heat dissipation. In addition, it is natural convection in a limited space outside the test section, and the heat transfer conditions are basically constant. Therefore, the two-phase heat dissipation loss ratio can be derived by fitting the heat dissipation data of single-phase flow:

$$\begin{aligned}\mathbf{lg}\boldsymbol{k} = &\left(-0.03338 + 2\times10^{-4}\,\Delta\boldsymbol{T} - 3\times10^{-6}\boldsymbol{G}\right)\boldsymbol{q} - 6\times10^{-4}\,\Delta\boldsymbol{T}^2 \\ &-0.00362\,\Delta\boldsymbol{T} - 5\times10^{-5}\boldsymbol{G} + 0.19232\end{aligned} \tag{11}$$

In this formula, $\Delta\boldsymbol{T}$ is the degree of subcooling (°C), $\boldsymbol{G}$ is the inlet mass flow rate (kg/s), and $\boldsymbol{q}$ is the heat flux density (kW/m^2).

So far, numerous of empirical, semiempirical and analytical two-phase flow void fraction correlations have been developed, and according to many review literatures these formulas can be mainly divided into slip ratio model, Lockhart-Martinelli parameter based model, drift flux model, $\boldsymbol{K}\alpha_H$ model, etc. (Vijayan et al., 2000; Dalkilic et al., 2009) According to Huang et al. (2013), the slip ratio model which essentially specify an empirical equation for the slip ratio S is more suitable for narrow

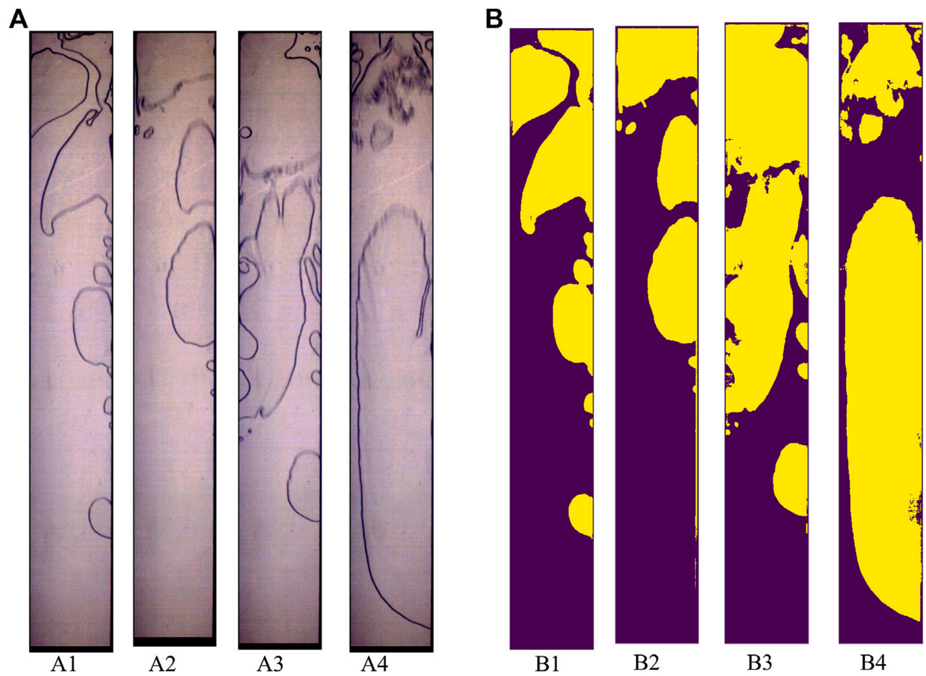

FIGURE 9 | Image processing results of different flow patterns. **(A)** Input images. **(B)** Output binarized images (A1, A2: slug flow with bubbles; A3, A4: churn flow).

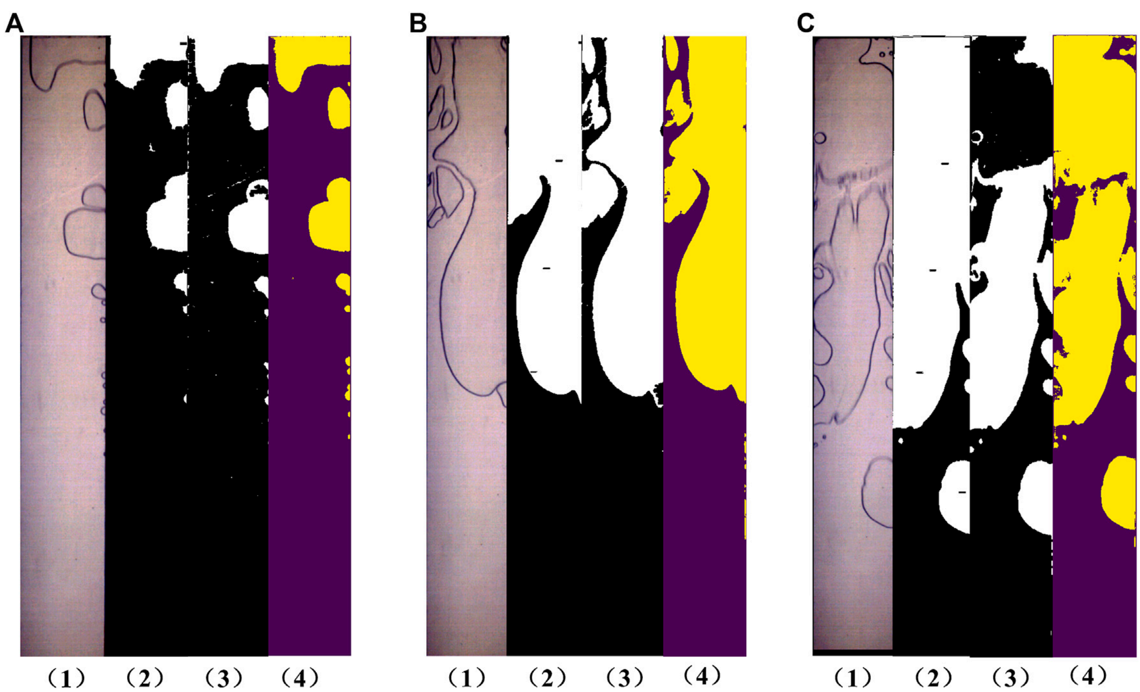

FIGURE 10 | Comparison of FCN model results in this paper with traditional algorithms **(A)** Condition A of low void fraction **(B,C)** Condition B and C of high void fraction. (1) Input experimental pictures; (2) Traditional edge detection/filling algorithm; (3) Two-step morphological method; (4) FCN method.

channels with relatively low outlet mass quality. Therefore, according to the survey, three commonly used calculation models of void fraction are selected as shown in **Table 3**.

The void fraction calculated by our FCN method is instantaneous and the data is time-averaged for comparing with the theoretical results：

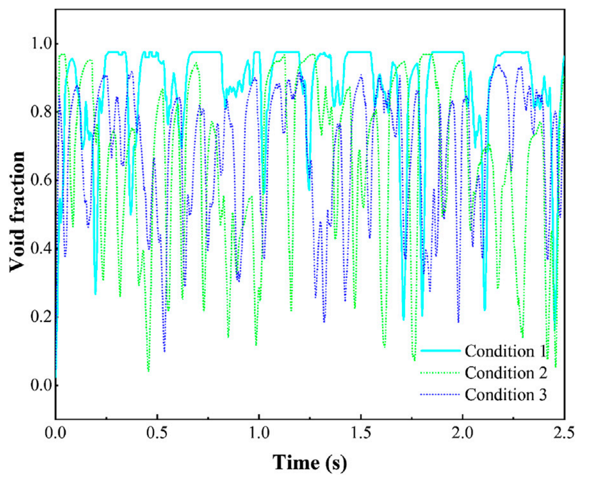

FIGURE 11 | Change of the outlet void fraction with time of different working conditions (0~4 s).

TABLE 3 | The vapor quality-void fraction conversion model selected in this paper.

Number	Authors	Vapor quality-void fraction conversion model
1	Zivi (1964)	$\boldsymbol{\alpha} = \left[1+\left(\frac{1-\boldsymbol{x}}{\boldsymbol{x}}\right)\left(\frac{\rho_v}{\rho_l}\right)\boldsymbol{S}\right]^{-1}, \boldsymbol{S} = 0.2+0.8\left[\frac{\frac{\rho_l}{\rho_v}+0.2(1-\boldsymbol{x})/x}{1+0.2(1-\boldsymbol{x})/x}\right]^{1/3}$
2	Smith (1969)	$\boldsymbol{\alpha} = \left[1+\left(\frac{1-\boldsymbol{x}}{\boldsymbol{x}}\right)\left(\frac{\rho_v}{\rho_l}\right)\boldsymbol{S}\right]^{-1}, \boldsymbol{S} = 0.4+0.6\left[\frac{\frac{\rho_l}{\rho_v}+0.4(1-\boldsymbol{x})/x}{1+0.4(1-\boldsymbol{x})/x}\right]^{1/2}$
3	Chisholm (1973)	$\boldsymbol{\alpha} = \left[1+\left(\frac{1-\boldsymbol{x}}{\boldsymbol{x}}\right)\left(\frac{\rho_v}{\rho_l}\right)\boldsymbol{S}\right]^{-1}, \boldsymbol{S} = \sqrt{1-\boldsymbol{x}+\frac{\boldsymbol{x}\rho_l}{\rho_v}}$

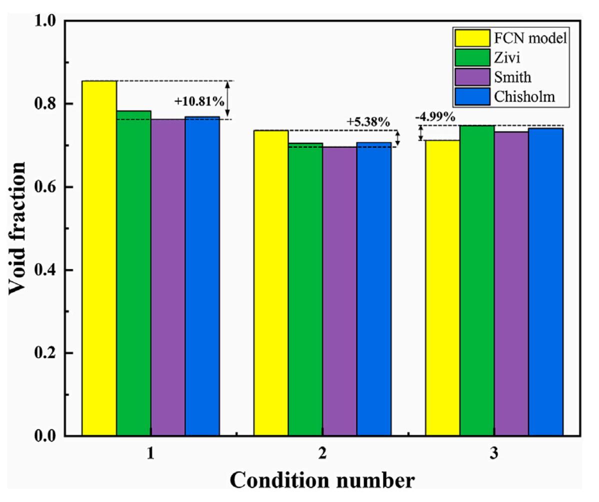

FIGURE 12 | Comparison results of the void fraction calculated by the method in this paper and the empirical formulas.

$$\bar{\boldsymbol{\alpha}} = \frac{\sum_{i=1}^{K}\boldsymbol{\alpha}_i}{\boldsymbol{K}} \tag{12}$$

Where $\bar{\boldsymbol{\alpha}}$ is the time-averaged result of the FCN model, $\boldsymbol{\alpha}_i$ is the instantaneous void fraction of the corresponding images in experimental data set, and $\boldsymbol{K}$ is the number of the experimental image set. The comparison results are listed in **Figure 12**. It shows that the relative deviation between the method in this paper and various empirical models is within ±11%, which illustrates the accuracy of the FCN model proposed in this paper. In addition, the neural network method uses the tensor operation method based on the pre-training weights, and the processing speed has also been improved. After further optimizing the network, it can be applied to real-time monitoring and online void fraction identification.

CONCLUSION

In this paper, a void fraction measurement method based on fully convolutional neural network (FCN) is proposed for the visualization system of the narrow channel two-phase flow boiling experiment. It can identify and extract gas phase from the flow images captured by a high-speed camera, and calculate the void fraction at different locations of the channel. The conclusion is summarized as follow:

(1) Introducing the FCN method based on deep supervised learning and data extraction into the gas-liquid two-phase recognition. FCN can extract information automatically from pixel level to abstract semantic concepts through multi-layer convolution operations. It also uses up-sampling layers and multi-scale fusion technology to further optimize the results. The method reduces the cost of manual design algorithm, and has extensive value for the gas-liquid identification of two-phase flow.

(2) Aiming at problems such as blurring of the gas-liquid interface and dramatic changes in the instantaneous void fraction when in high vapor quality of the narrow channel, the network structure has been adjusted to adapt specific problems. In the working conditions of different void fraction and flow patterns, FCN method realizes better recognition of the gas phase in images, and also realizes the measurement of the transient void fraction in the entire flow channel, which improves the generality of the gas-liquid recognition algorithm.

(3) The void fraction at the outlet of the flow channel is extracted and compared with the numerical results obtained by the energy conservation method and empirical formulas. The deviation between two methods is within ±11%, which verified the reliability of the FCN method. In the future, this method can be applied to real-time void fraction measurement and flow channel monitoring in complex conditions of narrow channels.

DATA AVAILABILITY STATEMENT

The raw data supporting the conclusions of this article will be made available by the authors, without undue reservation.

AUTHOR CONTRIBUTIONS

WC, YL, LP, and XY designed the experiment and the work in paper. WC designed the main algorithm, while YL and LP helped with the processing of experiment data, WC wrote the manuscript with support from HZ and XY and all other authors.

FUNDING

The Analyses and Tests for the key Safety Technology of Nuclear Heating Reactor NHR200-II supported this study.

ACKNOWLEDGMENTS

We gratefully wish to acknowledge the assistance of Yefei Liu to the experiment, and thank to other teachers and students in the laboratory.

SUPPLEMENTARY MATERIAL

The Supplementary Material for this article can be found online at: https://www.frontiersin.org/articles/10.3389/fenrg.2021.636813/full#supplementary-material.

REFERENCES

Bröder, D., and Sommerfeld, M. (2007). Planar shadow image velocimetry for the analysis of the hydrodynamics in bubbly flows. *Meas. Sci. Technol.* 18 (8), 2513. doi:10.1088/0957-0233/18/8/028

Cen, M., and Jung, C. (2018). "Fully convolutional siamese fusion networks for object tracking," in Proceedings of the Int. Conf. on Image Processing, Athens, Greece, October 7-October 10, 2018.

Chisholm, D. (1973). Pressure gradients due to friction during the flow of evaporating two-phase mixtures in smooth tubes and channels. *Int. J. Heat Mass Tran.* 16 (2), 347–358. doi:10.1016/0017-9310(73)90063-X

Dalkilic, A. S., Laohalertdecha, S., and Wongwises, S. (2009). Effect of void fraction models on the film thickness of R134a during downward condensation in a vertical smooth tube. *Int. Commun. Heat Mass Tran.* 36 (2), 172–179. doi:10.1016/j.icheatmasstransfer.2008.10.015

Fu, Y., and Liu, Y. (2016). Development of a robust image processing technique for bubbly flow measurement in a narrow rectangular channel. *Int. J. Multiphas. Flow* 84, 217–228. doi:10.1016/j.ijmultiphaseflow.2016.04.011

Hong, W., Liu, Y., and Zhou, Y. (2011). Investigation on gas-liquid two-phase flow void fraction across tube bundles based on images processing method. *Proc. CSEE* 31 (11), 74–78. doi:10.13334/j.0258-8013.pcsee.2011.11.001 [in Chinese]

Huang, D., Gao, P., Chen, C., and Lan, S. (2013). Effect of void fraction correlations on two-phase pressure drop during flow boiling in narrow rectangular channel. *Nucl. Eng. Des.* 265, 383–392. doi:10.1016/j.nucengdes.2013.09.011

Jahangir, S., Wagner, E. C., Mudde, R. F., and Poelma, C. (2019). Void fraction measurements in partial cavitation regimes by X-ray computed tomography. *Int. J. Multiphas. Flow* 120, 103085. doi:10.1016/j.ijmultiphaseflow.2019.103085

Jaworek, A., Krupa, A., and Trela, M. (2004). Capacitance sensor for void fraction measurement in water/steam flows. *Flow Meas. Instrum.* 15 (5-6), 317–324. doi:10.1016/j.flowmeasinst.2004.04.002

Jia, J., Babatunde, A., and Wang, M. (2015). Void fraction measurement of gas–liquid two-phase flow from differential pressure. *Flow Meas. Instrum.* 41, 75–80. doi:10.1016/j.flowmeasinst.2014.10.010

Karn, A., Ellis, C., Arndt, R., and Hong, J. (2015). An integrative image measurement technique for dense bubbly flows with a wide size distribution. *Chem. Eng. Sci.* 122, 240–249. doi:10.1016/j.ces.2014.09.036

Kawahara, A., Chung, P. Y., and Kawaji, M. (2002). Investigation of two-phase flow pattern, void fraction and pressure drop in a microchannel. *Int. J. Multiphas. Flow* 28 (9), 1411–1435. doi:10.1016/S0301-9322(02)00037-X

Lau, Y. M., Deen, N. G., and Kuipers, J. A. M. (2013). Development of an image measurement technique for size distribution in dense bubbly flows. *Chem. Eng. Sci.* 94, 20–29. doi:10.1016/j.ces.2013.02.043

Long, J., Shelhamer, E., and Darrell, T. (2015). "Fully convolutional networks for semantic segmentation," in Proceedings of the IEEE conference on computer vision and pattern recognition, Boston, MA, June 7–June 12 2015.

Maggiori, E., Tarabalka, Y., Charpiat, G., and Alliez, P.. "Fully convolutional neural networks for remote sensing image classification," in Proceedings of the 2016 IEEE International Geoscience and Remote Sensing Symposium, Beijing, China, July 10-July 15 2016.

Pan, L., Liu, Y., and Li, W. (2018). Measurement method of void fraction in narrow channel based on two-step morphological image method. *Yuanzineng Kexue Jishu Atomic Energy Sci. Technol.* 52, 2256–2262. doi:10.7538/yzk.2018.youxian.0204

Ronneberger, O., Fischer, P., and Brox, T. (2015). "U-net: convolutional networks for biomedical image segmentation," in proceedings of the international conference on medical image computing and computer-assisted intervention, Munich, Germany, October 5–October 9, 2015 (Cham: Springer), 234–241.

Simonyan, K., and Zisserman, A. (2014). Very deep convolutional networks for large-scale image recognition. Available at: https://arxiv.org/abs/1409.1556 (Accessed September 4, 2014).

Smith, S. L. (1969). Void fractions in two-phase flow: a correlation based upon an equal velocity head model. *Proc. Inst. Mech. Eng.* 184 (1), 647–664. doi:10.1243/pime_proc_1969_184_051_02

Srisomba, R., Mahian, O., Dalkilic, A. S., and Wongwises, S. (2014). Measurement of the void fraction of R-134a flowing through a horizontal tube. *Int. Commun. Heat Mass Tran.* 56, 8–14. doi:10.1016/j.icheatmasstransfer.2014.04.004

Triplett, K. A., Ghiaasiaan, S. M., Abdel-Khalik, S. I., and Sadowski, D. L. (1999). Gas–liquid two-phase flow in microchannels Part I: two-phase flow patterns. *Int. J. Multiphas. Flow* 25 (3), 377–394. doi:10.1016/S0301-9322(98)00054-8

Vigayan, P. K., Patil, A. P., and Pilkhwal, D. S. (2000). An assessment of pressure drop and void fraction correlations with data from two-phase natural circulation loops. *Heat Mass Tran.* 36 (6), 541–548. doi:10.1007/s002310000108

Winkler, J., Killion, J., and Garimella, S. (2012). Void fractions for condensing refrigerant flow in small channels. Part II: void fraction measurement and modeling. *Int. J. Refrig.* 35 (2), 246–262. doi:10.1016/j.ijrefrig.2011.08.012

Wu, B., Iandola, F., Jin, P. H., and Keutzer, K. (2017). "Unified, small, low power fully convolutional neural networks for real-time object detection for autonomous driving," in Proceedings of the IEEE Conference on Computer Vision and Pattern Recognition Workshops, Honolulu, HI, July 21–July 26, 2017.

Zahid, A. A., ur Rehman, S. R., Rushd, S., Hasan, A., and Rahman, M. A. (2020). Experimental investigation of multiphase flow behavior in drilling annuli using high speed visualization technique. *Front. Energy* 14, 635–643. doi:10.1007/s11708-018-0582-y

Zhao, Y., Bi, Q., Yuan, Y., and Lv, H. (2016). Void fraction measurement in steam–water two-phase flow using the gamma ray attenuation under high pressure and high temperature evaporating conditions. *Flow Meas. Instrum.* 49, 18–30. doi:10.1016/j.flowmeasinst.2016.03.002

Zivi, S. M. (1964). Estimation of steady-state steam void-fraction by means of the principle of minimum entropy production. *J. Heat Tran.* 86 (2), 247–251. doi:10.1115/1.3687113

Conflict of Interest: The authors declare that the research was conducted in the absence of any commercial or financial relationships that could be construed as a potential conflict of interest.

frontiers in Energy Research

ORIGINAL RESEARCH
published: 09 February 2021
doi: 10.3389/fenrg.2020.613852

Development and Validation of Multiscale Coupled Thermal-Hydraulic Code Combining RELAP5 and Fluent Code

Lin Sun[1], *Minjun Peng*[2], *Genglei Xia*[2], *Xuesong Wang*[1]* *and Mingyu Wu*[1]

[1]*Division of Reactor Engineering Technology Research, China Institute of Atomic Energy, Beijing, China,* [2]*Fundamental Science on Nuclear Safety and Simulation Technology Laboratory, Harbin Engineering University, Harbin, Heilongjiang, China*

In nuclear reactor system research, the multiscale coupled thermal-hydraulic (T-H) system code and CFD code is one of the most prevalent research areas, and it could help improve simulation fidelity and optimize nuclear reactor design. Additionally, a new idea known as the function fitting method (FFM) for coupling parameter distribution has been newly proposed for exchanging data on the coupling interface, which uses math equations to present the velocity distribution characteristics at the coupling interface. This method could improve the simulation error and numerical instability. To verify and validate the abovementioned FFM, a comparison between the velocity function shape by FFM and real velocity distribution was completed. Besides, the Edwards pipe blowdown test results were used to verify the coupled code. The results showed good agreement with experiment results, and a better simulation accuracy compared to previous work. The current work will establish the ability to explore multiscale coupled thermal-hydraulic operation characteristics which permit precise local parameter distribution.

Keywords: coupled RELAP5/fluent code, Edwards blowdown test, function fitting method, mutliscale thermal-hydraulic code, computational fluid dynamics

OPEN ACCESS

Edited by:
Xianping Zhong,
University of Pittsburgh, United States

Reviewed by:
Mehdi Hashemi-Tilehnoee,
Islamic Azad University, Iran
Jiankai Yu,
Massachusetts Institute of Technology, United States
Antonio Cammi,
Politecnico di Milano, Italy

****Correspondence:***
Xuesong Wang
wangxuesong@ciae.ac.cn

Specialty section:
This article was submitted to Nuclear Energy, a section of the journal Frontiers in Energy Research

Received: *04 October 2020*
Accepted: *11 December 2020*
Published: *09 February 2021*

Citation:
Sun L, Peng M, Xia G, Wang X and Wu M (2021) Development and Validation of Multiscale Coupled Thermal-Hydraulic Code Combining RELAP5 and Fluent Code. Front. Energy Res. 8:613852. doi: 10.3389/fenrg.2020.613852

INTRODUCTION

Nuclear safety is a top priority for nuclear power application and expansion. Estimate tools for increasing safety analysis and evaluation requirements need to become better and more precise. In the past few decades, on a system scale, the best estimate codes such as RELAP5 (Allison et al., 1993), RETRAN (McFadden et al., 1981), CATHARE (Barre and Bernard, 1990), and MARS (Jeong et al., 1999) have dominated nuclear reactor operation, safety analysis, and severe accident analysis. However, these codes can only present one-dimensional transient system behaviors, which can not provide the local characteristics of the reactor. As computational resources have dramatically developed, component scale analysis codes like COBRA (Stewart et al., 1977), RELAP5-3D (RELAP5-3D Code, 2012), VIPRE (Stewart et al., 1989), and local scale codes such as Fluent (Rohde et al., 2007), CFX (Höhne et al., 2010), and Star-CCM+ (Cardoni, 2011) have emerged. These computational fluid dynamic (CFD) codes can provide three-dimensional features, which have been applied in pressurized thermal shock (PTS) (Egorov et al., 2004), boron dilution and distribution in reactor vessels (Muhlbauer, 2003; Scheuerer et al., 2005), and so on. The above CFD application has faced the challenge of the computational cost of transient safety analysis. To conquer these difficulties, a compromised method of developing coupled codes based on system and CFD codes has been promoted.

Ronnie Andersson (Andersson et al., 2004) utilized a system and CFD code to analyze turbulence intensity and dissipation on multiphase flow in the reactor. Daniele Martelli (Martelli et al., 2017) coupled RELAP5/MOD3.3 and Fluent to simulate a NACIE experiment loop and loss of flow accident, which was in good agreement with experiment data. J-J. Jeong (Jeong et al., 1999) developed an integral modular code MARS coupled RELAP5 and sub-channel COBRA code, which adopted a semi-implicit method and dynamic memory allocation method. W. L. Weaver (Weaver et al., 2002; Weaver, 2005) developed a series of studies coupling RELAP5-3D and CFX, D.L. Aumiller (Aumiller et al., 2001; Aumiller et al., 2002) further coupled RELAP5-3D and CFD-FLOW3D based on the parallel virtual machine (PVM) method, both studies used the Edwards blowdown test to conduct the verification and validation (V&V) process. Nolan Anderson (Anderson, 2006; Anderson et al., 2008) also developed RELAP-3D and Fluent coupled code using PVM, for Very High Temperature Reactor (VHTR) lower plenum analysis.

The existing coupled code development technologies mainly include PVM, dynamic link library (DLL) (Li et al., 2014), and boundary files modification methods. Challenges in the coupling process (Ivanov and Avramova, 2007) mainly concern the method of coupling, coupling approach, spatial mesh overlays, time step algorithms, and coupling numeric and convergence schemes. Spatial mesh mapping, especially the data exchange at the coupling interface plays a key role in simulation accuracy and numerical convergence. Therefore, in this paper, a new method called the function fitting method (FFM) for coupling parameter distribution was proposed for coupling RELAP5 and Fluent, aiming at providing precise data exchange. An Edwards pipe blowdown test was used to verify and validate the coupled code.

COUPLING METHOD

For multiscale coupled thermal-hydraulic code, the kinds of variables that are transferred through the coupling interface must be considered as priority. The RELAP5 code sets the boundary conditions through time-dependent control volume (TMDPVOL) and time-dependent junction (TMDPJUN); while Fluent has a predetermined velocity-inlet, pressure-outlet, and outflow boundary conditions, etc.

Assuming that the control volume Ri (RELAP5-interface) is connected to the coupling interface between Fluent and RELAP5, the mass and energy conservation equations are solved in the control volume Ri. The junction j is also connected to Fluent and RELAP5, then the momentum conservation equation is solved in junction j, and the vector variables are stored in j (as shown in **Figure 1**). In fact, the RELAP5 interface control volume Ri and the junction j do not have realistic components in the RELAP5 system; its main function is to be used as a coupling interface, which is also known as a "ghost cell." This coupling interface is an overlapped computational domain.

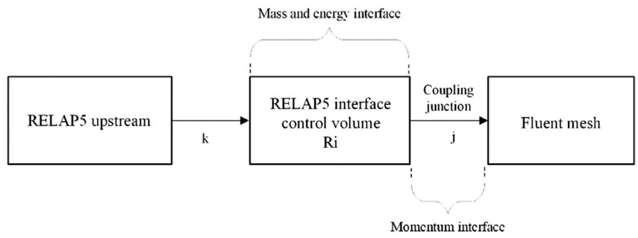

FIGURE 1 | The coupling interface control volumes between RELAP5 and Fluent.

Under this scenario, the downstream Fluent computational mesh is regarded as the downstream control volume of the RELAP5 portion, and the abovementioned mass, energy, and momentum conservation equations can be derived in the following forms:

$$P_{Ri}^{n+1} - P_{Ri}^{n} = b + g^1 v_{g,j}^{n+1} + g^2 v_{g,k}^{n+1} + f^1 v_{f,j}^{n+1} + f^2 v_{f,k}^{n+1} \tag{1}$$

$$v_{g,j}^{n+1} = A' \left(P_F^{n+1} - P_{Ri}^{n+1}\right) + C' \tag{2}$$

$$v_{f,j}^{n+1} = B' \left(P_F^{n+1} - P_{Ri}^{n+1}\right) + D' \tag{3}$$

where, P is the pressure and v is the fluid velocity. While, the subscript g and f stand for gas and fluid, respectively. The superscript n and $n+1$ represent the current and next time step.

Coefficients b, g^1, g^2, f^1, and f^2 are column vectors, these coefficient vectors are known variables under the current time step n. b is the source term in the equation, and the coefficient matrices g and f represent the convection effect. A', B', C', *and* D' are coefficients that contain only the current time step variable.

The exchange variables between RELAP5 and Fluent codes are listed in the following **Table 1**.

The data transfer between the coupling interface is bidirectional. While, Fluent passes parameters to RELAP5, which can be calculated by surface summation or averaging. For the mass flow rate, the sum of the Fluent surface cells is equal to that of the RELAP5 interface.

$$W_{gj}^{n+1} = \sum_{i=1}^{N_c} W_{gi}^{N} \tag{4}$$

$$W_{fj}^{n+1} = \sum_{i=1}^{N_c} W_{fi}^{N} \tag{5}$$

where, W is the mass flow rate and N_c stands for the Fluent cell numbers on the coupling interface.

Other variables like temperature, pressure, and void fraction, are represented by Φ, and can be described as follow:

$$\Phi_F^{n+1} = \frac{\sum_{i=1}^{N_c} \Phi_i^{n+1} |A_i|}{\sum_{i=1}^{N_c} |A_i|} \tag{6}$$

where, A_i is the area of cell surface i.

TABLE 1 | Data transfer between RELAP5 and Fluent.

Sequence	RELAP5 → Fluent	Fluent → RELAP5
1	Pressure (P)	Pressure (P)
2	Liquid density (rhof)	Liquid internal energy (uf)
3	Vapor density (rhog)	Vapor internal energy (ug)
4	Liquid temperature (tempf)	Void fraction (voidg)
5	Vapor temperature (tempg)	Liquid mass flow rate (mflowfj)
6	Void fraction (voidg)	Vapor mass flow rate (mflowgj)
7	Vapor velocity (velgj)	
8	Liquid velocity (velfj)	

For parameters passed from RELAP5 to Fluent, one-dimensional parameters obtained by the lumped parameter method of RELAP5 will be converted into the two-dimensional distribution of the Fluent interface. In past research, these data were generally averaged on the interface, but this method introduces errors into each calculation iteration. While, in some studies, the coupling boundary is set further afield so that it is far enough to minimize uneven effects on the interface. However, these two methods do not solve the different dimensional transformation problem of the coupling parameters. Therefore, in this paper, we worked on solving this issue by proposing a function fitting method for interface data.

FUNCTION FITTING METHOD

For nuclear power systems and equipment, most fluid areas are round tubes, such as pipes and fluid machinery (pumps, valves, etc.,). For the application of the RELAP5/CFD coupled code, the primary system and safety system are modeled by one-dimensional system codes to obtain the transient characteristics. However, the pressure vessel, lower plenum, and the core are modeled by the three-dimensional CFD code Fluent. The connection between the system and the local equipment are mostly long round tubes, and the fluid flow therein can be considered fully developed. The flow and heat transfer of single-phase and two-phase fluids for round tubes have been widely studied. Therefore, in this paper, the function fitting method (FFM) for coupling parameter distribution was proposed. This method can accurately convert the one-dimensional lumped variables into two-dimensional ones that satisfy the corresponding physical laws, thereby effectively improving the error of calculation instability and accelerating calculation convergence.

Fitting Function

The original intention of this method was to transfer the one-dimensional parameters into the two-dimensional surface ones through appropriate function fitting, and accurately reflect the real distribution. Therefore, for Newtonian viscous fluids, there are many mature empirical formulas for one-dimensional flow, and they can be used as one of the independent variables of the fitting function.

For the fully developed single phase turbulent flow in a round tube, the velocity distribution is relatively flat in the middle. While, in the viscous bottom layer near the wall surface, the velocity distribution changes sharply and the velocity gradient is relatively large. For the velocity distribution in the tube flow, the most influential factor is the Reynolds number and position. The flow velocity distribution function fitting method mainly considers the influence by friction coefficient and relative position.

The empirical formulas for the widely recognized turbulent flow frictional resistance coefficient are listed in **Table 2**.

Rr in **Table 2** is the relative roughness. The friction coefficient calculations for the Nikuradse and Colebrook models in the table are implicit, that is, f appears on both sides of the equation; therefore, either the equation is iteratively solved, or the solution is interpolated in the Moody diagram (Moody, 1944). These solution methods are very inconvenient (Haaland, 1983). Therefore, in the function fitting method, it is preferred to select the simple and accurate explicit friction coefficient calculation as one of the independent variables. After a large number of experiments, the Filonenko model was chosen because it is applicable in a wider range of Reynolds numbers. Besides, in related research, the experiments of scholars Romeo (Romeo et al., 2002), Fang (Fang et al., 2011), and Yıldırım (Yıldırım, 2009) have verified that this model is more accurate among the explicit friction relationship.

The function fitting method is also related to the position of the one-dimensional grid to the two-dimensional grid spatial mapping. Therefore, for the round tube coupling interface, the radial position of the round tube is selected as another independent variable. According to the characteristics of the flatness of the central cross-section, and the steep edge, the fitted mathematical function should also have the above characteristics.

The simplest and most straightforward method of the fitting function is to use piecewise polynomial fitting. However, the function obtained by this method requires multiple constraints, which is not suitable for practical application. In elementary functions, logarithmic function has the characteristics of rapid transition in the normalized (0–1) interval. Therefore, the fitting function must contain a logarithmic function term, which also requires the consideration of relative distance.

The term related to the friction coefficient is in the form of the polynomial and power function. The determination of the index needs to be verified by a large number of calculations, so that the obtained function conforms to the flow velocity distribution under different flow Reynolds numbers.

Finally, the conversion formula for the function fitting method is:

$$F(f, r) = 1 + 1.44f^{0.45} + 2.15f^{0.45}\log(1 - r/R) \tag{7}$$

where, F is the fitting function, r is the distance from the central axial line, and R is the inner radius.

The f in **Eq. 7** is the friction coefficient. Here, the Filonenko model is selected, namely:

$$f = (0.78\ln Re - 1.64)^{-2} \tag{8}$$

The coupling parameter velocity conversion from the system code RELAP5 to the CFD code Fluent can be expressed as:

TABLE 2 | Single phase turbulent flow friction factor in round pipe.

Order	Model	Formula	Reynolds number
1	von Karman (von Karman, 1937)	$\frac{1}{\sqrt{f}} = 2\log\left(\frac{1}{Rr}\right) + 1.74$	$4 \times 10^3 \le Re \le 10^8$
2	Nikuradse (Fang et al., 2011)	$\frac{1}{\sqrt{f}} = 2\log(Re\sqrt{f}) - 0.8$	$3 \times 10^3 \le Re \le 3.4 \times 10^6$
3	Blasius (Blasius, 1907)	$f = \frac{0.316}{Re^{1/4}}$	$Re \le 2 \times 10^4$
		$f = \frac{0.184}{Re^{1/5}}$	$Re \ge 2 \times 10^4$
4	Filonenko (Fang et al., 2011)	$f = (0.79\ln Re - 1.64)^{-2}$	$10^4 \le Re \le 10^8$
5	Colebrook (Colebrook, 1939)	$\frac{1}{\sqrt{f}} = -2\log\left(\frac{Rr}{3.7} + \frac{2.51}{Re\sqrt{f}}\right)$	$4 \times 10^4 \le Re \le 10^8$
6	Drew, McAdams, Koo (Schramm, 2006)	$f = 0.0056 + \frac{1}{2}Re^{-0.32}$	$3 \times 10^3 \le Re \le 3 \times 10^6$

$$u_{\mathrm{CFD}}(r) = u_{\mathrm{RELAP5}}\left[1 + 1.44f^{0.45} + 2.15f^{0.45}\log(1 - r/R)\right] \quad (9)$$

where, u_{CFD} is the fluid velocity at the Fluent coupling interface, while u_{RELAP5} is fluid velocity at the RELAP5 coupling junction.

In addition, for the coupling process between different thermal-hydraulic codes, attention should also be paid to the conservation of the coupling parameters. Especially for the coupling parameter distribution function fitting method, it is necessary to assure that the integral flow on the Fluent interface is equal to the total flow at the RELAP5 coupling junction, as follows:

$$W_j = \iint_A \rho u_{\mathrm{CFD}}\mathrm{d}A \quad (10)$$

where, W_j is the mass flow rate at the RELAP5 coupling junction and A is the area of the Fluent coupling interface.

Verification and Validation of Fitting Function

In order to verify and validate the accuracy of the function fitting method proposed in the previous section, Fluent was used to analyze the flow in a round tube under different conditions. Besides, the results have been compared with the fitting function under the corresponding Reynolds number. Since the independent and dependent variables of the fitting function are dimensionless, in the CFD verification, the corresponding size and speed are also normalized accordingly. A horizontal tube with a length of 500 mm and an inner diameter of 10 mm was chosen; and the velocity distribution at the center of the tube was compared with the fitting function. The selected pressure, temperature, flow rate, and corresponding Reynolds number were included within the pressurized water reactor (PWR) operation and accident conditions. The specific verification conditions are shown in **Table 3**.

In this V&V work, in order to accurately simulate the flow features in the boundary layer, the y plus value was confirmed as 30; the wall surface was divided into 20 boundary layers, the grid thickness of the first layer of the boundary layer was calculated to be 7×10^{-4} mm, and the growth ratio was 1.1. The mesh cross section is shown in **Figure 2**.

In **Figure 3**, the normalized velocity distribution is compared between the fitting function and Fluent results. Under different pressures, temperatures, velocities, and Reynolds numbers, the fitting function represented accurate results to prove its applicability. The x-axis of the fitting function was in a relative position to the axial center, and the y-axis was the normalized velocity, which determined that this function was not constrained by specific size.

VERIFICATION AND VALIDATION OF THE COUPLED CODE

In this paper, the Edwards pipe blowdown test was chosen to validate the multiscale coupled one dimensional (1D) and three dimensional (3D) code.

Edwards Pipe Blowdown Test

The original intention of the Edwards pipeline blowdown test was to simulate the phase change process in the safety analysis of the water-cooled reactor, which is very similar to the coolant loss process of the PWR loss of coolant accident (LOCA). The experimental facility contained a heating pipe filled with water, and the pressure was maintained above the saturation point. Before the glass plate at the end of the pipe was broken, the pressure was adjusted to the required level. During the blowdown test, measurement gauge stations were set up along the pipeline, with which pressure, temperature, and density changes were measured.

Before the blowdown process, the horizontal pipe was filled with supercooled water (602.15 K, 7.0 MPa). The ambient temperature was 293.15 K, and the ambient pressure was atmospheric pressure. The pipe was 4.096 m long and had an inner diameter of 73.15 mm. The design pressure of the pipeline was 17.2 MPa, and the design temperature was 616.5 K. The initial experimental pressure ranged from 3.55 to 17.34 MPa, and the temperature ranged from 514.8 to 616.5 K. The experiment layout is shown in **Figure 4**. The end of the pipe was the blowdown section, sealed by a toughened glass disc, the diameter of the glass disc was 88.9 mm, and the thickness was 12.7 mm. At the beginning of the experiment, the glass disc was ruptured by the lead pellet from a compressed air gun, and the water in the pipe was discharged into the environment. The reduction in the spray area accounted for 13% of the pipe cross-sectional area. A total of seven measuring gauge stations (GS1-GS7) were set up along the axial direction of the pipeline, and each was equipped with a facility for fitting fast response pressure and temperature transducers. The pipe was heated

TABLE 3 | Verification experiment conditions in horizontal round pipe.

Parameter	A	B	C
Velocity (m/s)	12.75	1.056	0.19
Density (kg/m^3)	763.87	922.20	988.50
Dynamic viscosity (kg/m·s)	9.74E-05	9.74E-05	8.93E-05
Reynolds	999932.5 (1 × 10^6)	99984.2 (1 × 10^5)	10015.5 (1 × 10^4)
Turbulence intensity (%)	2.85	3.79	5.06
Inlet pressure (MPa)	15.5	10.5	4.5
Outlet pressure (MPa)	15	10	4
Temperature (°C)	280	150	50

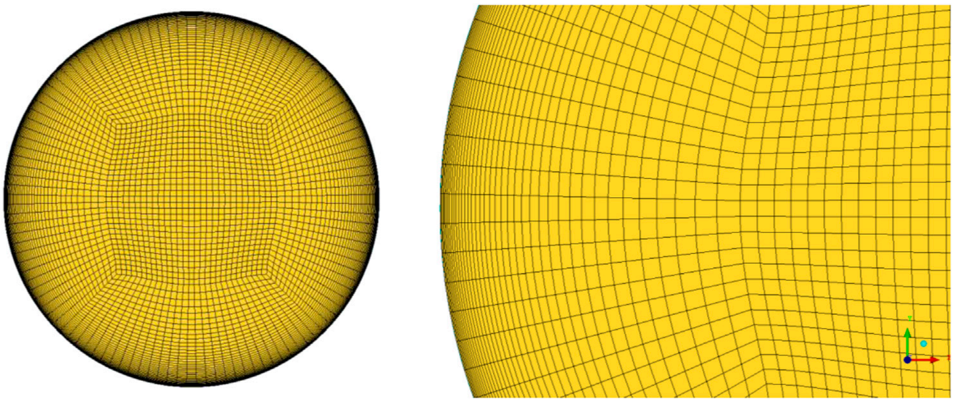

FIGURE 2 | Boundary layer mesh configuration on the cross section of the round pipe.

electrically with sheathe band heaters, formed to the curvature of the pipe. They covered approximately 70% of the pipe circumference and each had a capacity of 700 watts. Heat losses were reduced by using asbestos insulation.

In order to verify the RELAP5/Fluent coupled code, the Edwards pipe blowdown test was used as the benchmark problem in this paper. Meanwhile, the standalone RELAP5 code and other scholar's coupled code results (Li et al., 2014) were compared with our work.

Simulation Model

The standalone RELAP5 model nodalization is shown in **Figure 5**, in which the pipe component 003 PIPE stands for the experiment pipe, and the single junction component 004 SNGJUN connects the experiment pipe and rupture boundary. The time-dependent volume component 005 stands for the ruptured end of the pipe and also provides boundary conditions for the simulation. In RELAP5, the bubble radius change rate in the flash evaporation process is based on the Plesset-Zwick model (Plesset and Zwick, 1954), and the corresponding Nusselt solution is based on the Lee-Rypley model (Lee and Ryley, 1968):

$$Nu_b = 2.0 + 0.74Re_b^{0.5}Pr^{1/3} \tag{11}$$

where, the subscript b represents bubbles.

In the coupled code analysis, the Edwards pipeline simulation model was divided into two parts along the axial direction. The upstream was modeled by Fluent, and the downstream to the end of the pipeline was simulated by RELAP5 (as shown in **Figure 6**). The downstream RELAP5 part contained 10 mass and energy control volumes, and nine momentum junctions among each control volume. Since the Edwards blowdown test is a strong transient process, the maximum time step of RELAP5 was set to 0.0001 s. In each time step, the inlet boundary of RELAP5 provided the pressure, temperature, and void fraction to the outlet boundary of Fluent; the Fluent returned the void fraction, pressure, temperature, and mass flow rate of the gas and liquid phase inlet boundary condition of RELAP5.

For the Fluent calculation part, the two-phase Euler model was adopted for the multiphase flow simulation, and a bubble diameter d_{bubble} = 1 mm. The thermal phase change model was adopted for the rapid and intense evaporation-condensation process (ANSYS, 2015). The water properties were based on the National Institute of Standards and Technology (NIST) compressible gas model, which was important to capture the spread of pressure waves.

RESULTS AND ANALYSIS

The Edwards pipe blowdown test process can be divided into two periods: one is the rapid pressure discharge period caused by the single-phase water loss, and the other is the slower pressure discharge period by the loss of the two-phase mixture. The first

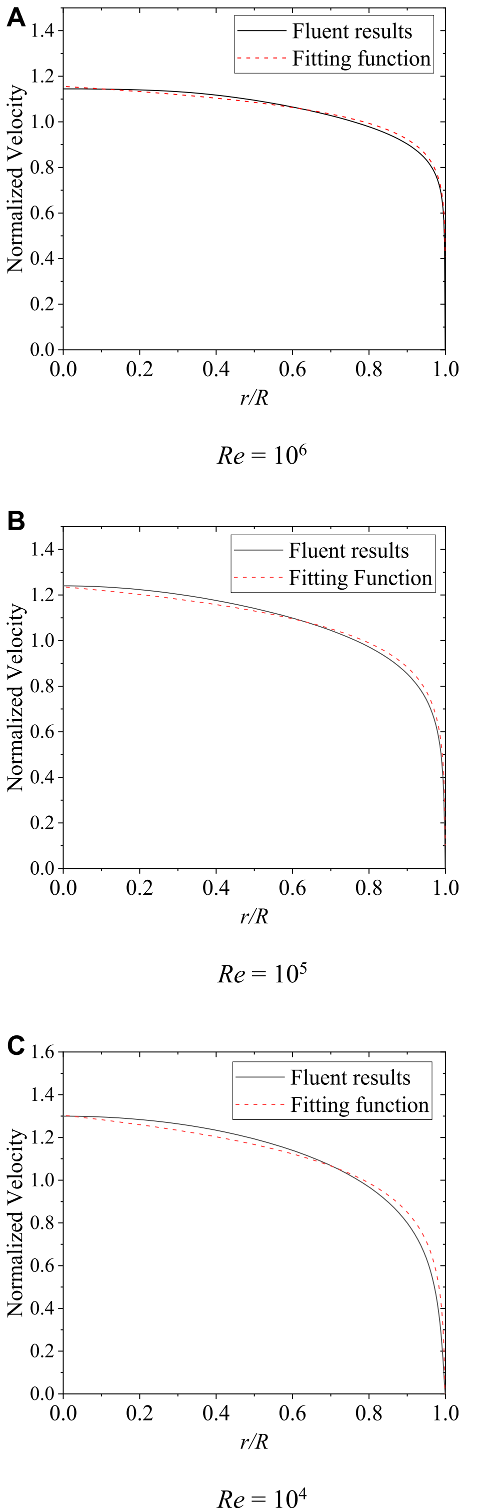

FIGURE 3 | Comparison of the fitting function and Fluent results. **(A)** $Re = 10^6$. **(B)** $Re = 10^5$. **(C)** $Re = 10^4$.

period happens almost instantaneously, at approximately 2 ms. The second period continues until the pressure is discharged close to the environment pressure.

Figure 7 shows the pressure variation of the GS-5. After the blowdown started, the pressure dropped sharply due to the rapid loss of relatively high-density supercooled water until saturation conditions were reached. The pressure drop during the discharge phase of the two-phase mixture was compensated by vapor generation. The pressure results simulated by the coupled Fluent/RELAP5 code was in good agreement with the Edwards pipeline test results (Edwards and O'Brien, 1970). The maximum deviation was 0.26 MPa, which corresponds to an error of 18.4% from the experiment results, which is acceptable for two-phase transient flow. The pressure results simulated by the coupled code was higher than the experiment and RELAP5 results. It is worth mentioning that the prediction of coupled analysis is not restricted by independent RELAP5. Compared with the coupled code with a simple boundary condition treatment from other papers, our results were closer to the experiment results.

Figure 8 shows the pressure variation at GS-7. The coupled code results were within a reasonable range compared to the experiment results. In 0–250 ms, the simulation results of the coupled code were close to the experimental results, after which the simulation results were higher than the experiment ones. The maximum pressure deviation between the coupled code and the test results was 0.41 MPa, and the corresponding error was 28%. The pressure drop process simulated by the Fluent/RELAP5 coupled code and the standalone RELAP5 code began earlier than in the experiment. This phenomenon was partly due to the thermal phase change flashing model in the Fluent code. Its flashing rate was determined by the temperature difference between each phase and their corresponding saturation temperature, which led to a faster pressure drop.

Figure 9 shows void fraction variation at GS-5. In the first millisecond, the vapor generation rate was relatively slow, and the coupled code results were slightly lower than the experiment ones. As the blowdown process reached saturation conditions, the largest increase rate of the void fraction occurred in the middle of the whole process. In the following period, due to the equilibrium state with the environment, the vapor generation rate decreased. The error between the coupled code results and the experiment ones can be attributed to the assumption that the average bubble size was simplified to a fixed value (1 mm) in the Fluent model. The size of the pre-existing nuclei in the sub-cooled liquid was substantially smaller than the prescribed 1 mm. This indicated a significant under-prediction of the interfacial area density available for the initiation of flashing. While the steam bubbles grew rapidly during the flashing process, which resulted in a mean size much larger than 1 mm in a short period (Liao and Lucas, 2017). Nevertheless, the uncertainty was weakened with the increase of the void fraction. The effects of prescribed bubble sizes were studied in Liao's paper (Liao et al., 2013).

Figure 10 shows the mass flow rate variation of the control volume at the coupling interface. Since there is no available experiment data in the Edwards pipe blowdown test, the results of the coupled code were compared with those of the standalone RELAP5 code. The results of the coupled Fluent/RELAP5 code showed similar trends with those of RELAP5. The mixture mass flow rate by the standalone RELAP5 code was

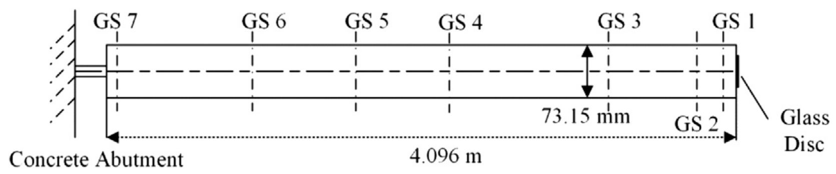

FIGURE 4 | Edwards blowdown test.

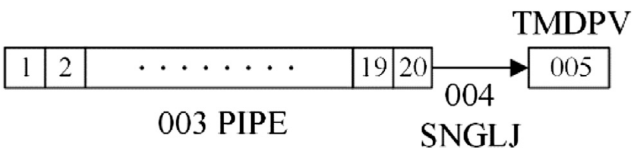

FIGURE 5 | RELAP5 nodalization of the Edwards blowdown test.

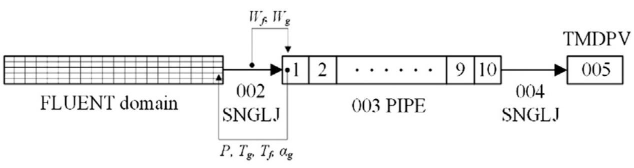

FIGURE 6 | RELAP5/Fluent coupling scheme for the Edwards pipe test.

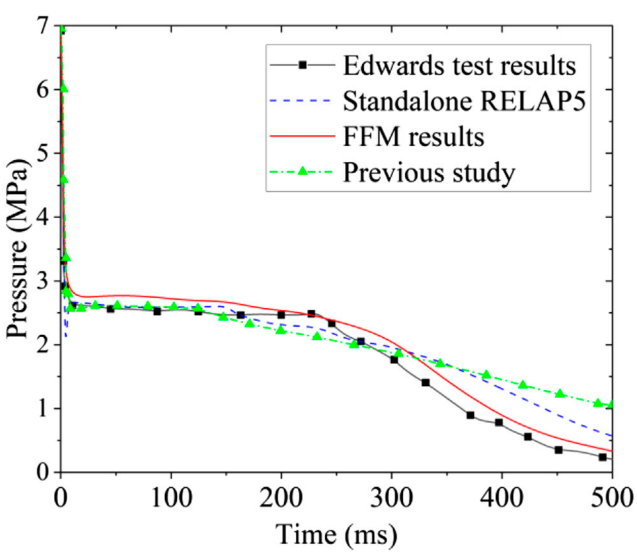

FIGURE 7 | Comparison of the pressure at GS-5.

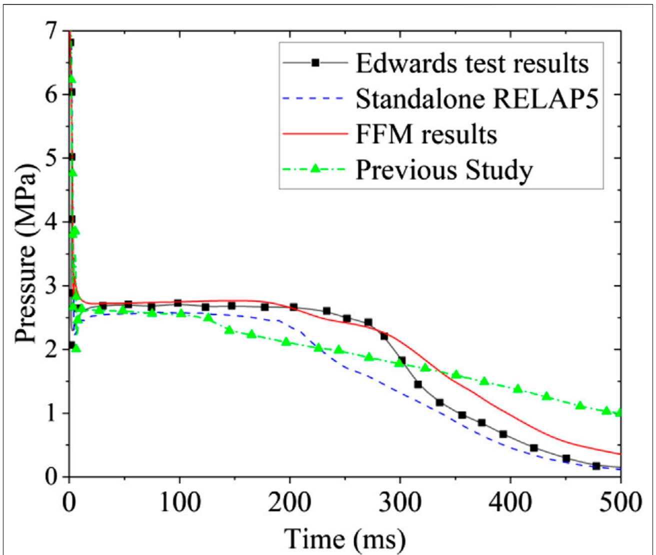

FIGURE 8 | Comparison of the pressure at GS-7.

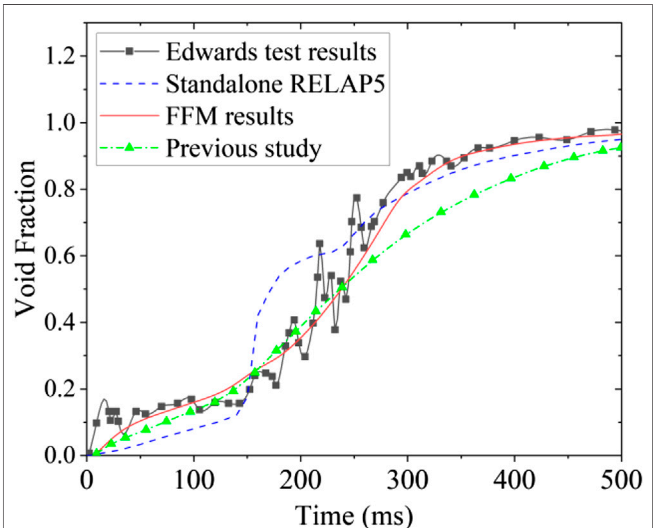

FIGURE 9 | Comparison of void fraction at GS-5.

larger than that of the coupled code, and the falling tendency of the mass flow rate variation simulated by the coupled code began earlier.

Figure 11 shows the mass flow rate variation at the break of the pipe. After the rupture of the end of the pipe, the discharge flow rate quickly reached the maximum value. The mass flow rate of the break simulated by the Fluent/RELAP5 coupled code was in good agreement with that of the standalone RELAP5, and the

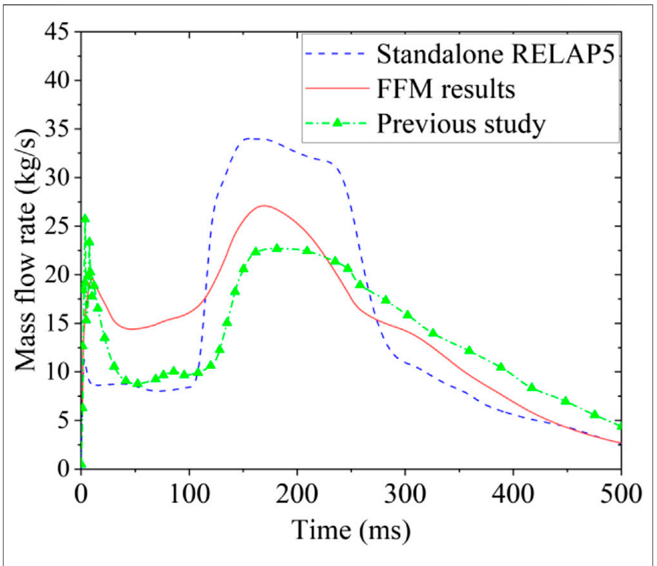

Figure 10 | Comparison of the mass flow rate of the mixture at the coupling interface.

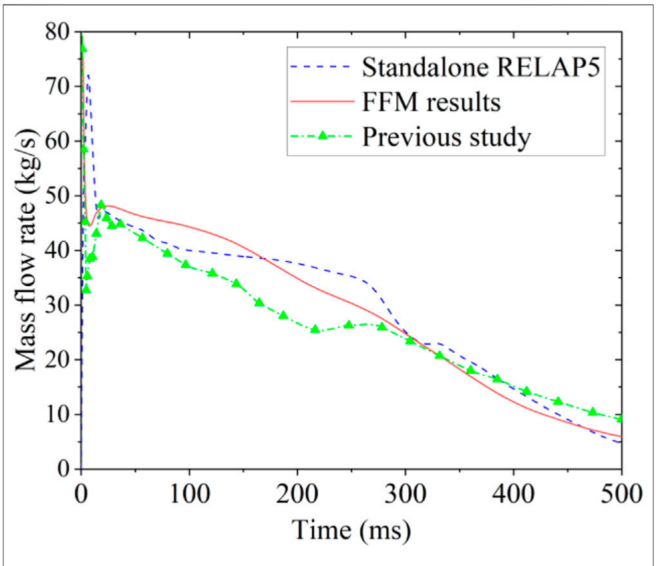

FIGURE 11 | Comparison of the mass flow rate of the mixture at the pipe exit.

falling trend of mass flow also showed a similar relationship with that of the pressure. Although there is a lack of experimental results for the break mass flow rate, the results in this paper were close to those of the standalone RELAP5. It also indicated that the function fitting method encountered smaller errors in the simulation, which weakened the error induced by the coupling parameter.

CONCLUSION

In this paper, a multiscale coupled thermal-hydraulic method was studied, and a coupled RELAP5/Fluent code was developed. To solve the problem of exchanging different dimensional thermal-hydraulic parameters through the coupling interface, the function fitting method was proposed. The physical distribution of different parameters was described by mathematical functions. The Edwards pipe blowdown test was used to verify the multiscale coupled thermal-hydraulic method. The results show that the FFM can help simulate the strong transient process accurately, and it can also improve the calculation accuracy when compared to the previous study that used uniform parameters distribution at the interface.

DATA AVAILABILITY STATEMENT

Due to the intellectual property limitations, the simulation data could not be published to the readers.

AUTHOR CONTRIBUTIONS

All authors listed have made a substantial, direct, and intellectual contribution to the work and approved it for publication.

FUNDING

The present work was supported by the China National Nuclear Corporation Science Fund for Talented Young Scholars (No. 167542).

REFERENCES

Allison, C., Berna, G., Chambers, R., Coryell, E., Davis, K., Hagrman, D., et al. (1993). Report No.: EGG-2720. SCDAP/RELAP5/MOD3. 1 code manual: MATPRO–a library of materials properties for light-water-reactor accident analysis. Volume 4, DT Hagrman, NUREG/CR-6150 .Available at: https://doi.org/10.2172/100327 (Accessed June 01, 1995)

Anderson, N. A. (2006). *Coupling RELAP5-3D and fluent to analyze a very high temperature reactor (VHTR) outlet plenum.* College Station, TX: Texas A&M University.

Andersson, R., Andersson, B., Chopard, F., and Norén, T. (2004). Development of a multiscale simulation method for design of novel multiphase reactors. *Chem. Eng. Sci.* 59, 4911–4917.

Anderson, N., Hassan, Y., and Schultz, R. (2008). Analysis of the hot gas flow in the outlet plenum of the very high temperature reactor using coupled RELAP5-3D system code and a CFD code. *Nucl. Eng. Des.* 238, 274–279. doi:10.1016/j.nucengdes.2007.06.008

ANSYS (2015). CFX multiphase workshop 09: Edwards test modelling a steam line break with the IAPWS EOS *ANSYS.* 9, 1–42.

Aumiller, D. L., Tomlinson, E. T., and Bauer, R. C. (2001). A coupled RELAP5-3D/CFD methodology with a proof-of-principle calculation. *Nucl. Eng. Des.* 205, 83–90. doi:10.1016/S0029-5493(00)00370-8

Aumiller, D. L., Tomlinson, E. T., and Weaver, W. L. (2002). An integrated RELAP5-3D and multiphase CFD code system utilizing a semi-implicit coupling technique. *Nucl. Eng. Des.* 216, 77–87. doi:10.1016/S0029-5493(01)00522-2

Barre, F., and Bernard, M. (1990). The CATHARE code strategy and assessment. *Nucl. Eng. Des.* 124, 257–284. doi:10.1016/0029-5493(90)90296-A

Blasius, H. (1907). *Grenzschichten in Flüssigkeiten mit kleiner Reibung*. Petit: Druck von BG Teubner.

Colebrook, C. F., (1939). Turbulent flow in pipes, with particular reference to the transition region between the smooth and rough pipe laws. *J. Inst. Civil Eng.* 11, 133–156. doi:10.1680/ijoti.1939.13150

Cardoni, J. N. (2011). *Nuclear reactor multi-physics simulations with coupled MCNP5 and STAR-CCM+*. MS thesis. Champaign (IL): University of Illinois at Urbana-Champaign

Edwards, A. T., and O'Brien, T. (1970). *Studies of phenomena connected with the depressurization of water reactors*. Risley, United Kingdom: United Kingdom Atomic Energy Authority.

Egorov, Y., Boucker, M., Martin, A., Pigny, S., Scheuerer, M., and Willemsen, S. (2004). Validation of CFD codes with PTS-relevant test cases. *5th Euratom Framework Programme ECORA project.* 2004, 91–116.

Fang, X., Xu, Y., and Zhou, Z. (2011). New correlations of single-phase friction factor for turbulent pipe flow and evaluation of existing single-phase friction factor correlations. *Nucl. Eng. Des.* 241, 897–902. doi:10.1016/j.nucengdes.2010.12.019

Haaland, S. E. (1983). Simple and explicit formulas for the friction factor in turbulent pipe flow. *J. Fluid Eng.* 105, 89–90.

Höhne, T., Krepper, E., and Rohde, U. (2010). Application of CFD codes in nuclear reactor safety analysis. *Science and Technology of Nuclear Installations.* 2010, 1–8. doi:10.1155/2010/198758

Ivanov, K., and Avramova, M. (2007). Challenges in coupled thermal-hydraulics and neutronics simulations for LWR safety analysis. *Ann. Nucl. Energy.* 34, 501–513. doi:10.1016/j.anucene.2007.02.016

Jeong, J.-J., Ha, K., Chung, B., and Lee, W. (1999). Development of a multi-dimensional thermal-hydraulic system code, MARS 1.3. 1. *Ann. Nucl. Energy.* 26, 1611–1642. doi:10.1016/S0306-4549(99)00039-0

Lee, K., and Ryley, D. J. (1968). The evaporation of water droplets in superheated steam. *J. Heat Trans.* 90, 445–451. doi:10.1115/1.3597540

Li, W., Wu, X., Zhang, D., Su, G., Tian, W., and Qiu, S. (2014). Preliminary study of coupling CFD code FLUENT and system code RELAP5. *Ann. Nucl. Energy.* 73, 96–107. doi:10.1016/j.anucene.2014.06.042

Liao, Y., and Lucas, D. (2017). Possibilities and limitations of CFD simulation for flashing flow scenarios in nuclear applications. *Energies.* 10, 139. doi:10.3390/en10010139

Liao, Y., Lucas, D., Krepper, E., and Rzehak, R. (2013). Flashing evaporation under different pressure levels. *Nucl. Eng. Des.* 265, 801–813. doi:10.1016/j.nucengdes.2013.09.027

Martelli, D., Forgione, N., Barone, G., and di Piazza, I. (2017). Coupled simulations of the NACIE facility using RELAP5 and ANSYS FLUENT codes. *Ann. Nucl. Energy.* 101, 408–418. doi:10.1016/j.anucene.2016.11.041

McFadden, J., Paulsen, M., Gose, G., Peterson, C., McClure, J., and Westacott, P. (1981). Report No.: EPRI NP-1850 CCM. RETRAN-02: A program for transient thermal-hydraulic analysis of complex fluid flow. Available at: https://www.osti.gov/biblio/6627455 (Accessed November 01, 1988)

Moody, L. F. (1944). Friction factors for pipe flow. *Trans. ASME.* 66, 671–684.

Muhlbauer, P. (2003). Review of CFD applications in primary loop and recommendations. *EVOL-ECORA-D02*, 24–47.

Plesset, M. S., and Zwick, S. A. (1954). The growth of vapor bubbles in superheated liquids. *J. Appl. Phys.* 25, 493–500. doi:10.1063/1.1721668

RELAP5-3D Code Development Team %J INEEL-EXT-98-00834, R. (2012). *RELAP5-3D code manual volume I: code structure, system models and solution methods*. Idaho Falls, ID: Idaho National Laboratory.

Rohde, U., Höhne, T., Kliem, S., Hemström, B., Scheuerer, M., Toppila, T., et al. (2007). Fluid mixing and flow distribution in a primary circuit of a nuclear pressurized water reactor—validation of CFD codes. *Nucl. Eng. Des.* 237, 1639–1655. doi:10.1016/j.nucengdes.2007.03.015

Romeo, E., Royo, C., and Monzón, A. (2002). Improved explicit equations for estimation of the friction factor in rough and smooth pipes. *Chem. Eng. J.* 86, 369–374. doi:10.1016/S1385-8947(01)00254-6

Scheuerer, M., Heitsch, M., Menter, F., Egorov, Y., Toth, I., Bestion, D., et al. (2005). Evaluation of computational fluid dynamic methods for reactor safety analysis (ECORA). *Nucl. Eng. Des.* 235, 359–368. doi:10.1016/j.nucengdes.2004.08.049

Schramm, L. L. (2006). *Emulsions, foams, and suspensions: fundamentals and applications*. Hoboken, NJ: John Wiley & Sons.

Stewart, C., Wheeler, C., Cena, R., McMonagle, C., Cuta, J., and Trent, D. (1977). *COBRA-IV: the model and the method*. Richland, WA: Pacific Northwest Labs.

Stewart, C., Cuta, J., Montgomery, S., Kelly, J., Basehore, K., George, T., et al. (1989). *VIPRE-01: a thermal-hydraulic code for reactor cores*. Palo Alto, CA: Electric Power Research Inst. Richland, WA: Pacific Northwest Lab.

von Karman, T. (1937). On the statistical theory of turbulence. *Proc. Natl. Acad. Sci. U. S. A.* 23, 98–105. doi:10.1073/pnas.23.2.98

Weaver, W. L., III (2005). Report No.: INL/EXT-05-00107. The application programming interface for the PVMEXEC program and associated code coupling system. Citeseer. , Available at: https://doi.org/10.2172/911219 (Accessed December 15, 2012)

Weaver, W. L., Tomlinson, E. T., and Aumiller, D. L. (2002). A generic semi-implicit coupling methodology for use in RELAP5-3D ©. *Nucl. Eng. Des.* 211, 13–26. doi:10.1016/S0029-5493(01)00422-8

Yıldırım, G. (2009). Computer-based analysis of explicit approximations to the implicit Colebrook–White equation in turbulent flow friction factor calculation. *Adv. Eng. Software.* 40, 1183–1190. doi:10.1016/j.advengsoft.2009.04.004

Conflict of Interest: The authors declare that the research was conducted in the absence of any commercial or financial relationships that could be construed as a potential conflict of interest.

frontiers in Energy Research

ORIGINAL RESEARCH
published: 12 February 2021
doi: 10.3389/fenrg.2021.641661

Data-Driven-Based Forecasting of Two-Phase Flow Parameters in Rectangular Channel

Qingyu Huang*, Yang Yu*, Yaoyi Zhang, Bo Pang, Yafeng Wang, Di Chen and Zhixin Pang

Science and Technology on Reactor System Design Technology Laboratory, Nuclear Power Institute of China, Chengdu, China

In the current nuclear reactor system analysis codes, the interfacial area concentration and void fraction are mainly obtained through empirical relations based on different flow regime maps. In the present research, the data-driven method has been proposed, using four machine learning algorithms (lasso regression, support vector regression, random forest regression and back propagation neural network) in the field of artificial intelligence to predict some important two-phase flow parameters in rectangular channels, and evaluate the performance of different models through multiple metrics. The random forest regression algorithm was found to have the strongest ability to learn from the experimental data in this study. Test results show that the prediction errors of the random forest regression model for interfacial area concentrations and void fractions are all less than 20%, which means the target parameters have been forecasted with good accuracy.

Keywords: data-driven method, two-phase flow, machine learning, interfacial area concentration, random forest regression

Edited by:
Xianping Zhong,
University of Pittsburgh, United States

Reviewed by:
Cenxi Yuan,
Sun Yat-Sen University, China
Jiankai Yu,
Massachusetts Institute of Technology, United States

****Correspondence:***
Qingyu Huang
huangqingyu950802@163.com
Yang Yu
yuzhaoyang1987@sina.com

Specialty section:
This article was submitted to Nuclear Energy, a section of the journal Frontiers in Energy Research

Received: *14 December 2020*
Accepted: *07 January 2021*
Published: *12 February 2021*

Citation:
Huang Q, Yu Y, Zhang Y, Pang B, Wang Y, Chen D and Pang Z (2021) Data-Driven-Based Forecasting of Two-Phase Flow Parameters in Rectangular Channel. Front. Energy Res. 9:641661. doi: 10.3389/fenrg.2021.641661

INTRODUCTION

In various industrial equipment of nuclear power systems, gas-liquid two-phase flow phenomenon is widespreaded. Research on the two-phase flow plays an important role in improving the safety and operational reliability of evaluation system equipment. At present, in traditional commercial nuclear reactor system safety analysis softwares such as Reactor Excursion and Leak Analysis Program (RELAP) 5 (Martin, 1995) and CATHARE (Barre and Bernard, 1990), two-fluid models are widely used in the two-phase flow and heat transfer processes. In order to improve the calculation accuracy of the two-fluid model, it is necessary to provide more accurate closure models for the two-fluid model, and the interface transport term must be accurately simulated (Guo, 2002). The interface transport term can be expressed as the product of the interfacial area concentration and interfacial transport driving force where the interfacial area concentration is defined as the interfacial area per unit mixture volume, which represents the effective area for mass-energy exchange between different phases. For two-phase flow system, the interfacial area concentration and void fraction are also two of the most important parameters.

In view of the importance of parameters such as the interfacial area concentration, a variety of measurement methods have been developed to obtain experimental data, such as probe method, high-speed camera method, chemical method, etc., and different types of empirical correlations have been established based on a large amount of data (Ishii, 1975; Kocamustafaogullari and Ishii, 1995; Su, 2013). However, the scope of application of these empirical correlations is relatively limited. Moreover, the acquisition of experimental data is costly with typical local features.

In recent years, with the continuous development of computer hardware, computing power as well as data collection and storage technology, artificial intelligence technology has made a qualitative leap in emerging applications and development in various fields. However, in the field of engineering, especially nuclear engineering, the application of data-driven methods, whether it is fault diagnosis, equipment health management or other aspects, is still subject to certain restrictions. There are many prediction and analysis methods based on data-driven routes, including machine learning, deep learning, information fusion, statistical analysis methods, signal processing analysis methods, etc. (Gammerman, 1996).

Machine learning (including deep learning), as known as the cornerstone of artificial intelligence technology, has become a popular research field in recent years. Implementation of machine learning completely starts from collecting operating parameters, constructing data analysis models through the learning of historical data, and then is conducted by using the trained models to give a predicted output for the actual input parameters. A review of the research and development status of learning-based methods used in reactor health and management, radiation detection and protection, as well as optimization illustrated that, at present, more and more researchers in various fields of nuclear science are showing enthusiasm for the data-driven parameters or states predictions, and these methods have become more practical with the rising of deep learning and other techniques in the past decade (Gomez-Fernandez et al., 2020). The most important application of machine learning in reactor health management is to use sensor data for parameter prediction and state classification to perform tasks such as stateful inspection, fault diagnosis, and life prediction control. Among them, Tennessee Valley Authority Sequoyah Nuclear Plant uses the artificial neural network to determine the variables that affect the heat rate and thermal performance (Guo and Uhrig, 1992). Advanced optimization algorithms are used to estimate local power peaking factor estimation in nuclear fuel (Montes et al., 2009). Nuclear reactor thermal-hydraulic research area has also shown interests in the application of machine learning: for instance, flow regime identification (Tambouratzis and Pàzsit, 2010), prediction of two-phase mixture density (Lombardi and Mazzola, 1997) and expert decision support systems trained by deep neural networks/long short-term memory which is developed to predict the progression of LOCA (Radaideh et al., 2020).

The data-driven method is more desired where the prediction task is more complex due to the enhancement of the data availability and reduce computational difficulty in some cases. In the present work, data-driven method is introduced in predicting two-phase flow parameters in rectangular channels, namely interfacial area concentration and voidfraction, by using four machine learning models: lasso regression, support vector regression, random forest regression and back propagation neural network. Additionally, the performance of four models for different parameters prediction will be discussed and compared in the present work. The remaining sections of this paper are organized as follows: Section *Data Acquisition* describes the experimental equipment and the process of data acquisition. The algorithms adopted in this paper are presented in Section *Algorithm*. The methods and test results of this paper are presented in Section *Methodology*. The result is further analyzed and discussed in Section *Discussion*. The conclusions drawn from this study are given in Section *Conclusion*.

DATA ACQUISITION

Introduction to the Experimental System

This experimental platform is shown in **Figure 1**, which can carry out the research of the vertical air-water two-phase flow in the channels with various cross-sectional area under normal temperature and pressure conditions. **Figure 1** is a schematic diagram of the experimental system, and **Figure 2** is the scene photo of the experimental system.

The experimental platform is mainly composed of water supply system, air supply system, air-water mixer, experimental section, instrumentation, and data acquisition system. The main part of experimental device is a rectangular channel with the total length of the experimental section about 1,500 mm and the channel size of 66 × 6 mm. The experimental section is all processed and bonded with transparent acrylic material for experimental observation. Four pressure measuring setpoints are distributed in the axial position, namely the entrance and three positions of the impedance void meters. The experiment uses three sets of electrodes as the void meters, and the measurement data can also be used for flow pattern identification and calibration. Conductivity probes are arranged at the position of the void meters to obtain local physical parameters such as the interfacial area concentration, void fraction, and bubble velocity. In order to provide a clear and intuitive explanation for the measurement data of the void meters and the conductivity probe, a high-speed camera is placed near the void meters and the conductivity probes. The probe measuring setpoints are arranged in the radial position with 30 ∼ 31 measuring setpoints, and the measuring setpoint arrangement positions are shown in **Figure 3**, where X represents the radial distance of the probes.

The specific experimental parameter ranges are shown in **Table 1** and the range of experimental conditions is shown in **Figure 4**. The experimental conditions are obtained by different flow regime. Black dots represent bubbly flow, red dots represent slug flow, green dots represent churn-turbulent flow, and blue dots represent annular flow. As far as the maximum uncertainty of the experiment is concerned, the values of liquid flow measurements, gas flow measurements, probe voltage acquisition, probe tip size measurements, and void meters are 3.2, 2.45, 1.23, 2 and 2.01%, respectively.

ALGORITHM

This chapter introduces the machine learning algorithms and principles used in this research, including lasso regression

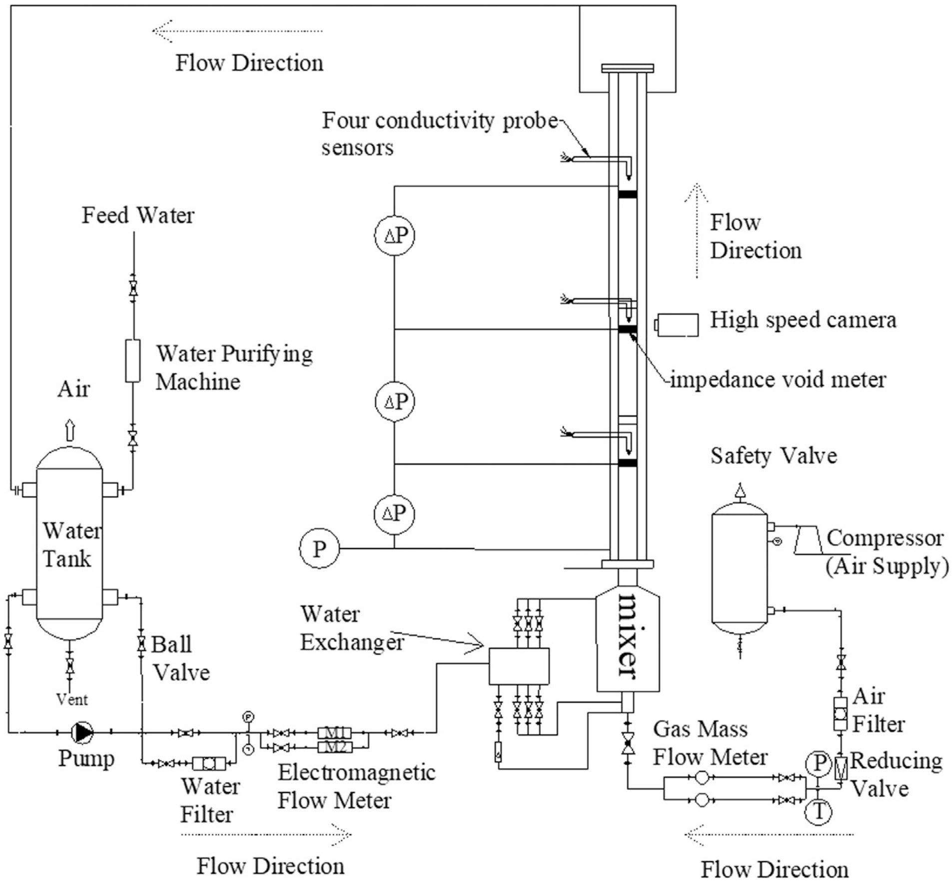

FIGURE 1 | Schematic diagram of the experimental loop system.

FIGURE 2 | A photograph of experimental system.

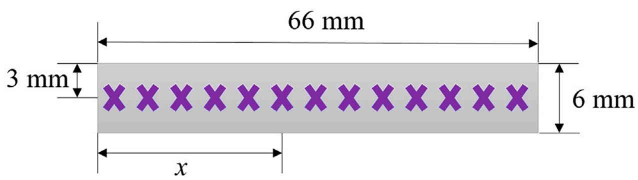

FIGURE 3 | The schematic of probe measuring setpoints in the radial position.

(LR), support vector regression (SVR), random forest regression (RFR) and back propagation neural network (BPNN).

Lasso Regression

Multiple linear regression refers to the study of the influence of changes in independent variables $\boldsymbol{x}_1, \boldsymbol{x}_2, \ldots, \boldsymbol{x}_m$ on dependent variable $\boldsymbol{y}$. The model can be expressed as:

$$y = \beta_0 + \beta_1 x_1 + \beta_2 x_2 + \cdots + \beta_m x_m + \varepsilon, \tag{1}$$

where $\beta_0, \beta_1, \beta_2, \ldots, \beta_m$ are unknown coefficients and ε is the independent identically distributed normal error.

In order to solve **Eq. 1**, methods such as least squares are usually used to estimate the parameters of the regression model from the perspective of error fitting, and the optimization goal can be expressed in matrix form as:

TABLE 1 | Experimental parameters of the rectangular channel.

Experimental section	Rectangle
Pipe size w × s/mm	6 × 66
Length L_1/mm	1,500
Measuring point location L_2/mm	266, 926, 1,482
Superficial gas velocity (j_g) m/s	0–10
Superficial liquid velocity (j_f) m/s	0–3
Temperature	Ambient temperature
Pressure	Ordinary pressure

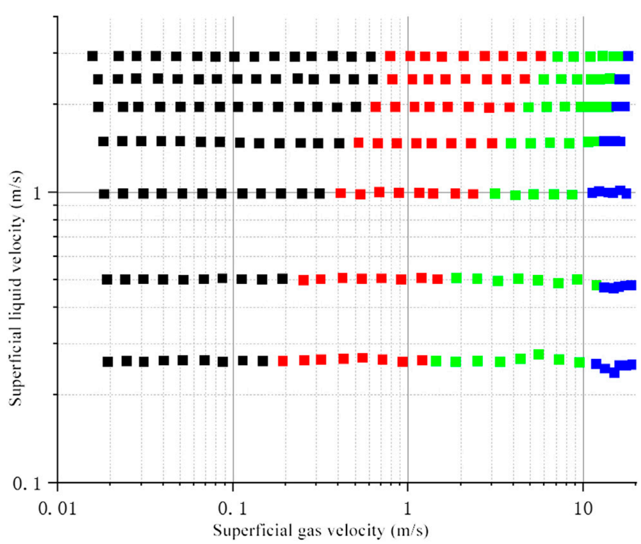

FIGURE 4 | Schematic diagram of experimental conditions.

$$\beta^* = \text{argmin}_\beta \frac{1}{m}\|y - X\beta\|^2 \tag{2}$$

However, the least squares method still has some shortcomings when facing multiple input features, for instance its unbiased estimation characteristics will lead to large variance. Lasso regression (least absolute shrinkage and selection operator) was proposed by Robert Tibshirani in 1996 based on Leo Breiman's non-negative garrote (Breiman, 1995; Tibshirani, 1996). It is a shrinkage estimation algorithm and its basic idea is to minimize the residual sum of squares under the constraint that the sum of the absolute values of the regression coefficients is less than a constant, and to reduce the non-zero components in the regression coefficients, thereby improving the accuracy of the prediction and the interpretability of the regression model. The objective equation of the lasso algorithm is:

$$\beta^* = \text{argmin}_\beta \frac{1}{m}\|y - X\beta\|^2 + \lambda\|\beta\| \tag{3}$$

where y is target variable, β is regression coefficient vector, X is the data matrix corresponding to explanatory variables and λ is the penalty parameter. Lasso regression is a quadratic programming problem that the solving algorithms include shooting algorithm, homotopy algorithm, etc.

Support Vector Regression

Support vector machine was originally used to deal with pattern recognition problems (Vapnik, 1998), but its sparse solution and good generalization make it suitable for regression problems. The generalization from SVM to SVR is accomplished by introducing an ε-tube, which reformulates the optimization problem to find the best approximation of the continuous-valued function, while balancing complexity and prediction error of prediction model. For nonlinear support vector machine regression, the basic idea is to map the data x to the high-dimensional Hilbert space $\phi(x)$ through a nonlinear mapping ϕ, and seek the regression linear hyperplane in this space, thereby solving the highly non-linear problems in the low-dimensional space. The linear model in the high-dimensional feature space is constructed as follows:

$$f(x) = \langle w \cdot \phi(x)\rangle + b, \tag{4}$$

where w is the weight vector, b is the bias constant and $\langle w \cdot \phi(x)\rangle$ is the inner product of the feature space. The optimal hyperplane regression estimation function is converted as follows:

$$f(x) = \sum_{i=1}^{n} (a_i - a_i^*) k(x_i, x_j) + b, \tag{5}$$

where a_i and a_i^* are lagrange multipliers, $k(x_i, x_j) = \phi(x_i) \cdot \phi(x_j)$ is kernel function. The types of kernels include polynomial kernel, Gauss radial basis function kernel, and sigmoid kernel, etc. while radial basis function kernel (RBF kernel) is selected as the kernel function in the present study because in some researches RBF kernel has been pointed out be appropriate for nonlinear systems, which is expressed as (Zhang and Li, 2006):

$$k(x_i, x_j) = e^{-\left(\|x_i - x_j\|^2 \div \sigma^2\right)} \tag{6}$$

Random Forest Regression

Random forest is an ensemble algorithm proposed by Breiman in 2001 (Breiman, 2001a; Breiman, 2001b). In general, the random forest shown in **Figure 5** is composed of multiple CART decision trees, which conducts classification or regression through bagging (bootstrap aggregating). The main idea of random forest regression method (RFR) is to extract multiple samples from the original sample, build a decision tree for each sample, and then use the average of all decision tree predictions as the final prediction result. RFR was pointed out that it has the advantages

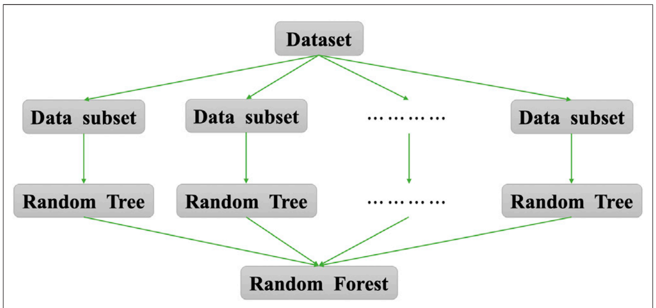

FIGURE 5 | The structure of Ramdom Forest.

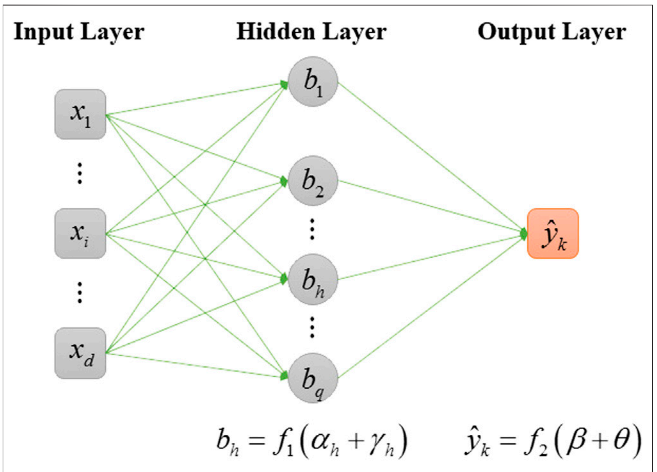

FIGURE 6 | Basic structure of BP neural network.

of fast training speed, strong adaptability to high-dimensional data sets, and strong robustness in the face of noise (Segal, 2004).

In principle, the random forest regression (RFR) is composed of a set of sub-decision trees $\{h(x, \theta_t), t = 1, 2, 3, \ldots T\}$, where θ_t is a random variable subject to independent and identical distribution, x represents the independent variable, and T represents the number of decision trees.

RFR uses the results of integrating multiple decision trees to take the mean value of $\{h(x, \theta_t)\}$ as the regression prediction result to eliminate the problems of overfitting and low precision of the decision tree model. The result is expressed as

$$\overline{h}(x) = \frac{1}{T}\sum_{t=1}^{T}\{h(x, \theta_t)\} \tag{7}$$

The RFR algorithm implementation process is as follows:

(1) Bagging is used to randomly generate sample subsets.
(2) Use the idea of random subspace by randomly extracting features, splitting nodes and building a regression sub-decision tree.
(3) Repeat the above steps to construct T regression decision subtrees to form a random forest (Pruning and other human intervention is not allowed in the process).
(4) Take the predicted values of T sub-decision trees and take the mean as the final prediction result.

Back Propagation Neural Network

Artificial neural network is a widely parallel interconnected network composed of adaptable simple units; its organization can simulate the interactive response of the biological neural system to real world objects (Kohonen, 1988). In the development of artificial neural networks, the error back-propagation algorithm occupies an important place (McClelland et al., 1986). The network based on this algorithm is referred to as BP network, which consists of one input layer, at least one hidden layer, and one output layer. The usually constructed BP neural network is a three-layer network. For regression prediction, the output layer usually has only one neuron.

Given the training set $D = \{(\boldsymbol{x}_1, y_1), (\boldsymbol{x}_2, y_2), \ldots, (\boldsymbol{x}_m, y_m)\}$, where $\boldsymbol{x}_i \in \mathbb{R}^d$, $y_i \in \mathbb{R}$. **Figure 6** shows a BP neural network with d input neurons, one output neuron, and q hidden layer neurons. The threshold of the output layer neuron is represented by θ, and the threshold of the h-th neuron in the hidden layer is represented by γ_h. The connection weight between the i-th neuron in the input layer and the h-th neuron in the hidden layer is v_{ih}, and the connection weight between the h-th neuron in the hidden layer and the output layer neuron is ω_h. The input received by the h-th neuron in the hidden layer is $\alpha_h = \sum_{i=1}^{d} v_{ih} x_i$, and the input received by the output layer neuron is $\beta = \sum_{h=1}^{q} \omega_h b_h$, where b_h is the output of the h-th neuron in the hidden layer.

For training example $(\boldsymbol{x}_k, y_k)$, assuming that the output of the neural network is $\hat{y}_k \in \mathbb{R}$, that is

$$\hat{y}_k = f_2(\beta + \theta) \tag{8}$$

Then the mean-square error of the network on $(\boldsymbol{x}_k, y_k)$ is

$$E_k = \frac{1}{2}(\hat{y}_k - y_k)^2 \tag{9}$$

For the hidden layer, we have

$$b_h = f_1(\alpha_h + \gamma_h) \tag{10}$$

where $f_1(\cdot)$ and $f_2(\cdot)$ are both activation functions. In consideration of regression prediction, $f_1(\cdot)$ in ourstudy is ReLU function, i.e.

$$f_1(x) = \max(0, x) \tag{11}$$

The function $f_2(\cdot)$ is preferable to the purelin function, i.e.

$$f_2(x) = x \tag{12}$$

The BP algorithm is based on a gradient descent strategy and adjusts the parameters in the direction of the negative gradient of the target. For the error E_k, given the learning rate η, we have

$$\Delta\omega_h = -\eta\frac{\partial E_k}{\partial \omega_h} = \eta(y_k - \hat{y}_k)f_1(\alpha_h + \gamma_h) \tag{13}$$

$$\Delta\theta = -\eta\frac{\partial E_k}{\partial \theta} = \eta(y_k - \hat{y}_k) \tag{14}$$

$$\Delta v_{ih} = -\eta\frac{\partial E_k}{\partial v_{ih}} = \eta(y_k - \hat{y}_k)\omega_h f_1'(\alpha_h + \gamma_h)x_i \tag{15}$$

$$\Delta\gamma_h = -\eta\frac{\partial E_k}{\partial \gamma_h} = \eta(y_k - \hat{y}_k)\omega_h f_1'(\alpha_h + \gamma_h) \tag{16}$$

The flow of BP algorithm is as follows:

(1) Set the network structure, input layer, hidden layer, output layer and learning rate η, where the output layer node number is set to 1;
(2) Randomly initialize the connection weight v_{ih}, ω_h and the threshold γ_h, θ in the network within the range of $(0, 1)$;
(3) Randomly select a training sample $(\boldsymbol{x}_k, y_k)$, and calculate the output $\hat{y}_k$ of the current sample according to the current parameters and **Eq. 8**;

TABLE 2 | The selected hyperparameters for each output.

Model	Hyperparameters	Group-I interfacial area concentration	Group-II interfacial area concentration	Group-I void fraction	Group-II void fraction
LR	Regularization parameter λ	0.1	0.0001	0.0001	0.0001
RFR	Number of trees	50	100	50	150
RFR	The maximum depth of the tree	11	11	11	11
RFR	Random state	9	7	5	9
SVR	Kernel function	Rbf	Rbf	Rbf	Rbf
SVR	Kernel coefficient	0.1	0.1	0.0556	0.1
SVR	Regularization parameter	100	100	100	94.74
SVR	Size of the kernel cache (MB)	50,000	50,000	50,000	50,000
BPNN	Batch size	256	512	512	512
BPNN	Epochs	200	300	150	200
BPNN	Processing units	128	128	128	128
BPNN	Learning rate	0.05	0.05	0.001	0.001
BPNN	Activiation function	ReLU	ReLU	ReLU	ReLU

(4) Calculate the weight correction $\Delta\omega_h$, Δv_{ih} and the threshold correction $\Delta\theta$, $\Delta\gamma_h$ according to **Eqs 13–16**;
(5) Update connection weights and thresholds:

$$\begin{gathered}\omega_h \leftarrow \omega_h + \Delta\omega_h,\\ v_{ih} \leftarrow v_{ih} + \Delta v_{ih},\\ \theta \leftarrow \theta + \Delta\theta,\\ \gamma_h \leftarrow \gamma_h + \Delta\gamma_h.\end{gathered}$$

(1) Go back to step 3) until all the training data are input;
(2) Go back to steps 2)–6) until the stop condition is reached.

METHODOLOGY

Data Preprocessing

In two-phase flow, considering the difference between the bubbles of different shapes and sizes, the bubbles were usually categorized into two bubble groups: group-I represents small-dispersed and distorted bubbles, whereas group-II represents cap/slug/churn-turbulent bubbles. (Ishii et al., 2002). Therefore, the interfacial area concentrations and void fractions are described by different bubbles characteristics of group-I and group-II respectively. The present research is based on real experimental measurement data that selects the axial distance Z, the radial distance X, superficial gas velocity J_g and superficial liquid velocity J_f as input features, and takes group-I interfacial area concentration, group-II interfacial area concentration, group-I void fraction, and group-II void fraction as outputs.

Since the units and dimensions of each input parameter are not the same, the data needs to be standardized before modeling. In this study, the mean variance normalization method was used to make the processed data set conform to the standard normal distribution, with a standard deviation of 1 and a mean of 0. The specific formula is as follows:

$$d_{norm} = (d - \mu)/\sigma, \tag{17}$$

where d_{norm} is the standardized data set, d is the original data set, μ is the average value, and σ is the standard deviation.

Model Performance Metrics

In this study, the coefficient of determination (R^2), the root-mean-square error (RMSE) and the coefficient of variation (CV) were selected as evaluation indicators of model performances. Supposing a series of data sets $y_1, \ldots, y_n$ includes n data points, and their corresponding model prediction values are $p_1, \ldots, p_n$.

The expression of the coefficient of determination R^2 is

$$\mathrm{R}^2 \equiv 1 - \frac{\sum_i (y_i - p_i)^2}{\sum_i (y_i - \bar{y})^2}, \tag{18}$$

where the closer the value of R^2 is to 1, the better the effect of model fitting.

The expression of RMSE is

$$\mathrm{RMSE} = \sqrt{\frac{1}{\mathrm{m}} \sum_{i=1}^{m} (y_i - p_i)^2}, \tag{19}$$

where m represents the number of samples, and the smaller the value, the smaller the error between the model prediction result and the true value.

In order to introduce the concept of percentage error rate to further explore the performance of the model, this paper selects the coefficient of variation (CV) to describe the model. The expression of the CV is

$$\mathrm{CV} = \frac{\sqrt{(1/m)\sum_{i=1}^{m} (y_i - p_i)^2}}{y} \times 100\% \tag{20}$$

When describing the model, the CV for a model aims to describe the model fit in terms of the relative sizes of the squared residuals and outcome value. The range of CV is between 0 and 100%. The smaller CV is, the more accurate the prediction of the model is.

Hyperparameters Tuning

In this study, the hyperparameter tuning process of four different models is implemented from using grid search

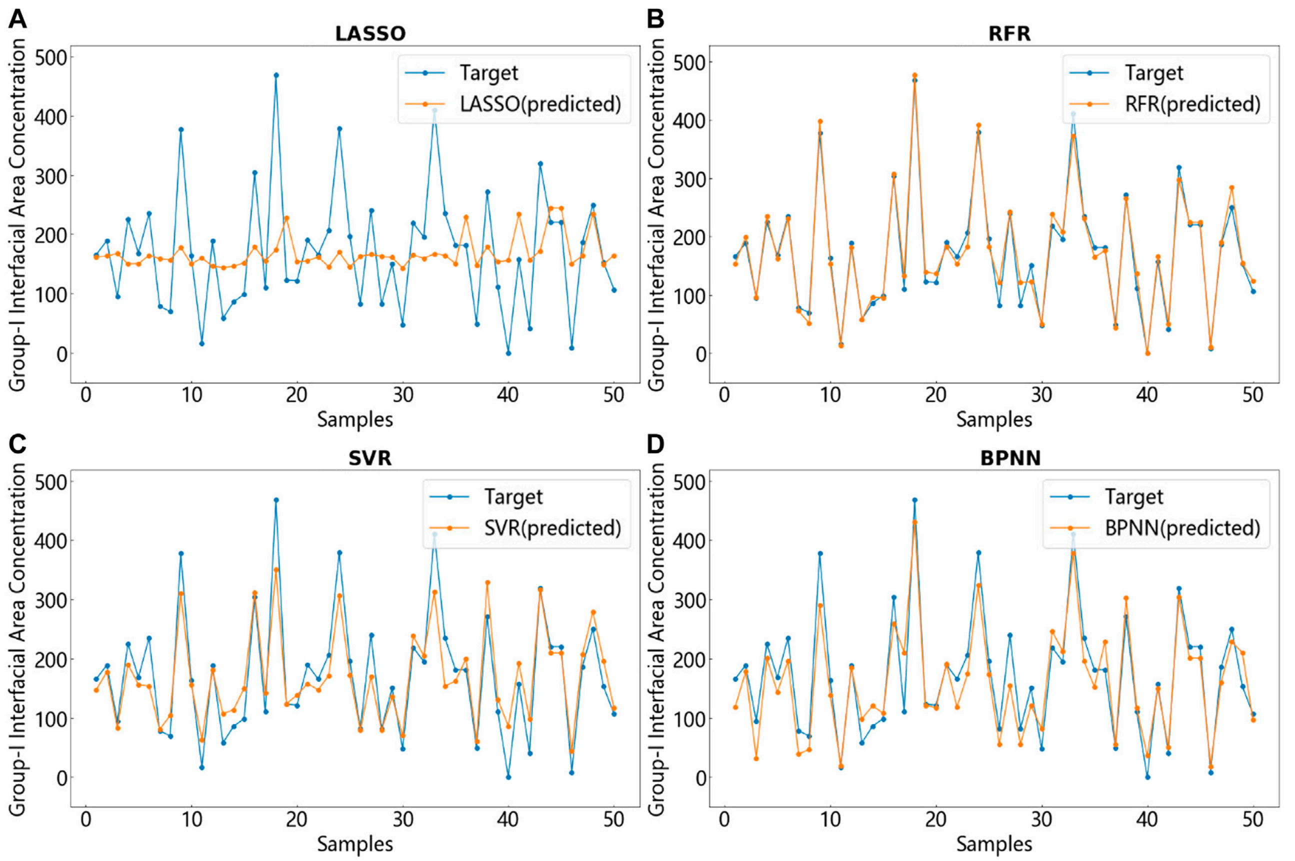

FIGURE 7 | Prediction of the group-I interfacial area concentration using four models and comparison with target values. **(A)** LASSO. **(B)** RFR. **(C)** SVR **(D)** BPNN.

method. The basic principle is to divide the interval of each parameter variable value into a series of small areas, and calculate the corresponding the target value (error in usual) determined by the combination of each hyperparameter variable values, and select the best one by one to obtain the minimum target value in the interval and its corresponding optimal hyperparameter. This method ensures that the search solution obtained is globally optimal or close to optimal. The hyperparameters optimization process in this study also considers the limits of the accuracy of the running results and the computational efficiency. However, the calculation time is not included in the model metric in this study.

For LR regression, the regularization parameter λ from **Eq. 3** is considered to be the most important indicator that affects the accuracy of the model. In theory, the larger the regularization parameter, the stronger the model's robustness against collinearity. However, if the regularization parameter is selected too big, all parameters β will be minimized, resulting in under-fitting. If the regularization parameter is selected too small, it will lead to improper solution to the over-fitting problem. When predicting the four sets of two-phase flow parameters, in order to expand the search for the appropriate range of λ, 50 sets of λ were selected for model optimization: an arithmetic sequence between 0.0001 and 0.1 (including 25 numbers) and an arithmetic sequence between 0.1 and 100 (including 25 numbers).

For the RFR model, the number of trees in the forest, the maximum depth of the tree and random state are commonly considered to be the key parameters that affect the performance of the model. Due to the few dimensions of input variables in this study, another hyperparameter that is often considered, namely the number of features to consider when looking for the best split, defaults to the maximum value 4 in this study. The three hyperparameters mentioned above are optimized using grid searchwith bounds selected as:

- the number of trees with bound: 50–250
- the maximum depth of the tree: 7–12
- random state: 1–12

For the SVR model, the kernel function is the RBF kernel which is better for nonlinear problems. Three major hyperparameters are also optimized using grid search with bounds selected as follows:

- Kernel coefficient with bound: 0.001–0.1
- Regularization parameter with bound: 0.1–100
- Size of the kernel cache (MB): 10,000–50,000

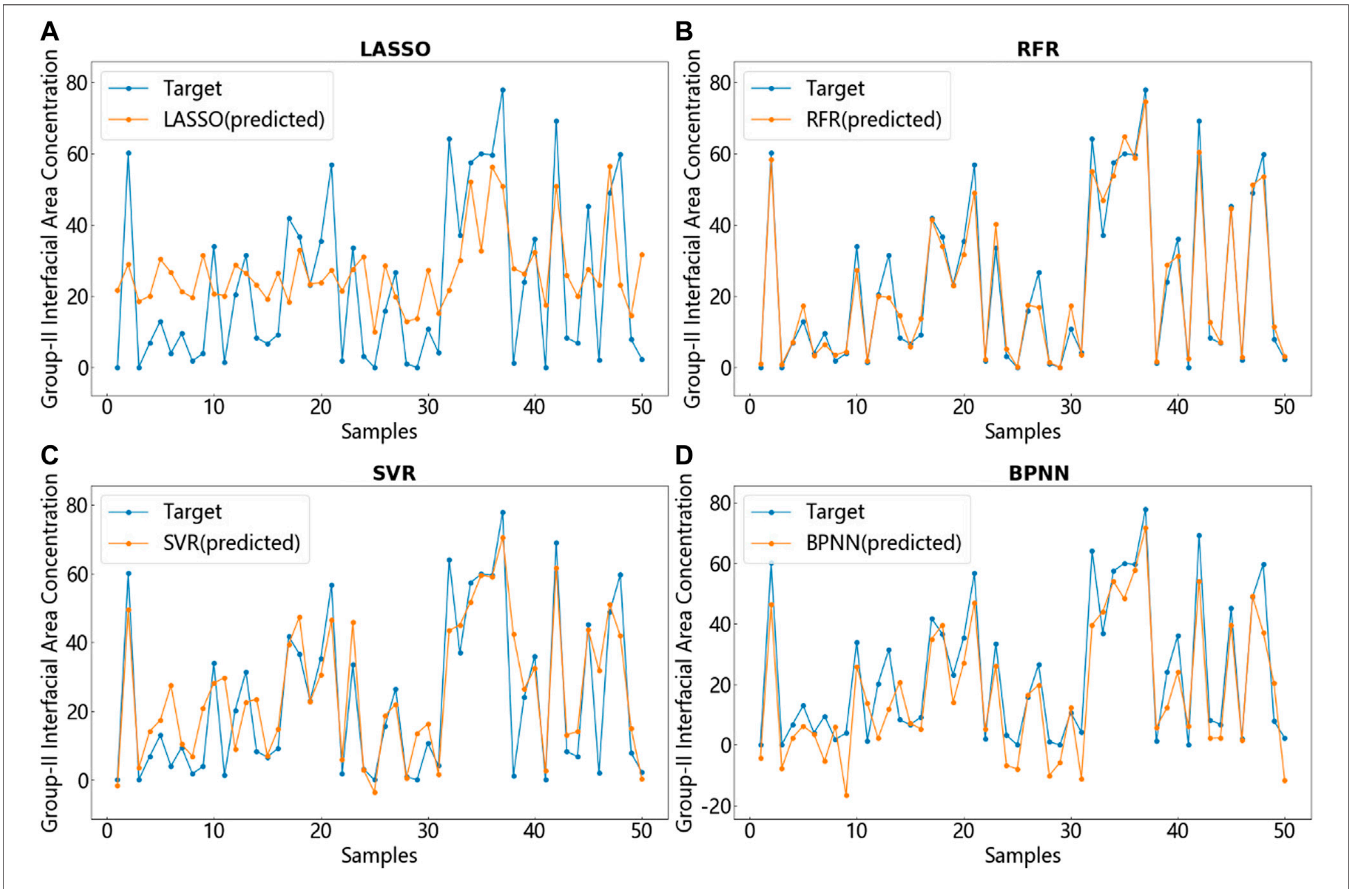

FIGURE 8 | Prediction of the group-II interfacial area concentration using four models and comparison with target values. **(A)** LASSO. **(B)** RFR. **(C)** SVR **(D)** BPNN.

Last but not least, for BPNN model, five major hyperparameters are optimized using grid search with bounds selected as follows:

- Batch size with bound: 512–1,024
- Epochs with bound:150–500
- Processing units: 64–128
- Learning rate: 0.001–0.05
- Activiation function: ReLU

The results of the optimum architecture of four models are listed in **Table 2**. It is worth mentioning that we directly selected ReLU, a piecewise linear function which is proven to be most effective for BP-NN (Nair and Hinton, 2010).

Model Training, Validation and Testing

The calculations of models were performed using an Apple laptop with Mac OS system (version 10.15), core Intel i5 5257U, 8 GB of RAM, and Intel Iris Graphics 6100 card with 1536 MB of the RAM. The utilization and implementation of the models in this study are done in the Python environment (Van Rossum and Drake, 1995).

For common machine learning problems, the data should be divided into training set, validation set and test set. The training set is used for model fitting, the validation set is used to adjust the hyperparameters of the model to prevent the model from overfitting and to make an initial assessment of the model's ability, and the test set is used to evaluate the generalization ability of the final model. In this study, all data were first divided into training set and test set at a ratio of 9:1. Cross-validation is selected as the method of model validation in the present work. Compared with the ordinary way with fixed validation set, cross-validation (Kohavi, 1995) contributes to obtain as much effective information as possible from the limited learning data. In general, the principle of cross-validation is to learn training samples from multiple directions, which can effectively avoid falling into local minimums and to a certain extent avoid over-fitting problems. In this study, the K-fold cross-validation method is used to achieve cross-validation whose idea is to divide the training set into k sub-samples, where a single sub-sample is retained as the data for the validation model, and the other k-1 samples are used for training. Cross-validation is conducted by repeating k times and each sub-sample is validated once. Hence, mean value of k-times' validation, or other combination methods are used to obtain a single final estimate. In this study, the most used cross validation method, namely 10-fold cross-validation was selected (McLachlan et al., 2005). In this study, assuming that a group of corresponding inputs and outputs are regarded as a data set, the number of data sets is 3,146 in total.

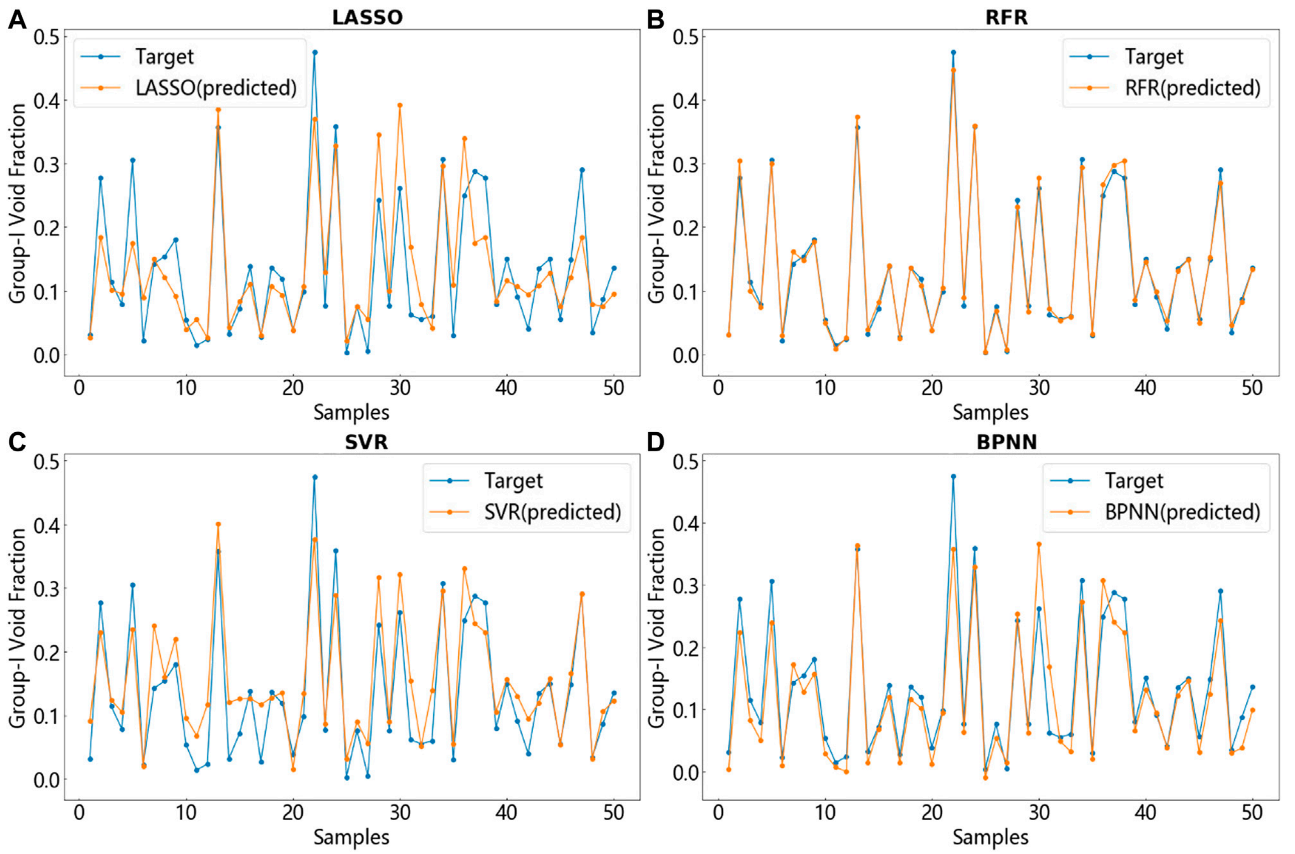

FIGURE 9 | Prediction of the group-I void fraction using four models and comparison with target values. **(A)** LASSO. **(B)** RFR. **(C)** SVR **(D)** BPNN.

DISCUSSION

In the previous section, the route that four two-phase flow parameters obtained from rectangular channel experiments are modeled and predicted by LR, RFR, SVR, and BPNN is introduced in detail. **Figures 7–10** respectively show the comparison between a part of the test set data and its corresponding real data. The blue line is the target data, that is, the true value while the orange-red line is the predicted value generated by the model. Each figure shows the comparison of the predictive capabilities of the four models for a single output. The unit of interfacial area concentration is $1/m$, and void fraction is a dimensionless parameter.

A phenomenon that can be clearly judged from the results shows that although each picture only takes 50 test set points (about 1/6 of the total number of test sets) and the corresponding real values for visual display, a strong nonlinear characteristic is still showed by the real data set. It can be seen from **Figures 7–10** that the predictive ability of LR is far inferior to the other three models. As a type of linear regression shipped with L1 regularization, one of the most crucial advantages of LR over non-linear models is LR usually performs great if the independent variables are linearly correlated with the dependent variable. However, non-linearity and scattered data features are obviously very disadvantageous and difficult for the LR algorithm because of its difficulty to capture the nonlinearity of dataset.

The performance of four models was measured by three metrics: R^2, RMSE and CV which are listed in **Table 3**. From the general distribution of the data, all models have significantly better predictive ability for group-I interfacial area concentration than group-II interfacial area concentration. Similarly, the predictive ability of all models for group-I void Fraction is significantly better than group-II void fraction. This phenomenon is consistent with the basic mechanism of two-phase flow, that is, the shape and size of the bubbles at the first interface are usually more regular and easier to predict than the bubbles at the second interface.

From the comparison of R^2 in **Table 3**, SVR and BPNN are significantly weaker than RFR in explaining experimental data in the present work. For the support vector regression, the prediction error CV of the model for the four outputs is in the range of 26–48%, reflecting that there is still a certain gap between its prediction performance and actual experimental data. It is undeniable that the main advantages of SVR are that its computing power and complexity which do not depend on the dimensionality of the input space, its flexibility in dealing with nonlinear data, and its stability in dealing with slight changes in data (Awad and Khanna, 2015). However, one of the most prominent drawbacks of SVR is, for samples with

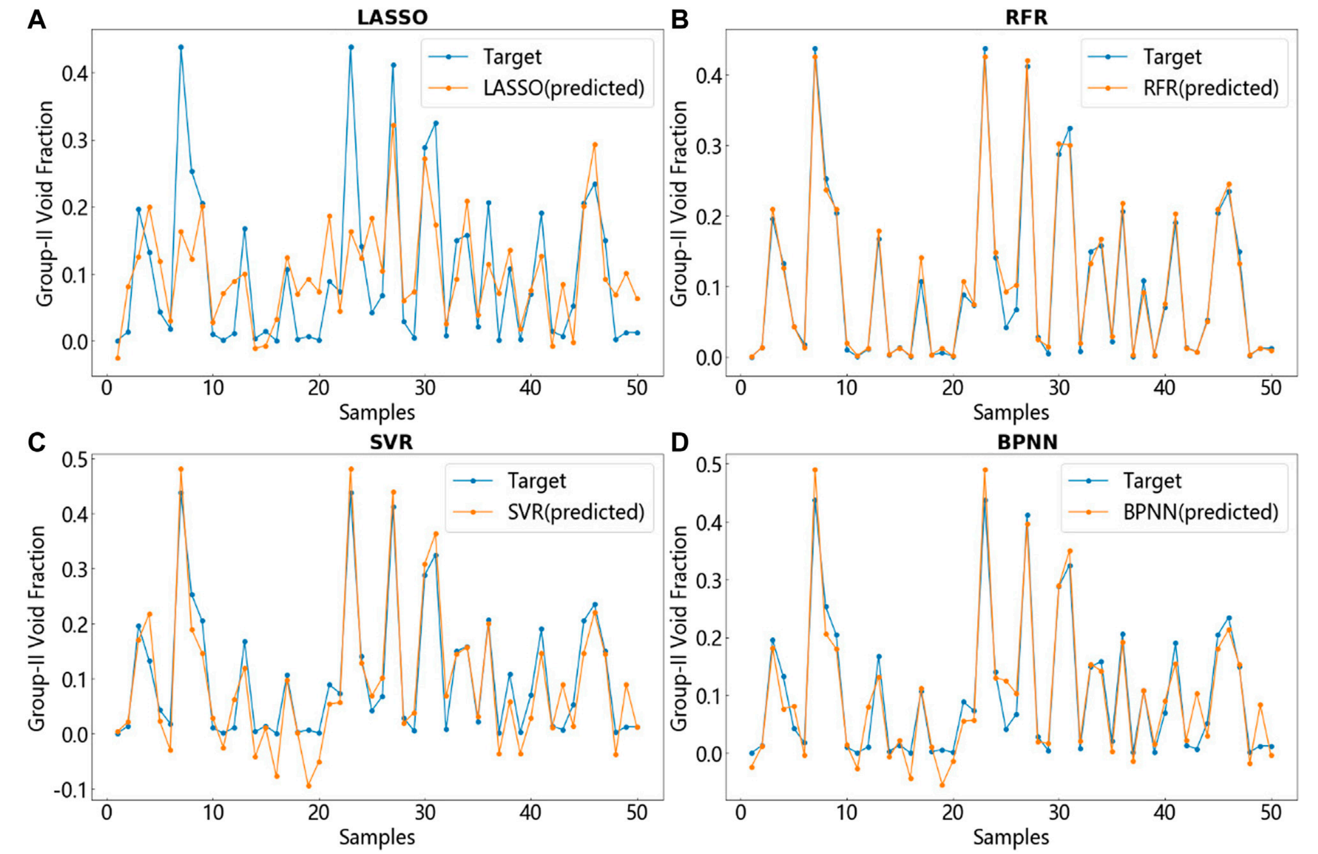

FIGURE 10 | Prediction of the group-II void fraction using four models and comparison with target values. **(A)** LASSO. **(B)** RFR. **(C)** SVR **(D)** BPNN.

TABLE 3 | The learning ability of the four models derived from the test set in terms of four two-phase flow parameter changes.

Metrics	Group-I interfacial area concentration			Group-II interfacial area concentration			Group-I void fraction			Group-II void fraction		
	R^2	RMSE	CV	R^2	RMSE	CV	R^2	RMSE	CV	R^2	RMSE	CV
LR	0.0625	94.35	56.48%	0.2533	19.83	75.50%	0.7767	0.046	38.17%	0.5273	0.078	87.60%
RFR	0.9296	25.85	15.47%	0.9464	5.31	19.29%	0.9858	0.012	9.62%	0.9817	0.015	17.26%
SVR	0.7932	44.31	26.53%	0.7016	12.54	47.85%	0.8168	0.041	34.57%	0.8645	0.042	46.90%
BPNN	0.8536	37.29	22.32%	0.8201	9.73	37.16%	0.9271	0.026	21.81%	0.9308	0.030	33.53%

discordant distributing complexities, the selection of reasonable parameters is very challenging (Liu et al., 2014), which is considered as the reason that SVR is not very satisfactory in terms of the data set fitting ability in the present research.

Finally, the two models RFR and BPNN are compared by using three metrics mentioned above. Although the interpretation of the data set by the two models is within an acceptable range, the prediction of the four outputs by RFR shows obviously higher accuracy rate. Although the neural network has a strong function approximation ability by preferentially fitting samples with higher discreteness in the data fitting process to achieve reduction in shavedness, but the learning ability of a single learner is always limited. By contrast, random forest, which belongs to ensemble learning, uses voting to solve the weak learning ability of a single learner and greatly improves the robustness of the model. For the prediction of the two sets of interfacial area concentrations, the errors of the RFR model are 15.47% and 19.49% while for the two sets of void fractions, the prediction errors of the RFR model are 9.62% and 17.26%. Moreover, it is worth mentioning that in the process of data preprocessing, the RFR requires simpler process, and the data required by its model does not need to be scaled. Because the numerical scaling does not affect the split point positions of the tree structure as well as the structure of the tree model. Moreover, the tree model cannot perform gradient descent because the tree model is constructed to find the best points by finding the optimal split points. Therefore, the tree model is stepped with non-differentiable step points, that means, the tree-structure model does not need to be normalized. In general, it is the distribution of the variables and the conditional probability between the variables instead of the values of the variables matter in tree-structure model. But for neural networks, the different feature ranges of the data will lead to catastrophic consequences such as gradient explosions. Consequently, the random forest regression algorithm shows robustness and effectiveness by taking advantage of the 'wisdom of the crowds' compared to other models in the present study. However, according to the mechanism of random forest regression in Section *Random Forest Regression*, the random forest regression model can only predict the data between the highest and lowest labels in the training data. For situations where the training and prediction inputs differ in their distributions, which named covariate shift (Tsuchiya et al., 2015), the characteristics of random forests that its disability to extrapolate will cause the attribute weights of its prediction outputs to be questionable. Therefore, it can be concluded that the explanatory and predictive capabilities of the random forest regression model for interfacial area concentration and void fraction in this study are better than those of the other three models, but whether the generalization ability of this model can be adapted to other working conditions still requires further exploration to verify. In addition, it is worth mentioning that, since the data used in this experiment is obtained from a rectangular channel of one size, this means that the size of the rectangular channel is not an input variable in this article. Therefore, it is unclear whether the generalization ability of the model obtained in this study can be applicable in rectangular channels of other sizes, which will be further explored in future research.

CONCLUSION

As an important cornerstone of artificial intelligence technology, machine learning has been widely used in many industries and various fields. The goal of this research is to explore the calculation of two-phase flow parameters based on data-driven methods in rectangular channels. In the paper, the four models, namely lasso regression, support vector machine regression, random forest regression and back propagation neural network regression were compared to mine and analyze the data collected through experiments, and the interfacial area concentration and void fraction were analyzed and predicted through the four models. It is found that the random forest regression is the most prominent algorithm among the four algorithms in terms of prediction accuracy, and meanwhile has strong anti-noise ability and good adaptability to nonlinear data. The prediction errors of four parameters including group-I interfacial area concentration, group-II interfacial area concentration, group-I void fraction and group-II void fraction predicted by the random forest regression are: 15.47, 19.29, 9.62 and 17.26%, respectively. In the future, data-driven methods are expected to be further applied in the prediction of other parameters of different flow conditions in rectangular channels, and the computational accuracy and efficiency of data-driven models could be improved further which shows the possibility of reducing the cost of experiment and replacing mechanical models in the nuclear reactor system safety analysis codes.

DATA AVAILABILITY STATEMENT

The datasets presented in this article are not readily available because Due to the nature of this research, participants of this study did not agree for their data to be shared publicly, so supporting data is not available. Requests to access the datasets should be directed to huangqingyu950802@163.com.

AUTHOR CONTRIBUTIONS

The authors confirm contribution to the paper as follows: study conception and design: QH and YY; data collection: YY; Data collation: QH, YY, and DC; Algorithms confirmation: QH; Implementation of Models: QH, YY, YZ, BP, and YZ; Analysis and interpretation of results: QH, YY, YZ, BP, and YW; Draft manuscript preparation: QH, YY, YZ, BP, and ZP. All authors reviewed the results and approved the final version of the manuscript.

REFERENCES

Awad, M., and Khanna, R. (2015). *Efficient learning machines: theories, concepts, and applications for engineers and system designers*. New York, NY: Springer Nature., 268.

Barre, F., and Bernard, M. (1990). The CATHARE code strategy and assessment. *Nucl. Eng. Des.* 124 (3), 257–284. doi:10.1016/0029-5493(90)90296-a

Breiman, L. (1995). Better subset regression using the nonnegative garrote. *Technometrics* 37 (4), 373–384. doi:10.1080/00401706.1995.10484371

Breiman, L. (2001a). Random forests. *Mach. Learn.* 45 (1), 5–32. doi:10.1023/a:1010933404324

Breiman, L. (2001b). Statistical modeling: the two cultures (with comments and a rejoinder by the author). *Stat. Sci.* 16 (3), 199–231. doi:10.1214/ss/1009213726

Gammerman, A. (1996). *Machine learning: progress and prospects*. London, UK: Royal Holloway.

Gomez-Fernandez, M., Higley, K., Tokuhiro, A., Welter, K., Wong, W. K., and Yang, H. (2020). Status of research and development of learning-based approaches in nuclear science and engineering: a review. *Nucl. Eng. Des.* 359, 110479. doi:10.1016/j.nucengdes.2019.110479

Guo, L. J. (2002). *Two-phase and multiphase flow dynamics*. Xi'an, China: Xi'an Jiaotong University Press.

Guo, Z., and Uhrig, R. E. (1992). Use of artificial neural networks to analyze nuclear power plant performance. *Nucl. Technol.* 99 (1), 36–42. doi:10.13182/nt92-a34701

Ishii, M., Kim, S., and Uhle, J. (2002). Interfacial area transport equation: model development and benchmark experiments. *Int. J. Heat Mass Tran.* 45 (15), 3111–3123. doi:10.1016/s0017-9310(02)00041-8

Ishii, M. (1975). Thermo-fluid dynamic theory of two-phase flow. Paris, Eyrolles, Editeur., NASA Sti/recon Technical Report A 75, 29657.

Kocamustafaogullari, G., and Ishii, M. (1995). Foundation of the interfacial area transport equation and its closure relations. *Int. J. Heat Mass Tran.* 38 (3), 481–493. doi:10.1016/0017-9310(94)00183-v

Kohavi, R. (1995). A study of cross-validation and bootstrap for accuracy estimation and model selection. *Ijcai* 14 (2), 1137–1145.

Kohonen, T. (1988). An introduction to neural computing. *Neural Networks* 1 (1), 3–16. doi:10.1016/0893-6080(88)90020-2

Liu, Y., Jiang, B., Yi, H., and Bo, C. (2014). Fault isolation for nonlinear systems using flexible support vector regression. *Math. Probl Eng.* 2014, 1–10. doi:10.1155/2014/713018

Lombardi, C., and Mazzola, A. (1997). Prediction of two-phase mixture density using artificial neural networks. *Ann. Nucl. Energy* 24 (17), 1373–1387. doi:10.1016/s0306-4549(97)00006-6

Martin, R. P. (1995). RELAP5/MOD3 code coupling model. *Nucl. Saf.* 36 (2), 290–298.

McClelland, J. L., and Rumelhart, D. E.PDP Research Group. (1986). *Parallel distributed processing*. Cambridge, MA: MIT press., Vol. 2, 20–21.

McLachlan, G. J., Do, K. A., and Ambroise, C. (2005). *Analyzing microarray gene expression data*. Hoboken, NJ: John Wiley & Sons.

Montes, J. L., Francois, J. L., Ortiz, J. J., Martín-del-Campo, C., and Perusquía, R. (2009). Local power peaking factor estimation in nuclear fuel by artificial neural networks. *Ann. Nucl. Energy* 36 (1), 121–130. doi:10.1016/j.anucene.2008.09.011

Nair, V., and Hinton, G. E. (2010). "Rectified linear units improve restricted Boltzmann machines," In Icml, Haifa, Israel, June 21–24, 2010.

Radaideh, M. I., Pigg, C., Kozlowski, T., Deng, Y., and Qu, A. (2020). Neural-based time series forecasting of loss of coolant accidents in nuclear power plants. *Expert Syst. Appl.* 160, 113699. doi:10.1016/j.eswa.2020.113699

Segal, M. R. (2004). *Machine learning benchmarks and random forest regression*. San Francisco, CA, Division of Biostatistics, University of California.

Su, G. H. (2013). *Thermal-hydraulic calculation method for nuclear power system*. Beijing, China: Tsinghua University Press.

Tambouratzis, T., and Pàzsit, I. (2010). A general regression artificial neural network for two-phase flow regime identification. *Ann. Nucl. Energy* 37 (5), 672–680. doi:10.1016/j.anucene.2010.02.004

Tibshirani, R. (1996). Regression shrinkage and selection via the lasso. *J. Roy. Stat. Soc. B.* 58 (1), 267–288. doi:10.1111/j.2517-6161.1996.tb02080.x

Tsuchiya, M., Yamauchi, Y., Yamashita, T., and Fujiyoshi, H. (2015). "Transfer forest based on covariate shift," 2015 3rd IAPR asian conference on pattern recognition (ACPR), Kuala Lumpur, Malaysia, November 2015 (New York: IEEE.), 760–764.

Van Rossum, G., and Drake, F. L., Jr. (1995). *Python reference manual*. Amsterdam: Centrum voor Wiskunde en Informatica.

Vapnik, V. (1998). "The support vector method of function estimation," in *Nonlinear modeling* (Boston, MA: Springer.), 55–85.

Zhang, G. Y., and Li, L. (2006). *Support vector machine and its application research*. Hunan: Hunan University.

Conflict of Interest: The authors declare that the research was conducted in the absence of any commercial or financial relationships that could be construed as a potential conflict of interest.

frontiers in Energy Research

METHODS
published: 05 March 2021
doi: 10.3389/fenrg.2021.637283

A Method of Containment Leakage Rate Estimation Based on Convolution Neural Network

Hao Wang, Jingquan Liu*, Guangyao Xie, Xianping Zhong and Xiangqi Fan

Department of Engineering Physics, Tsinghua University, Beijing, China

As the nuclear power plant containment is the third barrier to nuclear safety, real-time monitoring of containment leakage rate is very important in addition to the overall leakage test before an operation. At present, most of the containment leakage rate monitoring systems calculate the standard volume of moist air in the containment through monitoring parameters and calculate the daily leakage rate by the least square method. This method requires several days of data accumulation to accurately calculate. In this article, a new leakage rate modeling technique is proposed using a convolutional neural network based on data of the monitoring system. Use the daily monitoring parameters of nuclear power plants to construct inputs of the model and train the convolutional neural network with daily leakage rates as labels. This model makes use of the powerful nonlinear fitting ability of the convolutional neural network. It can use 1-day data to accurately calculate the containment leakage rate during the reactor start-up phase and can timely determine whether the containment leak has occurred during the start-up phase and deal with it in time, to ensure the integrity of the third barrier.

Keywords: containment leakage rate, convolution neural network, reactor start-up phase, data extrapolation, nuclear safety

OPEN ACCESS

Edited by:
Wenzhong Zhou,
Sun Yat-Sen University, China

Reviewed by:
Xinyu Wei,
Xi'an Jiaotong University, China
Yuan Yuan,
Sun Yat-Sen University, China

****Correspondence:***
Jingquan Liu
jingquan@tsinghua.edu.cn

Specialty section:
This article was submitted to Nuclear Energy, a section of the journal Frontiers in Energy Research

Received: *03 December 2020*
Accepted: *29 January 2021*
Published: *05 March 2021*

Citation:
Wang H, Liu J, Xie G, Zhong X and Fan X (2021) A Method of Containment Leakage Rate Estimation Based on Convolution Neural Network. Front. Energy Res. 9:637283. doi: 10.3389/fenrg.2021.637283

INTRODUCTION

In a nuclear power plant, the pressure boundary formed by the containment body and numerous perforated equipment, components and pipes that penetrate the body is the third and last barrier of a nuclear power plant (Sakaba et al., 2004). It is responsible for the important function of preventing radioactive materials from leaking into the external environment. The Safety Guide published by the International Atomic Energy Agency describes in detail the safety function requirements of the containment of radioactive materials under reactor operation and accident conditions. It emphasizes that the integrity of the containment structure should be maintained under design basis accidents, and the leakage rate cannot exceed the specified maximum value. Due to the existence of open-hole equipment, components, pipelines, and isolation valves through the reactor containment, it is of great significance to monitor the integrity of the containment.

In addition to regular containment integrity tests, it is necessary to monitor the containment leakage rate through the on-line monitoring system during the normal operation of the nuclear power plant (ANS, 2002). The on-line monitoring system of containment leakage rate (EPP system) is an important monitoring system of the nuclear power plant. It can monitor the gas leakage rate of containment during the operation of the unit, monitor the change of containment tightness, and keep the atmospheric pressure in the containment within an allowable range. When the leakage rate reaches the operation limit, the operator is informed to take necessary measures action.

At present, the EPP system of CPR1000 nuclear power plants mostly adopts SEXTEN2, which is developed by Division technique general of Electricite de France, for on-line monitoring of containment leakage rate during normal operation of the reactor (EDF/DTG, 2001). SEXTEN2 adopts the law of conservation of mass and relies on the physical model of ideal gas conservation to calculate the containment leakage rate. The parameters used in the calculation need to be representative enough, which means that there is some uncertainty in the transient process. The linear fitting method is used to calculate the leakage rate, and a certain amount of data accumulation is required to give the results that meet the requirements of accuracy and uncertainty. Therefore, the estimated leakage rate cannot be obtained until several days after the end of the overhaul and containment closure.

At present, the research of containment leakage rate is mainly about the method based on mass conservation and the measures to deal with the leakage. Huang et al. (2016) studied the leakage mechanism of the containment penetration, described the microleakage mechanism of the interface of the static seal structure based on the porous media seepage theory, and used Hertz contact theory to correlate the stress with the changes of the microstructure, and finally realized the calculation of the leakage rate independent of any experimental data. Li. (2015) introduced the calculation model and method of monitoring the containment leakage rate of M310 nuclear reactor during operation, analyzed the treatment of leakage rate curve under special conditions, and proved the rationality and effectiveness of the EPP system. Liang et al. (2015) analyzed the causes of the abnormal containment leakage rate of the new CPR1000 unit and gave preventive measures. Liu. (2017) found that the calculation of containment leakage rate in the reactor start-up stage was not accurate, and measures such as eliminating abnormal data were needed.

However, compared with the application of machine learning method in other fields, we can find that there is a lack of machine learning application in the calculation of containment leakage rate, especially in the reactor start-up stage. One of the important reasons is that the reactor will not shut down and restart frequently, so there is a lack of data on the containment leakage rate during the start-up phase of the reactor. Moreover, the traditional method based on mass conservation can only use the data a few days after the start-up of the reactor to deduce the leakage rate of the start-up phase, which leaves a hidden danger for the safety of the containment leakage rate monitoring. Based on the above reasons, this paper proposes a convolutional neural network (CNN) method to estimate the containment leakage rate during the reactor start-up phase. In this paper, the data of 10 start-up stages of CAP1000 reactor in a nuclear power plant is taken as a case study. And major contributions in this work are:

(1) The calculation method of containment leakage rate based on mass conservation adopted by the EPP system is introduced.
(2) CNN combined with data extrapolation is used to estimate the containment leakage rate from high-dimensional monitoring parameters.
(3) The result of an ordinary artificial neural network (ANN) is compared to prove the rationality of using CNN.

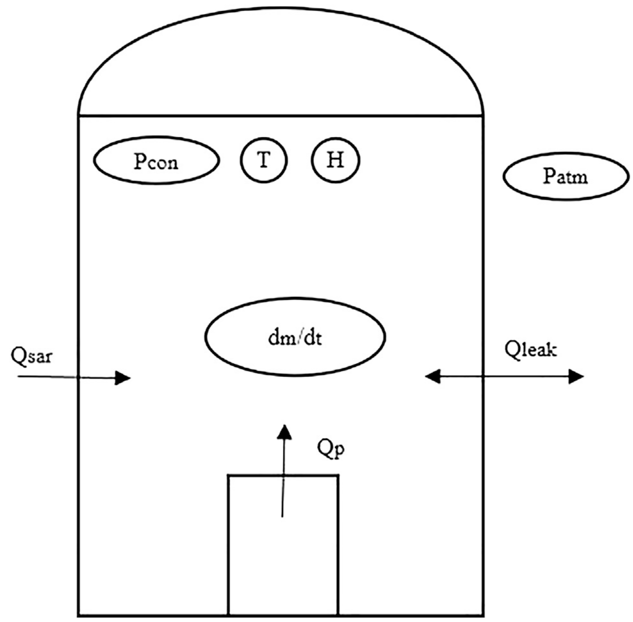

FIGURE 1 | Schematic diagram of gas mass balance in containment.

This paper is arranged as follows: The first section introduces the background and motivation; The second section introduces the calculation method of containment leakage rate based on mass conservation used in EPP system; The third section describes the proposed algorithm framework, and briefly introduces CNN. The case study and result are presented in the following sections. Finally, the Conclusion contains the conclusion and limitation of the work.

THE METHOD BASED ON PHYSICAL MODELS

Based on the physical models, the containment leakage rate is calculated according to the mass conservation of gas in the containment and equation of state of ideal gas (Zhang et al., 2014). The containment leakage rate cannot be measured directly, so the EPP system continuously measures and collects the pressure, temperature, humidity, and other parameters in the containment, and obtains the leakage rate through calculation. The containment leakage rate is defined as the mass change rate of dry air in containment within 24 h, which is generally called the dry air quality method (Chu and OuYang, 2010). The balance schematic diagram of the gas mass in the containment is shown in **Figure 1** (Guo, 2020). Qld is the daily leakage rate of the containment, Q_{sar} is air injection flow of instrument compressed air distribution system (SAR), T is temperature, P_{con} is average pressure in containment, H is humidity, P_{atm} is atmospheric pressure, Q_p is leakage of other pressure equipment, and Q_{leak} is containment leakage rate.

Considering the influence of the above factors, the variation of total gas mass in containment can be calculated by the following formula:

$$\frac{\Delta m}{\Delta t} = Q_{leak} + Q_p + Q_{sar}. \quad (1)$$

Let the average daily leakage rate $Q_{ld} = Q_{leak} + Q_p$, and then we can get the formula:

$$Q_{ld} = \frac{\Delta m}{\Delta t} - Q_{sar}. \quad (2)$$

Q_{leak} is a function of P_{con} and P_{atm}. Let $\Delta P = P_{con} - P_{atm}$, and the function can be expressed as $Q_{leak} = f(\Delta P)$. Then we can get **formula 3** and **formula 4**.

$$Q_{ld} = f(\Delta P) + Q_p, \quad (3)$$

$$f(\Delta P) + Q_p = \frac{\Delta m}{\Delta t} - Q_{sar}. \quad (4)$$

In the formula above, $\Delta m/\Delta t$ can be calculated by basic parameters, Q_p can be calculated by SAR system. After obtaining a series of coordinate points, Q_{ld} can be obtained by the least square method.

With the continuous operation of the unit, the pressure difference ΔP inside and outside the containment will change within a certain range. The online monitoring system of containment leakage rate calculates a ΔP and a Q_{ld} data every day. The relationship between Q_{ld} and pressure difference ΔP was fitted linearly. The intercept of the fitting line on the y-axis, that is, the leakage rate Q_{l0} when $\Delta P = 0$, represents the parasitic leakage rate, which is always above the y-axis. Because the leakage rate of containment is meaningful only when it corresponds to the internal and external pressure difference of containment, besides, the influence of parasitic leakage rate Q_P on Q_{leak} needs to be eliminated, and the leakage rate is converted into the leakage rate $Q_{l60} = 60 * \alpha$ at $\Delta P = 60$mbar, α is the linear slope. Q_{l60} is the theoretically calculated containment leakage rate.

THE METHOD BASED ON CNN

The physical models mentioned above require at least five consecutive valid Q_{ld} for the first Q_{l60} calculation, and the range of ΔP should be greater than 15 mbar. In the later fitting calculation, the data points (Q_{ld}, ΔP) will gradually increase until the full 20. That is to say, the accurate leakage rate level of the first day can be obtained 5 days after the start-up of the overhaul, which has a great impact on the real-time monitoring of the reactor containment. Therefore, this paper proposes a data-driven model based on the convolutional neural network. The leakage rate extrapolation method is used to construct the training data set from the historical data set to fit and predict the leakage rate calculation when the reactor is started after the overhaul. This method can be applied to the calculation method of containment leakage rate in the start-up stage and fills the blank that the containment leakage rate cannot be evaluated in the start-up stage.

Data-driven methods are widely used, ranging from simple linear fitting, polynomial fitting to complex physical relationship cleaning, which can be used to fit the functional relationship between input and output. In recent years, with the rise of artificial intelligence technology, various machine learning, and deep learning methods have been widely used in various fields because of their strong fitting ability and high prediction accuracy (Peng and Liu, 2014).

In essence, the calculated value of the containment leakage rate can be regarded as a function of the monitoring value of each monitoring quantity

$$Q_{l60} = f(\boldsymbol{X}), \quad (5)$$

where X is the matrix composed of the time series of monitoring parameters such as temperature, pressure, and humidity.

The problem solved by the data-driven model is to infer the functional relationship $y = f$ 10) between input X what is measured data of the monitoring system and output y that is corresponding to containment leakage rate Q_{l60} in this project. The data-driven method assumes that the specific form of f is unknown, but multiple groups of independent data can be obtained. In this case, the data-driven model uses a general parametric function to fit the data, so that the deviation between the model output value and the actual output value is as small as possible, so the fitting model is used as the approximation of the functional relationship between input and output.

Algorithm Framework

Based on the data of the monitoring system, this paper presents a calculation method of containment leakage rate using a convolutional neural network. **Figure 2** shows the flow of data within the framework of the proposed algorithm.

As can be seen from the figure, the process of model establishment mainly includes the following parts.

Step1: Collecting monitoring data of reactor start-up time from the historical database.
Step2: Extrapolate the leakage rate after 5 days of containment closure by extrapolation method to estimate leakage rate within 5 days after startup.

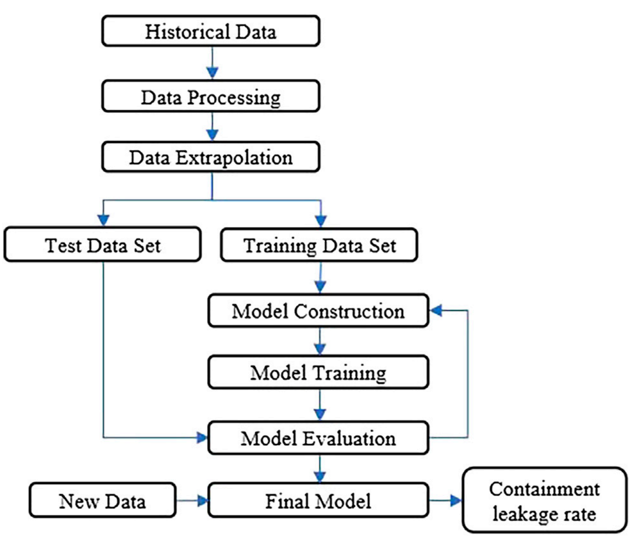

FIGURE 2 | The framework of the containment leakage rate calculation model.

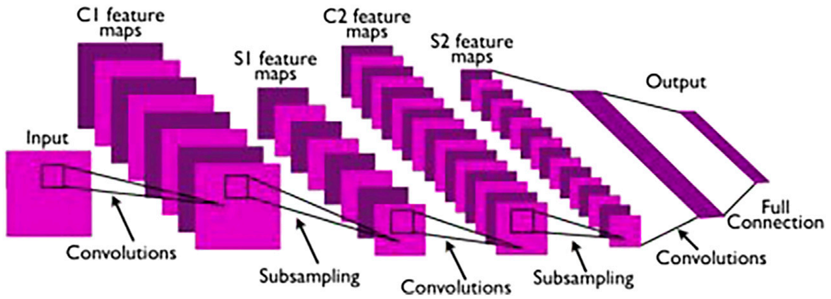

FIGURE 3 | The structure of a standard CNN.

Step3: Process raw data, such as data cleansing and data normalization.
Step4: Divide the processed data into two subsets, the training set and test set, and utilize the training data and modeling algorithm to develop the model. Attention should be paid to make sure there are enough samples in the training set.
Step5: Apply the model to the test set, and evaluate the model. The evaluation methods include mean square error, root mean square error, histogram or quantile map, etc.
Step6: After model evaluation, the model that does not meet the requirements needs to be retrained, and the model that meets the requirements is the final model.
Step7: Finally, the model can be applied to the new data to calculate the containment leakage.

Convolution Neural Network

A convolution neural network is a kind of nonlinear model, which can effectively process features from the original data and fit the results (Lawrence et al., 1997). CNN combines convolution operation with a multi-layer artificial neural network. In the process of feature extraction of the target, the method of local connection is adopted between the adjacent two layers of neurons, which realizes the local information perception and judgment, and reduces the complexity of the whole network by weight sharing, which greatly reduces the number of weights of the whole network, so it can quickly recognize the target (Hubel and Wiesel, 1962; Fukushima, 1980). At present, a two-dimensional convolutional neural network (2 days-CNN) is widely used. The standard CNN structure is shown in **Figure 3**, which mainly consists of the input layer, convolution layer, pooling layer, full connection layer, and output layer (Lecun et al., 2010).

CASE DESCRIPTION

In this work, the real monitoring data of a nuclear power plant is used to establish a model and predict the containment leakage rate within a few days of reactor start-up. In the past few years, there have been 10 overhaul and start-up cases of the two units H1 and H2 in the nuclear power plant. The data collected by the unit is one data point every half an hour, and each data point contains a total of 31 dimensions of data. The monitoring quantity includes the air intake of the pneumatic valve in containment, temperature, humidity, pressure, and other physical quantities related to containment leakage rate. Some monitoring measurements are listed in **Table 1**.

TABLE 1 | The important signals in the monitoring system.

Name of signal	Unit	Description
Q_{saravg}	m^3/h	Airflow rate
T_{avg}	°C	Average temperature
H_{avg}	%	Average humidity
DeltaP	hPa	Pressure difference
P_{con}	hPa	Containment pressure
P_{atm}	hPa	Atmospheric pressure

DATA PROCESSING

Before using the original data in the monitoring system, various types of data processing are needed to establish a better model. In this work, two processes are conducted.

Data Denoizing

Due to the influence of the external environment or sensor accuracy, the original data recorded by the monitoring system will have noise. In order to correct the noise, this paper carries out moving average noise reduction on the original data.

The principle of moving average is to modify the amplitude of other sampling points near a measurement point, so as to make the vibration curve smooth enough to achieve the purpose of noise reduction. In the moving average method, the surrounding points are simply averaged, or the nearby points are weighted average. In general, the average of five points nearby is based on the following formula:

$$y_i = \sum_{n=1}^{N} h_n x_{i-n} \quad i = 1, 2, \cdots, m, \tag{6}$$

where x is the data value obtained by sampling, y is the data after moving average, m is the number of measurement data, N is the average number of points, h is the weighted average factor. The value of the weighted average factor conforms to the following formula:

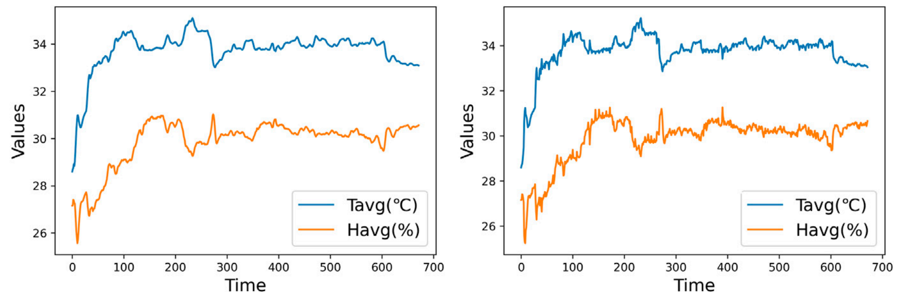

FIGURE 4 | The data with or without moving average.

$$\sum_{n=1}^{N} h_n = 1. \tag{7}$$

In this work, N is set to 5, and h is set to 0.2. **Figure 4** shows the effect of data denoizing. The left figure is the original data before noise reduction, and the right is the data after moving average. It can be seen that the burr in the original data is significantly reduced. With moving average Without moving average.

Data Normalization

Since the range of eigenvalues of the original data varies greatly, the ranges of all features should be standardized so that the contribution of each feature is comparable. In addition, in some machine learning algorithms, the objective function may not work properly without scaling. Various linear or nonlinear scaling methods can be used, such as rescale, mean normalization, standardization, etc. In this article, rescale is used to scale the range of features in [0, 1]. The general formula is as follows

$$X^* = \frac{X - \min(X)}{\max(X) - \min(X)}. \tag{8}$$

Where X is an original value, X^* is the normalized value.

It is worth pointing out that the general machine learning algorithm also needs to carry on the feature screening, in order to improve the modeling efficiency and reduce interference, but the deep learning algorithm has a strong processing ability for high-dimensional signals, so there is no need for feature screening.

MODEL CONSTRUCTING

The overall modeling steps of this work can be summarized as follows:

(1) The leakage rate Q_{160} data in the historical database after 5 days of containment closure was extrapolated by the extrapolation method, and the estimated leakage rate within 5 days after the startup was obtained.
(2) The input of training data is the matrix composed of the time series of each monitoring parameter in one day, and the output is the estimated leakage rate of corresponding time obtained by extrapolation.

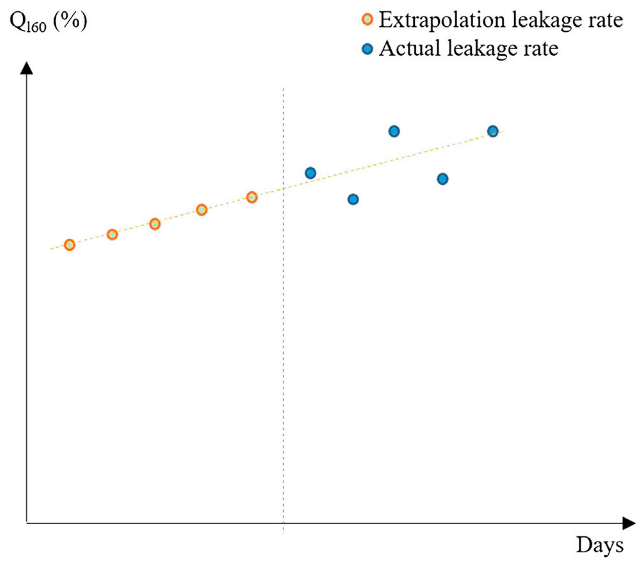

FIGURE 5 | Leakage rate extrapolation diagram.

(3) The CNN algorithm is used to train the neural network based on the constructed training set, and the model fitting results are obtained.
(4) The accuracy of the fitting model is evaluated by selecting test data from the historical database.

Extrapolation of Leakage Rate

The leakage rate extrapolation refers to the linear fitting of the leakage rate with time in a period after 5 days of reactor startup. The calculated leakage rate within 5 days after the reactor startup is extrapolated by the fitting line, which is used as the label of data-driven model training. As shown in **Figure 5**.

CNN Construction

In this work, the structure of the CNN as shown in **Figure 6** is used to fit the matrix composed of the time series within one day. The label in the training process is the leakage rate calculation value after linear fitting extrapolation. From the C1 layer to the P2

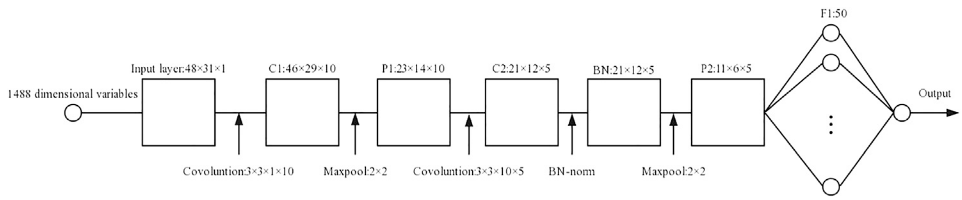

FIGURE 6 | The structure of the convolution neural network in this work.

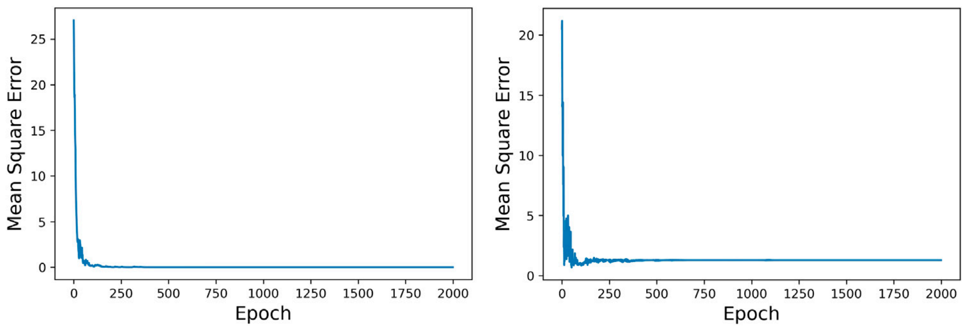

FIGURE 7 | Training and testing curves.

layer, it is responsible for feature selection, dimension reduction, and information fusion. The input sample is the data of one day, one data point every half hour, including 31-dimensional parameters. After normalization, each 1488-dimension sample in the input layer is resized to 48 × 31. For each layer, we use a 3 × 3 convolution kernel. The first convolution layer C1 has 10 groups, and the size of each group is 46 × 29. The second convolution layer C2 has five groups with a size of 21 × 12. The pool size of P1 and P2 is 2 × 2, and the maximum pool is used to reduce the number of parameters to prevent overfitting. BN normalized layer is used to prevent gradient explosion and accelerate convergence rate. There are 50 sigmoid neurons in the full junction layer F1 to calculate the output value. The final output value is the predicted leakage rate Q_{160}.

RESULT VERIFICATION

In this work, the 34 days data of 10 start-up processes were used to establish the model. The 27 days data were used as the training set, and the 7 days data were used as the test set. The loss function is the mean square error. **Figure 7** shows the change in loss function value. It can be seen that both the training loss and test loss decrease with the increase of model iterations and has reached a very low level at 2000 iterations. The reduction of training loss and test loss also shows that the modeling method is effective.

Figure 8 shows the results of this modeling. Each data point is the Q_{160} value within 5 days of the reactor startup. Intuitively, the training set and test set of the model have good performance.

To prove the rationality of choosing CNN in this work, this paper also uses two commonly used machine learning methods: Artificial neural network (ANN) and Support vector regression (SVR) to predict the containment leakage rate. All the steps are the same, except that CNN is replaced by ANN or SVR. The results of ANN and SVR are shown in **Figure 9** and **Figure 10**. And **Table 2** lists the performance differences of the three methods in the training set and the test set. R2 is the determination coefficient of the model, which is always less than or equal to 1, and the closer R2 is to 1, the better the fitting effect of the model.

From the above results, it can be seen that the results of CNN are significantly better than Ann and SVR in both training set and test set. The reason is that the EPP system has 31 kinds of parameters, which are recorded every half an hour. This means that the daily containment leakage rate is determined by a 48 × 31 dimensional parameter. In this case, CNN's advantage in fitting high-dimensional data can be reflected.

CONCLUSION

This work proposes a containment leakage rate estimation framework based on CNN. The data related to the containment leakage rate used in this case comes from a real CAP1000 nuclear power unit. The data is subsequently preprocessed and normalized. Through data extrapolation and CNN, the containment leakage rate of the reactor start-up phase can be obtained. Through the actual case study, the CNN model shows impressive performance. The comparison with ANN and SVR also shows the good performance of CNN in this work. The originality of this study is summarized below:

(1) We analyze the EPP system calculation method of containment leakage rate and its shortcomings.

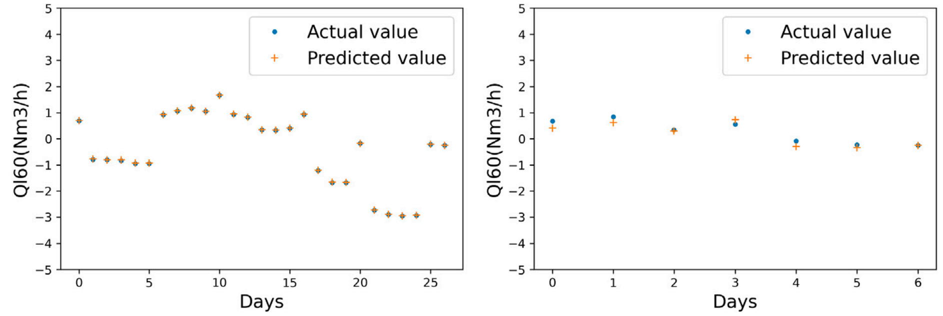

FIGURE 8 | Prediction results of the model on training set and test set.

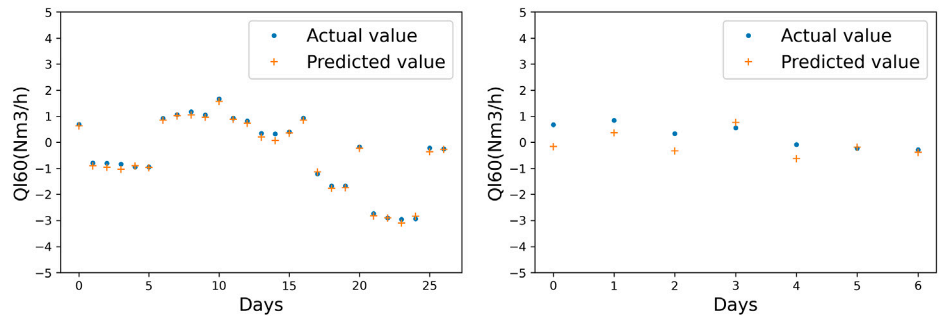

FIGURE 9 | Prediction results of ANN.

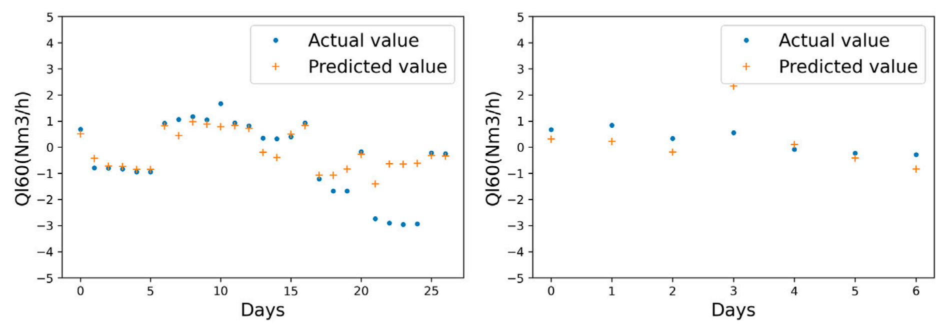

FIGURE 10 | Prediction results of SVR.

TABLE 2 | Comparison of results of CNN, ANN, and SVR.

Result	CNN	ANN	SVR
	Training set/Test set	Training set/Test set	Training set/Test set
MSE	0.00036/0.11	0.045/0.63	0.37/0.89
R2	0.99/0.78	0.95/0.49	0.57/0.38

(2) We propose a calculation model based on data extrapolation and CNN, which can estimate the containment leakage rate during the start-up phase of the reactor and assist in the assessment of containment integrity.

(3) We compare the performance of CNN with ANN and SVR in the model and prove that the CNN method has the best performance in this work.

Nevertheless, we observed some limitations of the research. First, we can do more research on the structure of CNN to make the model perform better. Then, because the reactor will not shut down and restart frequently, the amount of data in this work is not particularly large. And as the data accumulates, the model should be updated. These limitations will be addressed in our future work.

DATA AVAILABILITY STATEMENT

The raw data supporting the conclusion of this article will be made available by the authors, without undue reservation.

AUTHOR CONTRIBUTIONS

HW is responsible for method design and calculation. JL is responsible for data support. GX and XZ gives advice and guidance. XF collected some documents.

REFERENCES

ANS (2002). *American nuclear society standards committee working group ANS-56.8*. Illinois, IL, United States: American Nuclear Society 202, 14–15.

Chu, Y. J., and OuYang, Q. (2010). Comparison and analysis of methods for containment leakage rate calculation. *Nucl. Power Eng.* 31 (6), 33–37. doi:10.1016/S1876-3804(11)60004-9

EDF/DTG (2001). *SEXTEN2-LING AO system validation and test procedure (Unit in shutdown conditions)*. Paris, France: EDF/DTG.

Fukushima, K. (1980). Neocognitron: a self organizing neural network model for a mechanism of pattern recognition unaffected by shift in position. *Biol. Cybern* 36, 193–202. doi:10.1007/BF00344251

Guo, X. L. (2020). Study on the abnormal phenomenon of containment leakage rate monitoring system. *Sci. Tech. Vis.* 320 (26), 14–17. doi:10.19694/j.cnki.issn2095-2457.2020.26.03

Huang, X. M., Li, J., Xu, G., and Cheng, G. (2016). Study on leak mechanism and leakage rate prediction model of reactor containment sealing structure. *Nucl. Power Eng.* 3, 116–121. doi:10.13832/j.jnpe.2016.03.0116

Hubel, D. H., and Wiesel, T. N. (1962). Receptive fields, binocular interaction and functional architecture in the cat's visual cortex. *J. Physiol. (Lond)* 160 (1), 106. doi:10.1113/jphysiol.1962.sp006837

Lawrence, S., Giles, C. L., Tsoi, A. C., and Back, A. D. (1997). Face recognition: a convolutional neural-network approach. *IEEE Trans. Neural Netw.* 8 (1), 98–113. doi:10.1109/72.554195

Lecun, Y., Kavukcuoglu, K., and Farabet, Cle´ment. (2010). *Convolutional networks and applications in vision*. Proceedings of 2010 IEEE international symposium on circuits and systems, Paris, France, 30 May–2 June, 2010. doi:10.1109/ISCAS.2010.5537907

Li, X,. G. (2015). Calculation model and analysis of containment leakage rate of nuclear power plant. *Sci. Tech. Innovation Herald* 12 (36), 153–154. doi:10.16660/j.cnki.1674-098X.2015.36.153

Liang, B., Wang, L., and Han, Z. (2015). Causes and preventive measures of abnormal daily leakage rate of CPR1000 new unit. *Sci. Tech. Vis.* 160, 127–129. doi:10.19694/j.cnki.issn2095-2457.2016.06.089 Available at GIDA-global.org/care.

Liu, Y. F. (2017). Analysis and processing methods of the containment leak rate alarm during the startup period of the NPP. *China Nucl. Power* 10 (3), 399–404. doi:10.12058/zghd.2017.03.399

Peng, Y., and Liu, D. T. (2014). .Data-driven prognostics and health management: a review of recent advances. *Yi Qi Yi Biao Xue Bao/Chinese J. Scientific Instrument* 35, 481–495.

Sakaba, N., Iigaki, K., Kondo, M., and Emori, K. (2004). Leak-tightness characteristics concerning the containment structures of the httr. *Nucl. Eng. Des.* 233 (1–3), 135–145. doi:10.1016/j.nucengdes.2004.08.023

Zhang, C. W., Yang, Y. D., Qiao, Y., and Liang, B. (2014). The principle and data analysis of online monitoring system of containment leak rate. *Nucl. Saf.* 13 (2), 56–60. doi:10.16432/j.cnki.1672-5360.2014.02.003

Conflict of Interest: The authors declare that the research was conducted in the absence of any commercial or financial relationships that could be construed as a potential conflict of interest.

frontiers
in Energy Research

ORIGINAL RESEARCH
published: 17 March 2021
doi: 10.3389/fenrg.2021.641545

A Framework for Monitoring and Fault Diagnosis in Nuclear Power Plants Based on Signed Directed Graph Methods

*Wu Guohua[1,2], Yuan Diping[2], Yin Jiyao[2], Xiao Yiqing[1] and Ji Dongxu[3]**

[1]Harbin Institute of Technology, Shenzhen, China, [2]Shenzhen Urban Public Safety and Technology Institute, Shenzhen, China, [3]School of Science and Engineering Chinese University of Hong Kong, Shenzhen, China

When nuclear power plants (NPPs) are in a state of failure, they may release radioactive material into the environment. The safety of NPPs must thus be maintained at a high standard. Online monitoring and fault detection and diagnosis (FDD) are important in helping NPP operators understand the state of the system and provide online guidance in a timely manner. Here, to mitigate the shortcomings of process monitoring in NPPs, five-level threshold, qualitative trend analysis (QTA), and signed directed graph (SDG) inference are combined to improve the veracity and sensitivity of process monitoring and FDD. First, a three-level threshold is used for process monitoring to ensure the accuracy of an alarm signal, and candidate faults are determined based on SDG backward inference from the alarm parameters. According to the candidate faults, SDG forward inference is applied to obtain candidate parameters. Second, a five-level threshold and QTA are combined to determine the qualitative trend of candidate parameters to be utilized for FDD. Finally, real faults are identified by SDG forward inference on the basis of alarm parameters and the qualitative trend of candidate parameters. To verify the validity of the method, we have conducted simulation experiments, which comprise loss of coolant accident, steam generator tube rupture, loss of feed water, main steam line break, and station black-out. This case study shows that the proposed method is superior to the conventional SDG method and can diagnose faults more quickly and accurately.

Keywords: nuclear power plants, process monitoring, fault detection and diagnosis, signed directed graph, qualitative trend analysis

OPEN ACCESS

Edited by:
Xianping Zhong,
University of Pittsburgh, United States

Reviewed by:
Cenxi Yuan,
Sun Yat-Sen University, China
Jiankai Yu,
Massachusetts Institute of Technology, United States

****Correspondence:***
Ji Dongxu
jidongxu@cuhk.edu.cn

Specialty section:
This article was submitted to Nuclear Energy, a section of the journal Frontiers in Energy Research

Received: *14 December 2020*
Accepted: *01 February 2021*
Published: *17 March 2021*

Citation:
Guohua W, Diping Y, Jiyao Y, Yiqing X and Dongxu J (2021) A Framework for Monitoring and Fault Diagnosis in Nuclear Power Plants Based on Signed Directed Graph Methods. Front. Energy Res. 9:641545. doi: 10.3389/fenrg.2021.641545

INTRODUCTION

Nuclear power plants (NPPs) are large and complex systems. To ensure the reliability and safety of NPPs, process monitoring and fault detection and diagnosis (FDD) are implemented to provide online guidance for operators diagnosing the abnormal functioning of NPPs in an accurate and timely manner (Liu et al., 2013; Liu et al., 2014).

FDD techniques can be divided into data-driven, signal-based, and model-based methods in NPP (Ma and Jiang, 2011; Ma and Jiang, 2015). Data-driven FDD mainly relies on large datasets to establish relationships among various parameters and faults. It does this through multiple approaches, such as neural networks (Mo et al., 2007; Amal et al., 2011), principal component analysis (Gajjar et al., 2017), qualitative trend analysis (Maurya et al., 2005), and others (Žarković and

Stojković, 2017). Signal-based methods operate in the time domain and employ techniques such as wavelet analysis, time-frequency analysis, and spectral analysis (Ma and Jiang, 2011). There are two main approaches for model-based FDD. The first is based on the use of expert knowledge, such as expert systems (Kramer and Palowitch, 1987). The second is based on graph theory, that is, the model graphically displays relationships among the various parameters and faults as in a Bayesian network (Kang and Golay, 1999), a signed directed graph (Liu et al., 2016), and a dynamic uncertain causality graph (Zhou and Zhang, 2017).

FDD is difficult to achieve for NPPs using data-driven and signal-based methods. On the one hand, an NPP is a complex system and it is difficult to obtain real-time data. On the other hand, data-driven methods of diagnosis are "black box" in nature, which makes it difficult for operators to determine the cause of faults. Therefore, graph methods are currently widely used for FDD in NPPs.

As a type of qualitative FDD technique, a Signed Directed Graph (SDG) model, which does not require a precise mathematical model to establish, can contain a large amount of information about faults. SDG was applied in the chemical industry by Lapp and Powers (1977), and the concept of SDG was proposed by Iri et al. (1979). Compared with other data-driven methods, SDG has the significant advantage that SDG-based FDD can reveal fault propagation paths and comprehensively explain causes of failure (Chen et al., 2015; Maurya et al., 2004), which has led to it becoming widely implemented in industry. To improve the accuracy and sensitivity of SDG-based FDD, other methods are combined with SDG, which has resulted in variants such as the SDG-expert system (Kramer and Palowitch, 1987), SDG-principal component analysis (Hiranmayee and Venkatasubramanian, 1999), SDG-qualitative trend analysis (Gao and Wu, 2010), SDG-hazard and operability (Wang and Chen, 2009), SDG-fuzzy logic (Tarifa and Scenna, 2003; He et al., 2014), and SDG-Bayesian network (Peng et al., 2014).

Based on the above studies, we found that almost all research into SDG-based FDD technology has focused on inference, diagnosis, and modeling. However, because process monitoring is the first step of FDD in NPPs, process monitoring itself should be more closely studied. Furthermore, the safety threshold in NPPs is very conservative, which not only increases the difficulty of applying FDD but also makes incipient fault diagnosis difficult (Chung and Bien, 1994). To solve these problems, SDG combined with principal component analysis was proposed for FDD, and principal component analysis was applied to solve the threshold problem in process monitoring. SDG combined with qualitative trend analysis (QTA) is used to determine the qualitative trends of parameters in early failure and to conduct incipient fault diagnosis. However, SDG combined with other methods requires more in-depth research. Principal component analysis reduces the parameters, so it is difficult to guarantee the accuracy of FDD. QTA obtains the trend of parameters. When the parameters fluctuate within the normal range, misdiagnosis may occur.

This study combines five-level threshold, QTA, and SDG inference to solve these problems. *Signed Directed Graph Method* Section introduces the SDG method; *Process Monitoring for Nuclear Power Plants* Section presents the method of process monitoring; and *Monitoring and Fault Diagnosis Framework for Nuclear Power Plants* Section proposes a combination of five-level threshold, QTA, and SDG inference. In *Application Case Study* Section, we discuss a case study, and finally, present conclusions in *Conclusion* Section.

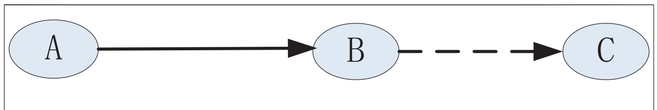

FIGURE 1 | Sketch map of an SDG model.

SIGNED DIRECTED GRAPH METHOD

Concepts and Principles

SDG models are described by nodes and directed edges which can express relationships among the parameters. An SDG model is defined as $G = (V, E)$, where$V = \{V_1, V_2, \ldots, V_n\}$represents parameter nodes; $V_i = \{+, 0, -\}$ is defined as node states: "0", "+", and "–" represent the normal state, higher than normal state and lower than normal state, respectively; $E = \{E_1, E_2, \ldots, E_m\}$ represent branch nodes, $E_i = \{+, -\}$ represents the directed edge, where "+", "–" indicate the cause node and effect node in positive and negative effects, respectively, which are expressed by a solid line or dotted line (Maurya et al., 2007). There also exists a "coupling of relations" in the SDG model, $\delta^+ : E \to V$ (the cause node of a branch); $\delta^- : E \to V$ (the effect node of a branch).

A fault's propagation path can be located by SDG inference. A "moment sample" includes all the values of the monitored parameters at the same time. According to the "moment sample", if $\varphi(\delta^+ E_k)\varnothing(E_k)\varphi(\delta^- E_k) = +$, then the directed edge is defined as a consistent path. An SDG model is presented as an example in **Figure 1**, which also gives an example of a consistent path. **Figure 1** shows that if:

$$\begin{aligned}&\varphi(A) = +, \varnothing(A-B) = +, \varphi(B) = +, \varphi(A)\varnothing(A-B)\\&\varphi(B) = +, \varnothing(B-C) = -,\\&\varphi(C) = +, \text{ so } \varphi(A)\varnothing(A-B)\varphi(B)\varnothing(B-C)\varphi(C) = +\end{aligned}$$

then A–B–C is a consistent path. In **Figure 1**, if a symbol is "+", the model means: A increases (+) → B increases (+) → C decreases (–), then nodes A, B, C constitute a consistent path. A consistent path can not only describe the fault's propagation path but also can explain the reason why failure occurs. Thus, the role of SDG-based FDD is to find all consistent paths in instantaneous samples of the system.

Signed Directed Graph-Based Fault Detection and Diagnosis

SDG inference is divided into forward inference and backward inference. Forward inference generally starts from the selected

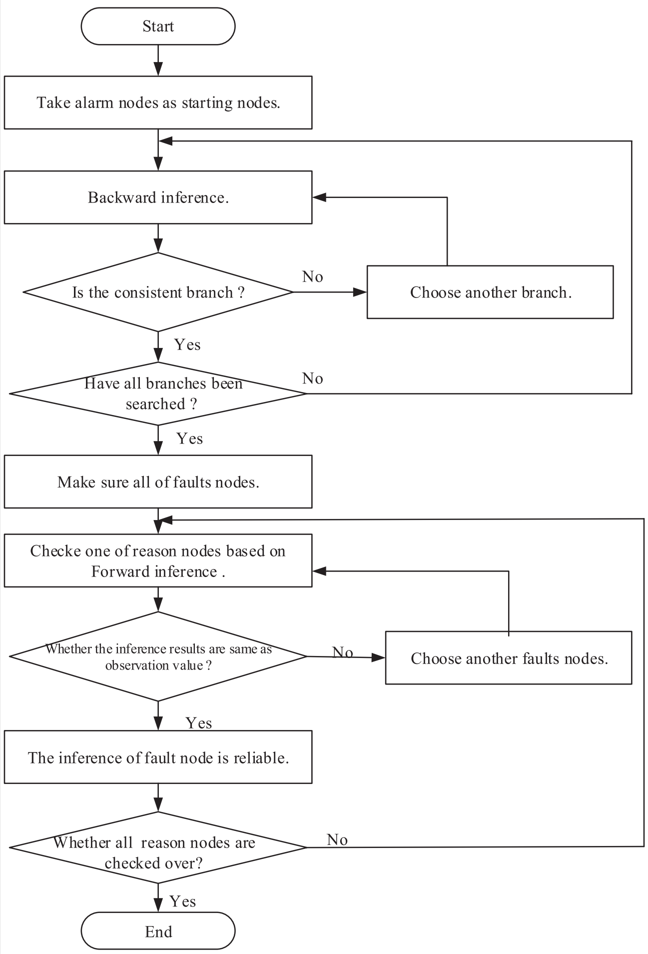

FIGURE 2 | Flow chart of SDG inference.

candidate fault node to find all consistent paths; its purpose is mainly to verify the correctness of FDD. Backward inference generally starts from the sign nodes back to the fault nodes based on a consistent path and is used for FDD (Mano et al., 2006). Forward inference and backward inference are usually combined for FDD. First, candidate faults are identified based on backward inference and forward inference is adopted from these candidate faults to remove false faults (Liu et al., 2014). The flow chart is shown in **Figure 2**.

An SDG model is shown in **Figure 3**. According to the alarm parameters *h*, *d*, *f*, candidate faults are identified based on backward inference and identifying a consistent path. Taking *d* as a starting node, *d*–*h* is a consistent path, which means nodes A and B are candidate faults. In the same way, taking *h*, *f* as starting nodes, then nodes A and B are again candidate faults. When candidate parameters {*d*, *e*, *f*, *h*} are identified based on forward inference, then the status of these candidate parameters is obtained by process monitoring. According to forward inference, A–*e* is not a consistent path, but all paths of node B have occurred; therefore, A is a false fault and B is a true fault.

PROCESS MONITORING FOR NUCLEAR POWER PLANTS

The purpose of process monitoring is to assess the states of parameters that are utilized for FDD. Here, the method of process monitoring is based on threshold and QTA methods.

Threshold Method

The threshold method assesses a parameter's status above the upper limit or below the lower limit. The method is easy to operate with software and easily understood by the operator, but it has some disadvantages: the thresholds in NPPs are more conservative, so alarm signals occur too late, and incipient fault diagnosis is difficult to achieve (Daneshvar and Rad, 2010). Therefore, the threshold method is not enough to achieve the goal of process monitoring and other methods should be added to improve the sensitivity of process monitoring.

Qualitative Trend Analysis

The purpose of QTA for process monitoring is to obtain a best-fit trend of parameters to assess the state of NPPs. Trend fitting is primarily based on linear least-squares (Frank, 1996). The main algorithm is as follows.

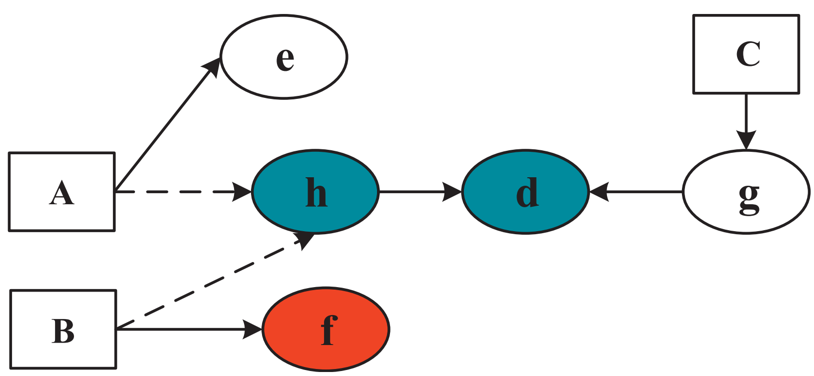

FIGURE 3 | Example of an SDG model.

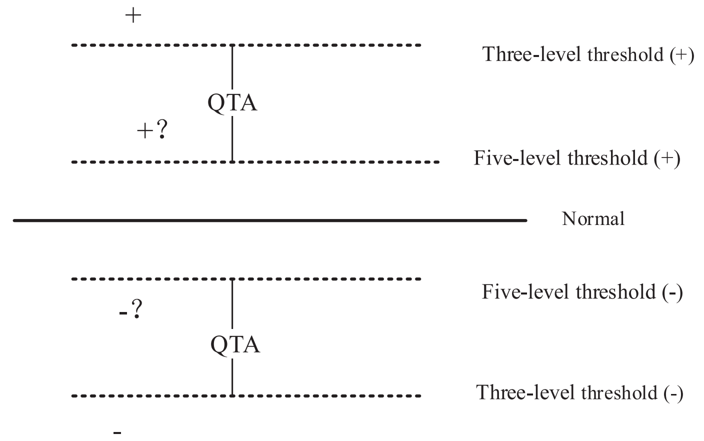

FIGURE 4 | Five-level threshold.

Parameters x, y are sampled with n sets of data $(x_1, y_1), (x_2, y_2), \ldots, (x_n, y_n)$. Assuming that x and y have a linear relationship, by the least squares method, the regression equation between x and y: $y = ax + b$ is achieved, where a, b minimize bias squares Q. A qualitative trend is achieved by calculating slope a. The fitting equations are shown by **Eqs. 1–3**. Values of $a > 0$, $a < 0$, $a = 0$ indicate that the parameter's status is high, low, and normal respectively.

$$Q = \sum_{i=1}^{n} (y_i - b - ax_i)^2 \tag{1}$$

$$a = \frac{\sum_{i=1}^{n} (x_i - \overline{x})(y_i - \overline{y})}{\sum_{i=1}^{n} (x_i - \overline{x})^2} \tag{2}$$

$$b = \overline{y} - a\overline{x} \tag{3}$$

The main disadvantage of QTA for process monitoring is that it may lead to misdiagnosis. When the system is in a state of disturbance, the parameters may remain high or low over a certain period, which leads to a misdiagnosis.

MONITORING AND FAULT DIAGNOSIS FRAMEWORK FOR NUCLEAR POWER PLANTS

Five-Level Threshold and Qualitative Trend Analysis

To mitigate the shortcomings of QTA and threshold methods in process monitoring, we propose a five-level threshold combined with QTA to improve the sensitivity of process monitoring.

1) Thresholds in nuclear power plants

Nodes are divided into two categories: parameter nodes and fault nodes. The statuses of parameter nodes are determined by the upper and lower limits (three-level threshold) of each parameter. A parameter's status may be in three states: "0", "1", or "−1". "1" indicates that the value of a parameter exceeds the upper limit, "0" indicates that values of a parameter are normal, and "−1" indicates that values of a parameter are below the lower limit (He et al., 2014). The calculation method is shown in **Eq. 4**:

$$\psi_i = \begin{cases} -1, & if \quad n_i < n_{il} \\ 0, & if \quad n_{il} < n_i < n_{ih} \ (1 \le i \le \alpha) \\ 1, & if \quad n_i > n_{ih} \end{cases} \tag{4}$$

2) Concept of a five-level threshold

The concept of a five-level threshold is shown in **Figure 4**. "±", "±?" stand for certain states and uncertain states of parameters respectively (Chung and Bien, 1994). A three-level threshold is currently used in NPPs. The five-level threshold, which is very sensitive to a parameter's variability, includes the three-level threshold. When parameters are within the three-level threshold, the status of a parameter is considered certain. When the parameters are between the five-level threshold and three-level threshold, the parameter's state is uncertain and the status of the parameter is identified using QTA.

3) U test

It is difficult to obtain the fault data of NPPs, but normal data are easy to acquire. Most parameters may appear as random variability in normal data, in which the values of parameters follow a normal distribution, but parameters may not always do so. The U-test is applied to determine whether the values of parameters follow a normal distribution. Calculating coefficients of skewness and kurtosis is the first step of the U test (Hao et al., 2009). For the time sequence $\{x_i, i = 1, 2, \ldots, N\}$ coefficients of skewness g and kurtosis k can be written as:

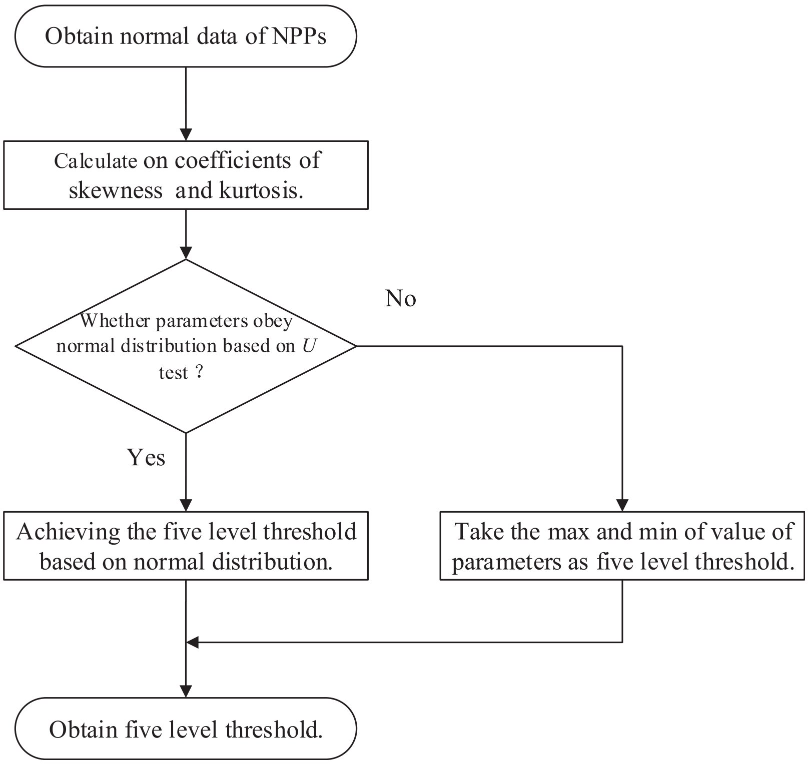

FIGURE 5 | Flow chart for calculation of five-level threshold.

$$g = \frac{\sum_{i=1}^{n} (x_i - \overline{x})^3}{(n-1)\sigma^3}, \tag{5}$$

$$k = \frac{\sum_{i=1}^{n} (x_i - \overline{x})^4}{(n-1)\sigma^4} - 3, \tag{6}$$

where$\sigma$is the standard deviation, $\overline{x}$ is the mean value, and n is the number of samples.

$$|g| < U_1 \tag{7}$$

$$|k| < U_2 \tag{8}$$

$$U_{1\alpha} = 1.96\sqrt{\frac{6(n-2)}{(n+1)(n+3)}} \tag{9}$$

$$U_{2\alpha} = 1.96\sqrt{\frac{24n(n-2)(n-3)}{(n+1)^2(n+3)(n+5)}} \tag{10}$$

If **Eqs. 6, 7** are satisfied, then parameters obey a normal distribution with time.

4) U test-based five-level threshold acquisition

Because it is difficult to obtain fault data from NPPs, the five-level threshold is obtained by handling the normal data of NPPs. The flow chart is shown in **Figure 5**.

5) Five-level threshold and qualitative trend analysis

When monitored parameters obey a normal distribution, the probability of parameters exceeding the five-level threshold is $0.00265\,(y < \overline{y}3\sigma \ or \ y > \overline{y} + 3\sigma)$ (Tarifa and Scenna, 1998). When the five-level threshold is met by the maximum and minimum values of parameters, the probability of these parameters exceeding the five-level threshold is lower than 0.00265. Therefore, it is reasonable to use the normal distribution to calculate the probability of parameters used to assess the abnormal state of NPPs.

The probability of parameters exceeding a five-level threshold over three continuous seconds is $0.002653^3 = 1.76 \times 10^{-8}$, as can be seen above. If an outside range based on the five-level threshold over three continuous seconds is considered as an abnormal process, then QTA based on least-square fitting can be used to obtain qualitative trends. The parameter c is defined in **Eq. 10** and can extract qualitative trends for FDD.

$$c = a*\psi_i > 0, \tag{11}$$

where$\psi_i$is shown in **Eq. 11**.

$$\psi_i = \begin{cases} -1 & \text{lower than five level threshold } (-) \text{ and higher than three level threshold } (-) \\ 0 & \text{normal} \\ 1 & \text{higher than five level threshold } (-) \text{ and lower than three level threshold } (-) \end{cases} \tag{12}$$

We propose the use of a five-level threshold in combination with QTA for incipient fault diagnosis. However, when the system is in a state of disturbance, the parameters may remain high or low over a certain time, which leads to misdiagnosis. To

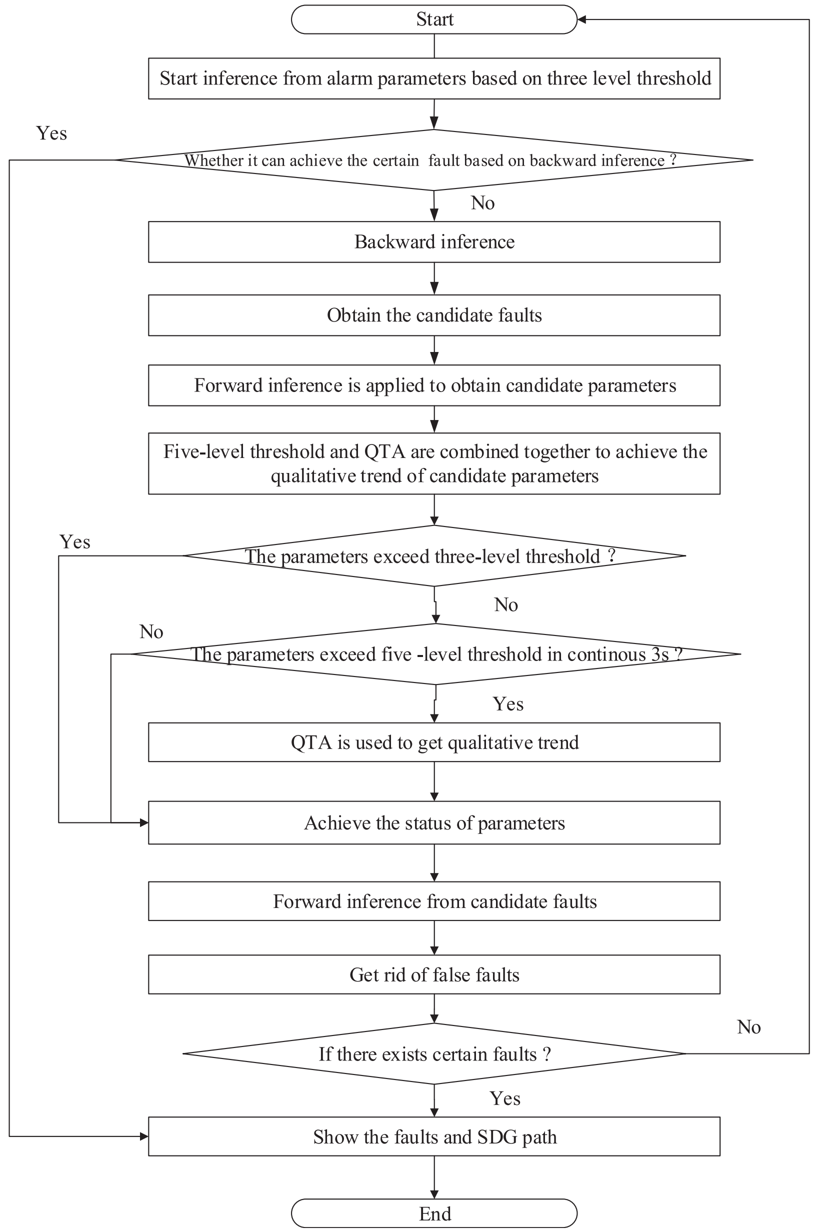

FIGURE 6 | Flow chart of process monitoring and FDD.

ensure the accuracy of FDD, SDG inference is proposed in combination with QTA and the five-level threshold.

Framework of Combining Process Monitoring and Signed Directed Graph-Based Inference for Fault Detection and Diagnosis

Five-level threshold, QTA, and SDG inference are combined to improve the veracity and sensitivity of process monitoring and FDD. Here, we assume that when the system is perturbed and parameters exceed the three-level threshold, failure occurs.

The steps of process monitoring and FDD are as follows:

Step 1: The SDG model is set up based on the flow chart and knowledge of systems in NPPs; although, at the same time, the SDG model should be modified and verified by simulation.

Step 2: The five-level threshold is achieved by data handling. The three-level threshold is initially applied for process monitoring, and when alarm signals appear as defined by the three-level threshold, candidate faults are identified by SDG backward inference.

Step 3: According to the identification of candidate faults, each fault is separately assessed by forward inference to determine candidate parameters.

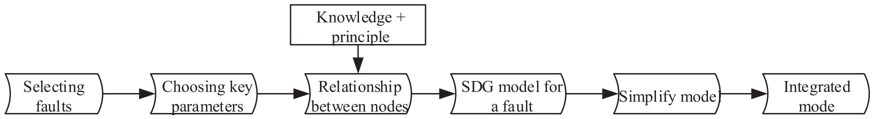

FIGURE 7 | Flow chart of SDG modeling.

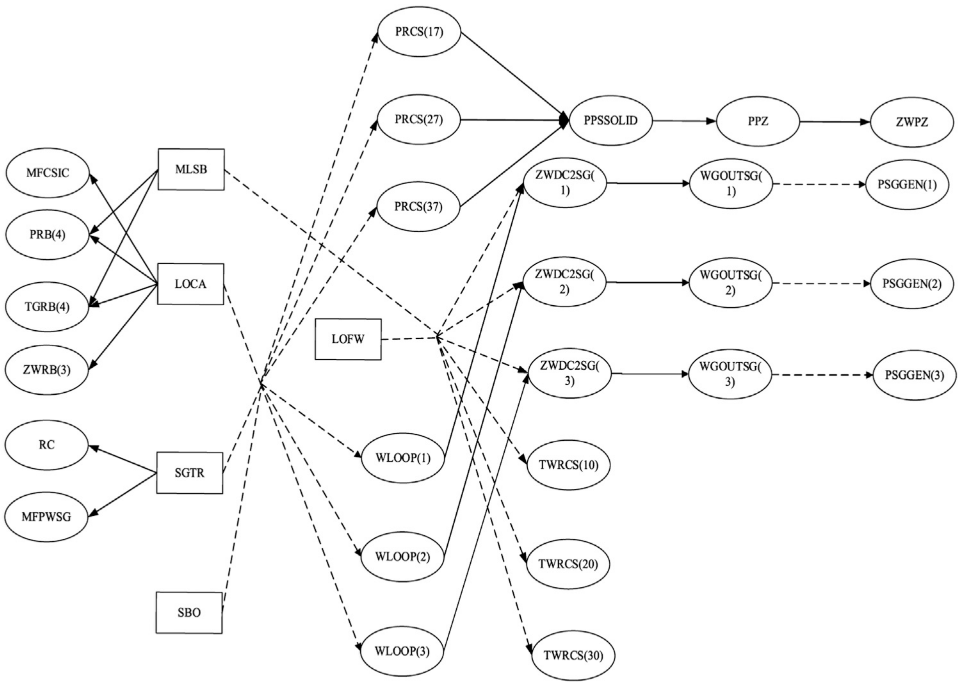

FIGURE 8 | SDG model for the pressurized water reactor.

Step 4: If the state of a candidate parameter is considered certain by the three-level threshold, this parameter state is used for FDD. If a candidate parameter's state is uncertain based on the three-level threshold, then five-level threshold and QTA are combined to determine the state of that parameter.

Step 5: According to the parameter's state, forward inference is used for FDD to reject false candidate faults.

Step 6: If a fault exists, then the result is shown in the NPP interface. If there is no fault, Steps 2–5 are repeated. The flow chart is shown in **Figure 6**.

APPLICATION CASE STUDY

1) Method of SDG modeling

According to the basic steps and principles of SDG modeling, the SDG model of a loss of coolant accident (LOCA), steam generator tube rupture, loss of feed water, main steam line break, and station black-out over three loops of the pressurized water reactor are created. The SDG model of an NPP is established by combining fundamental principles and existing knowledge. The steps for SDG modeling in NPPs are shown in **Figure 7**.

Analysis of the LOCA model: When a small LOCA occurs, the primary loop flow leaks, and with the containment of pressure, the temperature will rise. With the constant flow of leaking coolant, the pit water level will rise. The system pressure will have a short increase, but after a period of time, the loop pressure will continue to decrease, which reduces the system pressure and lowers the pressurizer water level and pressure. At the same time, the loop coolant flow will continue to decline. The LOCA of SDG can be built based on LOCA. As with SGTR and loss of feed water, the SDG model is built as shown in **Figure 8** (abbreviations are listed in **Table 1**).

2) Five-level threshold

First, three-level thresholds are achieved by NPPs according to the steps shown in **Figure 5**; then the five-level threshold is calculated and stored in a database.

3) Process monitoring and FDD

TABLE 1 | Abbreviation of parameters.

Parameters	Abbreviation	Parameters	Abbreviation
Flow of coolant in loop 1	WLOOP(1)	Temperature of cold leg in loop 1	TWRCS(10)
Flow of coolant in loop 2	WLOOP(2)	Temperature of cold leg in loop 2	TWRCS(20)
Flow of coolant in loop 3	WLOOP(3)	Temperature of cold leg in loop 3	TWRCS(30)
Water level in steam generator 1	ZWDC2SG(1)	Pressure of cold leg in loop 1	PRCS(10)
Water level in steam generator 2	ZWDC2SG(2)	Pressure of cold leg in loop 2	PRCS(20)
Water level in steam generator 3	ZWDC2SG(3)	Pressure of cold leg in loop 3	PRCS(30)
Flow in steam generator 1	WGOUTSG(1)	The average primary pressure in reactor coolant system	PPSSOLID
Flow in steam generator 2	WGOUTSG(2)	Pressure of pressurizer	PPZ
Flow in steam generator 3	WGOUTSG(3)	Water level in pressurizer	ZWPZ
Pressure in steam generator 1	PSGGEN(1)	Temperature of the containment	TRGB(4)
Pressure in steam generator 2	PSGGEN(2)	Pressure of the containment	PRB(4)
Pressure in steam generator 3	PSGGEN(3)	Radioactivity of condenser	RC
Radioactivity of sewage of steam generator	MFPWSG(14,1)	Radioactivity of the containment	MFCSIC
Pit water level	ZWRB(3)	Pressure of second-loop	PBS

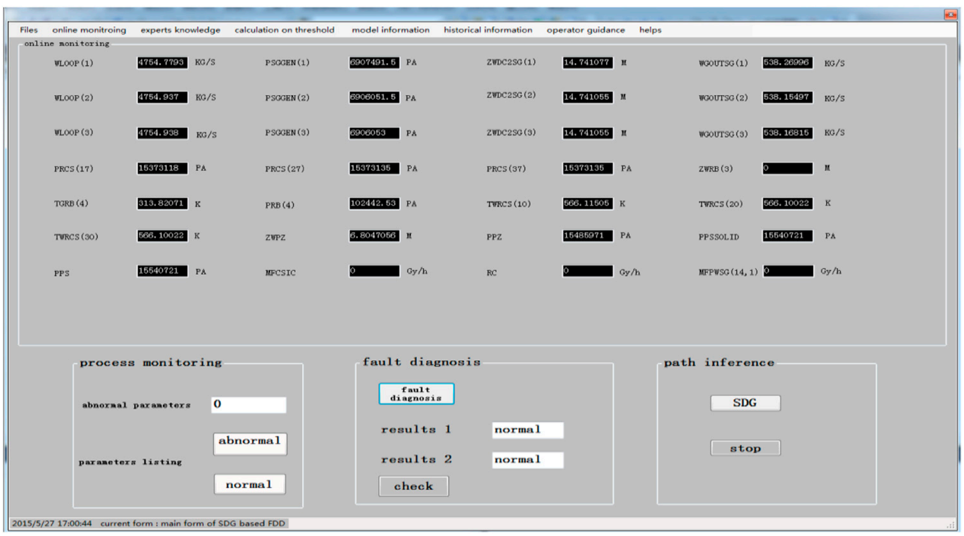

FIGURE 9 | FDD interface in the normal state.

Figure 9 shows the interface for process monitoring and FDD when the NPP is in a normal state (parameters in black are in a normal state; red indicates that the parameter is abnormal and the parameter status is "1"; green indicates that the parameter is abnormal and the parameter status is "−1"). When the NPP is in a normal state, there are no alarm signals and the values of parameters are displayed in real-time.

When LOCA occurs in 1000 s, the interface changed, as shown in **Figure 10**. The parameters that are monitored according to the flowchart shown in **Figure 6** are shown in **Figure 10**. **Figure 10** shows that FDD results in 2 based on a five-level threshold, QTA. SDG inference for LOCA and results 1 are based on an unknown threshold method. The results show that the speed of diagnosis based on a five-level threshold is faster than that for a single-threshold method.

When LOCA occurred, the PRB (4) first exceeded the three-level threshold; the corresponding process monitoring on PRB (4) is shown in **Figure 11**. On this basis, SDG backward inference was used to identify LOCA candidate faults. TGRB (4) was one of the candidate parameters based on candidate faults and SDG forward inference.

Process monitoring on TGRB (4) based on a five-level threshold, QTA, and SDG is shown in **Figure 12**. **Figure 12** shows that fitting of the curve improves the speed of process monitoring and ensures the accuracy of FDD.

When the simulator inserts a fault in 1000 s, the TGRB (4) starts to exceed the five-level threshold at 1004 s. At 1009 s, continuous 5 s exceeds the five-level threshold, QTA can identify abnormal parameters. When using the normal threshold method (three-level threshold), it is difficult to find parameters abnormalities. QTA can detect parameter abnormalities early, that is, within 1009–1034 s. It can recognize that the parameters are abnormal, and the common method can only find the parameters of abnormality after 1034 s.

FIGURE 10 | Interface of FDD when LOCA occurred.

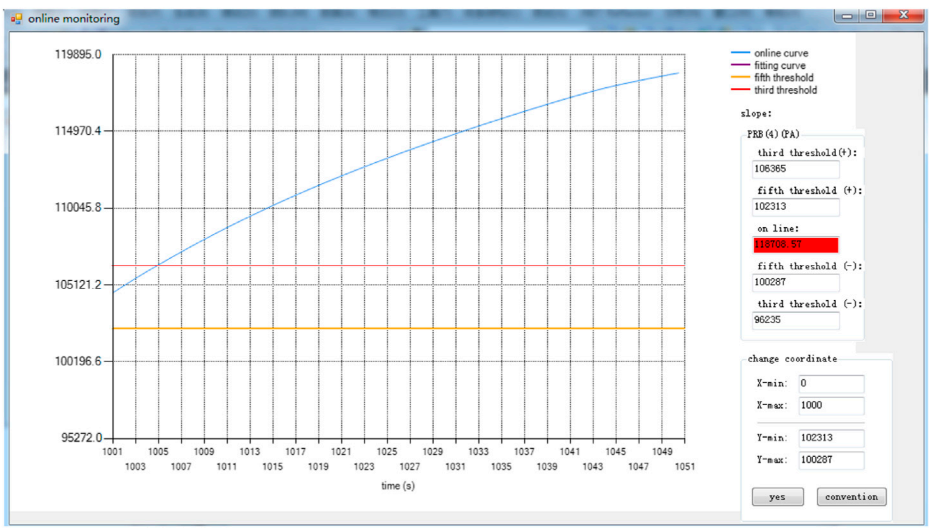

FIGURE 11 | Process monitoring on TGRB (4) when LOCA occurred.

QTA and threshold method realize parameter monitoring in the SDG model. The abnormality of TGRB (4) is first detected, and then the path (LOCA—TGRB (4)) is inferred based on the SDG model; according to the state of ZWPZ, PPZ, PPSSOLID, PRCS (17), the path is obtained: LOCA—PRCS (17) decreases—PPSSOLID decreases—PPZ decreases—ZWPZ decreases. The path is shown below. SDG inference to verify the accuracy of FDD results is shown in **Figure 13** for a LOCA accident. According to the obtained path, the possible failure is LOCA.

1) LOCA—pressure of the containment (PRB (4)) increases;
2) LOCA—radioactivity of the containment (MFCSIC) increases;
3) LOCA—temperature of the containment (TRGB (4)) increases;
4) LOCA—pit water level (ZWRB(3)) increases;
5) LOCA—pressure of cold leg in loop 1(PRCS(17)) decreases—the average primary pressure in the reactor coolant system (PPSSOLID) decreases—pressure of pressurizer (PPZ) decreases—water level in pressurizer (ZWPZ) decreases.

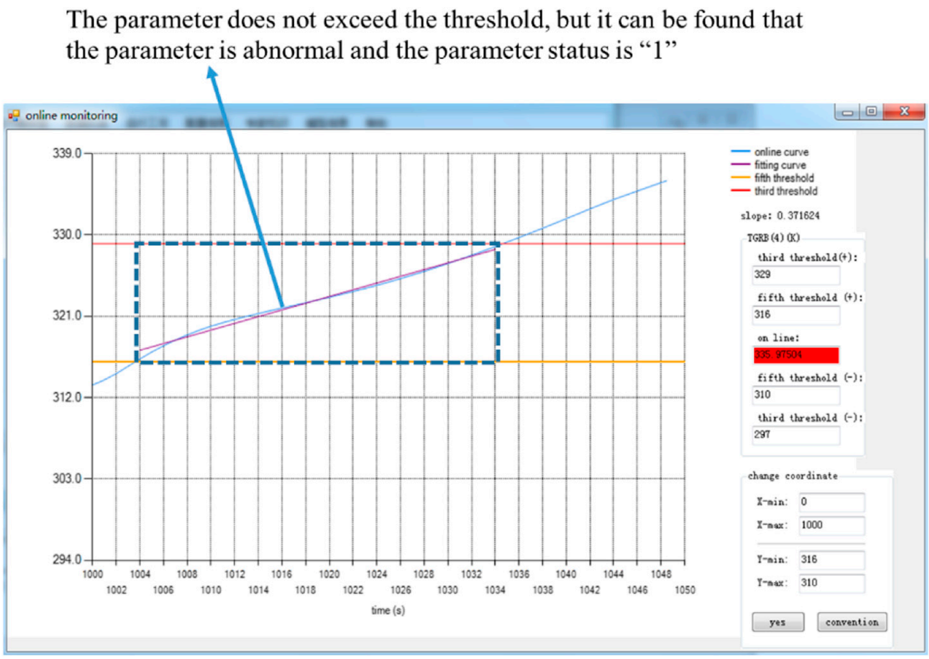

FIGURE 12 | Process monitoring on TGRB (4) when LOCA occurred.

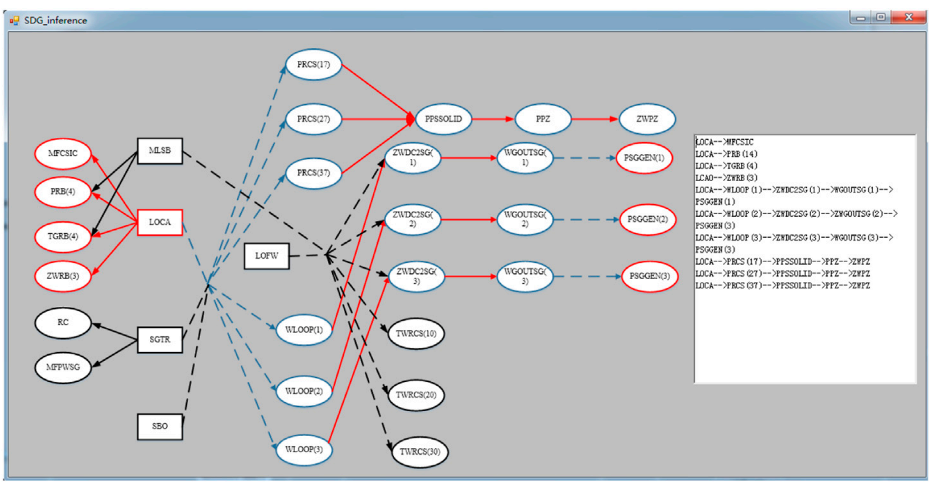

FIGURE 13 | Interface of SDG inference at the time the LOCA occurred.

CONCLUSION

Based on the characteristics of NPPs, this study proposes a method of process monitoring and FDD based on SDG. This method can increase the path of SDG, which is needed to guarantee the accuracy of FDD. The study has provided simulation-based examples that show the advantages of process monitoring and FDD by use of five-level threshold, QTA, and SDG methods:

1) It improves the sensitivity of process monitoring;
2) Incipient fault diagnosis is achieved and accuracy is improved;
3) Fault propagation paths are shown by SDG, which can explain the causes of faults.

Because of the complex structure of NPPs, the SDG model as established in this paper needs further refinement and will require different methods of establishment for different types of reactors. An SDG-based method combined with other quantitative methods is the subject of future research.

DATA AVAILABILITY STATEMENT

The raw data supporting the conclusion of this article will be made available by the authors, without undue reservation.

AUTHOR CONTRIBUTIONS

All authors listed have made a substantial, direct, and intellectual contribution to the work and approved it for publication.

FUNDING

This work is supported by National key research and development program (2019YFC0810705), National key research and development program (2018YFC0810601), R & D projects in key areas of Guangdong Province (2019B111102002).

ACKNOWLEDGMENTS

Thanks China Postdoctoral Science Foundation funded project.

REFERENCES

Amal, H., Pourahmadi, M., and Majidi-Maraghi, H. (2011). Fault diagnosis and classification based on wavelet transform and neural network. *Prog. Nucl. Energ.* 53, 41–47. doi:10.1016/j.pnucene.2010.12.001

Chen, J., Li, H., and Sheng, D. (2015). A hybrid data-driven modeling method on sensor condition monitoring and fault diagnosis powers plants. *Int. J. Electr. Power Energ. Syst.* 71, 274–284. doi:10.1016/j.ijepes.2015.03.012

Chung, H. Y., and Bien, Z. G. (1994). Incipient multiple fault diagnosis in real time with application to large-scale systems. *IEEE Trans. Nucl. Sci.* 41 (4), 1692–1703. doi:10.1109/23.322777

Daneshvar, M., and Rad, B. F. (2010). Data driven approach for fault detection and diagnosis of boiler system in coal fired power plant using principal component analysis. *Int. Rev. Autom. Control.* 3 (2), 198–208.

Frank, P. M. (1996). Analytical and qualitative model-based fault diagnosis-a survey and some new results. *Eur. J. Control* 2 (1), 6–28. doi:10.1016/s0947-3580(96)70024-9

Gajjar, S., Kulahci, M., and Palazoglu, A. (2017). Real-time fault detection and diagnosis using sparse principal component analysis. *J. Process Control* 64, 112–128. doi:10.1016/j.jprocont.2017.03.005

Gao, D., and Wu, C. G. (2010). Signed directed graph and qualitative trend analysis based fault diagnosis in chemical industry. *Chin. J. Chem. Eng.* 18 (2), 265–276. doi:10.1016/s1004-9541(08)60352-3

Hao, J. P., Xu, L. Q., and Gang, L. I. (2009). Skewness and kurtosis test of normal distribution for target detection precision. *J. North Univ. China* 30 (5), 472–476.

He, B., Chen, T., and Yang, X. H. (2014). Root cause analysis in multivariate statistical process monitoring: integrating reconstruction-based multivariate contribution analysis with fuzzy-signed directed graphs. *Comput. Chem. Eng.* 64, 167–177. doi:10.1016/j.compchemeng.2014.02.014

Hiranmayee, V., and Venkatasubramanian, V. (1999). PCA-SDG based process monitoring and fault diagnosis. *Control. Eng. Pract.* 7, 903–917. doi:10.1016/S0967-0661(99)00040-4

Iri, M., Aoki, K., and O'Shima, E. E. (1979). An algorithm for diagnosis of system failures in the chemical process. *Comput. Chem. Eng.* 3, 489–493. doi:10.1016/0098-1354(79)80079-4

Kang, C. W., and Golay, M. W. (1999). A Bayesian belief network-based advisory system for operational availability focused diagnosis of complex nuclear power systems. *Expert Syst. Appl.* 17 (1), 21–32. doi:10.1016/s0957-4174(99)00018-4

Kramer, M. A., and Palowitch, B. L. (1987). A rule-based approach to fault diagnosis using the signed directed graph. *AIChE J.* 33 (7), 1607–1078. doi:10.1002/aic.690330703

Lapp, S. A., and Powers, G. J. (1977). Computer-aided synthesis of fault-trees. *IEEE Trans. Rel.* 26 (2), 2–12. doi:10.1109/tr.1977.5215060

Liu, Y. K., Wu, G. H., Xie, C. L., and Duan, Z. Y., (2016). A fault diagnosis method based on signed directed graph and matrix for nuclear power plants. *Nucl. Eng. Des.*, 297, 166–174. doi:10.1016/j.nucengdes.2015.11.016

Liu, Y. K., Liu, Z., and Wu, X. T. (2014). Research on fault diagnosis with SDG method for nuclear power plant. *Atom. Energy Sci. Technol.* 48 (9), 1646–1653. doi:10.7538/yzk.2014.48.09.1646

Liu, Y. K., Peng, M. J., Xie, C. L., and Dang, Y. X.(2013). Research and design of distributed fault diagnosis system in nuclear power plant. *Prog. Nucl. Energ.* 68, 97–110. doi:10.1016/j.pnucene.2013.06.002

Ma, J., and Jiang, J. (2011). Applications of fault detection and diagnosis methods in nuclear power plants: a review. *Prog. Nucl. Energ* 53, 255–266. doi:10.1016/j.pnucene.2010.12.001

Ma, J., and Jiang, J. (2015). Semi supervised classification for fault diagnosis in nuclear power plants. *Nucl. Eng. Tech* 47 (2), 176–186. doi:10.1016/j.net.2014.12.005

Mano, R. M., Rengaswamy, R., and Venkatasubramanian, V. (2006). A signed directed graph-based systematic framework for steady-state malfunction diagnosis inside control loops. *Chem. Eng. Sci.* 61, 1790–1810. doi:10.1016/j.ces.2005.10.023

Maurya, M. R., Rengaswamy, R., and Venkatasubramanian, V. (2004). Application of signed digraphs-based analysis for fault diagnosis of chemical process flowsheets. *Eng. Appl. Artif. Intell.* 17, 501–518. doi:10.1016/j.engappai.2004.03.007

Maurya, M. R., Rengaswamy, R., and Venkatasubramanian, V. (2007). A signed directed graph and qualitative trend analysis-based framework for incipient fault diagnosis. *Chem. Eng. Res. Des.* 85 (10), 1407–1422. doi:10.1016/s0263-8762(07)73181-7

Maurya, M. R., Rengaswamy, R., and Venkatasubramanian, V. (2005). Fault diagnosis by qualitative trend analysis of the principal components. *Chem. Eng. Res. Des.* 83 (9), 1122–1132. doi:10.1205/cherd.04280

Mo, K., Lee, S. J., and Seong, P. H. (2007). A dynamic neural network aggregation model for transient diagnosis in nuclear power plants. *Prog. Nucl. Energy* 49, 262–272. doi:10.1016/j.pnucene.2007.01.002

Peng, Di., Geng, Z. Q., and Zhu, Q. X. (2014). A multilogic probabilistic signed directed graph fault diagnosis approach based on Bayesian inference. *Ind. Eng. Chem. Res.* 53, 9797–9804. doi:10.1021/ie403608a

Tarifa, E. E., and Scenna, N. J. (1998). A methodology for fault diagnosis in large chemical process and an application to a multistage flash desalination process: part I. *Rel. Eng. Syst. Saf.* 60 (1), 29–40. doi:10.1016/s0951-8320(97)00125-7

Tarifa, E. E., and Scenna, N. J. (2003). Fault diagnosis for a MSF using a SDG and fuzzy logic. *Desalination* 152, 207–214. doi:10.1016/s0011-9164(02)01065-2

Wang, H. Z., and Chen, B. Z. (2009). SDG-based HAZOP analysis of operating mistakes for PVC process. *Process Saf. Environ. Prot.* 87, 40–46. doi:10.1016/j.psep.2008.06.004

Žarković, M., and Stojković, Z. (2017). Analysis of artificial intelligence expert systems for power transformer condition monitoring and diagnostics. *Electr. Power Syst. Res.* 149, 125–136. doi:10.1016/j.epsr.2017.04.025

Zhou, Z., and Zhang, Q. (2017). Model event/fault trees with dynamic uncertain causality graph for better probabilistic safety assessment. *IEEE Trans. Rel.* 66 (99), 1–11. doi:10.1109/tr.2017.2647845

Conflict of Interest: The authors declare that the research was conducted in the absence of any commercial or financial relationships that could be construed as a potential conflict of interest.

frontiers in Energy Research

ORIGINAL RESEARCH
published: 10 May 2021
doi: 10.3389/fenrg.2021.665262

Diagnosis and Prediction for Loss of Coolant Accidents in Nuclear Power Plants Using Deep Learning Methods

Jingke She[1]*, *Tianzi Shi*[1], *Shiyu Xue*[1], *Yan Zhu*[1], *Shaofei Lu*[1], *Peiwei Sun*[2] and *Huasong Cao*[2]

[1] College of Computer Science and Electronic Engineering, Hunan University, Changsha, China, [2] School of Energy and Power Engineering, Xi'an Jiaotong University, Xi'an, China

A combination of Convolutional Neural Network (CNN), Long-Short Term Memory (LSTM), and Convolutional LSTM (ConvLSTM) is constructed in this work for the fault diagnosis and post-accident prediction for Loss of Coolant Accidents (LOCAs) in Nuclear Power Plants (NPPs). The advantages of ConvLSTM, such as effective feature determination and extraction, are applied to the classification of LOCA cases. The prediction accuracy is enhanced via the collaborative work of CNN and LSTM. Such a hybrid model is proved to be functional, accurate, and adaptive, offering quick accident judgment and a reliable decision basis for the emergency response purpose. It then allows NPPs to have an Artificial Intelligence (AI)-based solution for fault diagnosis and post-accident prediction.

Keywords: CNN, LSTM, ConvLSTM, LOCA, diagnosis, prediction

OPEN ACCESS

Edited by:
Xianping Zhong,
University of Pittsburgh, United States

Reviewed by:
Xingang Zhao,
Oak Ridge National Laboratory (DOE), United States
Jiankai Yu,
Massachusetts Institute of Technology, United States
Guohua Wu,
Harbin Institute of Technology, China

Correspondence:
Jingke She
shejingke@hnu.edu.cn

Specialty section:
This article was submitted to Nuclear Energy, a section of the journal Frontiers in Energy Research

Received: *07 February 2021*
Accepted: *13 April 2021*
Published: *10 May 2021*

Citation:
She J, Shi T, Xue S, Zhu Y, Lu S, Sun P and Cao H (2021) Diagnosis and Prediction for Loss of Coolant Accidents in Nuclear Power Plants Using Deep Learning Methods. Front. Energy Res. 9:665262. doi: 10.3389/fenrg.2021.665262

INTRODUCTION

The quick and accurate response to a Nuclear Power Plants (NPP) accident is critical to the safety of both the plant and the public. However, the accident model needed for fault diagnosis and post-accident prediction is hard to construct due to complex physical processes, nonlinear parameter variations, and multiple system factors. Assumptions have to be often made, whereas the accuracy of the model has to be sacrificed. Furthermore, most of the accidents behave as a nonlinear process, which makes the traditional statistical methods difficult to describe the system behavior and development trend. With the progress of machine learning, especially deep learning, describing accident behavior using data-based Artificial Intelligence (AI) models has become an effective way to avoid the above-mentioned problems. A large amount of simulated nuclear power plant data from previous research works has also settled a firm base to carry out AI models for fault diagnosis and post-accident prediction.

LOCA Classification

Loss of Coolant Accident (LOCA) is a type of severe accident that could happen during the operation of NPPs. The break of the Primary Heat Transport (PHT) system causes a fast and large loss of coolant, leading to the overheating of the reactor core. Hence, it is of great importance to timely determine the LOCA situation and evaluate its development. The break size has to be confirmed first since it determines both the flowrate at the break and the post-LOCA behavior of the system. As mentioned, building an accurate system model for this purpose is prevented by the complex accident process itself. Another challenge is that the break size varies due to different circumstances when the LOCA is taking place.

Researchers in recent years have explored possible methods to identify the LOCA case. Both Na et al. (2004) and Santhosh et al. (2011) trained their neural network (NN) models using a transient dataset generated by thermal-hydraulic codes to detect the break size of a LOCA. Later on, multi-connected Support Vector Machines (SVMs) were utilized to estimate the break size such that the LOCA type can be identified (Yoo et al., 2017). Tian et al. (2018) proposed a constraint-based random search algorithm for optimizing NN architectures for detecting the break size of a LOCA. Principal Component Analysis (PCA) was adopted by Sun et al. (2019) to identify the LOCA case happening at the Steam Generator (SG) tubes of a small modular reactor. Tanim et al. (2020) uses the PCTRAN prototype software to determine the unexpected interruption and loss of the coolant of the VVER-1200 reactor and their possible consequences on various parameters. Weglian et al. (2020) provides a single-top PRA fault tree for comprehensive assessment of the risk of various hazards such as the loss of coolant accidents. Deep learning models, as a data-driven method, is seldom found in previous LOCA diagnosis works. To avoid the complexity of building analytical system models, this work take ConvLSTM as a deep learning attempt to solve the LOCA diagnosis challenge.

The LOCA case is determined in this work using Convolutional Long-Short Term Memory (ConvLSTM) (Shi et al., 2015), which is improved in this work for data series classification. ConvLSTM is a variant of LSTM. It replaces the matrix multiplication of each gate in the LSTM unit with a convolution operation, such that the basic spatial features can be captured by convolution operations in multi-dimensional data. The main difference between ConvLSTM and LSTM is the input dimension. Input data to LSTM is one-dimensional. However, ConvLSTM can handle data that are one-dimensional, two-dimensional, and three-dimensional. The training dataset is obtained using an NPP control system design and validation platform (Sun et al., 2017). The design and validation platform mainly uses shared memory technology and an engineering simulator coupled with MATLAB/Simulink. Subsequently, the performance can be evaluated through simulations of abrupt load-transient changes and wide range-load changes. The coupling of the engineering simulator and MATLAB/Simulink generates an industry-grade simulation and validation platform, providing an effective tool for research on barely happened scenarios. The training dataset from such platform enables the ConvLSTM model to recognize features of different break sizes such that the LOCA type can be confirmed at an early stage of the accident.

Post-accident Prediction

Tracing critical system parameters and predicting their post-LOCA development assist the emergency response team to act in advance, reserving the safety margin as expected. However, knowing the break size is not enough to settle the decision basis. Depending on the operation status, a certain size PHT break may be followed with different system behaviors.

A nonlinear process, such as the post-LOCA trend, cannot be easily predicted using traditional statistical methods. In the past decade, various attempts have been taken for the prediction of processes in NPPs, such as (1) predicting the counter-current flow limitation at hot leg pipe during a small-break LOCA (Jeong, 2002); (2) predicting the water vessel level using Group Method of Data Handling (GMDH) (Park et al., 2013) and Deep Neural Network (DNN) (Koo et al., 2018); (3) predicting the leak flow rate of LOCA using Fuzzy Neural Network (FNN) (Kim et al., 2014); (4) monitoring the real-time condition of a LOCA using Time-Frequency Domain Reflectometry (TFDR) (Lee et al., 2017); (5) using RELAP5/MOD3.3 code to predict the LOCA of the main steam break (MSLB) on the third generation reactor with passive safety features (Yang et al., 2019); and (6) utilizing DNN/LSTM expert system to predict the loss of nuclear power plant coolant accident (Radaideh et al., 2020).

This work proposes a deep learning model combined with both Convolutional Neural Network (CNN) and Long-Short Term Memory (LSTM) for the post-LOCA prediction. It is considered that the prediction model has to understand the variation caused by both the break size and the operation status. To achieve this, the CNN part is introduced to deal with the multi-dimensional dataset. It recognizes and extracts the key features such that the prediction process is not misled. LSTM, as a deep learning model for long-time series prediction, is then utilized to calculate the post-LOCA development of critical system parameters.

THE HYBRID MODEL FOR LOCA DIAGNOSIS AND PREDICTION

The hybrid model constructed in this work consists of two major modules. The modified ConvLSTM model is responsible for LOCA diagnosis, followed by the "CNN+LSTM" module for post-LOCA prediction.

Improved ConvLSTM for LOCA Diagnosis

ConvLSTM model was originally proposed for prediction purposes (Shi et al., 2015). It has been widely applied to image and video processing areas (Feng et al., 2019; Mukherjee et al., 2019; Niu et al., 2019). In this work, it is chosen as the classifier for LOCA diagnosis due to the following considerations:

1. LOCA scenario consists of complicated system variations, such as uncertain break size, flowrate drop, pressure drop, etc. The expected classifier has to be capable of locating the key features of these parameters and extracting them for prediction. This can be satisfied by the convolutional structure of the ConvLSTM.
2. The diagnosis triggered by LOCA deals with time-series data, which is an essential function of the LOCA classifier. ConvLSTM can apply its LSTM structure for this objective.
3. The LOCA diagnosis deals with multiple features and time-series data. Both have to be taken care of simultaneously. The ConvLSTM, with the assistance of certain additional

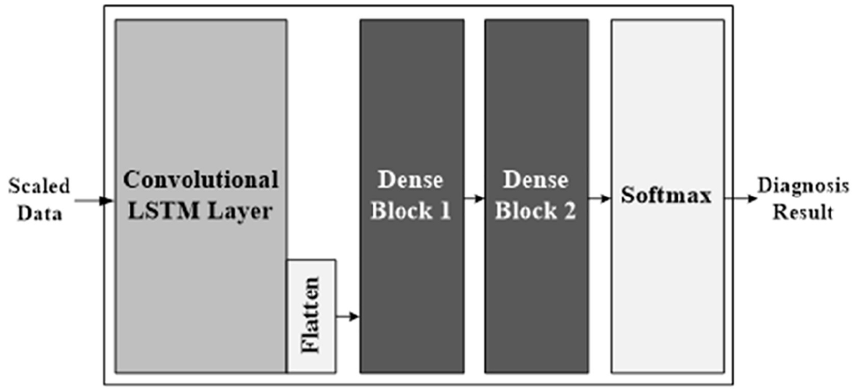

FIGURE 1 | Structure of the improved ConvLSTM.

structures, is capable of identifying and extracting key features from time-series data.

This work studies five Steam Generator Tube Rupture (SGTR) LOCA cases, i.e., break size of 0.2, 0.4, 0.6, 0.8, and 1.0 cm^2. Simulations are conducted using the mentioned platform (Sun et al., 2017) to obtain the dataset for model training and test. Each break case is simulated with different reactor power levels of 60, 70, 80, 90, and 100% to cover various operation statuses when the LOCA takes place. The traditional ConvLSTM layer is utilized in this work to extract key features from the normalized LOCA process dataset. Following it, there are two dense layers and a softmax function (Krizhevsky et al., 2012) to strengthen the classification performance. Using dense layers for classification has been verified by previous works (e.g., Kim and Medioni, 2010; Bi et al., 2019; Zhang et al., 2019). Dense layers used in these previous works have demonstrated qualified classification performance, which encourages its application to the classification of time-series data in this work. One of the two dense layers integrates the extracted features using 500 neural cells. The other one analyzes the results from the first one using five neural cells. Each cell in the second dense layer represents the probability of a break size. The softmax function is used after the dense layers, providing a probability list to indicate the classification result, i.e., the one with the largest probability. Critical system parameters, such as the pressurizer pressure and the coolant flowrate, are comprehensively examined by the model for a precise classification result. A brief illustration of the improved ConvLSTM is shown in **Figure 1**; while **Table 1** shows its parameter configuration.

TABLE 1 | Parameters of the Improved ConvLSTM.

Model parameters	Value
Filters	30
Kernel size	4
Dense_1 cells	500
Dense_2 cells	5
Activation function	Softmax

CNN+LSTM for Post-LOCA Prediction

The greatest challenge for post-LOCA prediction is the uncertainty of the process to be predicted. Although five typical break sizes are chosen to represent the LOCA scenarios, it is not a full coverage yet. Even for a chosen case, different NPP operation status at the LOCA moment could lead to various post-LOCA situations. Therefore, the prediction model needs to be aware of such uncertainty and be able to predict cases that are similar to the training ones.

In order to handle the uncertainty challenge, the prediction model is constructed with a combinational structure of CNN and LSTM. The convolutional computation from CNN, with the assistance of weight sharing and pooling operation, can effectively extract the major features at the early stage of the development. The LSTM model, as a variety of Recurrent Neural Network (RNN), is proficient at dealing with long-time series datasets such as LOCA data (She et al., 2019). Since the LOCA process is hard to predict due to complicated variations, two LSTM layers are used to increase the depth of the neural network. Two dense layers are also applied to the prediction results processing, ensuring a result with all necessary features.

The prediction model is trained using datasets of the five chosen LOCA cases. Total five sets of model weights are saved in a so-called "fault dictionary." Once the classification results, e.g., 0.2 cm^2 break, reaches the prediction model, it looks up the fault dictionary and loads the model with the corresponding "weight set-0.2" trained by such case. **Figure 2** below describes the model structure and **Figure 3** shows the process of using a fault dictionary. The parameter configuration is listed in **Table 2**.

EXPERIMENTS AND RESULTS

Experiments of this work are divided into two major stages. The proposed models are verified using industry simulation datasets first. A LOCA case is then picked up for the system integration test.

As mentioned, each LOCA case (0.2, 0.4, 0.6, 0.8, or 1.0 cm^2) is simulated under five kinds of operation status (60, 70, 80, 90, and 100% reactor power levels). Noise signals are introduced

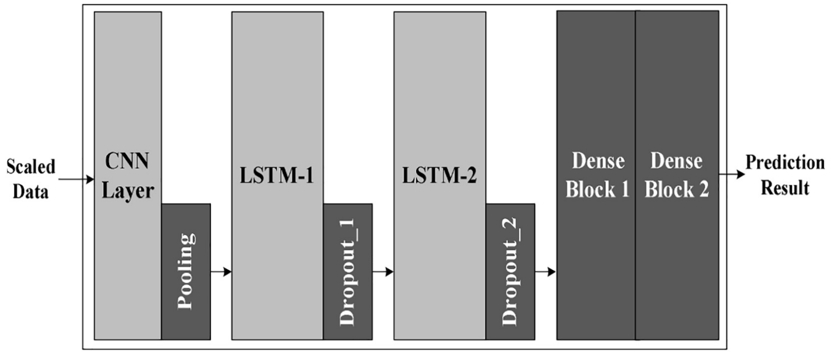

FIGURE 2 | Structure of the Post-LOCA prediction model.

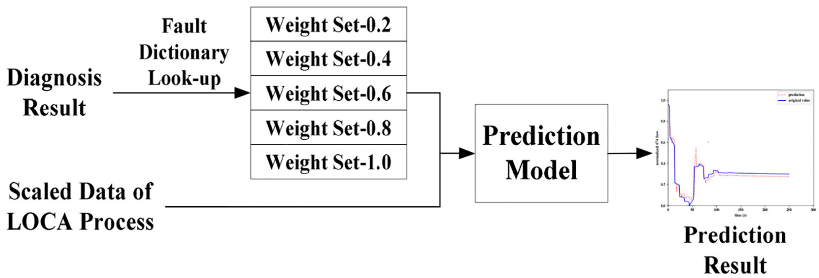

FIGURE 3 | Using fault dictionary for Post-LOCA prediction.

during the simulation such that the dataset is expanded and has a wider coverage of possible situations. Seventy-five percentage of the dataset is used for training purposes with the Rolling Update method applied; the rest of the dataset is used for the test experiments of both the classifier and the prediction model. The test dataset is also plotted as the "original value" in the result figures such that the comparison between the prediction results and the actual LOCA trend can be illustrated. All the data is denoised, smoothed, and then normalized to the maximum and minimum values.

Model Verification

Classifier Model Verification

The classifier verification uses test vectors composed of 10 system parameters, including core inlet temperature, core exit temperature, core outlet supercooling degree, pressurizer pressure, pressurizer water level, and five types of coolant flowrates. All the parameter values in one test vector belong to a chosen LOCA case. Adequate parameters in the test vector lead to a narrow classification scope, which guarantees accurate classification results.

During the classifier verification, there are totally 25 test vectors, 5 for each break size. And all contain the 10 crucial system parameters. They are fed into the model via a 50-timestep process that imitates the industry sampling process. The verification results are listed in **Table 3** below.

Results in **Table 3** demonstrate the classification performance of the proposed model. All the correct classifications are obtained at the first timestep and kept for the entire classification process. The sole misclassification case is the 0.4 cm^2 break size at 60%

TABLE 2 | Parameters of the Post-LOCA prediction model.

Model parameters	Value
Filters	8
Kernel size	2
Pooling size	4
LSTM_1 units	128
Dropout_1 odds	0.2
LSTM_2 units	64
Dropout_2 odds	0.2
Dense_1	16
Dense_2	1

TABLE 3 | Classifier verification results.

Break size (cm^2)	Test vectors	Correct results	Accuracy per size (%)	Total accuracy (%)
0.2	5	5	**100**	–
0.4	5	4	**80**	–
0.6	5	5	**100**	–
0.8	5	5	**100**	–
1.0	5	5	**100**	–
Total	**25**	**24**	–	**96**

The bold values represent data statistics, intermediate diagnosis results, and final diagnosis results.

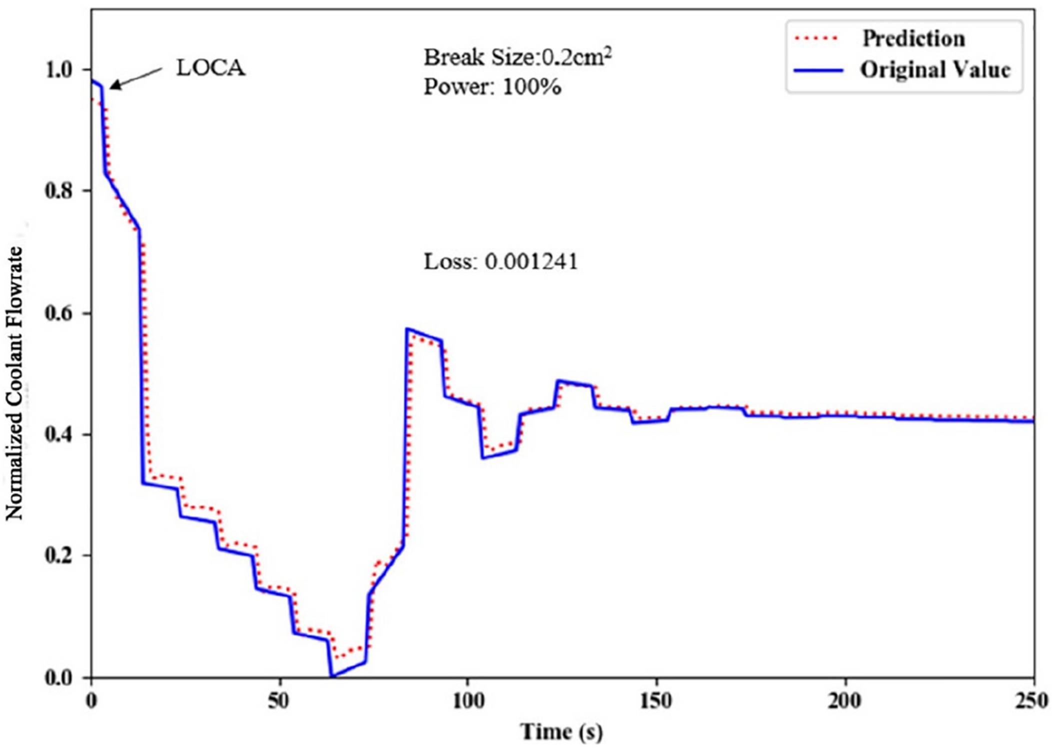

FIGURE 4 | Functionality verification of the prediction model.

reactor power level and it is misclassified as an adjacent case (0.6 cm^2 break at 60% power level).

Prediction Model Verification

The prediction model verification, however, consists of three sub-experiments:

(1) regular test of the "0.2 cm^2 break" model using a "0.2 cm^2 break" test vector;
(2) comparison experiments between a "pure LSTM" model and the "CNN+LSTM" model;
(3) adaptivity test of the "0.2 cm^2 break" model using a "1.0 cm^2 break" test vector.

(1) Functionality Verification

A regular test is performed to simply verify the model functionality. A 0.2 cm^2 break test vector, which is randomly picked from the dataset, is fed into the "CNN+LSTM" model trained by the 0.2 cm^2 break dataset. The coolant flowrate prediction result is shown in **Figure 4**.

The prediction given by the "CNN+LSTM" model matches the original value closely with a loss value of 1.241 $\times 10^{-3}$. The prediction capability of the proposed model is verified.

(2) Comparison Experiments

The comparison experiments are carried out for the coolant flowrate using all break sizes at 100% reactor power level, showing the performance comparison between the two models. The loss values via Mean Square Error (MSE) function are listed in **Table 4** to describe the difference.

With lower loss values derived by the "CNN+LSTM" model, the comparison of the results in **Table 4** clearly shows the advantage of using the "CNN+LSTM" structure. It is demonstrated that the CNN layer covers the shortage of the LSTM model when facing a multi-feature process.

(3) Adaptivity Verification

The third verification experiment is to prove that the prediction model in this work can adapt to an untrained but similar case. This is quite meaningful to accident scenarios with much uncertainty, such as the LOCA. For this experiment, the coolant flowrate dataset generated from the simulation of a 1.0 cm^2 break is applied to a prediction model trained by a 0.2 cm^2 break dataset, both at 100% power level. The prediction generated is illustrated in **Figure 5**.

The "1.0 cm^2 break" prediction curve generated by a "0.2 cm^2 break" model still follows the main trend of the test case. The loss value of 3.968 $\times 10^{-3}$ is larger than experiment (1) but

TABLE 4 | Comparison of prediction performance.

break size	0.2 cm^2	0.4 cm^2	0.6 cm^2	0.8 cm^2	1.0 cm^2
Loss value (LSTM)	0.003815	0.003746	0.003615	0.004126	0.003937
Loss value (CNN+LSTM)	**0.001241**	**0.002767**	**0.002864**	**0.002099**	**0.003121**

The bold values represent the loss value of the experimental model, and is better than the LSTM model.

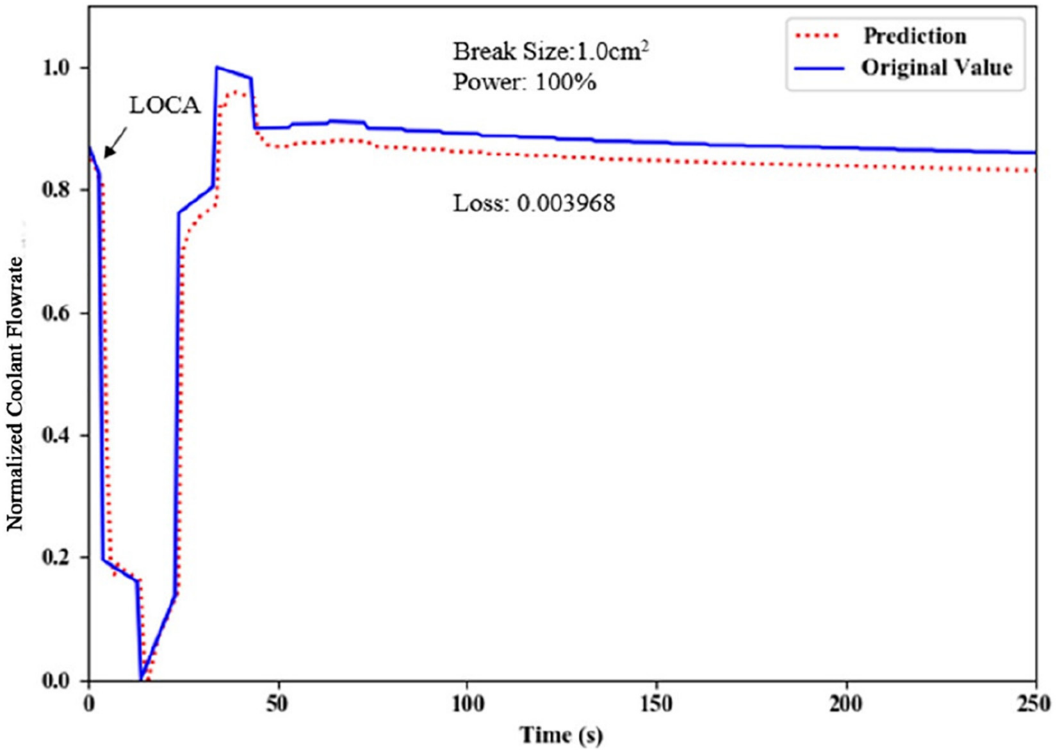

FIGURE 5 | Adaptivity verification of the prediction model.

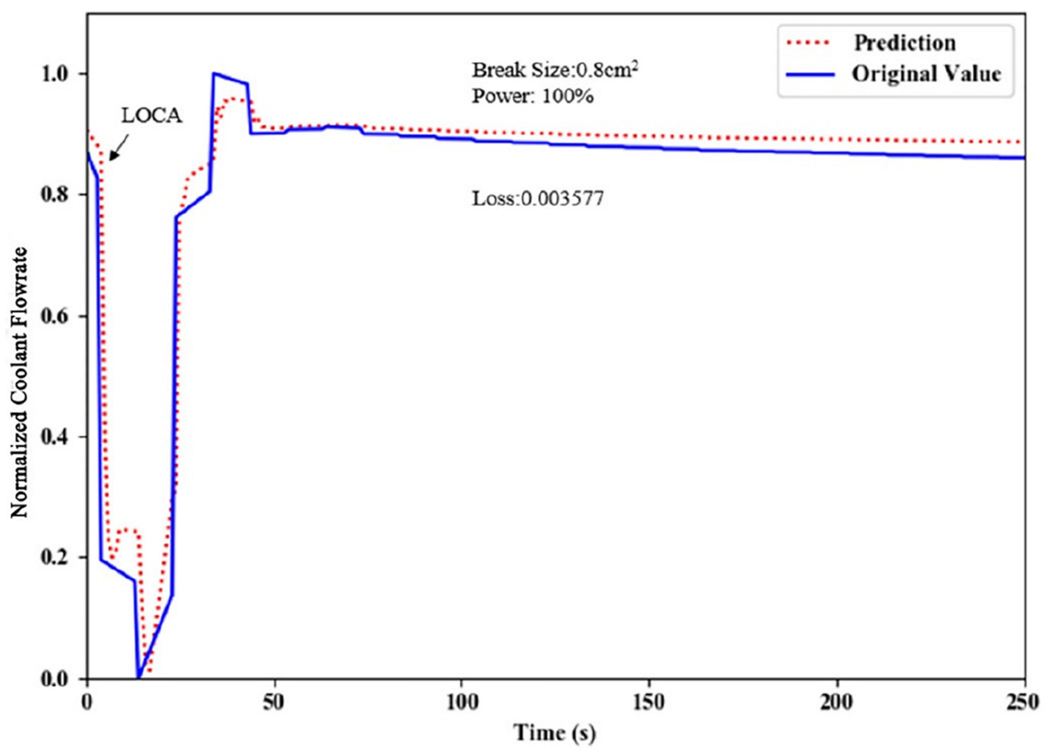

FIGURE 6 | Coolant flowrate prediction for 0.8 cm^2 break.

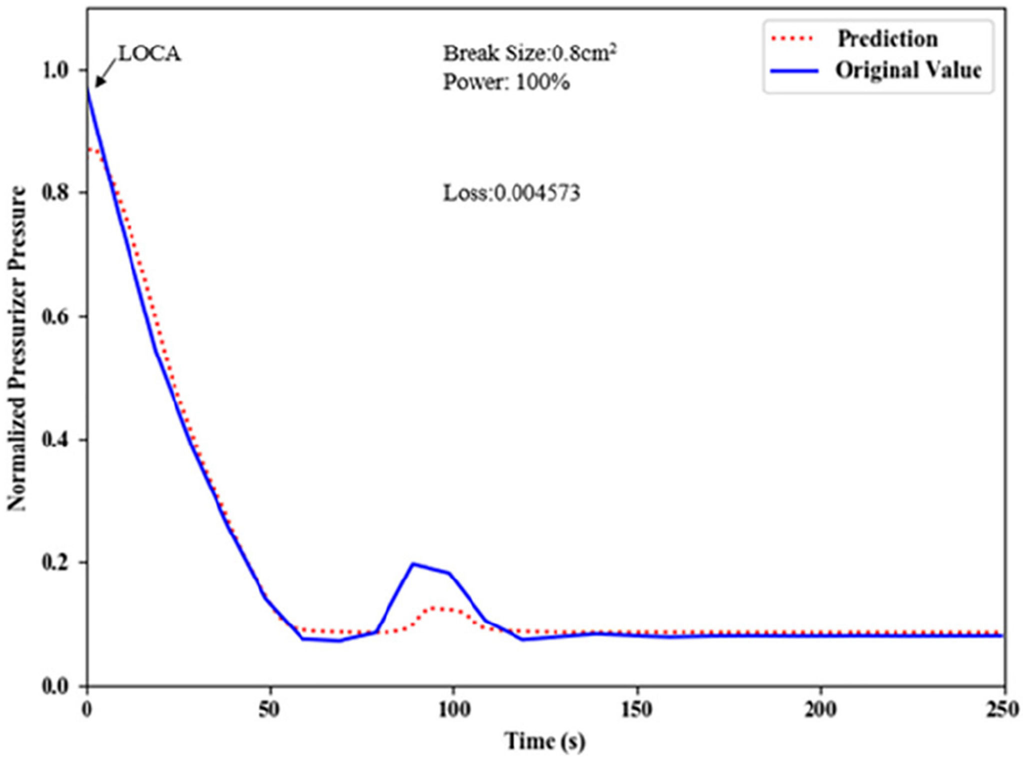

FIGURE 7 | Pressurizer pressure prediction for 0.8 cm^2 break.

still within the same order of magnitude. It has to be pointed out that 0.2 cm^2 break and 1.0 cm^2 break are two cases with the biggest difference in the given dataset group. Such a result signifies that any two of other case models can adapt to each other even closer. That is to say, when an uncertain scenario appears, the "CNN+LSTM" model has the potential to adapt to it and generate a meaningful prediction.

Based on the high-accuracy classification, the prediction showing functionality and adaptivity, and the better performance demonstrated in the comparison experiments, the hybrid LOCA diagnosis and prediction model has been proved to be accurate, functional, and adaptive.

Diagnosis and Prediction Experiment

This subsection presents one of the system integration experiments conducted from diagnosis to prediction for a given LOCA case, 0.8 cm^2 break at 100% power level. The purpose is to demonstrate the functionality and performance of the proposed hybrid model from a systematic view.

Predictions for two crucial system parameters, coolant flowrate, and pressurizer pressure, are selected to be shown in **Figures 6**, **7**, respectively.

It is noticed that, at the beginning of both **Figures 6**, **7**, the prediction appears underfitting. This is often observed in prediction using neural networks. In this work, the prediction model is trained for each break size separately and the trained weights are then stored in the fault dictionary. However, during the training process, all the data belong to the chosen break size are used, including data under different reactor power levels. Thus, it is hard to avoid the underfitting problem when the prediction test for 0.8 cm^2 break is performed against a certain reactor power.

The prediction curves also show underfitting at where dramatic changes are. This is exactly what has been mentioned as one of the great challenges to predict nonlinear processes. As can be seen from the following figures, the prediction is trying to catch with the sudden rises or drops. But when the quick nonlinear changes happen consecutively, the prediction can only develop in a lagging manner, leading to underfitting phenomena at those sharp turning points.

CONCLUSION

A hybrid model for LOCA diagnosis and prediction is proposed in this work. The ConvLSTM is used for fault type diagnosis, and the LOCA prediction is produced using CNN-LSTM. The datasets of different break sizes of LOCA are obtained from the experimental platform. The dataset is preprocessed and normalized for proper training and test dataset. The proposed diagnosis and prediction model is then tested and verified through rigorous experiments. With an improved structure, the fault diagnosis model based on ConvLSTM successfully reaches classification accuracy as high as 96%. The post-LOCA prediction model established by combining CNN and LSTM has also shown effective functionality and adaptability through three different sub-experiments. Its loss values (MSE) for all the test cases are kept as low as 10^{-3}, satisfying the accuracy expectation. Comparing to the LSTM model, the CNN-LSTM demonstrated its advantage of multi-feature processing, which provides a better prediction performance.

However, the model research proposed in this article has certain limitations. First of all, the sample datasets used in this experiment need to be further expanded to ensure the validity of the experiment. In addition, the model needs to be further verified using real LOCA data from the NPPs. Moreover, underfitting does appear in prediction results due to training strategy and consecutive inflection points, which implies the potential improvement of the prediction model in future work.

DATA AVAILABILITY STATEMENT

The raw data supporting the conclusions of this article will be made available by the authors, without undue reservation.

AUTHOR CONTRIBUTIONS

JS proposed the idea of using deep learning methods for LOCA diagnosis and prediction, established the main structure of the deep learning models used in this work, drafted most part of the manuscript, and coordinated the cooperation of all the co-authors. TS contributed to the programming, testing, and results analysis of the prediction model. SX preprocessed all the training and testing datasets, including using the rolling update method to generate proper test vectors. After building the diagnosis model, YZ finished all the diagnosis experiments and analysis. SL provided key instructions to the group members to ensure accurate and efficient research methodologies. PS and HC performed the simulations that produced all the datasets, using the industry-grade simulation tool. All authors contributed to the article and approved the submitted version.

ACKNOWLEDGMENTS

We would like to thank the financial and technical support from the following research projects and institutions, including but not limited to: (1) the Special Funds for Basic Scientific Research Business of the Central Universities (531118010070); (2) the Provincial Talents Gathering Project—Innovation Talents Plan (2018RS3050); (3) the Industrial Internet Innovation and Development Project of China: Digital Twin System for Automobile Welding and Casting Production Lines and Its Application Demonstration (TC19084DY); (4) the Special Funds for Construction of Innovative Provinces in Hunan Province of China (No. 2020SK2066, No. 2020GK2016); (5) the Hunan Xiangjiang Artificial Intelligence Academy; (6) the Central Research Institution of the State Power Investment Co. Ltd. (SPIC); and (7) the China Guangdong Nuclear (CGN) Research Institution Co. Ltd.

SUPPLEMENTARY MATERIAL

The Supplementary Material for this article can be found online at: https://www.frontiersin.org/articles/10.3389/fenrg.2021.665262/full#supplementary-material

REFERENCES

Bi, Q., Qin, K., and Li, Z. L. (2019). "Multiple instance dense connected convolution neural network for aerial image scene classification," in *In the Proceedings of IEEE International Conference on Image Processing*, (New York: IEEE), 2501–2505.

Feng, J., Wu, X. D., and Chen, J. T. (2019). "Joint multilayer spatial-spectral classification of hyperspectral images based on CNN and convLSTM," in *In Proceedings of IEEE International Geoscience and Remote Sensing Symposium* (Japan: Yokohama), 588–591.

Jeong, H. Y. (2002). Prediction of counter-current flow limitation at hot leg pipe during a small-break LOCA. *Ann. Nucl. Energy* 29, 571–583. doi: 10.1016/s0306-4549(01)00053-6

Kim, D. Y., Yoo, K. H., and Kim, J. H. (2014). Prediction of leak flow rate using fuzzy neural networks in severe post-LOCA circumstances. *IEEE Trans. Nucl. Sci.* 61, 3644–3652. doi: 10.1109/tns.2014.2357583

Kim, E., and Medioni, G. (2010). "Dense structure inference for object classification in aerial LIDAR dataset," in *In Proceedings of the 20th International Conference on Pattern Recognition*, (New York: IEEE), 3049–3052.

Koo, Y. D., Na, M. G., and Kim, K. S. (2018). "Prediction of nuclear reactor vessel water level using deep neural networks," in *In Proceedings of International Conference on Electronics, Information, and Communication*, (New York: IEEE), 1–3.

Krizhevsky, A., Sutskever, I., and Hinton, G. E. (2012). ImageNet classification with deep convolutional neural networks. *Adv. Neural Inf. Process. Syst.* 25, 1106–1114.

Lee, C. K., Kwon, G. Y., and Chang, S. J. (2017). Real-time condition monitoring of LOCA via time–frequency domain reflectometry. *IEEE T. Instrum. Meas.* 66, 1864–1873. doi: 10.1109/tim.2017.2664578

Mukherjee, S., Ghosh, S., and Ghosh, S. (2019). "Predicting video-frames using encoder-convLSTM combination," in *In Proceedings of IEEE International Conference on Acoustics, Speech and Signal Processing*, (United Kingdom: Brighton), 2027–2031.

Na, M. G., Shin, S. H., and Jung, D. W. (2004). Estimation of break location and size for loss of coolant accidents using neural networks. *Nucl. Eng. Des.* 232, 289–300. doi: 10.1016/j.nucengdes.2004.06.007

Niu, J. W., Li, S. J., and Mo, S. S. (2019). "Affective analysis for video frames using convLSTM network," in *In Proceedings of IEEE International Conference on Communications*, (New York: IEEE), 1–6. doi: 10.1109/taffc.2020.3004114

Park, S. H., Kim, J. H., and Na, M. G. (2013). "Rediction of reactor vessel water level using GMDH in severe accidents due to LOCA," in *In Proceedings of IEEE Nuclear Science Symposium and Medical Imaging Conference*, (New York: IEEE), 1–4.

Radaideh, M. I., Pigg, C., and Kozlowski, T. (2020). Neural-based time series forecasting of loss of coolant accidents in nuclear power plants. *Expert Syst. Appl.* 160:2020.

Santhosh, T. V., Kumar, M., and Thangamani, I. (2011). A diagnostic system for identifying accident conditions in a nuclear reactor. *Nucl. Eng. Des.* 241, 177–184. doi: 10.1016/j.nucengdes.2010.10.024

She, J. K., Xue, S. Y., and Sun, P. W. (2019). The Application of LSTM model to the prediction of abnormal operation in nuclear power plants. *Instrumentation* 26, 39–44.

Shi, X. J., Chen, Z. R., and Wang, H. (2015). "Convolutional LSTM network: a machine learning approach for precipitation nowcasting," in *In Proceedings* *of the 29th Annual Conference on Neural Information Processing Systems*, (New York: Cornell University), 802–810.

Sun, P. W., Wang, L. B., and Cao, H. S. (2019). "Fault Identification of a small modular reactor based on PCA method," in *In Proceedings of 27th International Conference on Nuclear Engineering*, (Ibaraki: Tsukuba International Conference Center).

Sun, P. W., Zhao, H. H., and Liao, L. T. (2017). Control system design and validation platform development for small pressurized water reactors (SPWR) by coupling an engineering simulator and MATLAB/Simulink. *Ann. Nucl. Energy* 102, 309–316. doi: 10.1016/j.anucene.2016.12.034

Tanim, M. M. H., Ali, M. F., and Shobug, M. A. (2020). "Analysis of Various types of Possible Fault and Consequences in VVER-1200 using PCTRAN," in *2020 International Conference for Emerging Technology (INCET)*, (New York: IEEE).

Tian, D., Deng, J., and Vinod, G. (2018). "A constraint-based random search algorithm for optimizing neural network architectures and ensemble construction in detecting loss of coolant accidents in nuclear power plants," in *In Proceedings of the 11th International Conference on Developments in eSystems Engineering*, (Huntsville: DeSE), 237–243.

Weglian, J., Riley, J., and Ferrante, F. (2020). "Combining Hazards into a Single-Top Fault Tree," in *2020 Annual Reliability and Maintainability Symposium (RAMS)*, (US: IEEE).

Yang, J., Yang, Y., and Deng, C. C. (2019). Best Estimate Plus Uncertainty analysis of a large break LOCA on Generation III reactor with RELAP5. *Ann. Nucl. Energy* 127:2019.

Yoo, K. H., Koo, Y. D., and Back, J. H. (2017). Identification of LOCA and estimation of its break size by multiconnected support vector machines. *IEEE Trans. Nucl. Sci.* 64, 2610–2617. doi: 10.1109/tns.2017.2743098

Zhang, C. J., Li, G. D., and Du, S. H. (2019). Multi-scale dense networks for hyperspectral remote sensing image classification. *IEEE Trans. Geosci. Remote Sens.* 57, 9201–9222. doi: 10.1109/tgrs.2019.2925615

Conflict of Interest: The authors declare that the research was conducted in the absence of any commercial or financial relationships that could be construed as a potential conflict of interest.

frontiers in Energy Research

ORIGINAL RESEARCH
published: 12 May 2021
doi: 10.3389/fenrg.2021.663296

Data-Driven Machine Learning for Fault Detection and Diagnosis in Nuclear Power Plants: A Review

Guang Hu[1], *Taotao Zhou*[2] *and Qianfeng Liu*[3]*

[1] *Institute of Thermal Energy Technology and Safety, National Research Center of Helmholtz Association, Karlsruhe Institute of Technology, Karlsruhe, Germany,* [2] *China Ship Development and Design Center, Wuhan, China,* [3] *Key Laboratory of Advanced Reactor Engineering and Safety, Institute of Nuclear and New Energy Technology, Tsinghua University, Beijing, China*

OPEN ACCESS

Edited by:
Xianping Zhong,
University of Pittsburgh, United States

Reviewed by:
Hyun Gook Kang,
Rensselaer Polytechnic Institute, United States
Jiankai Yu,
Massachusetts Institute of Technology, United States
Yunfei Zhao,
The Ohio State University, United States
Zhegang Ma,
Idaho National Laboratory (DOE), United States

Correspondence:
Qianfeng Liu
liuqianfeng@tsinghua.edu.cn

Specialty section:
This article was submitted to Bioenergy and Biofuels, a section of the journal Frontiers in Energy Research

Received: *02 February 2021*
Accepted: *13 April 2021*
Published: *12 May 2021*

Citation:
Hu G, Zhou T and Liu Q (2021) Data-Driven Machine Learning for Fault Detection and Diagnosis in Nuclear Power Plants: A Review. Front. Energy Res. 9:663296. doi: 10.3389/fenrg.2021.663296

Data-driven machine learning (DDML) methods for the fault diagnosis and detection (FDD) in the nuclear power plant (NPP) are of emerging interest in the recent years. However, there still lacks research on comprehensive reviewing the state-of-the-art progress on the DDML for the FDD in the NPP. In this review, the classifications, principles, and characteristics of the DDML are firstly introduced, which include the supervised learning type, unsupervised learning type, and so on. Then, the latest applications of the DDML for the FDD, which consist of the reactor system, reactor component, and reactor condition monitoring are illustrated, which can better predict the NPP behaviors. Lastly, the future development of the DDML for the FDD in the NPP is concluded.

Keywords: data-driven method, machine learning, fault detection and diagnosis, applications and development, nuclear power plant

INTRODUCTION

Nuclear Energy Development

Nuclear energy is of continuous interest as it can meet increasing energy demands of the world environmentally friendly (Jamil et al., 2016). On the one hand, nuclear power plants (NPPs) consist of many complex systems and components. On the other hand, NPPs are also highly dynamic and non-linear (Peng et al., 2018). In addition, the latest advances come to the further Generation IV NPPs (Yao et al., 2020). In particular, further NPPs greatly emphasize the economics, safety, and reliability over the previous NPPs (Locatelli et al., 2013).

This future of the NPP necessitates the high performance of the fault diagnosis and detection (FDD) in the nuclear industry (Oluwasegun and Jung, 2020). First, the FDD can be adopted in the reactor systems, components, and conditions. Later, it allows the reactor systems and components to be fully optimally used to their lifetime before the maintenance or disposal. Meanwhile, the FDD can reflect the current conditions and enable further prediction of possible malfunctions (Li et al., 2020). Therefore, an accurate and efficient FDD is of great importance to ensure the economics, safety, and reliability of the NPP.

Fault Detection and Diagnosis in NPP

To achieve its goal, the nuclear industry has increased popularity in adapting the FDD techniques (Rezaeianjouybari and Shang, 2020). And the research process of the FDD methods in the NPP can be described as follows.

First, the traditional FDD approach in the NPP belongs to the hardware redundancy method (Betta and Pietrosanto, 2000). For example, the same quantity can be measured by several sensors, and the voting scheme is also introduced for the sensor fault. However, the hardware redundancy principle can hardly suitable for other reactor systems and components (Lu and Upadhyaya, 2005). Thus, it comes to the limit checking method. Usually, it is adopted to monitor the specified parameter of the NPP to see whether the parameter exceeds the predefined value or not (Jamil et al., 2016). Nevertheless, it can only detect the fault when it exceeds a certain value, which could ignore the incipient fault stage. Additionally, the FDD method based on the analytical redundancy can overcome the disadvantages of both the hardware redundancy and limit checking approach (Nguyen et al., 2020). Meanwhile, it can predict the incipient anomalies, optimize the operation schedule, reduce the maintenance cost, and improve safety at the same time. Hence, the FDD method based on the analytical redundancy is of emerging interest in the NPP in these years.

Currently, the FDD methods based on the analytical redundancy can be basically classified into three main types: physic model-based, reliability-based, and data-driven methods (Wang et al., 2020). For the physic model-based techniques, the mathematical models are proposed to describe the research objects. Moreover, the reliability-based approaches adapt the probability theory and knowledge-based statics while it requires prior experience or knowledge of the system (Ma and Jiang, 2011; Jamil et al., 2016). However, it is not suitable for real industrial applications like the NPP as it is highly dynamic and non-linear (Zhao and Wang, 2018). At last, the data-driven approaches require no prior experience of the NPP and just only need the previous data for the model training (Betta and Pietrosanto, 2000; Razavi-Far et al., 2009; Wang et al., 2020). In recent years, it is a promising technique and of interest for the FDD in the NPP (Moshkbar-Bakhshayesh and Ghofrani, 2013; Ren et al., 2016; Utah and Jung, 2020; Nguyen et al., 2020).

Data-Driven Machine Learning Method

The data-driven approaches tend to be more suitable and able to predict without a prior knowledge of the NPP. At the same time, it potentially achieves high accuracy with low economic cost. Combined with the machine learning (ML) algorithms, the data-driven techniques have drawn increasing attention for the FDD in the NPP in the past decades (Ma and Jiang, 2011; Mandal et al., 2017a,b; Wang et al., 2020).

At present, the data-driven machine learning (DDML) methods, including the neural network, support vector machine (SVM), dimension reduction learning (DRL), ensemble learning (EL) or random tree (RT), regression approaches, and so on, have been applied to predict the NPP behaviors (Jamil et al., 2016; Saeed et al., 2020). Nevertheless, few researches concern with the state-of-the-art progress and future trends for both the DDML approach for the FDD and the NPP (Bartlett and Uhrig, 1992; Ma and Jiang, 2011; Moshkbar-Bakhshayesh and Ghofrani, 2013).

Especially, Bartlett and Uhrig (1992) briefly presented the artificial neural network (ANN) method for the FDD in the NPP. However, it only concerns the ANN method. In 2011, Ma and Jiang (2011) considered six areas of applications of the FDD in the NPP. Moreover, the transient diagnosis in the NPP was illustrated with the ANN approach (Moshkbar-Bakhshayesh and Ghofrani, 2013). However, there are either the specified component (system) or the outdated techniques in the available research. As the DDML techniques in the NPP sharp a lot in recent years (Rezaeianjouybari and Shang, 2020; Yao et al., 2020; Saeed et al., 2020), there exists a gap in the current state-of–the-art of the DDML techniques for the FDD in the NPP. In this review, the current classifications, principles, characteristics, and applications of the FDD in the NPP, followed by the discussion on the future development of the DDML method for the NPP state prediction, will be illustrated.

Scope of This Review

Compared with the physic model-based and reliability-based techniques, the data-driven methods have the superior advantage in the trade-off between the safety, reliability, and economics of the NPP. In addition, it has been considered as a promising future FDD direction from the encouraging results made by the recent studies. However, to the best of our knowledge, there still lacks research on comprehensive reviewing the state-of–the-art progress on the DDML for the FDD in the nuclear industry. Therefore, this review focuses on elaborating the DDML in the NPP, introducing the applications of the DDML in the NPP and illustrating the future development. In section "Overview of the DDML for FDD in NPP," principles and characteristics of the DDML for the FDD are discussed, including the supervised learning type, unsupervised learning type, and reinforcement learning type. Section "Development of DDML for FDD in NPP" shows the applications and further development of the DDML for the FDD. Section "Conclusion" explains the conclusions and remarks on the DDML for the FDD. It should be noted that this review would emphasize the DDML for the FDD in the nuclear industry.

OVERVIEW OF THE DDML FOR FDD IN NPP

Generally, the DDML for the FDD in the NPP can be classified into several types. First, these types include supervised learning, unsupervised learning, and reinforcement learning by the principle of the learning type. Second, these can be sorted into regression, instance-based learning, neural network, deep learning, dimension reduction, and kernel-based learning algorithms by the algorithm type. In addition, the detailed classifications of DDML for FDD in NPP are as shown in **Figure 1**. As for the DDML, it is of emerging interest for the FDD in the NPP. Hence, it is necessary to be illustrated in detail.

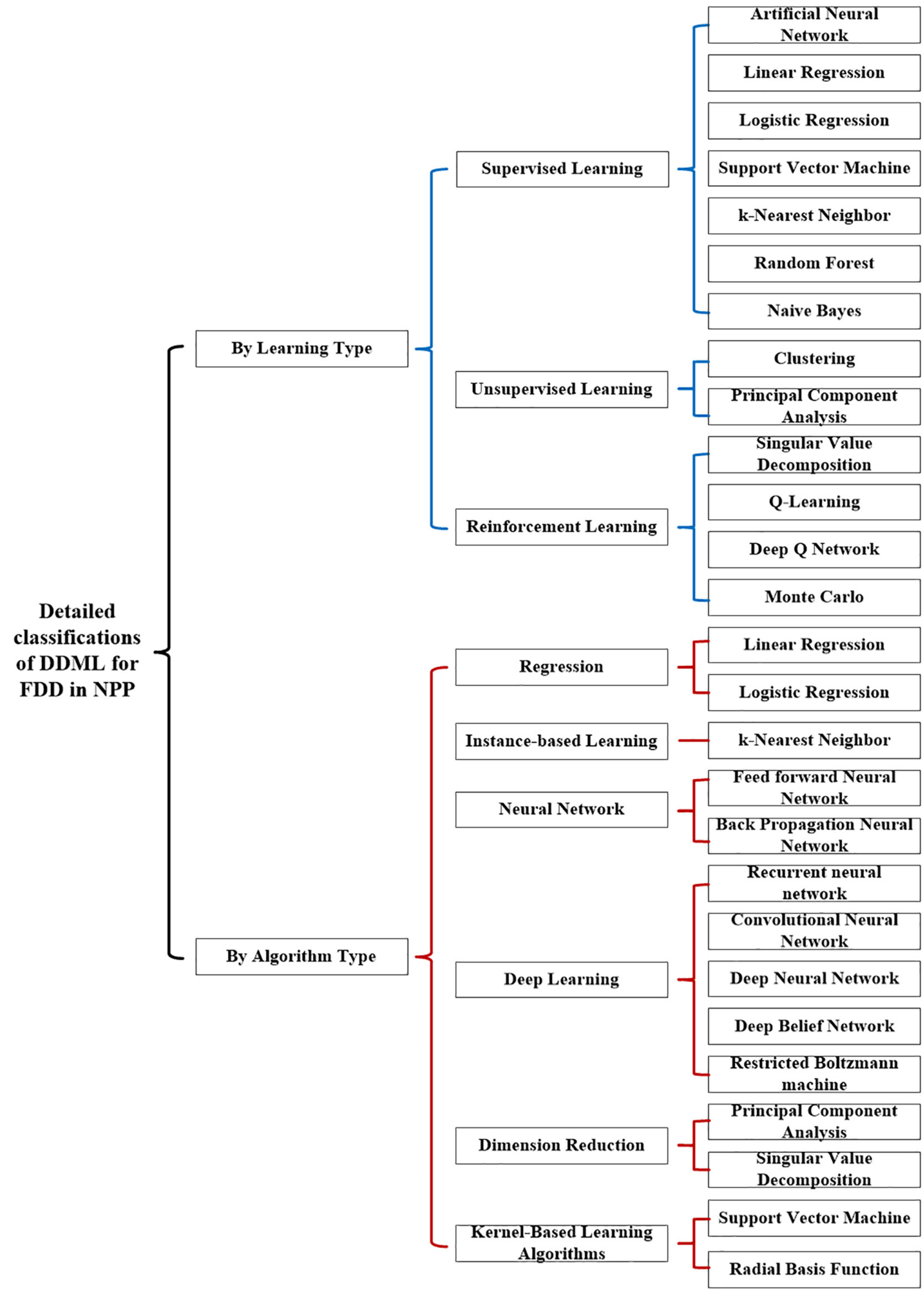

FIGURE 1 | Detailed classifications of data-driven machine learning (DDML) for the fault diagnosis and detection (FDD) in the nuclear power plant (NPP).

Finally, the research profile of the DDML for the FDD in the NPP is described as follows.

Supervised Learning Method

In **Table 1**, the ANN method, linear regression, logistic regression, SVM, k-nearest neighbor (kNN), RT, and naive Bayes (NB) for the FDD in the NPP belong to the supervised learning approaches.

Artificial Neural Network Approach

A typical ANN is constructed by three parts: the structure (the input signal, hidden layer, and output), learning algorithm (update the synaptic weights), and activation function. For

TABLE 1 | Status of the data-driven machine learning (DDML) of the supervised learning method for the fault diagnosis and detection (FDD) in the nuclear power plant (NPP).

References	Methods	Type	Characteristics
Aizpurua et al. (2018), Oluwasegun and Jung (2020), and Po (2020)	ANN	Supervised learning type	Quickly adjustment; require a lot of data
Hadad et al. (2011)	Linear regression	Supervised learning type	Direct and fast; abnormal value
Ayodeji et al. (2018)	Logistic regression		
Zio (2007), Liu et al. (2013), Ren et al. (2016), Moshkbar-Bakhshayesh (2020), Meng et al. (2020), and Wang et al. (2021)	SVM	Supervised learning type	Largest geometric interval; low efficiency
Biet (2012) and Liu et al. (2013)	kNN	Supervised learning type	Without modeling and training; large amount of calculation
Sharanya and Venkataraman (2018)	RT	Supervised learning type	Without dimensionality reduction; overfit
Liu et al. (2013) and Chen and Jahanshahi (2017)	NB	Supervised learning type	Easy to train; unable to process related parameters

example, the ANN approaches are taken for the FDD in the NPP like the control rod drive system and accident prevention system (Aizpurua et al., 2018; Po, 2020; Oluwasegun and Jung, 2020) as shown in **Figure 2**. In **Figure 2**, the input signals x_1, x_2, . . ., x_n are the control rod step number, coil current data, vibration data, coolant temperature, etc. They correspond to each synaptic weight w_1, w_2, . . ., w_n, respectively. After the procession of the summing junction and the activation function $\varphi(\cdot)$, the output $y(k)$ is obtained. Additionally, the ANN approach can quickly adjust to new problems. However, it requires a lot of data for the training and it is hard to select the meta parameters.

Regression Algorithm

Especially, the linear regression assumes that the dependent variable obeys a Gaussian distribution, whereas the logistic regression assumes that the dependent variable follows a Bernoulli distribution. Based on the linear regression, the logistic regression introduces non-linear factors through the Sigmoid function. For instance, Hadad et al. (2011) performed a linear regression analysis to evaluate the network performance in the NPP. In 2018, Ayodeji et al. (2018) combined the logistic regression with the SVM for the incipient fault diagnosis in the NPP. In particular, the regression algorithm is direct and fast while it also needs to handle the abnormal value.

Support Vector Machine Method

The basic idea of the SVM learning is to solve the separation hyperplane that can correctly divide the training dataset. In **Figure 3A**, the formula represents the separating hyperplane. In addition, w is the normal vector to the hyperplane with a magnitude w. The parameter b/w is the offset amount between the hyperplane and the origin. Furthermore, the two hyperplanes $wx - b = 1$ and $wx - b = -1$ are the margins of two classifies. Overall, the distance between the two margins is $2/w$. For a linearly separable dataset, there are infinitely such hyperplanes (i.e., perceptrons), whereas the separating hyperplane with the largest geometric interval is the only one. It has the largest geometric interval while the efficiency may not be high.

For the FDD in the NPP, Zio (2007) applied the SVM in the anomalies and malfunctions occurring in the feedwater system. Then, Liu et al. (2013) developed the SVM for monitoring the components of NPPs. In addition, Ren et al. (2016) proposed the SVM with sparse representation. Furthermore, Moshkbar-Bakhshayesh (2020) utilized the SVM for the control rod system. Meanwhile, Meng et al. (2020) combined the SVM and objective function method for the loose parts. At last, Wang et al. (2021) adopted the SVM together with the principal component analysis (PCA) and clustering algorithm for the sensor faults in the NPP.

k-Nearest Neighbor Technique

The principle of the kNN technique is described in **Figure 3B**. In the prediction of point x_u in **Figure 3B**, four neighboring samples belong to the category c_1 and only one neighboring sample belongs to the category c_2. Hence, the point x_u is classified as the category c_1. But from the visual observation, it should be more reasonable to divide into circular classification. According to this situation, a weight such as ω_1, ω_2, and ω_3 can be also added to the distance measurement. First, Liu et al. (2013) coupled the kNN technique with the SVM for monitoring the components of NPPs. Biet (2012) conducted the rotor FDD with the kNN technique and feature section in the NPP. On the one hand, the advantages of this algorithm are simple, easy to understand, and without modeling and training. And it is suitable for multi-classification problems. On the other hand, the shortcomings of this algorithm include the lazy algorithm and a large amount of calculation when classifying the test samples.

Random Tree Approach

The RT approach contains two parts, one is "random" and the other is "tree." It is based on the decision tree (DT). It can produce very high-dimensional (many features) data without dimensionality reduction or feature selection. And Sharanya and Venkataraman (2018) carried out the RT for the FDD of the coolant tower in the NPP. Meanwhile, it can judge the importance of features. However, the RT has been shown to overfit in some noisy classification or regression problems.

Naive Bayes Method

The NB is a classification method based on the Bayes' theorem and the independence assumption of characteristic conditions. For this technique, Liu et al. (2013) combined the NB with

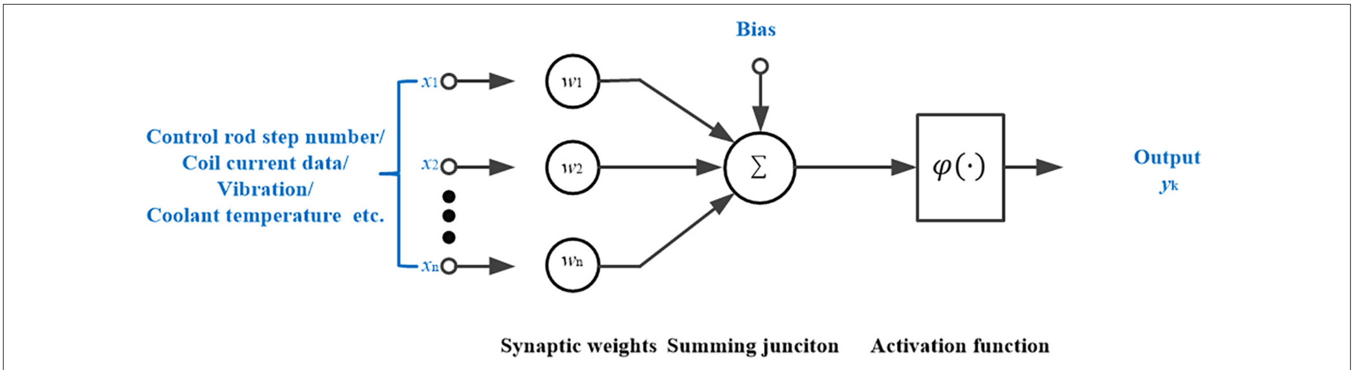

FIGURE 2 | The artificial neural network (ANN) approach for the fault diagnosis and detection (FDD) in the nuclear power plant (NPP).

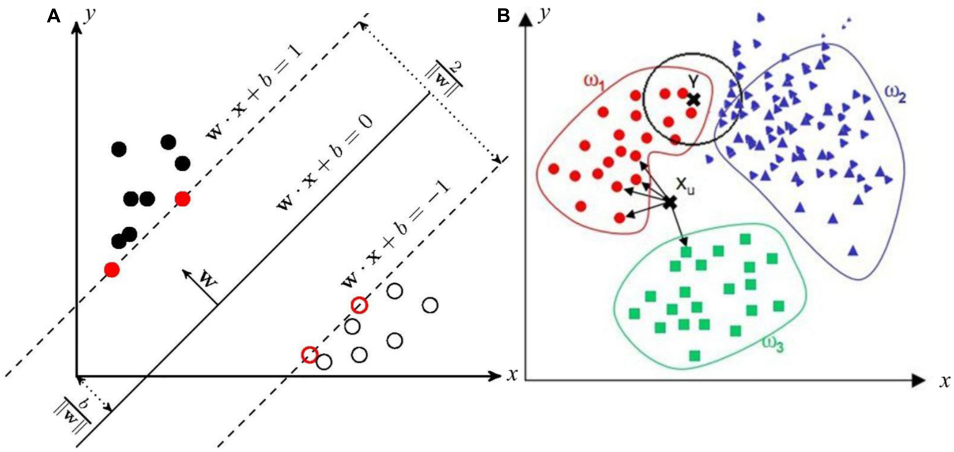

FIGURE 3 | The support vector machine (SVM) and k-nearest neighbor (kNN) method for the fault diagnosis and detection (FDD) in the nuclear power plant (NPP). **(A)** SVM **(B)** kNN.

SVM for components in the NPP. In 2017, Chen and Jahanshahi (2017) carried out the FDD of thermocouples with the naive Bayes method in the NPP. It is fast, easy to train, and has good performance. Meanwhile, it may fall short when the input variables are related.

Unsupervised and Reinforcement Learning Method

Then, the DDML methods of the unsupervised learning type for the FDD in the NPP include the clustering (Baraldi et al., 2013; Li et al., 2020; Wang et al., 2021) and PCA (Ayodeji et al., 2018; Ling et al., 2020; Yu et al., 2020; Wang et al., 2021) techniques as shown in **Table 2**.

Afterward, the DDML research of the reinforcement learning type gradually developed in **Table 2**. The DDML such as the singular value decomposition (SVD) (Mandal et al., 2017a), deep Q learning network (DQN) (Lee et al., 2020), and Monte Carlo (MC) (Rao et al., 2009; Wang et al., 2018) are adopted by the NPP.

Clustering

Clustering algorithm refers to the classification of a group of targets. Compared with other groups of the targets, the same group of the targets are more similar to each other. In 2013, Baraldi et al. (2013) adopted the clustering technique for the FDD of the pressurizer. Later, Li et al. (2020) proposed a clustering algorithm for the transient detection in the NPP. Furthermore, Wang et al. (2021) utilized the clustering algorithm together with the SVM and PCA for the sensor anomalies in the NPP. This algorithm can make the data meaningful. Meanwhile, the results with this algorithm become difficult to interpret for the unusual datasets.

Principal Component Analysis Approach

The PCA approach is a kind of the dimensionality reduction method, which pursues the purpose of using less information to summarize or describe the data. In 2018, Ayodeji et al. (2018) operated the PCA with the radial basis function (RBF) for the transient scenarios in the NPP. Then, Yu et al. (2020) detected the sensor faults with the PCA approach. Afterward, Ling et al. (2020) presented the FDD of the reactor coolant system in the NPP. Lastly, Wang et al. (2021) utilized the PCA together with the clustering algorithm and SVM for the sensor anomalies in the NPP. The main operation of the PCA approach is eigenvalue decomposition, which is easy to implement. Conversely, the

TABLE 2 | Status of the data-driven machine learning (DDML) of the unsupervised and reinforcement learning method for the fault diagnosis and detection (FDD) in the nuclear power plant (NPP).

References	Methods	Type	Characteristics
Baraldi et al. (2013), Li et al. (2020) and Wang et al. (2021)	Clustering	Unsupervised learning type	Make data meaningful; difficult to handle the unusual data
Ayodeji et al. (2018), Ling et al. (2020), Yu et al. (2020), and Wang et al. (2021)	PCA	Unsupervised learning type	Easy to implement; certain degree of vagueness
Mandal et al. (2017a)	SVD	Reinforcement learning type	No noise; only suits the numerical data
Lee et al. (2020)	DQN	Reinforcement learning type	A lot of samples; sophisticated parameter adjustment
Rao et al. (2009) and Wang et al. (2018)	MC	Reinforcement learning type	Without uncertainty; high a time and space complexity

meaning of each feature dimension of the principal component has a certain degree of vagueness, which is not as explanatory as the original sample feature.

Singular Value Decomposition Method

The SVD method also belongs to the dimensionality reduction means. It is to decompose a large matrix into a form that is easy to handle. For the FDD in the NPP, Mandal et al. (2017a) introduced the SVD method to the thermocouple sensors. This algorithm can simplify the data, remove the noise, and hence improve the algorithm results. In contrast, it only suits the numerical data.

Deep Q Learning Network Technique

The DQN algorithm is a method of approximating the Q learning through a neural network. In 2020, Lee et al. (2020) focused on developing the algorithm for converting all the currently manual activities in the NPP power-increase process to autonomous operations. Among them, the DQN algorithm is included. For the DQN algorithm, it can produce a large number of samples. Conversely, the DQN algorithm may not necessarily converge and require sophisticated parameter adjustment.

Monte Carlo Method

The MC method has its inherent capability in simulating the actual process and random behavior of the system. First, Rao et al. (2009) carried out the probabilistic safety assessment with the MC method in the NPP. Then, Wang et al. (2018) explored the cyber-attack scenarios with the MC method in the NPP. It can eliminate uncertainty in reliability modeling while this algorithm requires a high time and space complexity.

Algorithm Type Method

In the past decades, the DDML studies can be classified into regression, instance-based learning, neural network, deep learning, dimension reduction, and kernel-based learning algorithms and they are shown in **Table 3**. Especially, the DDML of the deep learning type is popular for the FDD in the NPP recently. In addition, it is one of the recent advancements in the ANN (Peng et al., 2018). Furthermore, the deep learning type includes the recurrent neural network (RNN) (Moshkbar-Bakhshayesh and Ghofrani, 2013; Ling et al., 2020; Rezaeianjouybari and Shang, 2020), convolutional neural network (CNN) (Chen and Jahanshahi, 2017; Yao et al., 2020; Chae et al., 2020), deep neural network (DNN) (Mo et al., 2007; Chae et al., 2020; Miki and Demachi, 2020; Rezaeianjouybari and Shang, 2020; Saeed et al., 2020; Utah and Jung, 2020), deep belief network or dynamic Bayesian network (DBN) (Mandal et al., 2017b; Peng et al., 2018; Oh and Lee, 2020; Vaddi et al., 2020; Zhao et al., 2020), and restricted Boltzmann machine (RBM) (Rezaeianjouybari and Shang, 2020).

Recurrent Neural Network Approach

The biggest difference between the RNN approach and the traditional neural network is that each time it will bring the previous output result to the next hidden layer and train together. In 2013, Moshkbar-Bakhshayesh and Ghofrani (2013) studied the advanced approaches, which include the RNN approach for the transient diagnosis in the NPP. Then, Rezaeianjouybari and Shang (2020) reviewed the RNN algorithm and DNN technique for the prognostics and health management (PHM) in the NPP. Afterward, Ling et al. (2020) presented the RNN approach and PCA for the FDD in the reactor coolant system in the NPP. Especially, the RNN has the ability to learn and execute complex data conversion over a long period of time. It also may cause the problem of the vanishing gradient.

Convolutional Neural Network Method

The CNN algorithm is iteratively trained with a certain model to extract the features. It has been adopted for crack detection (Chen and Jahanshahi, 2017), sensor fault conditions (Yao et al., 2020), and pipe corrosion (Chae et al., 2020). Additionally, the advantages of the CNN algorithm are that it can automatically perform the feature extraction and has no pressure on the high-dimensional data processing. Meanwhile, it needs to adjust the parameters need and requires a large size of the sample.

Deep Neural Network Technique

The DNN technique has been proposed for the transient detection (Mo et al., 2007), PHM (Rezaeianjouybari and Shang, 2020), fault state detection of the solenoid operated valves (Utah and Jung, 2020), and the novel fault scheme (Saeed et al., 2020) in the NPP. In addition, Chae et al. (2020) combined the long–short term memory (LSTM) network with the SVM and CNN approach to diagnose the pipe corrosion in the NPP. Finally, the LSTM network, which is an RNN approach, was also applied for the bear fault in the NPP (Miki and Demachi, 2020). It has a strong learning ability while the model design is complex.

TABLE 3 | Status of the data-driven machine learning (DDML) of the algorithm type method for the fault diagnosis and detection (FDD) in the nuclear power plant (NPP).

References	Methods	Type	Characteristics
Moshkbar-Bakhshayesh (2020)	FFBPNN	Neural network type	Fast classification; decrease in accuracy
Moshkbar-Bakhshayesh (2020)	BPNN	Neural network type	Self-learning ability; low efficiency
Moshkbar-Bakhshayesh and Ghofrani (2013), Ling et al. (2020), and Rezaeianjouybari and Shang (2020)	RNN	Deep learning type	Execute complex data; vanishing gradient
Chen and Jahanshahi (2017), Chae et al. (2020), and Yao et al. (2020)	CNN	Deep learning type	Automatically feature extraction; require a lot of sample
Mo et al. (2007), Chae et al. (2020), Miki and Demachi (2020), Rezaeianjouybari and Shang (2020), Saeed et al. (2020), and Utah and Jung (2020)	DNN	Deep learning type	Strong learning ability; complex model design
Mandal et al. (2017b), Oh and Lee (2020), Peng et al. (2018), Vaddi et al. (2020), and Zhao et al. (2020)	DBN	Deep learning type	Quickly adjustment; requirement of a lot of data
Rezaeianjouybari and Shang (2020)	RBM	Deep learning type	
Ayodeji et al. (2018) and Wang et al. (2019)	RBF	Kernel-based Type	Fast in convergence; require a lot of data

Deep Belief Network and RBM Method

The DBN method is a major method of the Bayesian network (BN). It was applied to classify the fault data of the thermocouple sensors (Mandal et al., 2017b), accident prediction (Peng et al., 2018), operation failure of the high temperature gas-cooled reactor (Zhao et al., 2020), loss of coolant accident (LOCA) identity (Oh and Lee, 2020) and cybersecurity threats (Vaddi et al., 2020) in the NPP. Lastly, the DBN can be seen as a stack of the RBM (Rezaeianjouybari and Shang, 2020). The DBN and RBM method belong to the neural network (NN) method. Hence, the pros and cons of the two techniques are the same as the ANN approach.

Other Techniques

For the kernel-based type approach, the above SVM comes to the first place. Followed with the SVM, the RBF was adopted for the transients monitoring (Ayodeji et al., 2018; Wang et al., 2019). It is fast in convergence while it requires a lot of data. In addition, Moshkbar-Bakhshayesh (2020) investigated the feed-forward back-propagation neural network (FFBPNN), backpropagation neural network (BPNN), DT and SVM for the uncontrolled withdrawal of control rods in the NPP. The advantages and disadvantages of these methods are shown in **Table 3**.

DEVELOPMENT OF DDML FOR FDD IN NPP

Currently, huge achievements have already been made in its applications to predict the behaviors of the NPP. Therefore, there is a need to summarize the latest applications of the DDML in the NPP. It can also open future prospects to improve the accuracy of the FDD and have insights into the underlying mechanisms.

Furthermore, the DDML is a promising area with a flexible and efficient fitting algorithm. It does not underlie physical knowledge. **Tables 4–6** summarize the approaches taken by a wide range of authors recently. Generally, the DDML for the FDD in the NPP can be classified into three areas: (1) reactor system, (2) reactor component, and (3) reactor condition monitoring.

Latest Applications of DDML for FDD in the NPP System

As shown in **Table 4**, the DDML has been utilized for the FDD in the reactor coolant system (Ayodeji and Liu, 2018a; Farber and Cole, 2020), secondary loop system (Dong and Zhang, 2020), instrumentation control system (Holbert and Lin, 2012), and feedwater system (Zio, 2007) in the NPP.

First, Ayodeji and Liu (2018a) proposed the SVM for the incipient fault conditions of the reactor coolant system in the pressurized water reactor. In addition, Farber and Cole (2020) combined the ANN with the physical model-based method for the loss of coolant accident (LOCA) of the reactor coolant system. Then, Dong and Zhang (2020) presented the causality graphs, which belong to the BN approach for the secondary loop system in the NPP. Afterward, Holbert and Lin (2012) integrated the fuzzy logic, which is a kind of the NN techniques for the instrumentation control system in the NPP. At last, Zio (2007) utilized the SVM approach for the feedwater system of a boiling water reactor.

TABLE 4 | Latest applications of the data-driven machine learning (DDML) for the fault diagnosis and detection (FDD) of the nuclear power plant (NPP) system.

References	Methods	Objectives
Ayodeji and Liu (2018a)	SVM	Reactor coolant system
Farber and Cole (2020)	ANN + physic model	
Dong and Zhang (2020)	BN (Causal graphs)	Reactor secondary loop system
Holbert and Lin (2012)	NN (fuzzy logic)	Instrumentation control system
Zio (2007)	SVM	Feedwater system

TABLE 5 | Latest applications of the data-driven machine learning (DDML) for the fault diagnosis and detection (FDD) of the nuclear power plant (NPP) component.

References	Methods	Objectives
Baraldi et al. (2013)	Clustering	Pressurizer
Zhang et al. (2020)	RNN (LSTM)	
Di et al. (2013)	PCA + Regression	Reactor coolant pump
Liu and Zio (2017)	SVM	
Lu and Upadhyaya (2005)	NN (GMDH)	Steam generator
Zhao and Upadhyaya (2005)	BN (causal graphs)	
Razavi-Far et al. (2009)	NN (fuzzy logic)	
Li et al. (2012)	PCA	
Ayodeji and Liu (2018b)	Regression	
Ayodeji and Liu (2019)	ML	
Oluwasegun and Jung (2020)	ANN	Control rod
Moshkbar-Bakhshayesh (2020)	DT + FFBPNN + SVM	
Biet (2012)	kNN + Sparse	Turbine generator
Zhang et al. (2013)	BN (causal graphs)	
Ren et al. (2016)	SVM + Sparse	Bearing
Zhao and Wang (2018)	DNN	
Miki and Demachi (2020)	RNN (LSTM)	
Upadhyaya et al. (2003)	PCA + NN (GMDH)	Sensors
Mandal et al. (2017a)	SVD	
Mandal et al. (2017b)	DBN	
Choi and Lee (2020)	RNN	
Yu et al. (2020)	PCA	
Nguyen et al. (2020)	Physic model	
Wang et al. (2021)	SVM + PCA + clustering	

TABLE 6 | Latest applications of the data-driven machine learning (DDML) for the fault diagnosis and detection (FDD) of the nuclear power plant (NPP) condition monitoring.

References	Methods	Objectives
Mo et al. (2007)	DNN	Transient diagnosis
Moshkbar-Bakhshayesh and Ghofrani (2013)	ANN	
Ma and Jiang (2011)	ANN	
Ma and Jiang (2011)	ANN	Loose part monitoring
Meng et al. (2020)	SVM	
Zhao and Upadhyaya (2005)	BN (causal graphs)	Incipient fault monitoring
Chen and Jahanshahi (2017)	CNN + NB	Crack monitoring
Chae et al. (2020)	SVM + CNN + LSTM	Pipe corrosion monitoring
Wang et al. (2018)	MC	Cyber-attack monitoring
Vaddi et al. (2020)	DBN	

Latest Applications of DDML for FDD in the NPP Component

In **Table 5**, the reactor components, which include the pressurizer (Baraldi et al., 2013; Zhang et al., 2020), reactor coolant pump (Di et al., 2013; Liu and Zio, 2017), steam generator (Lu and Upadhyaya, 2005; Zhao and Upadhyaya, 2005; Razavi-Far et al., 2009; Li et al., 2012; Ayodeji and Liu, 2018b, 2019), control rod (Moshkbar-Bakhshayesh, 2020; Oluwasegun and Jung, 2020), turbine generator (Biet, 2012; Zhang et al., 2013), bearing (Ren et al., 2016; Zhao and Wang, 2018; Miki and Demachi, 2020), and sensors (Upadhyaya et al., 2003; Mandal et al., 2017a,b; Choi and Lee, 2020; Nguyen et al., 2020; Yu et al., 2020; Wang et al., 2021) are captured by different modeling techniques.

Initially, Baraldi et al. (2013) tested the clustering for the FDD in the pressurizer in the NPP. Later, Zhang et al. (2020) applied the LSTM for the water lever prediction of the pressurizer. For the reactor coolant pump, Di et al. (2013) conducted the FDD for the reactor coolant pump with the PCA and kernel-based regression method. Finally, Liu and Zio (2017) predicted the leakage from the reactor coolant pump with the SVM.

However, Lu and Upadhyaya (2005) adopted the group method of data handling method (GMDH), which is a kind of the NN approach for modeling the interrelationship of the U-tube steam generator (UTSG). Zhao and Upadhyaya (2005) presented the causal graphs for a pressurized water reactor. Razavi-Far et al. (2009) detected the faults of the steam generator using the fuzzy logic technique. Meanwhile, the PCA (Li et al., 2012) and support vector regression (Ayodeji and Liu, 2018b) are also adopted for the FDD of the steam generator.

For the control rod, Oluwasegun and Jung (2020) provided the health monitoring with the ANN approach. Meanwhile, Moshkbar-Bakhshayesh (2020) predicted the uncontrolled withdrawal of control rods transient with the DT, FFBPNN, and SVM. In addition, Biet (2012) recoded the rotor faults of the turbine generator with the kNN and sparse. However, Zhang et al. (2013) developed the causal graphs for the FDD of the turbine generator. Furthermore, the SVM plus sparse, DNN, and LSTM approaches for the FDD of the roller bearing were also proposed, respectively (Ren et al., 2016; Zhao and Wang, 2018; Miki and Demachi, 2020). Lastly, various techniques, including the PCA, GMDH, SVD, DBN, RNN, and clustering, are carried out for the sensor faults correspondingly in the NPP as shown in **Table 4** (Upadhyaya et al., 2003; Mandal et al., 2017a,b; Choi and Lee, 2020; Nguyen et al., 2020; Yu et al., 2020; Wang et al., 2021).

Latest Applications of DDML for FDD in the NPP Condition Monitoring

To satisfy the reliability, safety, and economics of the NPP, the condition identification of the NPP is expected to become increasingly popular as shown in **Table 6** (Moshkbar-Bakhshayesh and Ghofrani, 2013).

For the transient monitoring, Mo et al. (2007) proposed the DNN for the NPP. Furthermore, the ANN method for the transient monitoring in the NPP is mainly reviewed (Moshkbar-Bakhshayesh and Ghofrani, 2013; Ma and Jiang, 2011). Additionally, the ANN and SVM approaches have been adopted for the loose part monitoring (Ma and Jiang, 2011; Meng et al., 2020). Meanwhile, the causal graphs are also utilized for the incipient fault monitoring (Zhao and Upadhyaya, 2005). Moreover, Chen and Jahanshahi (2017) detected cracks on the underwater metallic surfaces from the nuclear inspection videos with the CNN and NB techniques. Furthermore, three approaches, including the SVM, CNN, and LSTM, are combined for the flow-accelerated corrosion of the pipe in the NPP (Chae et al., 2020). Especially, the new threats of the cyber-attack scenarios in the NPP are identified with the MC and DBN methods (Wang et al., 2018; Cyber threats: Vaddi et al., 2020).

Further Development of DDML for FDD in NPP

The DDML is of emerging interest in the FDD in the NPP. As mentioned above, significant efforts have already been taken in the prediction of the NPP behaviors. The future development of the DDML for the FDD in the NPP can be concluded based on the latest applications of the DDML for the FDD in the NPP as described in sections "Latest Applications of DDML for FDD of NPP System" to "Latest Applications of DDML for FDD of NPP Condition Monitoring."

Combination of DDML and Physic Model-Based Approach

For the DDML, the training data input and the results output. Hence, it is commonly regarded as a "black box." Although the physic model-based techniques are difficult to be proposed to describe the research objects, it still has its advantages. However, the combination of the DDML and physic model-based approach can help better understanding of the physical process (Farber and Cole, 2020). Furthermore, the DDML can be illustrated the experiment data clearly if the physic model-based approach functions. It should be noted that the hybrid of the DDML and physic model-based approach may attribute to higher computational resources. Nevertheless, it can provide reasonable and accurate insights into the physical processes.

Hybrid of Different Time-Scale Methods

In **Tables 4–6**, various methods for the FDD of the reactor systems, reactor components, and reactor condition monitoring are illustrated generally. Among them, there are hybrid of two or more techniques (Upadhyaya et al., 2003; Di et al., 2013; Ren et al., 2016; Chae et al., 2020; Moshkbar-Bakhshayesh, 2020; Wang et al., 2021). In particular, the time scale of the physical process of each object differs, which corresponds to its suitable methods for the FDD. Especially, the hybrid of the two or more methods for the FDD can be a superior solution for the evolution of the NPP. By this hybrid, it can present both the short-time and long-time behaviors of the NPP.

Sparse Data Treatment

Due to the safety, reliability, and economic issues, there is usually a lack of the experiment data of the FDD in the NPP. For a reactor system, reactor component, and reactor condition monitoring, not every parameter or data can be obtained. Therefore, there is a need for the DDML approach that is suitable for the sparse data. Special DDML can meet the urgent requirement properly.

Accurate and Fast Simulations

From the above treatment, the experiment data are hardly obtained under some conditions. Hence, the simulations are commonly performed to generate the training data (Wang et al., 2020; Yu et al., 2020). An accurate and fast simulation can understand the system, component, or condition with relatively acceptable computation cost. Detailed simulations are costly. One solution is to create a database of the historic results for the simulations and then train the DDML model. Later, DDML can also contribute to the experiment design for reasonable relatively fewer experiments.

CONCLUSION

In this paper, the state-of-the-art progress on the DDML for the FDD in the nuclear industry, which is an emerging interest on both the DDML approach for the FDD and the NPP, is reviewed. The main conclusions are obtained.

First, the DDML for the FDD in the NPP, which includes the supervised learning type, unsupervised learning type, and so on, are classified clearly with their characteristics, which help a comprehensive overview of the DDML.

1. Then, principles of various DDML for the FDD in the NPP, in particular, the DDML of the supervised learning type and deep learning type are explained in detail.
2. Furthermore, the latest applications of the DDML for the FDD, which consist of the reactor system, reactor component, and reactor condition monitoring are illustrated.

Lastly, the future development of the DDML for the FDD in the NPP is concluded. Considering the accuracy, complexity, and computation amount, the combination of the DDML and physic model-based approach, hybrid of different time-scale methods, accurate, and fast simulations are the future trends for the FDD in the NPP.

Compared with the physic model-based and reliability-based techniques, the DDML have superior advantages in the trade-off between the safety, reliability, and economics of the NPP. With the advancement of the information technologies and ML algorithms, together with the hybrid of the various approaches in different time scales, the DDML is to be a promising technique for the advanced NPP modeling in the future.

DATA AVAILABILITY STATEMENT

All datasets presented in this study are included in the article/supplementary material.

AUTHOR CONTRIBUTIONS

GH illustrated and summarized the fault diagnosis and detection in the nuclear power plant. TZ dedicated his time to classifications and principles of the algorithms. QL designed the whole architecture and provided the required resources. All authors contributed to the article and approved the submitted version.

FUNDING

This work was supported by the Sichuan Science and Technology Project (Grant No. 2020YFSY0031). It was also partially supported by the National Science Foundation for Young Scientists of China (Grant No. 61703385).

REFERENCES

Aizpurua, J. I., McArthur, S. D., Stewart, B. G., Lambert, B., and Cross, C. J. (2018). Adaptive power transformer lifetime predictions through machine learning and uncertainty modeling in nuclear power plants. *IEEE Trans. Ind. Electron.* 66, 4726–4737. doi: 10.1109/tie.2018.2860532

Ayodeji, A., and Liu, Y. K. (2018a). Support vector ensemble for incipient fault diagnosis in nuclear plant components. *Nucl. Eng. Technol.* 50, 1306–1313. doi: 10.1016/j.net.2018.07.013

Ayodeji, A., and Liu, Y. K. (2018b). SVR optimization with soft computing algorithms for incipient SGTR diagnosis. *Ann. Nucl. Energy* 121, 89–100. doi: 10.1016/j.anucene.2018.07.011

Ayodeji, A., and Liu, Y. K. (2019). PWR heat exchanger tube defects: trends, signatures and diagnostic techniques. *Prog. Nucl. Energy* 112, 171–184. doi: 10.1016/j.pnucene.2018.12.017

Ayodeji, A., Liu, Y. K., and Xia, H. (2018). Knowledge base operator support system for nuclear power plant fault diagnosis. *Prog. Nucl. Energy* 105, 42–50. doi: 10.1016/j.pnucene.2017.12.013

Baraldi, P., Di Maio, F., and Zio, E. (2013). Unsupervised clustering for fault diagnosis in nuclear power plant components. *Int. J. Comput. Intelligence Syst.* 6, 764–777. doi: 10.1080/18756891.2013.804145

Bartlett, E. B., and Uhrig, R. E. (1992). Nuclear power plant status diagnostics using an artificial neural network. *Nucl. Technol.* 97, 272–281. doi: 10.13182/nt92-a34635

Betta, G., and Pietrosanto, A. (2000). Instrument fault detection and isolation: state of the art and new research trends. *IEEE Trans. Instrum. Meas.* 49, 100–107. doi: 10.1109/19.836318

Biet, M. (2012). Rotor faults diagnosis using feature selection and nearest neighbors rule: application to a turbogenerator. *IEEE Trans. Ind. Electron.* 60, 4063–4073. doi: 10.1109/tie.2012.2218559

Chae, Y. H., Kim, S. G., Kim, H. M., Kim, J. T., and Seong, P. H. (2020). A methodology for diagnosing FAC induced pipe thinning using accelerometers and deep learning models. *Ann. Nucl. Energy* 143:107501. doi: 10.1016/j.anucene.2020.107501

Chen, F. C., and Jahanshahi, M. R. (2017). NB-CNN: deep learning-based crack detection using convolutional neural network and Naïve Bayes data fusion. *IEEE Trans. Ind. Electron.* 65, 4392–4400. doi: 10.1109/tie.2017.2764844

Choi, J., and Lee, S. J. (2020). A sensor fault-tolerant accident diagnosis system. *Sensors* 20:5839. doi: 10.3390/s20205839

Di, M. F., Baraldi, P., Zio, E., and Seraoui, R. (2013). Fault detection in nuclear power plants components by a combination of statistical methods. *IEEE Trans. Reliab.* 62, 833–845. doi: 10.1109/tr.2013.2285033

Dong, C., and Zhang, Q. (2020). The cubic dynamic uncertain causality graph: a methodology for temporal process modeling and diagnostic logic inference. *IEEE Trans. Neural Netw. Learn. Syst.* 31, 4239–4253. doi: 10.1109/tnnls.2019.2953177

Farber, J. A., and Cole, D. G. (2020). Detecting loss-of-coolant accidents without accident-specific data. *Prog. Nucl. Energy* 128:103469. doi: 10.1016/j.pnucene.2020.103469

Hadad, K., Pourahmadi, M., and Majidi-Maraghi, H. (2011). Fault diagnosis and classification based on wavelet transform and neural network. *Prog. Nucl. Energy* 53, 41–47. doi: 10.1016/j.pnucene.2010.09.006

Holbert, K. E., and Lin, K. (2012). Nuclear power plant instrumentation fault detection using fuzzy logic. *Sci. Technol. Nucl. Installations* 2012:421070.

Jamil, F., Abid, M., Haq, I., Khan, A. Q., and Iqbal, M. (2016). Fault diagnosis of Pakistan research Reactor-2 with data-driven techniques. *Ann. Nucl. Energy* 90, 433–440. doi: 10.1016/j.anucene.2015.12.023

Lee, D., Arigi, A. M., and Kim, J. (2020). *Algorithm for Autonomous Power-Increase Operation Using Deep Reinforcement Learning and a Rule-Based System*. Piscataway, NJ: IEEE.

Li, F., Upadhyaya, B. R., and Perillo, S. R. (2012). Fault diagnosis of helical coil steam generator systems of an integral pressurized water reactor using optimal sensor selection. *IEEE Trans. Nucl. Sci.* 59, 403–410. doi: 10.1109/tns.2012.2185509

Li, X., Fu, X. M., Xiong, F. R., and Bia, X. M. (2020). Deep learning-based unsupervised representation clustering methodology for automatic nuclear reactor operating transient identification. *Knowl. Based Syst.* 204:106178. doi: 10.1016/j.knosys.2020.106178

Ling, J., Liu, G. J., Li, J. L., Chen, X. C., and You, D. D. (2020). Fault prediction method for nuclear power machinery based on Bayesian PPCA recurrent neural network model. *Nucl. Sci. Techniques* 31:75.

Liu, J., and Zio, E. (2017). SVM hyperparameters tuning for recursive multi-step-ahead prediction. *Neural Comput. Appl.* 28, 3749–3763. doi: 10.1007/s00521-016-2272-1

Liu, J., Seraoui, R., Vitelli, V., and Zio, E. (2013). Nuclear power plant components condition monitoring by probabilistic support vector machine. *Ann. Nucl. Energy* 56, 23–33. doi: 10.1016/j.anucene.2013.01.005

Locatelli, G., Mancini, M., and Todeschini, N. (2013). Generation IV nuclear reactors: current status and future prospects. *Energy Policy* 61, 1503–1520. doi: 10.1016/j.enpol.2013.06.101

Lu, B., and Upadhyaya, B. R. (2005). Monitoring and fault diagnosis of the steam generator system of a nuclear power plant using data-driven modeling and residual space analysis. *Ann. Nucl. Energy* 32, 897–912. doi: 10.1016/j.anucene.2005.02.003

Ma, J., and Jiang, J. (2011). Applications of fault detection and diagnosis methods in nuclear power plants: a review. *Prog. Nucl. Energy* 53, 255–266. doi: 10.1016/j.pnucene.2010.12.001

Mandal, S., Santhi, B., Sridhar, S., Vinolla, K., and Swaminathan, P. (2017a). A novel approach for fault detection and classification of the thermocouple sensor in nuclear power plant using singular value decomposition and symbolic dynamic filter. *Ann. Nucl. Energy* 103, 440–453. doi: 10.1016/j.anucene.2017.01.043

Mandal, S., Santhi, B., Sridhar, S., Vinolla, K., and Swaminathan, P. (2017b). Nuclear power plant thermocouple sensor-fault detection and classification using deep learning and generalized likelihood ratio test. *IEEE Trans. Nucl. Sci.* 64, 1526–1534.

Meng, J., Su, Y., and Xie, S. (2020). Loose parts detection method combining blind deconvolution with support vector machine. *Ann. Nucl. Energy* 149:107782. doi: 10.1016/j.anucene.2020.107782

Miki, D., and Demachi, K. (2020). Bearing fault diagnosis using weakly supervised long short-term memory. *J. Nucl. Sci. Technol.* 57, 1091–1100. doi: 10.1080/00223131.2020.1761473

Mo, K., Lee, S. J., and Seong, P. H. (2007). A dynamic neural network aggregation model for transient diagnosis in nuclear power plants. *Prog. Nucl. Energy* 49, 262–272. doi: 10.1016/j.pnucene.2007.01.002

Moshkbar-Bakhshayesh, K. (2020). Prediction of unmeasurable parameters of NPPs using different model-free methods based on cross-correlation detection of measurable/unmeasurable parameters: a comparative study. *Ann. Nucl. Energy* 139:107232. doi: 10.1016/j.anucene.2019.107232

Moshkbar-Bakhshayesh, K., and Ghofrani, M. B. (2013). Transient identification in nuclear power plants: a review. *Prog. Nucl. Energy* 67, 23–32. doi: 10.1016/j.pnucene.2013.03.017

Nguyen, T. N., Downar, T., and Vilim, R. (2020). A probabilistic model-based diagnostic framework for nuclear engineering systems. *Ann. Nucl. Energy* 149:107767. doi: 10.1016/j.anucene.2020.107767

Oh, C., and Lee, J. I. (2020). Real time nuclear power plant operating state cognitive algorithm development using dynamic Bayesian network. *Reliab. Eng. Syst. Saf.* 198:106879. doi: 10.1016/j.ress.2020.106879

Oluwasegun, A., and Jung, J. C. (2020). The application of machine learning for the prognostics and health management of control element drive system. *Nucl. Eng. Technol.* 52, 2262–2273. doi: 10.1016/j.net.2020.03.028

Peng, B. S., Xia, H., Liu, Y. K., Yang, B., Guo, D., Zhu, S. M., et al. (2018). Research on intelligent fault diagnosis method for nuclear power plant based on correlation analysis and deep belief network. *Prog. Nucl. Energy* 108, 419–427. doi: 10.1016/j.pnucene.2018.06.003

Po, L. C. (2020). Conceptual design of an accident prevention system for light water reactors using artificial neural network and high-speed simulator. *Nucl. Technol.* 206, 505–513. doi: 10.1080/00295450.2019.1641877

Rao, K. D., Gopika, V., Rao, V. S., Kushwaha, H. S., Verma, A. K., Srividya, A., et al. (2009). Dynamic fault tree analysis using Monte Carlo simulation in probabilistic safety assessment. *Reliab. Eng. Syst. Saf.* 94, 872–883. doi: 10.1016/j.ress.2008.09.007

Razavi-Far, R., Davilu, H., Palade, V., and Lucas, C. (2009). Model-based fault detection and isolation of a steam generator using neuro-fuzzy networks. *Neurocomputing* 72, 2939–2951. doi: 10.1016/j.neucom.2009.04.004

Ren, L., Lv, W., Jiang, S., and Xiao, Y. (2016). Fault diagnosis using a joint model based on sparse representation and SVM. *IEEE Trans. Instrum. Meas.* 65, 2313–2320. doi: 10.1109/tim.2016.2575318

Rezaeianjouybari, B., and Shang, Y. (2020). Deep learning for prognostics and health management: state of the art, challenges, and opportunities. *Measurement* 163:107929. doi: 10.1016/j.measurement.2020.107929

Saeed, H. A., Peng, M. J., Wang, H., and Zhang, B. W. (2020). Novel fault diagnosis scheme utilizing deep learning networks. *Prog. Nucl. Energy* 118:103066. doi: 10.1016/j.pnucene.2019.103066

Sharanya, S., and Venkataraman, R. (2018). "Empirical analysis of machine learning algorithms in fault diagnosis of coolant tower in nuclear power plants," in *International Conference on Computational Vision and Bio Inspired Computing, November 29*, (Cham).

Upadhyaya, B. R., Zhao, K., and Lu, B. (2003). Fault monitoring of nuclear power plant sensors and field devices. *Prog. Nucl. Energy* 43, 337–342. doi: 10.1016/s0149-1970(03)00046-5

Utah, M. N., and Jung, J. C. (2020). Fault state detection and remaining useful life prediction in AC powered solenoid operated valves based on traditional machine learning and deep neural networks. *Nucl. Eng. Technol.* 52, 1998–2008. doi: 10.1016/j.net.2020.02.001

Vaddi, P. K., Pietrykowski, M. C., Kar, D., Diao, X., and Zhao, Y. (2020). Dynamic Bayesian networks based abnormal event classifier for nuclear power plants in case of cyber security threats. *Prog. Nucl. Energy* 128:103479. doi: 10.1016/j.pnucene.2020.103479

Wang, H., Peng, M. J., Hines, J. W., Zheng, G. Y., Liu, Y. K., Upadhyaya, B. R., et al. (2019). A hybrid fault diagnosis methodology with support vector machine and improved particle swarm optimization for nuclear power plants. *ISA Trans.* 95, 358–371. doi: 10.1016/j.isatra.2019.05.016

Wang, H., Peng, M. J., Yu, Y., Saeed, H., Hao, C.-M., Liu, Y. K., et al. (2021). Fault identification and diagnosis based on KPCA and similarity clustering for nuclear power plants. *Ann. Nucl. Energy* 150:107786. doi: 10.1016/j.anucene.2020.107786

Wang, H., Peng, M., Xu, R., Ayodeji, A., and Xia, H. (2020). Remaining useful life prediction based on improved temporal convolutional network for nuclear power plant valves. *Front. Energy Res.* 8:584463.

Wang, W., Cammi, A., Di, M. F., Lorenzi, S., and Zio, E. (2018). A monte carlo-based exploration framework for identifying components vulnerable to cyber threats in nuclear power plants. *Reliab. Eng. Syst. Saf.* 175, 24–37. doi: 10.1016/j.ress.2018.03.005

Yao, Y., Wang, J., Long, P., Xie, M., and Wang, J. (2020). Small-batch-size convolutional neural network based fault diagnosis system for nuclear energy production safety with big-data environment. *Int. J. Energy Res.* 44, 5841–5855. doi: 10.1002/er.5348

Yu, Y., Peng, M. J., Wang, H., Ma, Z. G., and Li, W. (2020). Improved PCA model for multiple fault detection, isolation and reconstruction of sensors in nuclear power plant. *Ann. Nucl. Energy* 148:107662. doi: 10.1016/j.anucene.2020.107662

Zhang, J., Wang, X., Zhao, C., Bai, W., Shen, J., Li, Y., et al. (2020). Application of cost-sensitive LSTM in water level prediction for nuclear reactor pressurizer. *Nucl. Eng. Technol.* 52, 1429–1435.

Zhang, Q., Dong, C., Cui, Y., and Yang, Z. (2013). Dynamic uncertain causality graph for knowledge representation and probabilistic reasoning: statistics base, matrix, and application. *IEEE Trans. Neural Netw. Learn. Syst.* 25, 645–663.

Zhao, K., and Upadhyaya, B. R. (2005). Adaptive fuzzy inference causal graph approach to fault detection and isolation of field devices in nuclear power plants. *Prog. Nucl. Energy* 46, 226–240.

Zhao, L., and Wang, X. (2018). *A Deep Feature Optimization Fusion Method for Extracting Bearing Degradation Features*. Piscataway, J: IEEE.

Zhao, Y., Tong, J., Zhang, L., and Wu, G. (2020). Diagnosis of operational failures and on-demand failures in nuclear power plants: an approach based on dynamic Bayesian networks. *Ann. Nucl. Energy* 138:107181.

Zio, E. (2007). A support vector machine integrated system for the classification of operation anomalies in nuclear components and systems. *Reliab. Eng. Syst. Saf.* 92, 593–600.

Conflict of Interest: The authors declare that the research was conducted in the absence of any commercial or financial relationships that could be construed as a potential conflict of interest.

NOMENCLATURE

ANN	The artificial neural network
BPNN	The back propagation neural network
BN	The Bayesian network
CNN	The convolutional neural network
DBN	The deep belief network or dynamic Bayesian network
DDML	The data-driven machine learning
DNN	The deep neural network
DRL	The dimension reduction learning
DQN	The deep Q learning network
DT	The decision tree
EL	The ensemble learning
FDD	The fault diagnosis and detection
FFBPNN	The feed-forward back-propagation neural network
GMDH	The group method of data handling
kNN	The k-nearest neighbor
LOCA	The loss of coolant accident
LSTM	The long–short term memory
MC	The Monte Carlo
ML	The machine learning
NB	The naive Bayes
NN	The neural network
NPP	The nuclear power plant
PCA	The principal component analysis
PHM	The prognostics and health management
RBF	The radial basis function
RBM	The restricted Boltzmann machine
RNN	The recurrent neural network
RT	The random tree
SVD	The singular value decomposition
SVM	The support vector machine
UTSG	The U-tube steam generator
b	The model parameter
c_1, c_1, c_3	The category in the kNN method
w	The normal vector to the hyperplane
$w_1, \ldots, w_n$	The synaptic weights
w	The magnitude
$x_1, \ldots, x_n$	The input signals
x_u	The prediction point in the kNN method
y_k	The output signals
$\varphi(\cdot)$	The activation function

frontiers in Energy Research

REVIEW
published: 15 June 2021
doi: 10.3389/fenrg.2021.696785

Prognostics and Health Management in Nuclear Power Plants: An Updated Method-Centric Review With Special Focus on Data-Driven Methods

Xingang Zhao[1], Junyung Kim[2], Kyle Warns[2], Xinyan Wang[3], Pradeep Ramuhalli[1], Sacit Cetiner[1], Hyun Gook Kang[2] and Michael Golay[3]*

[1]Nuclear Energy and Fuel Cycle Division, Oak Ridge National Laboratory, Oak Ridge, TN, United States, [2]Department of Mechanical, Aerospace and Nuclear Engineering, Rensselaer Polytechnic Institute, Troy, NY, United States, [3]Department of Nuclear Science and Engineering, Massachusetts Institute of Technology, Cambridge, MA, United States

OPEN ACCESS

Edited by:
Wenzhong Zhou,
Sun Yat-Sen University, China

Reviewed by:
Sameer Al-Dahidi,
German Jordanian University, Jordan
Gyunyoung Heo,
Kyung Hee University, South Korea

****Correspondence:***
Xingang Zhao
zhaox2@ornl.gov

Specialty section:
This article was submitted to Nuclear Energy, a section of the journal Frontiers in Energy Research

Received: *17 April 2021*
Accepted: *26 May 2021*
Published: *15 June 2021*

Citation:
Zhao X, Kim J, Warns K, Wang X, Ramuhalli P, Cetiner S, Kang HG and Golay M (2021) Prognostics and Health Management in Nuclear Power Plants: An Updated Method-Centric Review With Special Focus on Data-Driven Methods.
Front. Energy Res. 9:696785.
doi: 10.3389/fenrg.2021.696785

In a carbon-constrained world, future uses of nuclear power technologies can contribute to climate change mitigation as the installed electricity generating capacity and range of applications could be much greater and more diverse than with the current plants. To preserve the nuclear industry competitiveness in the global energy market, prognostics and health management (PHM) of plant assets is expected to be important for supporting and sustaining improvements in the economics associated with operating nuclear power plants (NPPs) while maintaining their high availability. Of interest are long-term operation of the legacy fleet to 80 years through subsequent license renewals and economic operation of new builds of either light water reactors or advanced reactor designs. Recent advances in data-driven analysis methods—largely represented by those in artificial intelligence and machine learning—have enhanced applications ranging from robust anomaly detection to automated control and autonomous operation of complex systems. The NPP equipment PHM is one area where the application of these algorithmic advances can significantly improve the ability to perform asset management. This paper provides an updated method-centric review of the full PHM suite in NPPs focusing on data-driven methods and advances since the last major survey article was published in 2015. The main approaches and the state of practice are described, including those for the tasks of data acquisition, condition monitoring, diagnostics, prognostics, and planning and decision-making. Research advances in non-nuclear power applications are also included to assess findings that may be applicable to the nuclear industry, along with the opportunities and challenges when adapting these developments to NPPs. Finally, this paper identifies key research needs in regard to data availability and quality, verification and validation, and uncertainty quantification.

Keywords: prognostics and health management, planning and decision-making, condition-based maintenance, artificial intelligence, machine learning, data-driven methods, nuclear power plant

INTRODUCTION

Reducing anthropogenic greenhouse gas (GHG) emissions for climate change mitigation while expanding energy access to billions of people is a central global challenge of this century. As the world's second-largest low-carbon power source (second only to hydropower), nuclear power makes up more than one-quarter of annual low-carbon electricity supply worldwide and has avoided about 60 gigatons of GHG emissions over the past 50 years (IEA, 2019). At present, approximately 10% of global electricity generation is produced by nuclear power each year (IAEA, 2021). To achieve deep decarbonization targets, including the one limiting average global warming to 2°C in 2050 (Gao et al., 2017), it is imperative to maintain the existing nuclear share of electricity production (MIT, 2018).

Despite its important role in energy transitions to meet climate goals, the nuclear industry is facing an uncertain future in many countries, not only due to the March 2011 Fukushima accident in Japan but also more fundamentally for economic reasons. In advanced economies such as the United States, unfavorable market conditions—including weak growth in electricity demand, low natural gas prices, and increasing competition from renewables-based power supply—are putting pressure on the financial performance of existing nuclear power plants (NPPs), which may lead to their early retirements. One of the first thrusts being pursued to support economical nuclear power has been focused on life extensions of the legacy fleet, from the initial license period of 40 years (in most cases) to 50–60 years and possibly beyond. Life extensions are considerably cheaper than new construction and will be cost-competitive with any other electricity generation technology, as illustrated in **Figure 1** for the projected US levelized cost of electricity associated with different technologies in 2040. A new joint report (IEA and NEA, 2020) by the International Energy Agency (IEA) and the Nuclear Energy Agency (NEA) also concludes that prolonging the operation of existing nuclear assets, known as long-term operation (LTO), is the most affordable low-carbon solution. Unfortunately, the LTO of current NPPs alone—mostly light water reactors (LWRs)—can only provide temporary support for the transition to clean energy systems. New builds are necessary, and near-term interests are rising in LWR-based small modular reactors (SMRs) and mature Generation-IV concepts.

To achieve safe, reliable, and economical operation of NPPs, attention is turning to enhanced plant asset management methods within the activities of both legacy fleet LTO and new construction. Decades of global operational experience have shown that greater situational awareness of the condition of key structures, systems, and components (SSCs) is essential for managing and mitigating plant equipment degradation, particularly the aging-related degradation due to exposure to a harsh operating environment. While the traditional approaches to maintenance and aging management complied with the defense-in-depth policy (IAEA, 1996) and proved to be adequate for maintaining safety margins in the past, they were not optimized in terms of effort, time, or cost (Coble et al., 2012). Historically, corrective find-and-fix maintenance policies prevailed in the early days of the nuclear industry, which would incur overly long facility downtime and excessively high cost (Ayo-Imoru and Cilliers, 2018). The time-based periodic maintenance scheduling became widely employed since the 1970s. However, this strategy is generally conservative and often yields unnecessary planned inspection and maintenance that challenge the economics of nuclear generation. Meanwhile, it does not prevent plant downtime caused by unanticipated equipment failure, which leads to a significant amount of lost revenue: at least $1.2 million per day of plant shutdown for an

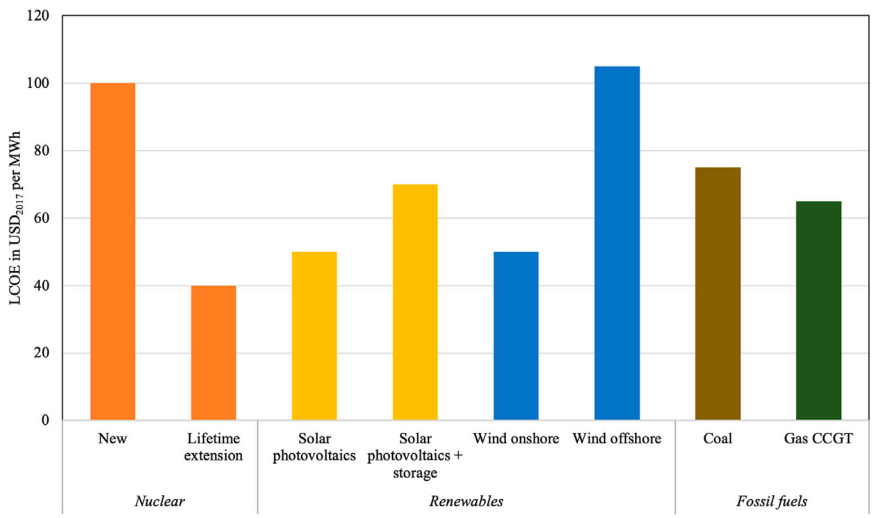

FIGURE 1 | Projected US LCOE by technology in 2040 [modified from IEA (2019)]. *Note for* **Figure 1**: LCOE = levelized cost of electricity, average cost to build and operate a power plant over its lifetime divided by the total electricity output of the plant over the same period; it represents the break-even price of electricity generation at a power production facility. CCGT = combined-cycle gas turbines. Estimates of nuclear lifetime extension are based on a 500 million USD investment to extend operations for 20 years. Other cost assumptions can be found in IEA (2019).

average NPP in the United States and France (NEI, 2011; Power Engineering International, 2017). Therefore, it is necessary to move from uneconomic find-and-fix or periodic maintenance strategies to the more cost-effective just-in-time repair policies.

The just-in-time repair is a predictive maintenance strategy that relies on continuous monitoring and full awareness of the equipment health condition throughout its life cycle, or in other words, the use of *prognostics and health management* (PHM) principles. The full PHM suite includes five modules: data acquisition, monitoring and anomaly detection, fault diagnostics, prognostics, and planning and decision-making. Through appropriate detection, diagnosis and prognosis, and mitigation actions, a robust PHM system will allow early warning of degradation in NPPs and will potentially preclude serious consequences due to faults and failures while helping alleviate the burden of unnecessary maintenance activities.

This paper provides an updated method-centric review of the full PHM suite in NPPs since the last major survey article by Coble et al. (2015) was published in 2015. The results of that survey are augmented with new progress made in the intervening years. In particular, recent advances in data-driven analysis methods—largely represented by those in artificial intelligence (AI) and machine learning (ML)—have enhanced applications ranging from robust anomaly detection to automated control and autonomous operation of complex systems. PHM in NPPs is one area where the application of those algorithmic advances can significantly improve the ability to perform enhanced asset management. Therefore, special attention is dedicated to the advances in data-driven diagnostic and prognostic methods. PHM technologies in non-nuclear power applications are also included to assess findings that may be applicable to the nuclear industry, along with the opportunities and challenges when adapting these developments to NPPs. "US NPP Monitoring and Maintenance: Historical Approach and Motivations for Prognostics and Health Management" Section summarizes the historical approach to monitoring and maintenance in US NPPs and outlines the PHM needs for improving the safety and economy of both LTO and new builds. "Prognostics and Health Management Framework and Modeling Approaches" Section describes the PHM framework, followed by the state of practice for each of its five modules with a focus on data-driven methods. "Research Needs for Deployment of Prognostics and Health Management in Nuclear Power Plants" Section identifies the overarching research needs to support the development and deployment of PHM in NPPs. "Summary" Section summarizes the key findings of this paper.

US NPP MONITORING AND MAINTENANCE: HISTORICAL APPROACH AND MOTIVATIONS FOR PROGNOSTICS AND HEALTH MANAGEMENT

The United States has the largest number of commercial nuclear reactors in the world. Its operating fleet [94 LWRs in 56 NPPs (IAEA, 2021) as of January 2021] has steadily generated about 20% of the nation's electricity since the mid-1990s (NEI, 2021a) at by far the highest capacity factor [93.4% in 2019 (US DOE, 2019)] of any energy source. Despite this performance and the fact that nuclear makes up more than half of the nation's clean energy (NEI, 2021b), nine reactors have been shut down in the United States before their licenses expired since 2012 due to unfavorable market conditions, and an additional five units are scheduled to retire in 2021 (US DOE, 2020a; US EIA, 2021a). The average age of US operating reactors is almost 40 years. The youngest unit, Tennessee's Watts Bar Nuclear Plant Unit 2, began operation in 2016 and was the nation's first new reactor in 20 years (US EIA, 2021b). Meanwhile, only two commercial reactors—2 AP1000 units at Georgia's Vogtle plant—are currently under construction (IAEA, 2021) in the country. To keep America's nuclear capacity from sharply declining and to enable clean energy transition, the current LWR fleet is undergoing 20-years life extensions from the original 40-years licenses; 85 reactors[1] have been approved by the US Nuclear Regulatory Commission (NRC) to operate 60 years through the initial license renewal applications (NEI, 2021c). To date, 53 reactors have already entered extended operation or LTO (US NRC, 2021a). Additionally, utilities are intending to operate up to 80 years through second 20-years extensions or subsequent license renewals; four reactors have been issued a second renewed license for extended LTO and six additional applications are under review (US NRC, 2021b).

To comply with the NRC's license renewal rule [Title 10, Part 54 of the *Code of Federal Regulations*, or 10 CFR 54 (US NRC, 1995)] and to continue to provide secure nuclear power generation, it is imperative to understand and manage the effects of SSC aging in NPPs. As described in Coble et al. (2012), the NRC monitoring and maintenance programs usually draw a distinction between active and passive SSCs.[2] The active SSCs—such as control rod drives, generators, sensors, motors, pumps, and valves—must move to perform their intended functions. Their performance monitoring and aging management have been historically covered by the Maintenance Rule (10 CFR 50.65) (US NRC, 2021c). The Maintenance Rule provides a performance-based approach to monitoring and improving the overall effectiveness of active component maintenance. However, it does not directly improve the economics of performing maintenance (Coble et al., 2012). Under the Maintenance Rule, a large majority of maintenance activities remain periodically scheduled. The passive SSCs—such as reactor pressure vessels (RPVs), heat exchangers, transformers, cables, support structures, and piping—do not move during normal functions. Their degradation and maintenance are managed through periodic in-service inspection as dictated by the plant's aging management program. As codified in 10 CFR 50.55a (US NRC, 2021d), nondestructive inspection

[1]The NRC has approved initial license renewal applications for 93 reactors. Unfortunately, eight of them have since ceased operations prematurely.

[2]The distinction between active and passive SSCs can be complicated. For example, pumps are active components, but their casings and support structures are considered passive.

requirements are specified for the in-service inspection of passive components.

As plants enter LTO, aging becomes a more challenging problem. Because it is of paramount importance to be warned of impending SSC faults and failures, the frequency of periodic inspection and maintenance will need to increase to compensate for potentially growing failure rates over time due to wear-out failures in active SSCs and for reduced safety margins toward the lowest allowable level due to degraded material characteristics in passive SSCs. The increased inspection frequency would cause extended (and sometimes unnecessary) downtime of plant safety-critical systems and eventually affect the industry's competitiveness. Transitioning from periodic maintenance scheduling to a more continuous, just-in-time health management approach is essential to ensure that the intended functions of NPP assets are maintained for the period of extended operation. Advanced monitoring techniques will provide the necessary support to this transition, along with advances in diagnostic and prognostic methods.

Currently, there is a growing interest in applying condition-based (rather than time-based) maintenance for active components and automated online monitoring (instead of periodic inspection) for passive components through the use of PHM. In fact, well-applied PHM technologies will benefit not only aging LWRs but also new builds, especially LWR-based SMRs [such as the pressurized water NuScale720 (US DOE, 2020b) and the boiling water GEH BWRX-300 (US DOE, 2020c)] and mature advanced reactor designs as part of the Generation-IV initiative [such as TerraPower's Natrium and X-energy's Xe-100 under the US Department of Energy [DOE]'s Advanced Reactor Demonstration Program (US DOE, 2020d)], into which inherent and passive safety features are extensively incorporated. These reactors have additional monitoring and surveillance needs over currently operating LWRs due to extended fuel cycles, exposure to harsher operating environments, use of innovative materials, and remote siting with reduced maintenance staffing levels (Coble et al., 2015). Traditional inspection techniques and maintenance policies will not meet such needs.

In addition to improving plant safety and reliability, PHM is also economically attractive for reducing operations & maintenance (O&M) costs compared to time-based and even traditional condition-based (i.e., without the use of PHM)[3] policies. The O&M costs represent a crucial disadvantage for the nuclear industry and comprise about two thirds of total generating costs in NPPs (Coble et al., 2015; Al Rashdan et al., 2018). As discussed in "Introduction" Section, periodic inspection and maintenance could lead to unnecessary and unanticipated repair or replacement of SSCs, incurring significant additional downtime and costs. Besides, compared to the traditional concept of condition-based maintenance (CBM), PHM-enabled CBM provides capabilities to achieve more proactivity in O&M, places stronger emphasis on the operation stage than the design stage, and rely on condition-based, facility-specific status identification rather than population statistics. While detailed cost-benefit analyses of using PHM in specific NPPs are yet to be conducted, Bond et al. (2011) suggest that applying PHM technologies to all key SSCs in the nation's legacy plants could result in an annual fleet-wide savings of more than $1 billion.[4] Furthermore, proper application of the complete PHM suite—especially with automated planning and decision-making capabilities—can effectively reduce labor reliance and frequency of O&M activities because labor costs account for approximately 80% of O&M costs in US plants.

PROGNOSTICS AND HEALTH MANAGEMENT FRAMEWORK AND MODELING APPROACHES

This paper reviews the full PHM suite, which utilizes sensor technologies and data analytics to monitor health conditions, detect anomalies, diagnose faults, predict the remaining useful life (RUL), and proactively manage failures (Droguett, 2020) in complex engineering systems such as NPP assets. The five modules/steps of a full PHM system are depicted in **Figure 2**, and each module will be elaborated on in the following subsections. To date, there has been no universally well-defined categorization of PHM systems partly due to lack of unifying PHM standards, which are needed for harmonized terminology, consistency of PHM methods, and compatibility/interoperability of PHM technology. A number of disparate industrial standards—mostly developed by the International Organization for Standardization (ISO) and the Institute of Electrical and Electronics Engineers (IEEE)—exist which pertain to different modules of a PHM system, such as ISO 13374 series for condition monitoring (CM) of industrial machines, ISO 13379 for diagnostics, ISO 13381 for prognostics, and IEEE P1856 for PHM of electronic systems. Vogl et al. (2014) surveyed existing PHM-related standards and identified areas for development of future standards.

In a PHM system, sensory data collected from a target SSC are continuously monitored for deviations from normal behavior, which are indicators of incipient faults or anomalies.[5] Once an anomaly is detected, it is important to diagnose the fault, or in

[3]It is important to notice that PHM is not a type of maintenance by itself but rather a set of tools that yield information which can be used as input to CBM. In other words, CBM can be adopted with or without the use of PHM. In fact, many traditional frameworks considered CBM but did not include the treatment of PHM techniques/methods. To mark the difference with the traditional concept of CBM (i.e., CBM without implementation of PHM), new terms for PHM-enabled CBM have been introduced in the literature, including CBM+ and CBM/PHM. A comprehensive review on the role of PHM in CBM systems, which is not the focus of this paper, can be found in Guillén et al. (2016).

[4]The annual fleet-wide O&M costs in the US are estimated to be around $12 billion in 2017 US dollars. This is calculated with an annual O&M cost of $120 per kW for an average US plant of 36 years old (in 2017) (SargentLundy, 2018) and a total capacity of 100 GW (NEI, 2021c).

[5]The terms "faults" and "anomalies" have been used interchangeably in the literature. Technically speaking, they have a subtle difference in meaning: anomalies refer to deviations indicated by sensor measurements, whereas faults refer to the actual physical manifestations of such deviations in a monitored SSC.

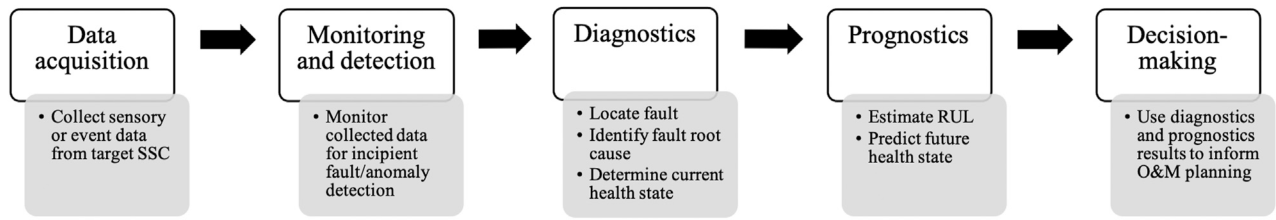

FIGURE 2 | Five modules/steps of PHM [adapted and extended from Coble et al., 2015)].

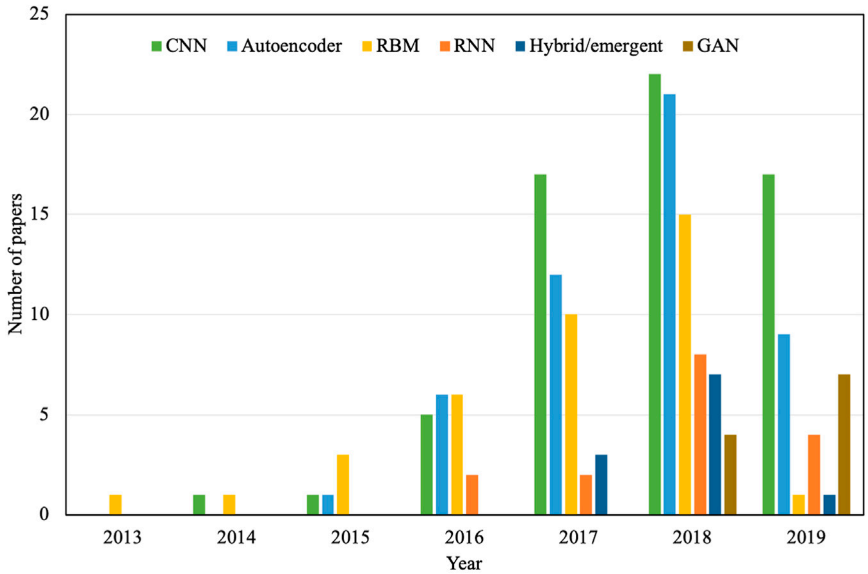

FIGURE 3 | Breakdown of published papers on DL in PHM between 2013 and September 2019 (modified from Rezaeianjouybari and Shang (2020)) *Note for* **Figure 3**: DL architecture–share of total publications as follows: CNN (convolutional neural network)—32.1%; autoencoder—26.8%; RBM (restricted Boltzmann machine)—19.6%; RNN (recurrent neural network)—9.2%; hybrid/emergent—6.7%; GAN (generative adversarial network)—5.6%.

other words, to locate the fault to a specific component or area of a structure (i.e., fault isolation) and to determine the root cause of the fault (i.e., fault identification). Depending on how the SSC will degrade, an appropriate prognostic model is then applied to estimate its RUL. Finally, O&M planning is informed by integrating prognostic calculations and risk assessment of proposed mitigation actions based on the current and postulated future health states of the target SSC to achieve optimal (and ultimately autonomous) control and decision-making.

Besides traditional modeling tools, the recent advancements in AI and ML technologies provide opportunities for leveraging emerging data-driven algorithms to effectively address PHM problems, especially those of diagnostics and prognostics. Details will be provided in the corresponding subsections. **Figure 3** illustrates the growing research interest in the application of one such algorithmic example for PHM: deep learning (DL), a quickly developing subfield of ML. Through a systematic review of state-of-the-art DL-based PHM frameworks, Rezaeianjouybari and Shang (2020) recently presented the benefits and potentials of DL technologies in the PHM paradigm, especially in the presence of high-volume and multidimensional data streams that contain real-time information about the degradation and health condition of the system of interest.

Data Acquisition: Emerging Sensor Technologies

Traditional reliability analyses rely on population statistics rather than condition-based status identification. Thus, they do not provide any useful insight regarding a specific SSC's current or future state. The process of data acquisition from the target equipment is necessary to make an accurate, reliable prediction of individual SSC health. Collected data can be either event or sensory data (Atamuradov et al., 2017). Event data are O&M logs containing actions taken by the operator or maintenance staff in response to events that occurred to the physical asset and are not the focus of this paper. Sensory data are measurements tracked via sensors installed on the target

TABLE 1 | Comparison of different sensor technologies.

Sensor technology		Location (surface/embedded/remote)	Operation type (active/passive)	Used in nuclear/non-nuclear industry	References
Magnetic anisotropy	MBN	Surface	Passive	Nuclear/non-nuclear	Spasojevic et al. (1996), Stefanita (2008), McCloy et al. (2013), Li et al. (2015), Deng et al. (2018)
	MAE	Surface	Passive	Nuclear/non-nuclear	Stefanita (2008), Li et al. (2015), Makowska et al. (2017)
Piezoelectricity	Piezoelectric thin film	Surface	Active/passive	Nuclear/non-nuclear	Komagome and Matsumoto (2002), Takahashi and Matsumoto (2009), Sharma et al. (2012)
	PWAS	Surface	Active/passive	Nuclear/non-nuclear	Cuc et al. (2007), Daw et al. (2014), Si and Baier (2015), Dziendzikowski et al. (2016), Ebrahimkhanlou et al. (2016), Haider et al. (2017), Park et al. (2017), Bhuiyan et al. (2018), Bhuiyan and Giurgiutiu (2018), Hong et al. (2018), Qiu et al. (2018), Reinhardt et al. (2018)
Optical fiber	FBG	Surface/embedded	Active/passive	Nuclear/non-nuclear	Morana et al. (2016), Chen (2018), Calderoni et al. (2019)
Hybrid PZT/FBG		Surface/embedded	Active/passive	Non-nuclear	Qing et al. (2005), Wu et al. (2009), Wang et al. (2020a)
Visual vibrometry		Remote	Active	Non-nuclear	Wadhwa et al. (2013), Chen et al. (2017), Davis et al. (2017)
Electrical impedance		Surface	Active	Nuclear/non-nuclear	Lee et al. (2014), Shin et al. (2016), Fleming et al. (2019)

equipment. Various types of sensors are needed to monitor key health related parameters in nuclear SSCs. Examples of such parameters include vibration, electrical signatures (current/voltage) and position measures in active SSCs, localized change in material properties (mechanical, magnetic, optical, thermal, or electrical) in passive SSCs, as well as general measurands of process conditions (such as temperature, flow, pressure) that may be associated with equipment degradation.

Due to the harsh operating environments (such as radiation, high pressure, high temperature) encountered in some parts of the NPP systems, many of the existing sensors that are widely used in other industries for abovementioned measurands may not survive. This section surveys recent research efforts to improve sensor survivability and measurement sensitivity for nuclear instrumentation. Some of the emerging sensing techniques, including those in use for nuclear applications and those which are deemed useful in the near future for CM inside NPPs, are briefly described in the following six subsections and compared in **Table 1**.

Magnetic Anisotropy

Magnetic properties of ferromagnetic materials depend on the direction in which they are measured. This phenomenon is known as *magnetic anisotropy* (Stefanita, 2008). *Magnetic Barkhausen noise* (MBN)—the electromagnetic waves emitted during a ferromagnetic material's magnetization process—allows one to characterize magnetic anisotropy without regard to its origin (Spasojevic et al., 1996). Several studies have utilized MBN to continuously or periodically monitor material structure degradation, such as in structural steels of nuclear reactors (McCloy et al., 2013). Another effect produced by the movement of magnetic domain walls is the *magneto acoustic emission* (MAE). Acoustic signals are generated by the sudden and discontinuous changes in magnetization, which involve localized deformations (Stefanita, 2008). Simply put, the magnetic signal from a sensing coil corresponds to MBN (Deng et al., 2018), whereas the acoustic signal from a piezoelectric (PZT) sensor corresponds to MAE (Makowska et al., 2017). Li et al. (2015) investigated magnetic anisotropy of α-iron containing nonmagnetic particles for checking integrity of a nuclear RPV and suggested the possibility of using magnetic technologies for nondestructive evaluation of RPV embrittlement.

Piezoelectricity

Progress in sensor technology development has enabled the use of *PZT transducers*, which can be mounted on the surface or embedded inside host structural materials. Once they are integrated with the host structure, PZT elements are utilized as sensors to deliver signals in real-time. Simultaneously, they can also serve as actuators to generate diagnostic stress waves into the structure to detect, localize, and quantify damage in the materials. Various studies have proposed techniques using *piezoelectric thin films* attached to a material surface (Komagome and Matsumoto, 2002; Takahashi and Matsumoto, 2009; Sharma et al., 2012). By measuring the electric potential distribution on the piezoelectric film, the location, the aperture shape, and the defect's depth can be estimated. The *piezoelectric wafer active sensor* (PWAS), another type of PZT sensor, has emerged as one of the major sensing techniques. PWASs were developed as convenient enablers for generating and receiving Lamb waves—a type of ultrasonic guided waves propagating between two parallel surfaces without much energy loss—for structural health monitoring in space applications (Cuc et al., 2007). Radiation influence on their sensing capability and survivability has been investigated to determine the reliability of PWAS-based methods for PHM in extreme nuclear environments (Haider et al., 2017). Additionally, research of PZT sensors using Lamb waves has been ongoing, and their capabilities for impact localization (Si and Baier, 2015; Park et al., 2017; Qiu et al., 2018), acoustic emission detection (Bhuiyan et al., 2018; Bhuiyan and Giurgiutiu, 2018), and damage detection in isotropic and composite plates

(Dziendzikowski et al., 2016; Ebrahimkhanlou et al., 2016; Hong et al., 2018) have been explored. In-pile instrumentation development activities using PZT sensors have also been conducted recently—such as under several DOE Nuclear Energy programs investigating the use of new fuels and materials for advanced and existing reactors—to address crosscutting needs for irradiation testing by providing higher-fidelity, real-time data with increased accuracy and resolution from smaller, compact sensors that are less intrusive (Daw et al., 2014; Reinhardt et al., 2018).

Optical Fiber

Measurement techniques based on *optical fibers* have demonstrated the capability to provide multi-sensing (measuring different operational parameters within a single sensor configuration, such as temperature, pressure, and strain) and multiplexing (communicating data collected at multiple locations through the single line) instrumentation. They are intrinsically immune to electromagnetic interference, electrically passive, and widely available at a reasonable cost. Beyond the use as a light guide, several optical sensors and related measurement techniques have been considered for nuclear applications. *Fiber Bragg grating* (FBG) sensors have been the focus of many research efforts due to their demonstrated potential for high-temperature operation in a radioactive environment and their multiplexing capability. An FBG is achieved by creating a periodic modulation of the refractive index of the fiber core, which generates a distributed reflector characterized by its period and modulation depth. Several recent studies (Morana et al., 2016; Chen, 2018; Calderoni et al., 2019) have shown the effectiveness of certain radiation-resistant FBG sensor types—such as femtosecond-etched FBGs and germanosilicate singlemode FBGs—in monitoring diverse physical parameters for in-reactor instrumentation.

Piezoelectric-Fiber Hybrid Sensor System

A hybrid PZT/FBG system offers the best decoupling of actuator and sensor signals because the two devices apply different mechanisms for signal transmission. The PZT transducers rely on electrical channels to actuate or detect dynamic responses, whereas the FBG sensors rely on optical means to measure quasi-static or relatively low frequency responses (Wu et al., 2009). In other words, such a hybrid system uses piezoelectric actuators to input a controlled excitation to the structure and uses fiber optic sensors to capture the corresponding structural response (Qing et al., 2005). More generally, the accuracy and stability of SSC health monitoring can be potentially improved by constructing a hybrid sensor network and integrating multi-source sensor information (Wang et al., 2020a). Such hybrid sensor systems have not seen applications in NPPs but should not face hurdles given the respective success of PZT and FBG sensors.

Visual Vibrometry

Visual testing has played a prominent role in inspecting civil infrastructures. Recently, researchers have been able to use computer vision techniques to analyze small motions in videos. Those techniques amplify imperceptibly small motions in specified frequency bands, effectively producing a visualization of an object's operational deflection shapes (Wadhwa et al., 2013). Video cameras provide the benefit of long-range measurements and enable the collection of a large amount of data at once since each pixel can be considered as a sensor. Objects tend to vibrate in a set of preferred modes, and the shapes and frequencies of the modes depend on the structure and material properties of an object. Focusing on the case where geometry is known or fixed, information about an object's vibration modes can be extracted from video and used to make inferences about that object's material properties (Davis et al., 2017). A camera-based vibration measurement methodology was also recently demonstrated for civil infrastructure by measuring an antenna tower's ambient vibration response (Chen et al., 2017). Future research is needed to investigate the application of visual vibrometry inside NPPs with radiation exposure, such as for nuclear containment systems.

Electrical Impedance

Electrical impedance–based sensing is a relatively mature measurement field with broad nuclear applications, including passive structure, standby component, and in-pile monitoring. Lee et al. (2014) proposed laser-based mechanical impedance (LMI) measurement, utilizing a fiber-guided laser ultrasound system to generate and measure LMI response for damage detection in NPP pipes. Shin et al. (2016) suggested an online monitoring technique for standstill motors based on an impedance analysis method. More recently, Fleming et al. (2019) developed an impedance-based diameter gauge consisting of an electrically conductive concentric ring around fuel cladding, such that the electrical impedance between the ring and cladding could be measured.

Condition Monitoring and Fault Detection

Condition monitoring describes a suite of activities for providing state estimation and early warning of anomalous behavior. It is a crucial step of the PHM framework, and the effectiveness of PHM largely depends on the accuracy of the CM process (Ayo-Imoru and Cilliers, 2018). The process of fault detection attempts to recognize incipient faults and failures[6] from CM data and quantification of the inconsistencies between the actual and the expected behavior of the monitored SSC in nominal conditions (Atamuradov et al., 2017).

The instrumentation and control (I&C) systems in NPPs receive large amounts of sensory data from various components to enable and support safe and reliable power generation by controlling the system variables. However, most raw data collected by sensors are not ready to be used directly, and appropriate data manipulation is required. The multidimensionality of high-volume data and redundancy

[6]As defined in Isermann and Ballé (1997), a *fault* is "an unpermitted deviation of at least one characteristic property or parameter of the SSC from the acceptable/usual/standard operating conditions;" in contrast, a failure is "a permanent interruption of the SSC's ability to perform a required function under specified conditions."

among data attributes are examples of challenges faced by CM and fault detection. Therefore, the feature selection process—including choosing high-quality attributes, removing collinear features, and selecting an optimal subset from the original data set—is usually needed (Chandrashekar and Sahin, 2014). The objective of feature selection is to find a subset of variables from the full array of raw sensor data that can efficiently describe the input data stream while reducing effects from error/noise or irrelevant information (Guyon and Elisseeff, 2003).

Feature Selection Methods

Feature selection methods can be divided into three categories: filters, wrappers, and embedded methods. *Filter methods* pick up the intrinsic properties of the features measured by univariate statistics. In general, filter methods use variable ranking techniques as the principal criteria for variable selection. A suitable ranking criterion is used to score the input variables, and thresholds are applied to filter out the less relevant features. Several studies (John et al., 1994; Blum and Langley, 1997; Kohavi and John, 1997) have presented various definitions and measurements for the relevance of a variable. The widely used metrics such as mutual information, Fisher score, relief, separability, and correlation are all under the umbrella of the filter methods. The primary advantage of filter methods is their speed and ability to scale to large data sets. They are computationally light and are not prone to overfitting (Lazar et al., 2012). They also do not rely on the learning algorithm. One of the drawbacks of filter methods is that the selected subset might not be optimal because a redundant subset might be obtained. Besides, essential features that are less informative on their own but are informative when combined with other features could be discarded in error (Xu et al., 2010). Bommert et al. (2020) recently published a comprehensive survey analyzing 22 filter methods concerning runtime and accuracy in high-dimensional classification data.

Wrapper methods use the predictor as a black box and the predictor performance as the objective function to evaluate the variable subset. They search through the space of feature subsets using a learning algorithm and calculate the estimated accuracy of the learning algorithm for each feature that can be added to or removed from the feature subset. Also, they depend on a classification algorithm used to evaluate the candidate solutions (i.e., subsets of features) generated by a search algorithm and thus are more computationally expensive. Wrapper methods often provide more accurate results than filter methods (Pudil and Somol, 2008), although one needs to take extra care to prevent overfitting and wrappers usually scale poorly to large data sets (Das, 2001). The selection process is based on a specific learning algorithm trying to fit on a given data set. In general, it follows a greedy search approach by evaluating all the possible combinations of features against the evaluation criterion. For instance, the branch and bound algorithm (Narendra and Fukunaga, 1977), genetic algorithm (Goldberg, 1989), particle swarm optimization (Kennedy and Eberhart, 1995), adaptive floating search (Somol et al., 1999), recursive feature elimination (Guyon et al., 2002), and similarity measure (Chen and Chen, 2015) are all under the category of the wrapper methods.

Embedded methods complete the feature selection process within the construction of the ML algorithm itself. This method category combines the qualities of both filters and wrappers. The search for an optimal subset of features is embedded into the classifier construction and can be seen as a search in the combined space of feature subsets and hypotheses. The embedded methods use an independent measure to decide the best subsets for a given cardinality and use the learning algorithm to select the optimal subset among the best subsets across different cardinalities. Therefore, they are specific to a given learning algorithm and have the advantage of taking into consideration the interaction of features with the classification model (like wrapper methods) while being far less computationally intensive (like filter methods) (Saeys et al., 2007). Regularization and tree-based models are some common methods that use embedded feature selection. The weights of a classifier can also be used to rank the features for their removal, and the features can be selected by conducting sensitivity analysis on the corresponding weights. Several methods (Archibald and Fann, 2007; Mundra and Rajapakse, 2010; Zhang et al., 2015a) used support vector machines (SVMs)[7] as classifiers, optimizing the SVM equation and assigning weights to each feature. In some other studies (Setiono and Liu, 1997; Verikas and Bacauskiene, 2002; Romero and Sopena, 2008; Yang and Ong, 2011), an artificial neural network (ANN) was applied for the same purpose.

As examples in the nuclear field, Deleplace et al. (2020) recently used a separability-based feature selection metric (i.e., filter method) to enhance accuracy of fault detection in NPP water screen cleaners; Peng et al. (2018a) applied correlation analysis (i.e., filter method) for dimensionality reduction of NPP transient data simulated from their personal computer transient analyzer; Zio et al. (2006) selected features for early transient detection by means of genetic algorithms (i.e., wrapper method); Moshkbar-Bakhshayesh (2021) investigated six different feature selection techniques for parameter estimation in an NPP, among which the ANN with Bayesian regularization (i.e., embedded method) gave the most accurate results.

Anomaly Detection Methods

One can attempt to derive first principles–based analytical models to describe the expected nominal or faulty SSC behavior if its underlying physical mechanisms/relationships are well understood. In an engineering system, *physics-based* models are attractive for three reasons: first, they consider mechanical, material, and operational characteristics explicitly; second, they can be developed and evaluated even before the system has been built and operated; and third, they can be used to understand behavior over a broad range of operational and material conditions (Coble et al., 2012). Unfortunately, it is challenging, time-consuming, and often impossible to model a complex, nonlinear system with first principles and mathematical functions alone (Mirnaghi and Haghighat, 2020). Furthermore,

[7]SVMs have become the reference for many classification problems because of their flexibility, computational efficiency, and capacity to handle high-dimensional data.

the physical foundation in such models is inevitably diluted by the use of simplifying (sometimes unjustified) assumptions to make up for runtime performance or incomplete domain knowledge (Coble et al., 2012; Zhao et al., 2020a). In contrast, *data-driven* approaches have shown the potential to characterize system operations and develop system models due to their independence in modeling and sole reliance on system data (Yang and Rizzoni, 2016).

With the development of sensor technologies—which enable routine collection of online data for numerous system variables—various anomaly detection approaches based on multivariate statistics have gained attention. *Principal component analysis* (PCA) and *partial least squares* (PLS) are two basic multivariate statistical techniques (Severson et al., 2016), and many applications based on those techniques have been considered for detecting faults (Harrou et al., 2013; Liu et al., 2013; Rato and Reis, 2013; Mnassri et al., 2015; Jia and Zhang, 2016; Li et al., 2016; Jiao et al., 2017; Jiang and Yan, 2018). Once the detection method is selected, a metric for identifying faults is needed. In PCA- and PLS-based methods, Hotelling's t-squared statistic (Hotelling, 1933)—a generalization of Student's t-statistic in multivariate hypothesis testing—is widely used to detect anomalies with specific thresholds. The sum of squared prediction error (Box, 1954), also known as the Q statistic, is another metric that denotes the change of the events that are not explained by the model of principal components (Mujica et al., 2011). In the nuclear field, Li et al. (2019a) recently applied an improved PCA method using data pre-processing and false alarm reducing techniques for NPP sensor fault detection, which reduced the false alarms of both t-squared and Q statistics.

Traditional multivariate statistical-based methods have inherent limitations. Calculating monitoring statistics and thresholds of the PCA- or PLS-based methods is made under the assumptions that data from sensors are Gaussian-distributed and linearly correlated and that the process is operated under a single stationary condition (Ge et al., 2013). In practice, most of these assumptions may be violated. Various research efforts using data-driven methods have been developed to relax assumptions in the traditional statistical-based methods. *Independent component analysis* (ICA), finding both statistically independent and non-Gaussian components, is a reliable alternative for fault detection (Li and Wang, 2002). Stefatos and Ben Hamza (2010) further introduced the dynamic ICA technique, extending the advantages behind ICA to detect faults in a time-correlated environment. Cai and Tian (2014) developed a non-Gaussian process based on robust ICA to alleviate the effect of outliers. Ajami and Daneshvar (2012) showed the validity and effectiveness of ICA for fault detection of a typical turbine system, which are found in an NPP.

The *Gaussian mixture model* (GMM) is another commonly used technique for non-Gaussian data processing. Yu (2012) proposed a nonlinear kernel GMM-based inferential monitoring approach for fault detection, which projected data from a raw measurement space into a high-dimensional kernel space so that the GMM could be estimated in the feature space satisfying multivariate Gaussianity. Karami and Wang (2018) proposed an adaptive GMM for automatic fault detection in nonlinear systems. Ma et al. (2019) presented a nuclear application by using a GMM-based early fault detection method on 30 sets of real data from reciprocating compressors containing three fault types.

More recently, *SVM variants*—which do not require the data to be Gaussian—have emerged. Liu and Zio (2018) developed a k-nearest neighbors–based fuzzy SVM to reduce the computational burden and tackle the issue of data imbalance and outliers. Several applications exist for fault detection in NPP assets using SVM-based models (Jamil et al., 2018; Lin and Wu, 2019; Meng et al., 2020).

Fault Diagnostics

Within the overarching area of PHM, fault diagnostics begins after a fault has been detected during the CM process. Diagnostics is further divided into *fault isolation*, which seeks to identify the piece of equipment or component from which the fault originates, and *fault identification*, which determines the cause of the fault. Logically, these two subtasks of fault diagnostics are often performed as a single analysis. The analysis is based upon fault symptoms, which primarily take the form of available features or signatures of the fault, obtained in the form of sensed data and measurements. A common classification scheme for diagnostics problems is by modeling method, in which the problem is approached using either a *model-based* or a *data-driven* method. This is not a completely clear distinction, though, as some overlap can exist between the two approaches, and various hybrid approaches can be developed. One specific area of overlap is in the use of *rule-based expert systems* for fault diagnosis. These expert systems rely on "if-then" rules to diagnose a system's state given its fault symptoms. It will be seen that the development of "if-then" rules can be done by either model-based or data-driven methods.

This review places emphasis on developments in data-driven methods for PHM. However, a brief review of advances in model-based methods is still deemed beneficial to the reader interested in fault diagnostics or PHM in general. As such, the following subsections will survey model-based methods first; then rule-based expert systems, namely those which rely on fuzzy rule bases; and finally, data-driven methods. Additionally, the interested reader can refer to Li et al. (2020) for a second review of diagnostic methods.

Model-Based Methods

According to Yang (2004), who presented a review of both model-based and data-driven methods, common model-based methods include the use of observers or statistical filters, checks of the parity between plant models and sensor outputs, generation of residuals in the frequency domain, use of causal graphical models (such as signed directed graphs and fault trees), and approaches based on qualitative physics (such as qualitative simulation and qualitative process theory). A common classification scheme for these methods is that filtering, parity, and frequency approaches are grouped as quantitative methods, and that graphical models and qualitative physics are considered qualitative methods.

In the area of filtering-based methods, Gautam et al. (2019) used an extended Kalman filter for fault identification and performed fault isolation for single and simultaneous multiple-sensor faults in an NPP with a recursive least squares estimate. An advancement to the parity space method was performed by Cho and Jiang (2018) for nuclear applications, in which Fisher discriminant analysis (FDA) was used to address the issue where the number of fault classes exceeds the total independent residual signatures. Lee and Shin (2018) proposed a method using time-frequency domain reflectometry and k-means clustering to determine the fault location and faulty line in a multi-core I&C cable system to assure the safety and reliability of NPP operation. Advances in qualitative causal graphs for NPP asset fault diagnosis include those on signed directed graphs (Liu et al., 2016) and dynamic uncertain causality graphs (Zhao et al., 2017a).

Rule-Based Methods

Rule-based methods operate by firing specific "if-then" rules to determine the consequence associated with a measured/detected fault symptom. Rule bases have traditionally been developed using expert judgment and prior knowledge about the system. Although a system based on engineering knowledge may be attractive, issues in classical rule-based systems can include rule bases growing to unmanageable size to describe an increasing number of scenarios and the potential for a rule-based system to fail when it encounters a situation for which there is currently no rule (Coble et al., 2012). Another large difficulty encountered by the standard rule-based method is how to operate when there is not complete certainty as to which rule should be activated given the measured symptoms. This situation typically arises when the symptom cannot be simply classified into a single qualitative category, such as "low" or "high." The most common means of handling this uncertainty is by using a *fuzzy rule–based system*. Similar methods have also received some attention, such as the use of confidence degrees (Deng et al., 2017) or the development of a belief rule-based expert system (Xu et al., 2017). However, fuzzy rule–based fault diagnostic tools are still the most prominently used method in the literature to deal with uncertainty.

Fuzzy rule bases, and the fuzzy logic in general on which they operate, act as a nonlinear mapping between inputs and outputs by means of determining the degree of membership to which "crisp" inputs belong to "fuzzy" qualitative states and using the fuzzy states to determine the consequence of the given inputs. Fuzzy rule bases have found application for fault diagnosis in various disciplines and numerous components—many of which are found in NPPs—including induction motors (Shetgaonkar, 2017), other standard rotating machinery (Da Silva et al., 2017), spur gears (Krishnakumari et al., 2017), bearings (Berredjem and Benidir, 2018), power transformers (Husain, 2018), diesel generators (Nain and Varde, 2013), distributed sensor networks (Bhajantri, 2018), and high-power lithium-ion batteries (Wu et al., 2017).

Despite their advantages over traditional rule-based fault diagnosis, fuzzy rule–based systems are the subject of ongoing research to improve their performance. Work by Yan et al. (2019) and Rodríguez Ramos et al. (2019) both addressed identifying multiple faults using fuzzy rule–based systems. Du et al. (2020) proposed a self-organizing fuzzy logic classifier based on the harmonic mean difference for application in bearing fault diagnosis. That approach in particular is an example of a rule-based method also potentially being classed as a data-driven method because measured fault features were used to train a fuzzy classifier. As a means of further characterizing the uncertainty present in signals and measurements, Wang et al. (2019a) introduced an interval-valued fuzzy spiking neural P system,[8] also demonstrated on an example case with the presence of multiple faults.

Data-Driven Methods

Data-driven methods generally rely on a large amount of process data, typically historical, to develop models and reasoning methods (Yang, 2004). Methods traditionally classed as data-driven methods comprise ANNs–discriminative methods (for traditional neural networks), models based on Bayesian statistics or utilizing Bayesian networks (BNs)—generative methods, SVMs–discriminative, and PCA–generative (if unsupervised) or discriminative (supervised). Often, combinations of these methods are used. In addition, many more methods considered as data-driven exist, which have seen less applications in the nuclear field than those presented in this section.

The *ANNs* constitute a large subject area in data-driven methods for fault diagnostics, and research of ANNs is an extensive field unto itself due to the vast number of techniques and types of neural networks in use. Lin et al. (2021) developed a nearly autonomous management and control (NAMAC) system for advanced reactors and proposed to apply a feed-forward neural network (FFNN) model for NAMAC's diagnostic digital twin (DT) layer; Gomes and Canedo Medeiros (2015) used a network of Gaussian radial basis functions (RBFs) to identify accidents in an NPP; Banerjee et al. (2020) demonstrated use of an ANN to identify nuclear reactor sensor and actuator faults in the presence of a proportional–integral–derivative controller; Ayo-Imoru and Cilliers (2018) implemented an ANN while using a plant simulator as a dynamic reference. A common theme in the literature sees ANNs working in tandem with some other technique to transform sensory data into a form usable by the ANN. As examples, Messai et al. (2015) and Tagaris et al. (2019) both used data from wavelet transformations; Lee et al. (2021) transformed the number of plant state variables into a 2D image and used a convolutional neural network (CNN) to process the image as a means of diagnosing abnormal states; Saeed et al. (2020) implemented a long short-term memory (LSTM) network and CNN after performing PCA; and Ayodeji et al. (2018) tested the effectiveness of an RBF network and an Elman neural network (ENN) after using PCA to perform noise filtering for NPP fault diagnosis.

[8]Spiking neural P systems are one of the recently developed spiking neural network (SNN) models inspired by the way neurons communicate (Wang et al., 2016). Known as the third generation of neural networks, SNNs use time to encode information and employ the concept of individual spikes. Those features make SNNs biologically more realistic (Fan et al., 2020).

Another common trend, both in the literature surrounding ANNs for diagnostics and AI as a whole, is the increased interest in utilizing DL methods. In application to NPP fault diagnostics, DL architectures have been applied by Ahmed et al. (2017), Mandal et al. (2017), Peng et al. (2018a), and Kim et al. (2019). Outside of the nuclear industry, Yu et al. (2018) applied DL for fault diagnosis in wind turbines, and Ren et al. (2019) developed a DL diagnoser in autonomous vehicles.

In the current state of the industry, the application of *BNs* to diagnostics is sparser than those of ANNs. Unlike black-box data-driven methods such as ANNs, the BN approach offers transparent model interpretability, reasoning under uncertainty, and graphical representation capability to emulate the target SSC's physical behavior (Zhao and Golay, 2020). However, constructing the BN knowledge base is a cumbersome and time-consuming process, and problems using BNs can become intractable for complex scenarios. Wu et al. (2018a) developed a BN framework for fault diagnosis in NPPs with multi-source sensor nodes, and Zhao et al. (2020b) proposed a method to diagnose operational and on-demand failures using dynamic BNs (DBNs). A large body of work on using BNs as fault diagnosers also exists outside the nuclear field. Cai et al. (2017) provided a detailed review of BNs for application in fault diagnosis. Wang et al. (2018) proposed an improved BN method by determining the network structure with a hybrid technique of process knowledge and data-driven correlation, which was validated with the Tennessee Eastman Process open-source benchmark (Downs and Vogel, 1993). Areas where BNs have seen application, in addition to those discussed in Cai et al. (2017), include the general case of industrial processes (Yu and Zhao, 2019), hydroelectric generation systems (Xu et al., 2019), and ground-source heat pumps (Cai et al., 2014). Lastly, as a method used in combination with ANNs, Bayesian statistics was used in Tolo et al. (2019) as a means of connecting a set of neural network architectures for early accident detection in NPPs.

Research efforts directed toward *SVMs* have been primarily focused on improving the optimization of SVM parameters and then applying the SVM to the problem of fault diagnostics. In the nuclear field, Wang et al. (2019b) developed an improved particle swarm optimization, and Zhang et al. (2015b) used a hybrid of the bare bones particle swarm optimization and differential evolution. Beyond simply developing a better means of parameter optimization, Wang et al. (2021) introduced a hybrid least squares SVM method for fault diagnosis in NPPs. Another approach beyond optimization was to separately train an ensemble of SVMs and combine them after training (Ayodeji and Liu, 2018).

Developments involving *PCA* are mostly fault diagnosers that utilize PCA combined with another tool, as was observed during the discussion of ANNs. An example of using PCA for fault diagnosis without combination with another major method is that of Li et al. (2018a), which presented an optimized PCA method for fault identification and reconstruction of NPP sensors. An approach fundamental to PCA, however, was the development of statistical methods to reduce the number of false alarms raised by PCA (Li et al., 2018b). Approaches having seen fusion with PCA for fault diagnosis in NPPs include FDA (Jamil et al., 2016), conditional Gaussian networks (Atoui et al., 2015), multilevel flow modeling (Peng et al., 2018b), ENNs (Liu et al., 2017), and SVMs (Xin et al., 2019). Additionally, Wang et al. (2017) used a semiparametric PCA in combination with a BN.

Prognostics

Prognostics is one of the major tasks in PHM as its results are directly used to support proactive decision-making for maintenance practices. The prognostics module is typically defined as the process of predicting the remaining time before the equipment can no longer perform a particular function (i.e., RUL) (Atamuradov et al., 2017). Prognostic calculations cannot be done in isolation and depend largely on the stages of monitoring, detection, and diagnostics: the accuracy of these stages will all affect RUL estimation. It is desirable to develop generalizable prognostic methods that can accurately predict the future equipment state given a set of measurements correlated to the equipment's current state (Ramuhalli et al., 2020). An appropriate estimate of the equipment's RUL can improve overall plant performance and reduce costs by optimizing O&M activities. Therefore, prognostics is seen as one of the most beneficial aspects of PHM (Hess, 2002).

Paradoxically, prognostics is an underdeveloped element of PHM systems (Vogl et al., 2019), especially in the nuclear industry (Coble et al., 2015; Ayo-Imoru and Cilliers, 2018). Unlike fault detection and diagnostics, the prognostic technology is just emerging and often is deemed immature due to lack of uncertainty calculations, method verification and validation, and risk assessment for PHM system development (Saxena et al., 2010). Although many approaches to prognostics have been proposed in the literature, the state of practice is mainly at the research level and much of the published work has been exploratory. There is no universally accepted methodology for all prognostic problems (Lee et al., 2011; Coble et al., 2012). A variety of models have been developed for application to specific situations or specific classes of components. As such, prognostic algorithms can be categorized according to different criteria. Based on the recent publications (Atamuradov et al., 2017; Lei et al., 2018; Taheri et al., 2019; Vogl et al., 2019; Baur et al., 2020; Bektas et al., 2020; Ramuhalli et al., 2020) that contain a comprehensive review of prognostics, these algorithms can be loosely divided into four categories according to their basic techniques or methodologies: *physics-based* methods, *knowledge-based* methods, *data-driven* methods, and *hybrid* methods.

Physics-Based Methods

Physics-based prognostic methods attempt to describe the evolving SSC degradation process based on a comprehensive mathematical model—usually in the form of a series of ordinary or partial differential equations—that represents the underlying physics of failure and encodes the first-principles input-output relationship. The derived mathematical model is combined with CM data to identify model parameters, which are then used to predict the future evolution of SSC health state. A commonly illustrated physics-based method example in the literature is a crack growth model for which Paris' law (also known as the Paris–Erdogan equation) (Paris and Erdogan, 1963) or the Forman equation (Forman, 1972) is used to relate the growth rate of a fatigue crack to the stress intensity factor and the number of fatigue cycles. Some other examples include prediction of bearing deterioration, turbine creep evolution, pipeline tube degradation, battery life, and gearbox failure (Qiu et al., 2002; Liao and Kottig, 2014; Hu et al., 2016).

When the failure mechanism is well known and correctly captured, a physics-based prognostic model should yield highly robust and accurate RUL prediction for a specific type of component and require less data for tuning (Baur et al., 2020). Unfortunately, the underlying physical processes leading to failure are often not completely understood or cannot be explicitly modeled. In this case, simplifying assumptions and estimations must be made to facilitate model development, raising skepticism about the model's applicability to real-world engineering systems (An et al., 2015; Coble et al., 2015). Due to their nature of being component-specific, physics-based methods can hardly be reconfigured to fit alternative domains, and most of them are only applicable at the component or subsystem level (Baur et al., 2020; Bektas et al., 2020). When applied to system-level prognostic problems or when multiple failure modes need to be represented (which is the case for a typical SSC in a nuclear facility), the model complexity and associated computational cost may become prohibitive for online analysis and decision-making. For these reasons, Coble et al. (2015) concluded that physics-based methods would be preferable for high-cost, high-risk equipment, such as electronic components in which failure data needed to develop empirical methods might not exist.

Knowledge-Based Methods

Knowledge-based (also known as experience-based or rule-based) prognostic methods are solely built upon expert knowledge. Such methods do not rely on a physical model of the system. Their implementation is relatively simple; however, they are applicable only in cases where expert knowledge exists to mimic human-like representation and reasoning with algorithm families that employ expert systems or fuzzy logics.

Analogous to rule-based diagnostic methods (see "Rule-Based Methods" Section), *expert systems* for prognostics aim to translate explicit knowledge from experts into human-coded "if-then" rules that closely resemble the way a domain specialist solves the same problem (Liao and Kottig, 2014). They do not perform well when a huge number of rules are needed and cannot handle new situations that are not explicitly coded. Compared with expert systems, *fuzzy logic–based* prognostic methods are more robust and can handle the uncertainty intrinsic to expert knowledge (Jardine et al., 2006). For complex systems and in the presence of high-volume data, fuzzy logics are typically used in conjunction with data-driven approaches—such as ANN to create a hybrid *neuro-fuzzy* (NF) model (Lei et al., 2018)—for systematized dimensionality reduction and membership function optimization. The stand-alone knowledge-based methods have been much less studied or recommended by recent publications than the other method categories (Atamuradov et al., 2017) due to their inherent limitations.

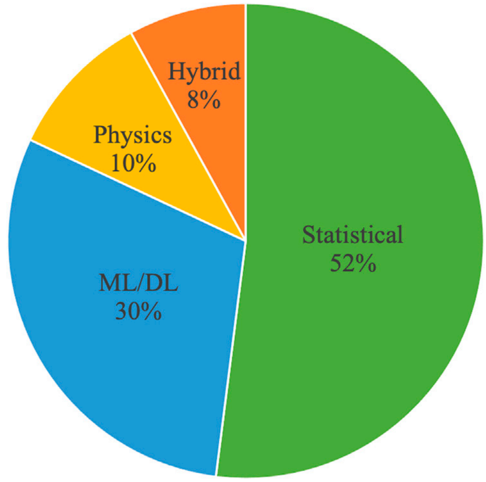

FIGURE 4 | Distribution of method categories in 274 recently published papers on machinery health prognostics [modified from Lei et al. (2018)].

The *similarity-based* prognostics is an alternative knowledge-based approach—such as the one proposed by Liu et al. (2019) for the RUL prediction of a gas turbine—that removes the requirements to model qualitative knowledge from domain experts. Although this approach is sometimes classified under data-driven methods, it actually follows the rule-based modeling philosophy of similarity evaluation between a monitored case and a library of previously known failures (Taheri et al., 2019; Bektas et al., 2020), which does not give enough insight into the current or future condition of the specific SSC in question.

Data-Driven Methods

Data-driven prognostic methods directly use CM data for the target SSC and do not incorporate first-principles information or expert knowledge. They rely on trends within the observed data to construct mathematical models to estimate future states of the monitored equipment. As will be further elaborated in this section, the mathematical approaches range from conventional statistical methods to advanced ML and DL techniques. In data-driven methods, no mechanism or input-output relationship needs to be known a priori to produce acceptable results, and the method development/implementation cost is relatively low (Diez-Olivan et al., 2019). Therefore, these methods are highly flexible and can be deployed at any level (component, subsystem, or system level) of the physical asset, which is of particular interest to large, complex systems (Ramuhalli et al., 2020; Sun et al., 2010). As shown in **Figure 4**, *statistical-based* and *ML/DL-based* data-driven methods have attracted most of the research attention in machinery prognostics. However, prognostic models that use a data-driven approach usually require large amounts of data covering a broad range of conditions, including run-to-failure data for degradation models. Availability of run-to-failure data for a particular SSC can be a key challenge (Sutharssan et al., 2015), which is the case of safety-critical systems in NPPs (Coble et al., 2015). The performance and confidence level of RUL predictions are bound to the quantity and quality of available data that are used to infer model parameters and to determine failure thresholds. Furthermore, data-driven methods cannot extrapolate beyond the domain spanned by the training data (Ramuhalli et al., 2020).

Statistical-Based Prognostics

Statistical-based prognostic methods, also known as empirical prognostic methods, are a grey-box approach that treats asset degradation as a stochastic process subject to different sources of variability and uncertainty (Baur et al., 2020). In statistical methods, RUL is a random variable whose probability density function is determined based on empirical data. Distinguished by its data-driven nature and ability to incorporate the uncertainty of the degradation process, this method category has been heavily focused upon in the literature, as illustrated in **Figure 4** for the field of machinery prognostics. Multiple review papers (Si et al., 2011; Ye and Xie, 2015; Lei et al., 2018; Taheri et al., 2019; Baur et al., 2020; Bektas et al., 2020) have surveyed statistical-based models systematically and have included their advancements in recent years. To unify apparently confusing terminologies used by different authors while minimizing repetition, a summary is provided in this section.

Statistical-based prognostics can be generally classified into two subcategories. Models in the first subcategory are based upon time-series CM data that *directly* describe the underlying degradation process of the monitored SSC. Both regression- and Markovian-based models fall into this subcategory. In *regression-based* models, forecasting of time-series data is achieved by using auto-regressive moving average processes, which assume that the future state of the target SSC is linearly dependent of both past observations and normally distributed random noise. These models are easy to implement with low computational cost, but their performance is heavily affected by the trend information of historical observations, which may be unreliable during incipient failure stage and for long-term forecasts (Baur et al., 2020). Recent examples of using regression-based prognostic models include Qian et al. (2014) for bearing wear-out, Barraza-Barraza et al. (2017) for crack growth in aluminum plates, Nguyen et al. (2018) for NPP steam generator degradation, and Mei et al. (2020) for shear building structural damage. In *Markovian-based* models, the degradation process is assumed to transform within a finite state space that satisfies the Markov (or memoryless) property. With a well-established theoretical basis to support these models, the Markovian approach was first introduced into the field of prognostics by Kharoufeh (2003). It was later refined by Kharoufeh and Cox (2005) and Kharoufeh et al. (2010). This version of Markovian models was not widely adopted by the PHM community because all the health states would need to be observed directly. Moreover, the memoryless assumption may not be valid for some real degradation processes, and a large volume of data or empirical knowledge is typically required for constructing the state transition probability matrix.

Models in the second subcategory rely on partially observed state processes and *indirect* CM data (i.e., data that can only indirectly indicate the underlying health state of the monitored SSC, such as vibration data). *Stochastic filtering-based* methods, which are based on the Bayes' theorem, fall into this subcategory. Built upon DBNs, *Kalman filter* and *particle filter* are two of the most common types of filtering algorithms. The basic Kalman filter algorithm is designed for linear Gaussian problems, and some of its enhanced versions have been proposed; the particle filter algorithm is a sequential Monte Carlo method and is a better choice in nonlinear, non-Gaussian systems. Due to their ability to characterize the future uncertainty of degradation processes by updating the probabilistic state estimation from online measurements, both filtering methods have seen many applications in machinery RUL prediction (Lei et al., 2018) and were introduced by Ramuhalli et al. (2010) for prognostics of NPP components. Similar to, yet simpler than the filtering-based models, *hidden Markov models* (Ghahramani, 2001) are extensions of the standard Markovian approach to incorporate unobservable health states. The hidden Markov models and their variants [e.g., hidden semi-Markov models (Yu, 2010)] have been applied to the PHM framework since the beginning of this century (Baur et al., 2020). However, their capabilities are still limited by the memoryless assumption.

Machine Learning–Based Prognostics

ML-based prognostic methods attempt to learn degradation patterns and predict RUL directly from available observations (or extracted features) using ML or DL techniques. Numerous opportunities have arisen from the continuously fast-growing trends of AI and ML to effectively address the problems of prognostics, especially those in complex multidimensional, nonlinear systems with large amounts of training data representative of true data range and variability. No prior physical understanding of the analyzed SSC is required in ML-based methods. However, as a black-box approach, the results are hard to interpret due to their lack of transparency. The ML-based methods generally provide point estimates of RUL instead of a probabilistic treatment unless additional uncertainty quantification—usually with Bayesian inference methods—is performed. A more fundamental comparison of statistical- and ML-based methods can be found in Bzdok et al. (2018). A variety of ML algorithms have been used for prognostics, which can be loosely grouped into variants of ANN, Gaussian process regression (GPR), and SVM.

The *ANNs* are the most common modeling techniques in data-driven methods for prognostics (Bektas et al., 2020), just like for fault diagnostics (see "Data-Driven Methods" Section). Comprehensive surveys of ANN architectures—in the context of DL—and their recent applications in machinery prognostics have been presented by Rezaeianjouybari and Shang (2020), Khan and Yairi (2018), and Wang et al. (2020b). Among the multiple types of ANNs in use, *FFNNs* and *recurrent neural networks* (RNNs) are the most popular. The FFNNs are the simplest form of ANN and have been mainly used to learn the relationship between the health index[9] and RUL (Lei et al., 2018). Lin et al. (2021) recently implemented FFNNs into the prognostic DT of their NAMAC system for advanced reactors. The RNNs, descendants of FFNN, are distinguished by their ability to handle time-series data explicitly. Standard RNNs suffer from vanishing and exploding gradients when learning long-term temporal dependencies; the gated recurrent unit (GRU) and LSTM networks are RNN variants to remedy that problem. Generally, GRUs are computationally less expensive and better suited for smaller data sets, whereas LSTMs work better with large data sets (Rezaeianjouybari and Shang, 2020). A limited number of studies in the literature have applied GRU for prognostic tasks, such as Zhao et al. (2018) for milling machine cutter tool wear prediction, Li et al. (2019b) for rolling bearing RUL, and Chen et al. (2019) for a nonlinear degradation process using the US National Aeronautics and Space Administration's commercial modular aero-propulsion system simulation (C-MAPSS) turbofan engine data. LSTM-based networks have gained greater attention in applications of RUL prediction. Some recent studies include Ramuhalli et al. (2020) using NPP asset data from the feedwater and condensate system (FWCS) of a boiling water reactor (BWR); Zhao et al. (2017b) using a convolutional bidirectional LSTM and raw sensory data from high-speed milling machine cutters for a real-life tool wear test; Zhang et al. (2018), Wu et al. (2018b), and Elsheikh et al. (2019) using different variants of LSTM on the C-MAPSS data set; Shi and Chehade (2021) using a novel dual-LSTM framework for both change point detection and RUL prediction on the same C-MAPSS data; and Bampoula et al. (2021) using LSTM autoencoders to estimate RUL in a cyber-physical production system. Besides the above two commonly used ANNs, several other variants—such as wavelet neural network (Javed et al., 2014), CNN variants (Wang et al., 2019c; Zhu et al., 2019), generative adversarial network (Khan et al., 2018), and reinforcement learning (Kozjek et al., 2020)—can be found in the literature of prognostics.

The *GPR* models build upon Gaussian processes—cumulative damage processes of random variables with joint multivariate Gaussian distributions—to predict future health states. In contrast to ANNs, this approach is adaptable to both small- and large-size data sets, although it often suffers from high complexity in terms of computation and storage (Rasmussen, 2004). As elaborated in the modules of fault detection ("Condition Monitoring and Fault Detection" Section) and diagnostics ("Data-Driven Methods" Section), *SVMs* are well-established supervised learning tools based on the core concept of support vectors. Different SVM variants have been applied to the machinery RUL prediction (Lei et al., 2018). In the nuclear domain, Liu et al. (2015) proposed a dynamic-weighted probabilistic SVM model to evaluate fault scenarios in the reactor coolant pump of a typical pressurized water reactor, and Ramuhalli et al. (2020) applied SVM with both a linear kernel and an optimized Gaussian kernel on a BWR FWCS data source. Compared with ANNs, SVM-based models usually perform better on small data sets and can guarantee a unique solution (i.e., global minimum) to a given problem. However, their performance is strongly correlated with the selected kernel functions.

[9]The health index, computed from diagnostics, is an indicator of the ability of the monitored SSC to meet its functional goals.

Hybrid Methods

The physics-based, knowledge-based, and data-driven prognostic methods each have their own strengths and limitations. While appropriate method selection depends on knowledge of the system behavior and available data, a hybrid or fusion approach attempts to integrate the advantages of different method types for improved RUL prediction results. Additionally, in the real world, no single method is deemed adequate to account for all the possible faults and failure modes of an analyzed system (Baur et al., 2020; Venkatasubramanian, 2005). As shown in **Figure 4**, this area of research is still at its early development stage. The hybrid methods can consist of any combination of the previously described approaches. Of special interest is the ensemble of physics- and ML/DL-based techniques where both physics-of-failure knowledge and experimental data can be properly leveraged (Dourado and Viana, 2020). In this way, the combined approach fosters a physical interpretation of the input-output relationship instead of a black-box treatment while not requiring as accurate physical understanding or large-size data as stand-alone counterparts would do (Zhao et al., 2020a). Another popular direction is to develop hybrid prognostic tools under the Bayesian framework (e.g., Kalman filter and particle filter) because of their robustness and ability to reason under uncertainty. This direction has been the subject of several research studies and has been applied to various applications like rotating machinery, batteries, and electrolytic capacitors (Taheri et al., 2019).

Some hybrid models use one method to predict health state and another one to estimate RUL, while other models attempt to apply both method types to RUL forecasting (Ramuhalli et al., 2020). The selection of the actual model and method is usually driven by the problem and specific to the application. As an example in nuclear systems, Gurgen et al. (2020) recently proposed a physics-guided RNN (with LSTM blocks) prognostic model within the NAMAC system to predict the evolution of fuel centerline temperature in loss of flow transient conditions and demonstrated its superior performance over pure data-driven prognosis. In other fields, research related to the hybrid approach has been much more active (Liao and Kottig, 2014; Atamuradov et al., 2017). Goebel et al. (2006) combined a physics-based model of fault initiation and an empirical model of condition-based fault propagation rate to estimate RUL of avionic roller bearings. Liu et al. (2012) developed a hybrid method to improve the accuracy and transparency of long-horizon lithium-ion battery health state forecasting by leveraging particle filter and ANN predictors (FFNN, NF and recurrent NF). Eker et al. (2019) presented a unified approach integrating the short-term prediction of a physics-based model with the longer-term projection of a data-driven model and validated with run-to-failure observations for crack growth and filter clogging. Yucesan and Viana (2020) proposed a physics-informed neural network model that merged physics- and data-driven layers within a deep neural network to predict main bearing failure in wind turbines.

Decision-Making

Once the current and postulated future health states of a monitored SSC are determined based on CM data and diagnostic/prognostic modeling, it is of crucial importance to be able to act in a timely and correct fashion on possible (incipient) faults/failures before they progress to becoming emergencies. Therefore, decision-making is deemed an indispensable module in the full PHM suite. In this context, the process of decision-making refers to using outputs from the previous modules—failure analysis and probability of failure (POF) estimate from diagnostics, RUL prediction from prognostics—to inform O&M planning and the selection of optimal maintenance action among several alternative options to be executed for the most beneficial operational performance. This process can be conducted by human labors with different operator decision support levels, or ultimately through autonomy-enabled technologies. If properly implemented, this module will play an impactful and beneficial role in asset integrity management as well as planning for O&M activities and staffing levels.

While the study of decision theories has a rich history, autonomy—i.e., operation without relying on human intervention—is in large part an advancement that appeared with the invention of computers and programmable devices that could perform fairly complex computations. Significant technological advances in controls and autonomy have been demonstrated in robotics, aerospace, unmanned aerial vehicles, and self-driving automobiles. However, autonomous control has not been extensively studied for any operating NPP or any new reactor concept (Wood et al., 2017). The nuclear industry lags far behind some other industries (such as avionics and electronics) in transferring the current human-based roles and responsibilities to cutting-edge machines, systems, and controls. To date, NPP equipment surveillance, diagnostics, and prognostics have been mostly used for offline asset management and modest decision support, but those technologies are not being fully leveraged for intelligent, optimal O&M planning and control. To achieve the desired operational efficiency with a reduced staffing burden, autonomous decision-making capabilities must be developed and demonstrated in the nuclear power context.

Given the current status and apparent gaps for NPPs, this section first provides a summary of general approaches used in decision-making, all of which are driven by data to a certain extent. [See Cetiner et al. (2014) and Cetiner and Ramuhalli (2019) for more detailed surveys]. A pioneering study in the nuclear domain by Ramuhalli et al. (2017) is then briefly presented to showcase the ability to integrate diagnostics and prognostics results with supervisory control systems for making risk-informed autonomous decisions that utilize real-time information on component conditions.

Decision-Making Methods

Statistical Decision Theory

Statistical decision theory is concerned with making decisions based on statistical knowledge, which sheds light on the uncertainties involved in the decision problem. The field of classical statistics is directed toward using sample information arising from statistical investigation to make inferences about the use of the data; in contrast, statistical decision theory attempts to combine sample information with other aspects of the problem to make the best decision. In addition to sample information, two other types of information are typically relevant. The first is the knowledge of possible consequences of decisions. Often this knowledge can be quantified by determining the loss that would be incurred for each possible decision and for various possible values of uncertainties. The second type, prior information, generally comes from past experience about similar situations involving similar uncertainties. The approach to statistics that seeks to utilize prior information is called Bayesian analysis. The Bayesian approach is one of the most commonly referred mathematical methods that are exclusively used in decision-making processes in a wide range of applications. Recent examples of applying Bayesian analysis for decision support in nuclear systems are Cai and Golay (2021), who proposed a DBN-based framework capable of analyzing interactions between system status and human activities for the 2011 Fukushima accident scenarios; and Kim et al. (2021), who coupled functional modeling with DBN to study a station blackout scenario leading to a seal loss of coolant accident in an NPP.

Rule-Based Decision-Making

A rule-based model 1) identifies the system state, 2) associates the state with a task, and 3) accesses stored rules to perform the task. Plant *operating procedures* (OPs) are essentially rule-based decision modules executed by human operators. OPs are developed for normal operation to ensure that the plant is run within the operational limits and conditions and to provide instructions for the safe conduct of all modes of normal operation. For abnormal conditions and design-basis accidents, either event-based or symptom-based procedures are created. A means of automating the plant procedural system is to implement the rules through decision tables, which associate conditions with actions to perform. In a recent paper by Hanna et al. (2020), an answer set programming representation of an NPP was presented, which included rules encoding the plant behavior for fast procedure lookup.

Utility Theory

Economists developed utility theory to explain and predict human decision-making under risk and uncertainty. The fundamental assumption underlying utility theory is that of a rational decision maker who always chooses the alternative for which the expected value of the utility is maximized. Built into this assumption is a further supposition that a code of rationality is accepted and utilized by human decision makers, making it possible to construct a mathematical representation that allows the prediction of human behavior. Utility theory can serve as a foundational building block for a decision-making system intended for real-time autonomous control. Given a collection of seemingly viable alternative solutions, implementation risks determined for each alternative can be compared to find a minimum risk solution. Independent loss and gain functions related to plant OPs or other decision strategies can be formulated and represented as nonlinear relationships. An exemplary implementation of the utility theory for NPPs can be found in Yildiz (2003), where an influence diagram-based advisory model was proposed to offer decision support to the plant personnel.

Markov Decision Process

For sequential decision problems in stochastic environments, the same principle of maximum expected utility still applies, but optimal decision-making will require reasoning about future sequences of actions and observations. *Markov decision processes* (MDPs) provide a mathematical framework for modeling decision-making in situations where outcomes are partly random and partly under the control of a decision maker. MDPs have been used successfully in a wide range of autonomous control problems—for autonomous driving (Thrun et al., 2006; Brechtel et al., 2014) in particular—and typically solve an optimization problem using dynamic programming (DP) for selecting the right decision. A *partially observable MDP* (POMDP) is a generalization of an MDP that models a decision process in which it is assumed that an MDP represents the system dynamics but not all states are observable. Instead, the measurements received by the model are incomplete and usually noisy predictions. Therefore, the model must estimate a posterior distribution over a possible state space. POMDPs compute a value function over a belief space. A belief is a function of an entire probability distribution. An exact solution to a POMDP yields the optimal action for each possible belief over the state space, maximizing the value function. However, this maximization procedure requires an iterative algorithm that is far from practical. For any reasonable number of states, sensors, and actuators, the complexity of the value function is prohibitive. One recommended solution to that challenge is the use of differential DP—a DP-based optimal control algorithm of the trajectory optimization class—as it optimizes only over the unconstrained control space. A promising implementation of POMDP can be found in Kochenderfer (2015) for an automated airborne collision avoidance system, leading to significant improvements to safety and operational performance of aircraft.

Discrete Event Models

Many artificial devices and systems and some natural systems demonstrate only discrete values or outcomes. These types of systems are best described as *discrete event systems* (DESs). The opening and closing of valves or commencing a pump startup process are examples of discrete event processes in an NPP. The processes are typically tied to OPs, and plant operators handle their controls. DESs satisfy the properties that 1) the state-space is a discrete set and 2) the state-transition mechanism is event-driven. Time in such systems is not an appropriate independent variable, and conventional differential equation approaches such as modern control theory do not apply to them. The DESs are typically modeled by *finite state automata* or *Petri nets*. Those models use a defined state-transition structure to describe the possible events in each state of the system, and they differ in how they represent state information. A detailed comparison between a finite state automation and a Petri net approach can be found in Aubry et al. (2016). Decision-making models for DESs have an established industrial track record; applications range from robotics to self-driving cars (Costelha and Lima, 2012; Badue et al., 2021).

From Enhanced Risk Monitors to Supervisory Control: A Pioneering Study

In the nuclear industry, successful implementations of autonomous controls seek to address both the probabilistic and deterministic aspects of decision-making. In other words, a risk-informed decision-making framework is needed for the plant control systems to maintain system variables within prescribed operating ranges. As shown in **Figure 5**, the *probabilistic* portion of the decision-making engine identifies decision options and provides the likelihood of success for each option given the status of the plant/systems and component health. It captures the uncertainties associated with sensors and those that arise from modeling assumptions used in inferences. On the other hand, the *deterministic* portion further evaluates the identified alternative success paths and generates a single solution that represents the best operational strategy. The evaluation metrics determine the cost function for finding the optimal decision, and additional constraints—such as regulatory rules and operating guidelines—can be enforced in the deterministic assessment phase.

A study on risk-informed decision-making using real-time equipment condition information was recently performed by Ramuhalli et al. 2017 (Liu et al., 2012), in which the *enhanced risk monitor* (ERM) methodology (Ramuhalli et al., 2014) was integrated with a plant *supervisory control system* (SCS) framework (Cetiner et al., 2016). The ERM methodology interprets components of interest based on sensory data and streamlines condition assessment, diagnostics, prognostics, and risk monitors that expand on probabilistic risk assessment (PRA) by incorporating the dynamically changing plant configuration. The functionality of ERMs can be further augmented to include uncertainty bounds and O&M-based risk metrics (in contrast to the traditional safety-based metrics, such as core damage frequency). As a proactive asset management philosophy, the ERM methodology can offer greater situational awareness to plant supervisory control and O&M planning routines.

The SCS framework is specifically designed to address the need for plant coordination/control that accounts for component degradation in its decision-making. Focused upon non-safety systems, the SCS integrates information from multiple sources, utilizes predefined success criteria, and evaluates plant control actions to ensure that the plant operates within a defined operational envelope. Using RUL and POF information from ERMs as inputs, the decision-making module in the integrated ERM-SCS is invoked only if any of the RUL values is estimated to

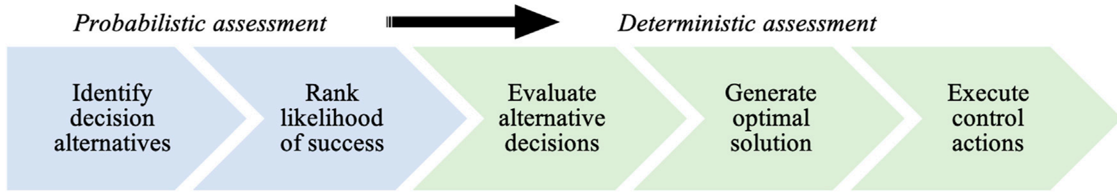

FIGURE 5 | Core elements within the generalized framework for autonomous decision-making.

be larger than the time to the next outage. Decision-making involves two steps: the probabilistic assessment using data acquired from individual ERM terminals to update the event tree/fault tree models with real-time failure probability estimations, and the deterministic assessment based on the multi-attribute utility theory to rank action paths that will not trip the plant's safety system and generate an optimal solution for the operational strategy of the plant. The solution is verified using a lower-order model of the plant to ensure that the recomputed RULs of all components fall within the prescribed criteria.

RESEARCH NEEDS FOR DEPLOYMENT OF PROGNOSTICS AND HEALTH MANAGEMENT IN NUCLEAR POWER PLANTS

Implementation of PHM technologies is a key need for improving the safety and economics of NPPs moving forward with both LTO and new builds. "Prognostics and Health Management Framework and Modeling Approaches" Section has provided a method-centric survey of research in PHM since the 2015 review (Coble et al., 2015), and it can be seen that most advances and corresponding modeling approaches have originated in non-nuclear applications. As such, those developments represent the current state of the art in PHM technologies and methods. Adapting those developments to the nuclear industry may face additional challenges due to the unique operational framework and licensing requirements of NPPs. Additionally, further investigation is needed in several general areas to bring PHM from the research arena to commercial deployment. This section attempts to identify the overarching research needs and technical gaps which still must be addressed to support the development and deployment of PHM in nuclear power generation, including challenges specific to NPPs, a unifying framework for connecting PHM and PRA, verification and validation of PHM models, as well as efforts to evaluate uncertainties and their propagation.

Prognostics and Health Management Feasibility and Challenges Specific to Nuclear Power Plants

Even though significant research has been undertaken to develop PHM—notably, fault detection and diagnostics—for nuclear applications, very limited pilot applications and implementations have resulted in success outside a laboratory setting (Hashemian, 2011; Ramuhalli et al., 2016). The vast majority of modeling approaches described in "Prognostics and Health Management Framework and Modeling Approaches" Section should be widely applicable to nuclear assets in theory; however, implementing PHM in NPPs is quite different from implementing it in other industries because the nuclear industry has been facing a series of specific challenges.

- *Operational compatibility*: As introduced in "US NPP Monitoring and Maintenance: Historical Approach and Motivations for Prognostics and Health Management" Section, PHM technologies in the nuclear industry typically differentiate between active and passive SSCs. PHM for active SSCs is necessary to support the day-to-day application of O&M planning and controls. The health conditions of those assets need to be closely integrated into real-time control decisions to manage *in situ* degradation of critical equipment that could challenge the overall system's operation or safety. PHM for passive SSCs will inform longer-term decision-making. The evolving degradation of these assets under specified operational conditions informs long-term risk assessment, maintenance planning, and outage scheduling. For both SSC types, the deployment of PHM systems should not pose an unacceptable increase in risk to the existing components/ structures of the plant in terms of instrumentation constraints (Pham et al., 2012). Typically, the number of installed sensors available is small in NPPs—particularly for passive SSCs (Coble et al., 2015)—because operational compatibility is limited. Novel inspection methods and advanced sensing techniques are needed to perform measurements without compromising the plant's integrity. Optimizing sensor placement for both legacy and new reactors is also an actively pursued research area to provide adequate and minimally intrusive coverage at a reasonable cost. In the case of new reactors, such needs should be incorporated in the initial design phase to avoid retrofitting.
- *Sensor reliability*: In addition to the compatibility concern, the sensors are often considered to be a weak link in NPPs because they are sometimes less reliable than the assets they monitor (Pham et al., 2012). Advanced sensor validation and qualification will help overcome sensor reliability issues. Additionally, sensors that can withstand the harsh operating environments (such as radiation, high pressure, high

temperature) encountered in some parts of the NPP systems are desired, and their reliability needs to be evaluated carefully.

- *Regulatory scrutiny*: Nuclear power generation is justifiably a heavily regulated industry owing to the risks associated with plant accidents and radiation exposure to the public. The introduction of any new technology or methodology that may impact safety and protection systems in an NPP is scrutinized to such an extent that many research advances are never implemented and deployed (Ayo-Imoru and Cilliers, 2018). This is a significant challenge that makes adopting PHM in the nuclear industry a very daunting task. The SSCs in NPPs are categorized as safety-related and non-safety-related (Pham et al., 2012). The safety-related SSCs are relied upon to remain functional during and following a design-basis event. For those SSCs, in many countries, including the United States, it is impossible to add any additional I&C or even change the maintenance practice without prior approval from the regulators. The implementation of PHM for such assets will certainly bear heavy burdens of justification for approval. Another hurdle for PHM of safety-related SSCs is that most of those assets are stand-by during the plant's normal operation, and their CM can be challenging itself regardless of the regulatory burdens. The non-safety-related SSCs do not require regulatory treatment. However, their unavailability may still carry significant risk in terms of preventing safety-related SSCs from fulfilling their function, triggering transients, or causing actuation of a safety-related system. This fact makes non-safety-related SSCs—usually referred to as the balance of plant assets—ideal candidates for coverage under the PHM framework.
- *Nuclear-applicable standards*: As briefly mentioned in "Prognostics and Health Management Framework and Modeling Approaches" Section, industrial standards for CM, diagnostics, and prognostics exist; however, those standards are largely not specific to the nuclear industry and have not been reviewed by the NRC (in the United States) for application to NPPs. Additionally, a unifying PHM standard that is applicable to generic assets is still missing. Some of the existing and pending standards are potentially relevant to SSCs in NPPs though. As an example, the IEEE P1856 standard covering PHM for electronic systems has broad applicability in digital I&C systems of NPPs. Besides, this IEEE standard provides a framework for developing a general PHM standard for any complex engineering system, as well as specific standards for nuclear SSCs. Developing nuclear-applicable PHM standards is a desired next step. Further efforts will be needed to have those standards reviewed and endorsed by the regulators, without which PHM cannot be deployed for safety-related systems (as mentioned in the bullet point above).
- *Data availability and quality*: There is a growing realization that although the nuclear power enterprise is more than 50 years old, most of the recorded operational data are not publicly available or useful from the perspective of plant reliability and production improvement. The underlying cause is threefold: justifiable protection of intellectual property and security (for safety-related data), low availability of run-to-failure data in most SSCs, and lack of customer needs for relevant data (until very recently). With most modeling tools reviewed in this paper, the effectiveness of the proposed PHM system is unfortunately constrained by the quality of data that can be ultimately reflected in these models. The data-driven methods—particularly those powered by ML/DL—require access to large quantities of data from anomalies observed in the field to train and validate PHM models. To support PHM development and deployment in the nuclear industry, a long-term campaign for coupled model building and data collection is needed, and initiatives to set a road map for coordinated data sharing are highly recommended. In the interim, the artificial/synthetic data obtained from high-fidelity simulations may be used before moving to actual operating data as they become available.
- *Physics-of-failure knowledge*: The NPP consists of various complex multidimensional, nonlinear engineered systems, many being exposed to potentially severe thermal, chemical, and radiological stressors. The underlying physics of certain failure modes for some systems (and their subsystems/components) remains too poorly understood to develop physics-based diagnostic and prognostic models. Research efforts to enhance physics-of-failure knowledge will also help with accurate sensor placement, especially for passive SSCs (Coble et al., 2012). Furthermore, developing high-fidelity physical models can be expensive and time-consuming. It is deemed more realistic and appropriate to leverage both experimental data and physics-of-failure knowledge within a hybrid framework to fully describe the failure modes and degradation process of a monitored asset.

Intersection of Prognostics and Health Management and Probabilistic Risk Assessment

Opportunities emerge as the modern industry moves toward the vision of a data-driven "Industry 4.0" paradigm (Farsi and Zio, 2019). Advances in digital I&C systems, low-cost sensors, and high-performance computing architectures offer new promises and insights for not only PHM but also PRA as means to enhance the safety and reliability of complex engineering systems such as NPPs. So far, PHM has been primarily focused on developing and implementing algorithms for component-level (or simple subsystem-level) health assessment. Significant challenges remain to be solved to develop system-level PHM tools, including component interactions, environmental effects, system nonlinearity, uncertainty propagation, and scalability concern (Atamuradov et al., 2017). On the other hand, PRA is mainly involved with using risk and reliability engineering methods to provide a system-level perspective with emphasis on engineering knowledge and systems logic modeling. Although PRA is well-established in high-consequence industries (such as nuclear), it has largely been used as an offline, static methodology, and few studies have recently attempted to incorporate online CM data within the implementation of dynamic PRA (Moradi and Groth, 2020). Both PHM and PRA technologies bring unique advantages and disadvantages, and they appear to have complementary characteristics that can be synergized in the context of complex engineering systems.

To date, only a handful of research publications have explored the potential intersection of PHM and PRA for complex systems. As introduced in "From Enhanced Risk Monitors to Supervisory Control: A Pioneering Study" Section, Ramuhalli et al. (2014) developed an ERM framework that integrated component-specific time-dependent failure information from PHM models into PRA to provide a dynamic risk measure. Similarly, Yadav et al. (2018) proposed a dynamic PRA model incorporating plant component health conditions using a PHM model based on sensor-based degradation data. More recently, Zhou et al. (2020) proposed a time-dependent common cause failure model by integrating degradation states of components inferred from multi-sensor data and demonstrated using an experimental study of three identical centrifugal pumps. Moradi and Groth (2020) reviewed the limited literature on PHM–PRA intersection and introduced a modernized risk assessment approach to systematically integrate those two families of techniques, considering that complex systems can be modeled as a multilevel hierarchical structure with interactive components. The component/subsystem-level analysis is reflective of the model development aspects of PHM, and the system-level analysis is reflective of those of PRA. In that vein, further research needs include developing of a physically interpretable logic model for learning, inference, and information updating as well as finding suitable risk metrics for assessing the logic model performance.

Verification and Validation

As compared to the amount of research put toward methods and frameworks for PHM, the state of research and effort toward verification and validation (V&V) remains nearly unchanged from the previous review by Coble et al. (Coble et al., 2015). A common trend in the literature is the tendency to perform V&V as one segment of research into a full PHM system, but that task is typically focused on a specific application rather than being an investigation of rigorous and robust V&V methods or frameworks. One work that has addressed this matter (Sun et al., 2016) introduced four performance metrics and two quantitative evaluation methods to provide one unified procedure for determining the trustworthiness of prognostic systems. That work was focused upon prognostics in general; however, there are challenges specific to V&V in the nuclear realm, namely data availability and regulation. Statistically significant data are lacking for V&V of prognostic algorithms across all relevant NPP SSCs. A desired action item at the overall DOE–industry level is to develop benchmark test beds for common data generation and collaborative method V&V efforts. Additionally, in the United States, any V&V methodology proposed will need approval and endorsement from the NRC, which would require a review of all data and models proposed to be used from a regulatory standpoint.

Uncertainty Quantification and Propagation

As emphasized throughout "Prognostics and Health Management Framework and Modeling Approaches" Section, the need to quantify uncertainty in PHM model predictions is of paramount importance, especially in data-driven models. A systematic uncertainty analysis can help reveal both reducible and irreducible sources of variability to aid in managing the overall uncertainty in RUL estimates, which is the last step of PHM before integrating it with O&M planning and control (Coble et al., 2015). The field of research in quantifying model uncertainty is not specific to the nuclear industry and is still evolving. A variety of uncertainty sources are involved in PHM, all of which can be categorized as a subset of one of the following: model input uncertainty, model discretization uncertainty, and model form uncertainty (Ewing et al., 2018; Dewey et al., 2019).

- *Model input uncertainty* comes from the uncertainty of any input parameters, such as uncertainty of material properties (e.g., electric conductivity, elastic modulus), operating conditions, and sensor readings. The overall accuracy of sensors in PHM systems can be compromised by several sources of uncertainty. Firstly, a sensor experiences a natural variation (e.g., a temperature sensor might have a natural uncertainty of ±0.5°). The quantization error from the analog-to-digital converter (ADC) is another source. Most sensors capture analog data that is then converted into digital data through an ADC, and loss of information is unavoidable given an ADC's inherently limited precision. Furthermore, as sensors age, their accuracy decreases, and their variability increases. The level of such degradation is generally not specified by the manufacturers and is hard to quantify, and so-called "uncertainty of uncertainties" will emerge over long lifespans. As a result, to accurately estimate the overall uncertainty of sensor measurements, all the sources of uncertainty should be acknowledged and taken into account.
- *Model discretization uncertainty* refers to the uncertainty of treating continuous parameters as discretized variables, such as modeling space as discretized meshes and time as time steps. Quantification of this source of uncertainty could be achieved by comparing analytical solutions or another numerical analysis with a different level of discretization.
- *Model form uncertainty* arises from the inconsistency between the implemented mathematical model and the real physical world, notably simplifications and approximations made in theories and model implementations. This type of uncertainty source can be estimated by validating with real-world observations or high-fidelity simulations.

Typically, Bayesian inference methods are adopted for quantifying the model prediction uncertainties (Atamuradov et al., 2017; Ramuhalli et al., 2020) because they naturally incorporate information about the target SSC with prior knowledge (e.g., past analysis results, expert opinion) (Coble et al., 2012). Several Bayesian uncertainty quantification approaches have been used in the literature, including BNs (see "Data-Driven Methods" Section), filtering algorithms (such as Kalman filter and particle filter, see "Statistical-Based Prognostics" Section), relevance vector machines (Saha and Goebel, 2008), Bayesian neural networks (Benker et al., 2020), and their variants. Some non-Bayesian approaches have also been proposed for use in the problem of uncertainty estimation, each of which is well suited to specific algorithms or applications. Examples of such approaches include closed-form equations, bootstrapping, and Monte Carlo methods (Coble et al., 2012; Ramuhalli et al., 2012).

In addition to evaluating uncertainty in each module of a PHM system, it is also important to understand how uncertainty in one module can propagate to later modules as well as how uncertainties for individual components will propagate through subsystems, systems, and the whole plant. The latter task can be addressed by prognostic-informed PRA analysis in the ERM framework (Ramuhalli et al., 2014) to integrate sources of uncertainty and their propagation through the ERM calculations. The resulting uncertainty bounds in the ERM output can then be used to perform a probabilistic assessment of the changes in plant O&M and safety risk metrics due to component degradation.

SUMMARY

The contributions of this review paper are threefold: 1) it provides the nuclear industry community with a systematic overview of the full PHM spectrum and an updated in-depth survey of its modeling approaches; 2) it places a strong emphasis on the state of the art of data-driven methods for PHM, primarily driven by recent advances in AI and ML; and 3) it identifies the overarching gaps that still must be addressed by the nuclear industry and PHM communities to support the development and deployment of PHM in NPPs.

To achieve safe and economical operation of NPPs in a competitive energy market, attention is turning to enhanced methods for plant asset management and greater situational awareness of the health condition of key SSCs throughout their life cycles. Interest is growing in applying condition-based (rather than time-based) maintenance for active SSCs and automated online monitoring (instead of periodic inspection) for passive SSCs through the use of PHM principles. Through appropriate detection, diagnosis & prognosis, and mitigation actions, a robust PHM system will allow early warning of degradation in NPPs and will potentially preclude serious consequences due to faults and failures while helping alleviate the burden of unnecessary maintenance activities. Proper application of the full PHM suite will provide improvements to plant reliability and availability and effectively reduce O&M costs and labor reliance.

The full PHM suite utilizes sensor technologies to monitor health conditions, detect anomalies, diagnose faults, predict RUL, and proactively manage failures in complex engineering systems such as NPPs. A complete PHM system proceeds in five modules/steps.

1) *Data acquisition*: The process of data acquisition from the SSC of interest is necessary to make an accurate, reliable prediction of its health. Collected data can be either sensory or event data. Sensory data are measurements tracked via installed sensors from the target equipment and the focus of "Data Acquisition: Emerging Sensor Technologies" Section, which introduces some of the emerging sensing techniques that have been used for nuclear applications or which are deemed useful soon for CM inside NPPs.
2) *Monitoring and detection*: Data collected from a target SSC are continuously monitored for deviations from normal behavior, which are indicators of anomalies. As explained in "Condition Monitoring and Fault Detection" Section, the process of fault detection attempts to recognize incipient faults and failures. Multidimensional, high-volume raw data collected by sensors are not ready to be used directly, and appropriate feature selection is required. "Feature Selection Methods" Section describes the three categories of feature selection methods: filters, wrappers, and embedded methods. In "Anomaly Detection Methods" Section, research efforts using data-driven methods for detecting anomalies are highlighted. In particular, various fault detection approaches based on multivariate statistics have gained attention.
3) *Fault diagnostics*: Once an anomaly is detected, it is vital to diagnose the fault, or in other words, to locate the fault to a specific component or area of a structure (i.e., fault isolation) and to determine the root cause of the fault (i.e., fault identification). As detailed in "Fault Diagnostics" Section, diagnostics can be approached using either a model-based method ("Model-Based Methods" Section), a rule-based method ("Rule-Based Methods" Section), or a data-driven method ("Data-Driven Methods" Section). The distinctions are not completely clear, however, and various hybrid approaches can be developed.
4) *Prognostics*: Depending on how the SSC will degrade, an appropriate prognostic model is then applied to estimate its RUL. Viewed as one of PHM's most beneficial aspects, prognostics is paradoxically an underdeveloped module, especially in the nuclear industry. There is no universally accepted methodology for all prognostic problems, and a variety of algorithms have been developed for application to specific situations or classes of components. Based on a collection of recent review papers, "Prognostics" Section divides these algorithms into four model categories: physics-based ("Physics-Based Methods" Section), knowledge-based ("Knowledge-Based Methods" Section), data-driven ("Data-Driven Methods" Section), and hybrid ("Hybrid Methods" Section) models. The data-driven prognostic models—from conventional statistical methods ("Statistical-Based Prognostics" Section) to advanced ML/DL techniques ("Machine Learning-Based Prognostics" Section)—are of particular interest to large complex systems, and they have been the topic of most research in the field of machinery prognostics. A hybrid approach further integrates the strengths of different model types for improved RUL prediction results.

5) *Decision-making*: O&M planning is informed by the integration of prognostic calculations and risk assessment of proposed mitigation actions based on the current and postulated future health states of the target SSC to achieve optimal (and ultimately autonomous) control and decision-making. As an indispensable step of the broader PHM philosophy, the module of autonomous decision-making has not been extensively studied in the nuclear realm. Given the current status and apparent gaps for NPPs, "Decision-Making" Section first summaries general methods used in decision-making ("Decision-Making Methods" Section). The study presented in "From Enhanced Risk Monitors to Supervisory Control: A Pioneering Study" Section showcases the ability to integrate diagnostics and prognostics results with supervisory control systems for making risk-informed autonomous decisions that utilize real-time information on component conditions.

Even though significant research has been undertaken and more extensive efforts are underway—such as current DOE projects around development of DTs and autonomous control capabilities—to develop PHM systems for nuclear applications, the nuclear industry still lags behind some other industries in bringing PHM from the research arena to commercial deployment. "Research Needs for Deployment of Prognostics and Health Management in Nuclear Power Plants" Section has identified the overarching research needs and technical gaps which still must be addressed to support the development and deployment of PHM in nuclear power generation, including PHM feasibility and challenges specific to NPPs due to the industry's unique operational framework and licensing requirements; a unifying framework for connecting PHM and PRA to synergize their complementary characteristics in the context of complex systems; benchmark test beds for common data generation and collaborative method V&V efforts; and systematic uncertainty quantification and propagation, especially in the case of data-driven methods.

AUTHOR CONTRIBUTIONS

XZ: conceptualization and organization; literature search, collection and review; writing (original draft and revisions). JK: literature search, collection and review; writing (original draft and revisions). KW and XW: literature search, collection and review; writing (original draft). PR and SC: literature search; writing (review & editing); supervision. HK and MG: writing (review & editing); supervision; funding acquisition.

FUNDING

The information presented in this paper was developed from materials collected for the US Department of Energy Nuclear Energy Enabling Technologies project under contract number DE-NE0008873.

ACKNOWLEDGMENTS

We would like to thank Walter Koncinski for his assistance in editing and formatting of the manuscript. We are also thankful to Birdy Phathanapirom and Justin Weinmeister for their technical comments and feedback.

REFERENCES

Ahmed, I., Heo, G., and Kassim, M. (2017). *Fault Detection and Diagnosis of Nuclear Power Plant Using Deep Learning Architecture*. Jeju, Korea: Trans Korean Nuclear Society.

Ajami, A., and Daneshvar, M. (2012). Data Driven Approach for Fault Detection and Diagnosis of Turbine in thermal Power Plant Using Independent Component Analysis (ICA). *Int. J. Electr. Power Energ. Syst.* 43, 728–735. doi:10.1016/j.ijepes.2012.06.022

Al Rashdan, A., Smith, J., Germain, St. S., Ritter, C., Agarwal, V., Boring, R., et al. (2018). Development of a Technology Roadmap for Online Monitoring of Nuclear Power Plants. Technical Report, INL/EXT-18-52206. Idaho Falls, ID: US Department of Energy, Office of Nuclear Energy. Light Water Reactor Sustainability Program. doi:10.2172/1492833

An, D., Kim, N. H., and Choi, J.-H. (2015). Practical Options for Selecting Data-Driven or Physics-Based Prognostics Algorithms with Reviews. *Reliability Eng. Syst. Saf.* 133, 223–236. doi:10.1016/j.ress.2014.09.014

Archibald, R., and Fann, G. (2007). Feature Selection and Classification of Hyperspectral Images With Support Vector Machines. *IEEE Geosci. Remote Sensing Lett.* 4, 674–677. doi:10.1109/LGRS.2007.905116

Atamuradov, V., Medjaher, K., Dersin, P., Lamoureux, B., and Zerhouni, N. (2017). Prognostics and Health Management for Maintenance Practitioners - Review, Implementation and Tools Evaluation. *Int. J. Progn Heal Manag.* 8, 1–31. doi:10.36001/ijphm.2017.v8i3.2667

Atoui, M. A., Verron, S., and Kobi, A. (2015). Fault Detection with Conditional Gaussian Network. *Eng. Appl. Artif. Intelligence* 45, 473–481. doi:10.1016/j.engappai.2015.07.020

Aubry, J.-F., Brinzei, N., and Mazouni, M.-H. (2016). "Comparison Petri Nets - Finite State Automaton," in *Syst. Dependability Assess. Benefits Petri Net Model.* (Hoboken, NJ, USA: John Wiley & Sons), 25–33. doi:10.1002/9781119262114.ch3

Ayodeji, A., and Liu, Y.-k. (2018). Support Vector Ensemble for Incipient Fault Diagnosis in Nuclear Plant Components. *Nucl. Eng. Technol.* 50, 1306–1313. doi:10.1016/j.net.2018.07.013

Ayodeji, A., Liu, Y.-k., and Xia, H. (2018). Knowledge Base Operator Support System for Nuclear Power Plant Fault Diagnosis. *Prog. Nucl. Energ.* 105, 42–50. doi:10.1016/j.pnucene.2017.12.013

Ayo-Imoru, R. M., and Cilliers, A. C. (2018). A Survey of the State of Condition-Based Maintenance (CBM) in the Nuclear Power Industry. *Ann. Nucl. Energ.* 112, 177–188. doi:10.1016/j.anucene.2017.10.010

Badue, C., Guidolini, R., Carneiro, R. V., Azevedo, P., Cardoso, V. B., Forechi, A., et al. (2021). Self-driving Cars: A Survey. *Expert Syst. Appl.* 165, 113816. doi:10.1016/j.eswa.2020.113816

Bampoula, X., Siaterlis, G., Nikolakis, N., and Alexopoulos, K. (2021). A Deep Learning Model for Predictive Maintenance in Cyber-Physical Production Systems Using LSTM Autoencoders. *Sensors* 21, 972. doi:10.3390/s21030972

Banerjee, S., Deng, J., Gorse, C., Vajpayee, V., Becerra, V., and Shimjith, S. R. (2020). ANN Based Sensor and Actuator Fault Detection in Nuclear Reactors. 2020 8th International Conference on Control, Mechatronics and Automation (ICCMA), November 6-8, 2020, Moscow, Russia, 88–94. doi:10.1109/ICCMA51325.2020.9301579

Barraza-Barraza, D., Tercero-Gómez, V. G., Beruvides, M. G., and Limón-Robles, J. (2017). An Adaptive ARX Model to Estimate the RUL of Aluminum Plates Based on its Crack Growth. *Mech. Syst. Signal Process.* 82, 519–536. doi:10.1016/j.ymssp.2016.05.041

Baur, M., Albertelli, P., and Monno, M. (2020). A Review of Prognostics and Health Management of Machine Tools. *Int. J. Adv. Manuf Technol.* 107, 2843–2863. doi:10.1007/s00170-020-05202-3

Bektas, O., Marshall, J., and Jones, J. A. (2020). Comparison of Computational Prognostic Methods for Complex Systems Under Dynamic Regimes: A Review of Perspectives. *Arch. Computat Methods Eng.* 27, 999–1011. doi:10.1007/s11831-019-09339-7

Benker, M., Furtner, L., Semm, T., and Zaeh, M. F. (2020). Utilizing Uncertainty Information in Remaining Useful Life Estimation via Bayesian Neural Networks and Hamiltonian Monte Carlo. *J. Manufacturing Syst*. doi:10.1016/j.jmsy.2020.11.005

Berredjem, T., and Benidir, M. (2018). Bearing Faults Diagnosis Using Fuzzy Expert System Relying on an Improved Range Overlaps and Similarity Method. *Expert Syst. Appl.* 108, 134–142. doi:10.1016/j.eswa.2018.04.025

Bhajantri, L. B. (2018). Fuzzy Logic Based Fault Detection in Distributed Sensor Networks. *Int. J. Sci. Res. Comput. Sci. Eng.* 6, 27–32. doi:10.26438/ijsrcse/v6i2.2732

Bhuiyan, M. Y., and Giurgiutiu, V. (2018). The Signatures of Acoustic Emission Waveforms from Fatigue Crack Advancing in Thin Metallic Plates. *Smart Mater. Struct.* 27, 015019. doi:10.1088/1361-665X/aa9bc2

Bhuiyan, M. Y., Bao, J., Poddar, B., and Giurgiutiu, V. (2018). Toward Identifying Crack-Length-Related Resonances in Acoustic Emission Waveforms for Structural Health Monitoring Applications. *Struct. Health Monit.* 17, 577–585. doi:10.1177/1475921717707356

Blum, A. L., and Langley, P. (1997). Selection of Relevant Features and Examples in Machine Learning. *Artif. Intelligence* 97, 245–271. doi:10.1016/S0004-3702(97)00063-5

Bommert, A., Sun, X., Bischl, B., Rahnenführer, J., and Lang, M. (2020). Benchmark for Filter Methods for Feature Selection in High-Dimensional Classification Data. *Comput. Stat. Data Anal.* 143, 106839. doi:10.1016/j.csda.2019.106839

Bond, L. J., Ramuhalli, P., Tawfik, M. S., and Lybeck, N. J. (2011). Prognostics and Life beyond 60 Years for Nuclear Power Plants. 2011 IEEE Conference on Prognostics and Health Management, June 20-23, 2011, Denver, CO. doi:10.1109/ICPHM.2011.6024316

Box, G. E. P. (1954). Some Theorems on Quadratic Forms Applied in the Study of Analysis of Variance Problems, I. Effect of Inequality of Variance in the One-Way Classification. *Ann. Math. Statist.* 25, 290–302. doi:10.1214/aoms/1177728786

Brechtel, S., Gindele, T., and Dillmann, R. (2014). Probabilistic Decision-Making under Uncertainty for Autonomous Driving Using Continuous POMDPs. 17th International IEEE Conference on Intelligent Transportation Systems (ITSC). Qingdao, China, 392–399. doi:10.1109/ITSC.2014.6957722

Bzdok, D., Altman, N., and Krzywinski, M. (2018). Statistics versus Machine Learning. *Nat. Methods* 15, 233–234. doi:10.1038/nmeth.4642

Cai, Y., and Golay, M. W. (2021). A Framework Analyzing System Status and Human Activities: Illustrated Using 2011 Fukushima Nuclear Power Plant Accident Scenarios. *Nucl. Eng. Des.* 373, 111025. doi:10.1016/j.nucengdes.2020.111025

Cai, L., and Tian, X. (2014). A New Fault Detection Method for Non-Gaussian Process Based on Robust Independent Component Analysis. *Process Saf. Environ. Prot.* 92, 645–658. doi:10.1016/j.psep.2013.11.003

Cai, B., Liu, Y., Fan, Q., Zhang, Y., Liu, Z., Yu, S., et al. (2014). Multi-source Information Fusion Based Fault Diagnosis of Ground-Source Heat Pump Using Bayesian Network. *Appl. Energ.* 114, 1–9. doi:10.1016/j.apenergy.2013.09.043

Cai, B., Huang, L., and Xie, M. (2017). Bayesian Networks in Fault Diagnosis. *IEEE Trans. Ind. Inf.* 13, 2227–2240. doi:10.1109/TII.2017.2695583

Calderoni, P., Hurley, D., Daw, J., Fleming, A., and McCary, K. (2019). "Innovative Sensing Technologies for Nuclear Instrumentation," in 2019 IEEE International Instrumentation and Measurement Technology Conference (I2MTC), Auckland, New Zealand. doi:10.1109/I2MTC.2019.8827129

Cetiner, S., and Ramuhalli, P. (2019). Transformational Challenge Reactor Autonomous Control System Framework and Key Enabling Technologies. Technical Report, ORNL/SPR-2019/1178. Oak Ridge, TN: Oak Ridge National Laboratory. doi:10.2172/1530084

Cetiner, S., Muhlheim, M. D., Flanagan, G. F., Fugate, D. L., and Kisner, R. A. (2014). Development of an Automated Decision-Making Tool for Supervisory Control System. Technical Report, ORNL/TM-2014/363. Oak Ridge, TN: Oak Ridge National Laboratory. doi:10.2172/1252136

Cetiner, S., Muhlheim, M. D., Guler-Yigitoglu, A., Belles, R. J., Greenwood, M. S., Harrison, T. J., et al. (2016). Supervisory Control System for Multi-Modular Advanced Reactors. Technical Report, ORNL/TM-2016/693. Oak Ridge, TN: Oak Ridge National Laboratory. doi:10.2172/1615832

Chandrashekar, G., and Sahin, F. (2014). A Survey on Feature Selection Methods. *Comput. Electr. Eng.* 40, 16–28. doi:10.1016/j.compeleceng.2013.11.024

Chen, G., and Chen, J. (2015). A Novel Wrapper Method for Feature Selection and its Applications. *Neurocomputing* 159, 219–226. doi:10.1016/j.neucom.2015.01.070

Chen, J. G., Davis, A., Wadhwa, N., Durand, F., Freeman, W. T., and Büyüköztürk, O. (2017). Video Camera–Based Vibration Measurement for Civil Infrastructure Applications. *J. Infrastruct Syst.* 23, 1–11. doi:10.1061/(ASCE)IS.1943-555X.0000348

Chen, J., Jing, H., Chang, Y., and Liu, Q. (2019). Gated Recurrent Unit Based Recurrent Neural Network for Remaining Useful Life Prediction of Nonlinear Deterioration Process. *Reliability Eng. Syst. Saf.* 185, 372–382. doi:10.1016/j.ress.2019.01.006

Chen, K. P. (2018). High Spatial Resolution Distributed Fiber-Optic Sensor Networks for Reactors and Fuel Cycle Systems. University of Pittsburgh. Pittsburgh, PA: Final Report for DE-NE0008303. doi:10.2172/1475174

Cho, S., and Jiang, J. (2018). Optimal Fault Classification Using Fisher Discriminant Analysis in the Parity Space for Applications to NPPs. *IEEE Trans. Nucl. Sci.* 65, 856–865. doi:10.1109/TNS.2018.2803658

Coble, J. B., Ramuhalli, P., Bond, L. J., Hines, J. W., and Upadhyaya, B. R. (2012). Prognostics and Health Management in Nuclear Power Plants: A Review of Technologies and Applications. Technical Report, PNNL-21515. Richland, WA: Pacific Northwest National Laboratory. doi:10.2172/1047416

Coble, J., Ramuhalli, P., Bond, L., Hines, J. W., and Upadhyaya, B. (2015). A Review of Prognostics and Health Management Applications in Nuclear Power Plants. *Int. J. Progn Heal Manag.* 6, 1–22. doi:10.36001/ijphm.2015.v6i3.2271

Costelha, H., and Lima, P. (2012). Robot Task Plan Representation by Petri Nets: Modelling, Identification, Analysis and Execution. *Auton. Robot* 33, 337–360. doi:10.1007/s10514-012-9288-x

Cuc, A., Giurgiutiu, V., Joshi, S., and Tidwell, Z. (2007). Structural Health Monitoring with Piezoelectric Wafer Active Sensors for Space Applications. *AIAA J.* 45, 2838–2850. doi:10.2514/1.26141

Da Silva, R. R., Costa, E. D. S., De Oliveira, R. C. L., and Mesquita, A. L. A. (2017). Fault Diagnosis in Rotating Machine Using Full Spectrum of Vibration and Fuzzy Logic. *J. Eng. Sci. Technol.* 12, 2952–2964.

Das, S. (2001). Filters, Wrappers and a Boosting-Based Hybrid for Feature Selection. *Proc. Eighteenth Int. Conf. Mach. Learn.*, 74–81. doi:10.5555/645530.658297

Davis, A., Bouman, K. L., Chen, J. G., Rubinstein, M., Buyukozturk, O., Durand, F., et al. (2017). Visual Vibrometry: Estimating Material Properties from Small Motions in Video. *IEEE Trans. Pattern Anal. Mach. Intell.* 39, 732–745. doi:10.1109/TPAMI.2016.2622271

Daw, J., Rempe, J., Palmer, J., Ramuhalli, P., Keller, P., Montgomery, R., et al. (2014). NEET In-Pile Ultrasonic Sensor Enablement-Final Report. INL/EXT-14-32505. Idaho Falls, ID: Idaho National Laboratory. doi:10.2172/1166037

Deleplace, A., Atamuradov, V., Allali, A., Pellé, J., Plana, R., and Alleaume, G. (2020). Ensemble Learning-Based Fault Detection in Nuclear Power Plant Screen Cleaners. *IFAC-PapersOnLine* 53, 10354–10359. doi:10.1016/j.ifacol.2020.12.2773

Deng, X.-W., Gao, Q.-S., Zhang, C., Hu, D., and Yang, T. (2017). Rule - Based Fault Diagnosis Expert System for Wind Turbine. *ITM Web Conf.* 11, 07005. doi:10.1051/itmconf/20171107005

Deng, Y., Li, Z., Chen, J., and Qi, X. (2018). The Effects of the Structure Characteristics on Magnetic Barkhausen Noise in Commercial Steels. *J. Magnetism Magn. Mater.* 451, 276–282. doi:10.1016/j.jmmm.2017.11.041

Dewey, H. H., DeVries, D. R., and Hyde, S. R. (2019). "Uncertainty Quantification in Prognostic Health Management Systems," in 2019 IEEE Aerospace Conference, Big Sky, MT, USA, 1–13. doi:10.1109/AERO.2019.8741821

Diez-Olivan, A., Del Ser, J., Galar, D., and Sierra, B. (2019). Data Fusion and Machine Learning for Industrial Prognosis: Trends and Perspectives towards Industry 4.0. *Inf. Fusion* 50, 92–111. doi:10.1016/j.inffus.2018.10.005

Dourado, A., and Viana, F. A. C. (2020). Physics-Informed Neural Networks for Missing Physics Estimation in Cumulative Damage Models: A Case Study in Corrosion Fatigue. *J. Comput. Inf. Sci. Eng.* 20, 061007. doi:10.1115/1.4047173

Downs, J. J., and Vogel, E. F. (1993). A Plant-wide Industrial Process Control Problem. *Comput. Chem. Eng.* 17, 245–255. doi:10.1016/0098-1354(93)80018-I

Droguett, E. L. (2020). "The PHM Perspective," in ASME-SERAD and UMD-CRR Interactive Seminar & Pre-workshop on the Intersection of PRA and PHM, October 2, 2020.

Du, W., Guo, X., Wang, Z., Wang, J., Yu, M., Li, C., et al. (2020). A New Fuzzy Logic Classifier Based on Multiscale Permutation Entropy and Its Application in Bearing Fault Diagnosis. *Entropy* 22, 27. doi:10.3390/e22010027

Dziendzikowski, M., Kurnyta, A., Dragan, K., Klysz, S., and Leski, A. (2016). *In Situ* Barely Visible Impact Damage Detection and Localization for Composite Structures Using Surface Mounted and Embedded PZT Transducers: A Comparative Study. *Mech. Syst. Signal Process.* 78, 91–106. doi:10.1016/j.ymssp.2015.09.021

Ebrahimkhanlou, A., Dubuc, B., and Salamone, S. (2016). Damage Localization in Metallic Plate Structures Using Edge-Reflected Lamb Waves. *Smart Mater. Struct.* 25, 085035. doi:10.1088/0964-1726/25/8/085035

Eker, O. F., Camci, F., and Jennions, I. K. (2019). A New Hybrid Prognostic Methodology. *Int. J. Progn Heal Manag.* 10, 1–13. doi:10.36001/ijphm.2019.v10i2.2727

Elsheikh, A., Yacout, S., and Ouali, M.-S. (2019). Bidirectional Handshaking LSTM for Remaining Useful Life Prediction. *Neurocomputing* 323, 148–156. doi:10.1016/j.neucom.2018.09.076

Ewing, M. E., Liechty, B. C., and Black, D. L. (2018). A General Methodology for Uncertainty Quantification in Engineering Analyses Using a Credible Probability Box. *J. Verif. Valid. Uncertain. Quantif.* 3, 021003. doi:10.1115/1.4041490

Fan, S., Paul, P., Wu, T., Rong, H., and Zhang, G. (2020). On Applications of Spiking Neural P Systems. *Appl. Sci.* 10, 7011. doi:10.3390/app10207011

Farsi, M. A., and Zio, E. (2019). Industry 4.0: Some Challenges and Opportunities for Reliability Engineering. *Int. J. Reliabl Risk Safe Theor. App* 2, 23–34. doi:10.30699/IJRRS.2.1.4

Fleming, A., Al Rashdan, A., Jensen, C., and Calderoni, P. (2019). An Impedance-Based Diameter Gauge for In-Pile Fuel Deformation Measurements. *Instrumentation Sci. Technol.* 47, 611–626. doi:10.1080/10739149.2019.1616207

Forman, R. G. (1972). Study of Fatigue Crack Initiation from Flaws Using Fracture Mechanics Theory. *Eng. Fracture Mech.* 4, 333–345. doi:10.1016/0013-7944(72)90048-3

Gao, Y., Gao, X., and Zhang, X. (2017). The 2 °C Global Temperature Target and the Evolution of the Long-Term Goal of Addressing Climate Change-From the United Nations Framework Convention on Climate Change to the Paris Agreement. *Engineering* 3, 272–278. doi:10.1016/J.ENG.2017.01.022

Gautam, S., Tamboli, P. K., Roy, K., Patankar, V. H., and Duttagupta, S. P. (2019). Sensors Incipient Fault Detection and Isolation of Nuclear Power Plant Using Extended Kalman Filter and Kullback-Leibler Divergence. *ISA Trans.* 92, 180–190. doi:10.1016/j.isatra.2019.02.011

Ge, Z., Song, Z., and Gao, F. (2013). Review of Recent Research on Data-Based Process Monitoring. *Ind. Eng. Chem. Res.* 52, 3543–3562. doi:10.1021/ie302069q

Ghahramani, Z. (2001). An Introduction to Hidden Markov Models and Bayesian Networks. *Int. J. Patt. Recogn. Artif. Intell.* 15, 9–42. doi:10.1142/S0218001401000836

Goebel, K., Eklund, N., and Bonanni, P. (2006). "Fusing Competing Prediction Algorithms for Prognostics," in IEEE Aerospace Conference, Big Sky, MT, USA. doi:10.1109/AERO.2006.1656116

Goldberg, D. E. (1989). *Genetic Algorithms in Search, Optimization and Machine Learning*. Boston, MA, USA: Addison-Wesley Longman Publishing Co., Inc.

Gomes, C. R., and Canedo Medeiros, J. A. C. (2015). Neural Network of Gaussian Radial Basis Functions Applied to the Problem of Identification of Nuclear Accidents in a PWR Nuclear Power Plant. *Ann. Nucl. Energ.* 77, 285–293. doi:10.1016/j.anucene.2014.10.001

Guillén, A. J., Crespo, A., Macchi, M., and Gómez, J. (2016). On the Role of Prognostics and Health Management in Advanced Maintenance Systems. *Prod. Plann. Control.* 27, 991–1004. doi:10.1080/09537287.2016.1171920

Gurgen, A., Lin, L., and Dinh, N. (2020). Development and Assessment of Physics-Guided Machine Learning for Prognosis System. *Trans. Am. Nucl. Soc.*, 272–275. doi:10.13182/T123-33503

Guyon, I., and Elisseeff, A. (2003). An Introduction to Variable and Feature Selection. *J. Mach Learn. Res.* 3, 1157–1182. doi:10.5555/944919.944968

Guyon, I., Weston, J., Barnhill, S., and Vapnik, V. (2002). Gene Selection for Cancer Classification Using Support Vector Machines. *Mach Learn.* 46, 389–422. doi:10.1023/A:1012487302797

Haider, M. F., Lin, B., Yu, L., and Giurgiutiu, V. (2017). Sensing Capabilities of Piezoelectric Wafer Active Sensors in Extreme Nuclear Environment. *Proc. Soc. Photo-Optical Instrum. Eng.* 10169. doi:10.1117/12.2260162

Hanna, B. N., Trieu, L. L. T., Son, T. C., and Dinh, N. T. (2020). An Application of ASP in Nuclear Engineering: Explaining the Three Mile Island Nuclear Accident Scenario. *Theor. Pract. Logic Program.* 20, 926–941. doi:10.1017/S1471068420000241

Harrou, F., Nounou, M. N., Nounou, H. N., and Madakyaru, M. (2013). Statistical Fault Detection Using PCA-Based GLR Hypothesis Testing. *J. Loss Prev. Process Industries* 26, 129–139. doi:10.1016/j.jlp.2012.10.003

Hashemian, H. M. (2011). On-line Monitoring Applications in Nuclear Power Plants. *Prog. Nucl. Energ.* 53, 167–181. doi:10.1016/j.pnucene.2010.08.003

Hess, A. (2002). "Prognostics, from the Need to Reality-From the Fleet Users and PHM System Designer/developers Perspectives," in Proceedings, IEEE Aerospace Conference, Big Sky, MT, USA. doi:10.1109/AERO.2002.1036118

Hong, X., Liu, Y., Liufu, Y., and Lin, P. (2018). Debonding Detection in Hidden Frame Supported Glass Curtain walls Using the Nonlinear Ultrasonic Modulation Method with Piezoceramic Transducers. *Sensors* 18, 2094. doi:10.3390/s18072094

Hotelling, H. (1933). Analysis of a Complex of Statistical Variables into Principal Components. *J. Educ. Psychol.* 24, 417–441. doi:10.1037/h0071325

Hu, Y., Baraldi, P., Di Maio, F., and Zio, E. (2016). Online Performance Assessment Method_newline for a Model-Based Prognostic Approach. *IEEE Trans. Rel.* 65, 718–735. doi:10.1109/TR.2015.2500681

Husain, Z. (2018). Fuzzy Logic Expert System for Incipient Fault Diagnosis of Power Transformers. *Ijeei* 10, 300–317. doi:10.15676/ijeei.2018.10.2.8

IAEA (1996). *Defence in Depth in Nuclear Safety. INSAG-10, a Report by the International Nuclear Safety Advisory Group*. Vienna, Austria: International Atomic Energy Agency.

IAEA (2021). "The Database on Nuclear Power Reactors," in *Power Reactor Information System* (Vienna, Austria: International Atomic Energy Agency). Retrieved in January 2021. https://pris.iaea.org/pris/.

IEA and NEA (2020). *Projected Costs of Generating Electricity*. 2020 Edition. Paris, France: International Energy Agency and OECD Nuclear Energy Agency.

IEA (2019). *Nuclear Power in a Clean Energy System*. Paris, France: International Energy Agency.

Isermann, R., and Ballé, P. (1997). Trends in the Application of Model-Based Fault Detection and Diagnosis of Technical Processes. *Control. Eng. Pract.* 5, 709–719. doi:10.1016/S0967-0661(97)00053-1

Jamil, F., Abid, M., Haq, I., Khan, A. Q., and Iqbal, M. (2016). Fault Diagnosis of Pakistan Research Reactor-2 with Data-Driven Techniques. *Ann. Nucl. Energ.* 90, 433–440. doi:10.1016/j.anucene.2015.12.023

Jamil, F., Abid, M., Adil, M., Haq, I., Khan, A. Q., and Khan, S. F. (2018). Kernel Approaches for Fault Detection and Classification in PARR-2. *J. Process Control.* 64, 1–6. doi:10.1016/j.jprocont.2018.01.003

Jardine, A. K. S., Lin, D., and Banjevic, D. (2006). A Review on Machinery Diagnostics and Prognostics Implementing Condition-Based Maintenance. *Mech. Syst. Signal Process.* 20, 1483–1510. doi:10.1016/j.ymssp.2005.09.012

Javed, K., Gouriveau, R., and Zerhouni, N. (2014). SW-ELM: A Summation Wavelet Extreme Learning Machine Algorithm with A Priori Parameter Initialization. *Neurocomputing* 123, 299–307. doi:10.1016/j.neucom.2013.07.021

Jia, Q., and Zhang, Y. (2016). Quality-related Fault Detection Approach Based on Dynamic Kernel Partial Least Squares. *Chem. Eng. Res. Des.* 106, 242–252. doi:10.1016/j.cherd.2015.12.015

Jiang, Q., and Yan, X. (2018). Parallel PCA-KPCA for Nonlinear Process Monitoring. *Control. Eng. Pract.* 80, 17–25. doi:10.1016/j.conengprac.2018.07.012

Jiao, J., Zhao, N., Wang, G., and Yin, S. (2017). A Nonlinear Quality-Related Fault Detection Approach Based on Modified Kernel Partial Least Squares. *ISA Trans.* 66, 275–283. doi:10.1016/j.isatra.2016.10.015

John, G. H., Kohavi, R., and Pfleger, K. (1994). *Irrelevant Features and the Subset Selection Problem. Mach. Learn. Proc*. New Brunswick, NJ: Morgan Kaufmann Publishers, 121–129. doi:10.1016/B978-1-55860-335-6.50023-4

Karami, M., and Wang, L. (2018). Fault Detection and Diagnosis for Nonlinear Systems: A New Adaptive Gaussian Mixture Modeling Approach. *Energy and Buildings* 166, 477–488. doi:10.1016/j.enbuild.2018.02.032

Kennedy, J., and Eberhart, R. (1995). "Particle Swarm Optimization," in Proceedings of ICNN'95 - International Conference on Neural Networks, November 27-December 1, 1995, Perth, WA (Perth, WA, Australia: IEEE). doi:10.1109/ICNN.1995.488968

Khan, S., and Yairi, T. (2018). A Review on the Application of Deep Learning in System Health Management. *Mech. Syst. Signal Process.* 107, 241–265. doi:10.1016/j.ymssp.2017.11.024

Khan, S. A., Prosvirin, A. E., and Kim, J.-M. (2018). "Towards Bearing Health Prognosis Using Generative Adversarial Networks: Modeling Bearing Degradation," in 2018 International Conference on Advancements in Computational Sciences (ICACS), Lahore, Pakistan. doi:10.1109/ICACS.2018.8333495

Kharoufeh, J. P., and Cox, S. M. (2005). Stochastic Models for Degradation-Based Reliability. *IIE Trans.* 37, 533–542. doi:10.1080/07408170590929009

Kharoufeh, J. P., Solo, C. J., and Ulukus, M. Y. (2010). Semi-Markov Models for Degradation-Based Reliability. *IIE Trans.* 42, 599–612. doi:10.1080/07408170903394371

Kharoufeh, J. P. (2003). Explicit Results for Wear Processes in a Markovian Environment. *Operations Res. Lett.* 31, 237–244. doi:10.1016/S0167-6377(02)00229-8

Kim, T. K., Park, J. K., Lee, B. H., and Seong, S. H. (2019). Deep-learning-based Alarm System for Accident Diagnosis and Reactor State Classification with Probability Value. *Ann. Nucl. Energ.* 133, 723–731. doi:10.1016/j.anucene.2019.07.022

Kim, J., Zhao, X., Shah, A. U. A., and Kang, H. G. (2021). System Risk Quantification and Decision Making Support Using Functional Modeling and Dynamic Bayesian Network (under review).

Kochenderfer, M. J. (2015). *Decision Making Under Uncertainty: Theory and Application*. Cambridge, MA, USA: The MIT Press. doi:10.7551/mitpress/10187.001.0001

Kohavi, R., and John, G. H. (1997). Wrappers for Feature Subset Selection. *Artif. Intelligence* 97, 273–324. doi:10.1016/S0004-3702(97)00043-X

Komagome, Y., and Matsumoto, E. (2002). Visualization of Back Surface Defects by Piezoelectric Film. *Jae* 14, 425–428. doi:10.3233/jae-2002-418

Kozjek, D., Malus, A., and Vrabič, R. (2020). Multi-objective Adjustment of Remaining Useful Life Predictions Based on Reinforcement Learning. *Proced. CIRP* 93, 425–430. doi:10.1016/j.procir.2020.03.051

Krishnakumari, A., Elayaperumal, A., Saravanan, M., and Arvindan, C. (2017). Fault Diagnostics of spur Gear Using Decision Tree and Fuzzy Classifier. *Int. J. Adv. Manuf Technol.* 89, 3487–3494. doi:10.1007/s00170-016-9307-8

Lazar, C., Taminau, J., Meganck, S., Steenhoff, D., Coletta, A., Molter, C., et al. (2012). A Survey on Filter Techniques for Feature Selection in Gene Expression Microarray Analysis. *IEEE/ACM Trans. Comput. Biol. Bioinf.* 9, 1106–1119. doi:10.1109/TCBB.2012.33

Lee, C.-K., and Shin, Y.-J. (2018). Multi-core cable Fault Diagnosis Using Cluster Time-Frequency Domain Reflectometry. 2018 IEEE International Instrumentation and Measurement Technology Conference (I2MTC), May 14-17, 2018, Houston, TX1–6. doi:10.1109/I2MTC.2018.8409561

Lee, J., Ghaffari, M., and Elmeligy, S. (2011). Self-maintenance and Engineering Immune Systems: Towards Smarter Machines and Manufacturing Systems. *Annu. Rev. Control.* 35, 111–122. doi:10.1016/j.arcontrol.2011.03.007

Lee, H., Sohn, H., Yang, S., and Yang, J. (2014). Monitoring of Pipelines in Nuclear Power Plants by Measuring Laser-Based Mechanical Impedance. *Smart Mater. Struct.* 23, 065008. doi:10.1088/0964-1726/23/6/065008

Lee, G., Lee, S. J., and Lee, C. (2021). A Convolutional Neural Network Model for Abnormality Diagnosis in a Nuclear Power Plant. *Appl. Soft Comput.* 99, 106874. doi:10.1016/j.asoc.2020.106874

Lei, Y., Li, N., Guo, L., Li, N., Yan, T., and Lin, J. (2018). Machinery Health Prognostics: A Systematic Review from Data Acquisition to RUL Prediction. *Mech. Syst. Signal Process.* 104, 799–834. doi:10.1016/j.ymssp.2017.11.016

Li, R. F., and Wang, X. Z. (2002). Dimension Reduction of Process Dynamic Trends Using Independent Component Analysis. *Comput. Chem. Eng.* 26, 467–473. doi:10.1016/S0098-1354(01)00773-6

Li, Y., Xu, B., Hu, S., Li, Y., Li, Q., and Liu, W. (2015). Simulation of Magnetic Hysteresis Loops and Magnetic Barkhausen Noise of α-iron Containing Nonmagnetic Particles. *AIP Adv.* 5, 077168. doi:10.1063/1.4927548

Li, G., Qin, S. J., and Yuan, T. (2016). Data-driven Root Cause Diagnosis of Faults in Process Industries. *Chemometrics Intell. Lab. Syst.* 159, 1–11. doi:10.1016/j.chemolab.2016.09.006

Li, W., Peng, M., Liu, Y., Jiang, N., Wang, H., and Duan, Z. (2018). Fault Detection, Identification and Reconstruction of Sensors in Nuclear Power Plant with Optimized PCA Method. *Ann. Nucl. Energ.* 113, 105–117. doi:10.1016/j.anucene.2017.11.009

Li, W., Peng, M., and Wang, Q. (2018). False Alarm Reducing in PCA Method for Sensor Fault Detection in a Nuclear Power Plant. *Ann. Nucl. Energ.* 118, 131–139. doi:10.1016/j.anucene.2018.04.012

Li, W., Peng, M., and Wang, Q. (2019). Improved PCA Method for Sensor Fault Detection and Isolation in a Nuclear Power Plant. *Nucl. Eng. Technol.* 51, 146–154. doi:10.1016/j.net.2018.08.020

Li, X., Jiang, H., Xiong, X., and Shao, H. (2019). Rolling Bearing Health Prognosis Using a Modified Health index Based Hierarchical Gated Recurrent Unit Network. *Mechanism Machine Theor.* 133, 229–249. doi:10.1016/j.mechmachtheory.2018.11.005

Li, D., Wang, Y., Wang, J., Wang, C., and Duan, Y. (2020). Recent Advances in Sensor Fault Diagnosis: A Review. *Sensors Actuators A: Phys.* 309, 111990. doi:10.1016/j.sna.2020.111990

Liao, L., and Kottig, F. (2014). Review of Hybrid Prognostics Approaches for Remaining Useful Life Prediction of Engineered Systems, and an Application to Battery Life Prediction. *IEEE Trans. Rel.* 63, 191–207. doi:10.1109/TR.2014.2299152

Lin, T.-H., and Wu, S.-C. (2019). Sensor Fault Detection, Isolation and Reconstruction in Nuclear Power Plants. *Ann. Nucl. Energ.* 126, 398–409. doi:10.1016/j.anucene.2018.11.044

Lin, L., Athe, P., Rouxelin, P., Avramova, M., Gupta, A., Youngblood, R., et al. (2021). Development and Assessment of a Nearly Autonomous Management and Control System for Advanced Reactors. *Ann. Nucl. Energ.* 150, 107861. doi:10.1016/j.anucene.2020.107861

Liu, J., and Zio, E. (2018). A Scalable Fuzzy Support Vector Machine for Fault Detection in Transportation Systems. *Expert Syst. Appl.* 102, 36–43. doi:10.1016/j.eswa.2018.02.017

Liu, J., Wang, W., Ma, F., Yang, Y. B., and Yang, C. S. (2012). A Data-Model-Fusion Prognostic Framework for Dynamic System State Forecasting. *Eng. Appl. Artif. Intelligence* 25, 814–823. doi:10.1016/j.engappai.2012.02.015

Liu, Q., Qin, S. J., and Chai, T. (2013). Decentralized Fault Diagnosis of Continuous Annealing Processes Based on Multilevel PCA. *IEEE Trans. Autom Sci. Eng.* 10, 687–698. doi:10.1109/TASE.2012.2230628

Liu, J., Vitelli, V., Zio, E., and Seraoui, R. (2015). A Novel Dynamic-Weighted Probabilistic Support Vector Regression-Based Ensemble for Prognostics of Time Series Data. *IEEE Trans. Rel.* 64, 1203–1213. doi:10.1109/TR.2015.2427156

Liu, Y.-K., Wu, G.-H., Xie, C.-L., Duan, Z.-Y., Peng, M.-J., and Li, M.-K. (2016). A Fault Diagnosis Method Based on Signed Directed Graph and Matrix for Nuclear Power Plants. *Nucl. Eng. Des.* 297, 166–174. doi:10.1016/j.nucengdes.2015.11.016

Liu, Y-K., Ayodeji, A., Wen, Z., Wu, M., Peng, M., and Yu, W. (2017). A cascade Intelligent Fault Diagnostic Technique for Nuclear Power Plants. *J. Nucl. Sci. Technol.* 55, 254–266. doi:10.1080/00223131.2017.1394228

Liu, Y., Hu, X., and Zhang, W. (2019). Remaining Useful Life Prediction Based on Health index Similarity. *Reliability Eng. Syst. Saf.* 185, 502–510. doi:10.1016/j.ress.2019.02.002

Ma, B., Zhao, Y., Zhang, Y., Jiang, Q. L., and Hou, X. Q. (2019). Machinery Early Fault Detection Based on Dirichlet Process Mixture Model. *IEEE Access* 7, 89226–89233. doi:10.1109/ACCESS.2019.2927104

Makowska, K., Piotrowski, L., and Kowalewski, Z. L. (2017). Prediction of the Mechanical Properties of P91 Steel by Means of Magneto-Acoustic Emission and Acoustic Birefringence. *J. Nondestruct Eval.* 36, 43. doi:10.1007/s10921-017-0421-9

Mandal, S., Santhi, B., Sridhar, S., Vinolia, K., and Swaminathan, P. (2017). Nuclear Power Plant Thermocouple Sensor Fault Detection and Classification Using

Deep Learning and Generalized Likelihood Ratio Test. *IEEE Trans. Nucl. Sci.* 64, 1. doi:10.1109/TNS.2017.2697919

McCloy, J. S., Ramuhalli, P., and Henager, Jr., C. (2013). Use of First Order Reversal Curve Measurements to Understand Barkhausen Noise Emission in Nuclear Steel. *Proc. 39th Annu. Rev. Prog. Quant. Nondestruct. Eval.* 1511, 1709–1716. doi:10.1063/1.4789247

Mei, L., Li, H., Zhou, Y., Li, D., Long, W., and Xing, F. (2020). Output-Only Damage Detection of Shear Building Structures Using an Autoregressive Model-Enhanced Optimal Subpattern Assignment Metric. *Sensors* 20, 2050. doi:10.3390/s20072050

Meng, J., Su, Y., and Xie, S. (2020). Loose Parts Detection Method Combining Blind Deconvolution with Support Vector Machine. *Ann. Nucl. Energ.* 149, 107782. doi:10.1016/j.anucene.2020.107782

Messai, A., Mellit, A., Abdellani, I., and Massi Pavan, A. (2015). On-line Fault Detection of a Fuel Rod Temperature Measurement Sensor in a Nuclear Reactor Core Using ANNs. *Prog. Nucl. Energ.* 79, 8–21. doi:10.1016/j.pnucene.2014.10.013

Mirnaghi, M. S., and Haghighat, F. (2020). Fault Detection and Diagnosis of Large-Scale HVAC Systems in Buildings Using Data-Driven Methods: A Comprehensive Review. *Energy and Buildings* 229, 110492. doi:10.1016/j.enbuild.2020.110492

MIT (2018). *The Future of Nuclear Energy in a Carbon-Constrained World: An Interdisciplinary MIT Study*. MIT Energy Initiative.

Mnassri, B., El Adel, E. M., and Ouladsine, M. (2015). Reconstruction-based Contribution Approaches for Improved Fault Diagnosis Using Principal Component Analysis. *J. Process Control.* 33, 60–76. doi:10.1016/j.jprocont.2015.06.004

Moradi, R., and Groth, K. M. (2020). Modernizing Risk Assessment: A Systematic Integration of PRA and PHM Techniques. *Reliability Eng. Syst. Saf.* 204, 107194. doi:10.1016/j.ress.2020.107194

Morana, A., Mellier, F., Cheymol, G., Destouches, C., Di Salvo, J., Girard, S., et al. (2016). Irradiation Campaign in the EOLE Critical Facility of Fiber Optic Bragg Gratings Dedicated to the Online Temperature Measurement in Zero Power Research Reactors. *IEEE Trans. Nucl. Sci.* 63, 2887–2894. doi:10.1109/TNS.2016.2618906

Moshkbar-Bakhshayesh, K. (2021). Investigating the Performance of the Supervised Learning Algorithms for Estimating NPPs Parameters in Combination with the Different Feature Selection Techniques. *Ann. Nucl. Energ.* 158, 108299. doi:10.1016/j.anucene.2021.108299

Mujica, L., Rodellar, J., Fernández, A., and Güemes, A. (2011). Q-statistic and T2-Statistic PCA-Based Measures for Damage Assessment in Structures. *Struct. Health Monit.* 10, 539–553. doi:10.1177/1475921710388972

Mundra, P. A., and Rajapakse, J. C. (2010). SVM-RFE with MRMR Filter for Gene Selection. *IEEE Trans.on Nanobioscience* 9, 31–37. doi:10.1109/TNB.2009.2035284

Nain, A., and Varde, P. V. (2013). "Fuzzy Rule-Based Approach for Diagnostics in Nuclear Plant Diesel Generators," in Proceedings of the International Symposium on Engineering under Uncertainty: Safety Assessment and Management (ISEUSAM - 2012) January, 2012, Kolkata, India (Springer India), 981–996. doi:10.1007/978-81-322-0757-3_67

Narendra, P. M., and Fukunaga, K. (1977). A Branch and Bound Algorithm for Feature Subset Selection. *IEEE Trans. Comput.* C-26, 917–922. doi:10.1109/TC.1977.1674939

NEI (2011). *Nuclear Energy's Economic Benefits - Current and Future (White Paper)*. Washington, DC: Nuclear Energy Institute.

NEI (2021a). US Nuclear Generating Statistics. Washington, DC: Nuclear Energy Institute. Available at: https://www.nei.org/resources/statistics/us-nuclear-generating-statistics. Retrieved in January 2021

NEI (2021b). Nuclear Provides Carbon-free Energy 24/7. Washington, DC: Nuclear Energy Institute. Available at: https://www.nei.org/fundamentals/nuclear-provides-carbon-free-energy. Retrieved in January 2021

NEI (2021c). Initial License Renewal Filings for US Nuclear Power Plants. Washington, DC: Nuclear Energy Institute. Available at: https://www.nei.org/resources/statistics/us-nuclear-license-renewal-filings Accessed January 29, 2021. Retrieved in January 2021

Nguyen, H-P., Fauriat, W., Zio, E., and Liu, J. (2018). "A Data-Driven Approach for Predicting the Remaining Useful Life of Steam Generators," in 2018 3rd International Conference on System Reliability and Safety (ICSRS). Barcelona, Spain. doi:10.1109/ICSRS.2018.0004910.1109/icsrs.2018.8688716

Paris, P., and Erdogan, F. (1963). A Critical Analysis of Crack Propagation Laws. *J. Basic Eng.* 85, 528–533. doi:10.1115/1.3656900

Park, W. H., Packo, P., and Kundu, T. (2017). Acoustic Source Localization in an Anisotropic Plate without Knowing its Material Properties - A New Approach. *Ultrasonics* 79, 9–17. doi:10.1016/j.ultras.2017.02.021

Peng, B.-S., Xia, H., Liu, Y.-K., Yang, B., Guo, D., and Zhu, S.-M. (2018). Research on Intelligent Fault Diagnosis Method for Nuclear Power Plant Based on Correlation Analysis and Deep Belief Network. *Prog. Nucl. Energ.* 108, 419–427. doi:10.1016/j.pnucene.2018.06.003

Peng, M.-j., Wang, H., Chen, S.-s., Xia, G.-l., Liu, Y.-k., Yang, X., et al. (2018). An Intelligent Hybrid Methodology of On-Line System-Level Fault Diagnosis for Nuclear Power Plant. *Nucl. Eng. Technol.* 50, 396–410. doi:10.1016/j.net.2017.11.014

Pham, B. T., Agarwal, V., Lybeck, N. J., and Tawfik, M. S. (2012). Prognostic Health Monitoring System: Component Selection Based on Risk Criteria and Economic Benefit Assessment. Technical Report, INL/CON-11-23571. Idaho Falls: Idaho National Laboratory.

Power Engineering International (2017). Offline Reactor Costing EDF $1.2m Per Day. Available at: https://www.powerengineeringint.com/decentralized-energy/equipment-technology/offline-reactor-costing-edf-1-2m-per-day/.

Pudil, P., and Somol, P. (2008). Identifying the Most Informative Variables for Decision-Making Problems - a Survey of Recent Approaches and Accompanying Problems. *Aop* 16, 37–55. doi:10.18267/j.aop.131

Qian, Y., Yan, R., and Hu, S. (2014). Bearing Degradation Evaluation Using Recurrence Quantification Analysis and Kalman Filter. *IEEE Trans. Instrum. Meas.* 63, 2599–2610. doi:10.1109/TIM.2014.2313034

Qing, X., Kumar, A., Zhang, C., Gonzalez, I. F., Guo, G., and Chang, F.-K. (2005). A Hybrid Piezoelectric/fiber Optic Diagnostic System for Structural Health Monitoring. *Smart Mater. Struct.* 14, S98–S103. doi:10.1088/0964-1726/14/3/012

Qiu, J., Seth, B. B., Liang, S. Y., and Zhang, C. (2002). Damage Mechanics Approach for Bearing Lifetime Prognostics. *Mech. Syst. Signal Process.* 16, 817–829. doi:10.1006/mssp.2002.1483

Qiu, L., Deng, X., Yuan, S., Huang, Y., and Ren, Y. (2018). Impact Monitoring for Aircraft Smart Composite Skins Based on a Lightweight Sensor Network and Characteristic Digital Sequences. *Sensors* 18, 2218–2227. doi:10.3390/s18072218

Ramuhalli, P., Bond, L. J., Griffin, J. W., Dixit, M., and Henager, C. H. (2010). "A Bayesian Prognostic Algorithm for Assessing Remaining Useful Life of Nuclear Power Components," in Proc. 7th Int. Top. Meet. Nucl. Plant Instrumentation, Control. Human-Machine Interface Technol. (NPIC&HMIT 2010), Las Vegas, NV, USA, 875–886.

Ramuhalli, P., Griffin, J. W., Fricke, J. M., and Bond, L. J. (2012). An Assessment of Uncertainty in Remaining Life Estimation for Nuclear Structural Materials. Proc. 8th Int. Top. Meet. Nucl. Plant Instrumentation, Control. San Diego, CA, USA, 1325–1337.

Ramuhalli, P., Hirt, E. H., Coles, G. A., Bonebrake, C. A., Ivans, W. J., Wootan, D. W., et al. (2014). An Updated Methodology for Enhancing Risk Monitors with Integrated Equipment Condition Assessment. Technical Report, PNNL-23478. Richland, WA: Pacific Northwest National Laboratory. doi:10.2172/1168934

Ramuhalli, P., Veeramany, A., Bonebrake, C. A., Ivans, W. J., Coles, G. A., and Hirt, E. H. (2016). "Evaluation of Enhanced Risk Monitors for Use on Advanced Reactors," in Proc. 24th Int. Conf. Nucl. Eng. Charlotte, NC, USA. doi:10.1115/ICONE24-60040

Ramuhalli, P., Bonebrake, C. A., Dib, G., Roy, S., and Cetiner, S. (2017). "Integration and Assessment of Component Health Prognostics in Supervisory Control Systems," in Proc. 10th Int. Top. Meet. Nucl. Plant Instrumentation, Control Hum. Mach. Interface Technol. (San Francisco, CA, USA, 1423–1431.

Ramuhalli, P., Walker, C., Agarwal, V., and Lybeck, N. J. (2020). Development of Prognostic Models Using Plant Asset Data. Technical Report, ORNL/TM-2020/1697. Oak Ridge, TN: Oak Ridge National Laboratory. doi:10.2172/1661211

Rasmussen, C. E. (2004). *Gaussian Processes in Machine Learning* in *Lect. Notes Comput. Sci.* (Berlin, Heidelberg: Springer), 63–71. doi:10.1007/978-3-540-28650-9_4

Rato, T. J., and Reis, M. S. (2013). Fault Detection in the Tennessee Eastman Benchmark Process Using Dynamic Principal Components Analysis Based on Decorrelated Residuals (DPCA-DR). *Chemometrics Intell. Lab. Syst.* 125, 101–108. doi:10.1016/j.chemolab.2013.04.002

Reinhardt, B., Daw, J., and Tittmann, B. R. (2018). Irradiation Testing of Piezoelectric (Aluminum Nitride, Zinc Oxide, and Bismuth Titanate) and Magnetostrictive Sensors (Remendur and Galfenol). *IEEE Trans. Nucl. Sci.* 65, 533–538. doi:10.1109/TNS.2017.2775163

Ren, J., Ren, R., Green, M., and Huang, X. (2019). A Deep Learning Method for Fault Detection of Autonomous Vehicles. 2019 14th International Conference on Computer Science & Education (ICCSE), August 19-21, 2019, Toronto, ON, Canada. 749–754. doi:10.1109/ICCSE.2019.8845483

Rezaeianjouybari, B., and Shang, Y. (2020). Deep Learning for Prognostics and Health Management: State of the Art, Challenges, and Opportunities. *Measurement* 163, 107929. doi:10.1016/j.measurement.2020.107929

Rodríguez Ramos, A., Domínguez Acosta, C., Rivera Torres, P. J., Serrano Mercado, E. I., Beauchamp Baez, G., Rifón, L. A., et al. (2019). An Approach to Multiple Fault Diagnosis Using Fuzzy Logic. *J. Intell. Manuf* 30, 429–439. doi:10.1007/s10845-016-1256-4

Romero, E., and Sopena, J. M. (2008). Performing Feature Selection With Multilayer Perceptrons. *IEEE Trans. Neural Netw.* 19, 431–441. doi:10.1109/TNN.2007.909535

Saeed, H. A., Peng, M.-j., Wang, H., and Zhang, B.-w. (2020). Novel Fault Diagnosis Scheme Utilizing Deep Learning Networks. *Prog. Nucl. Energ.* 118, 103066. doi:10.1016/j.pnucene.2019.103066

Saeys, Y., Inza, I., and Larranaga, P. (2007). A Review of Feature Selection Techniques in Bioinformatics. *Bioinformatics* 23, 2507–2517. doi:10.1093/bioinformatics/btm344

Saha, B., and Goebel, K. (2008). "Uncertainty Management for Diagnostics and Prognostics of Batteries Using Bayesian Techniques," in 2008 IEEE Aerospace Conference, Big Sky, MT, USA. doi:10.1109/AERO.2008.4526631

Sargentand Lundy, L. L. C. (2018). Nuclear Power Plant Life Extension Cost Development Methodology. Final Report, Project 13527-001. Chicago, IL: Eastern Research Group, Inc., US Environmental Protection Agency.

Saxena, A., Celaya, J., Saha, B., Saha, S., and Goebel, K. (2010). Metrics for Offline Evaluation of Prognostic Performance. *Int. J. Progn Heal Manag.* 1, 1–20. doi:10.36001/ijphm.2010.v1i1.1336

Setiono, R., and Liu, H. (1997). Neural-network Feature Selector. *IEEE Trans. Neural Netw.* 8, 654–662. doi:10.1109/72.572104

Severson, K., Chaiwatanodom, P., and Braatz, R. D. (2016). Perspectives on Process Monitoring of Industrial Systems. *Annu. Rev. Control.* 42, 190–200. doi:10.1016/j.arcontrol.2016.09.001

Sharma, T., Je, S.-S., Gill, B., and Zhang, J. X. J. (2012). Patterning Piezoelectric Thin Film PVDF-TrFE Based Pressure Sensor for Catheter Application. *Sensors Actuators A: Phys.* 177, 87–92. doi:10.1016/j.sna.2011.08.019

Shetgaonkar, S. S. (2017). Fault Diagnosis in Induction Motor Using Fuzzy Logic. 2017 International Conference on Computing Methodologies and Communication (ICCMC), July 18-19, 2017, Erode, India, 289–293. doi:10.1109/ICCMC.2017.8282693

Shi, Z., and Chehade, A. (2021). A Dual-LSTM Framework Combining Change point Detection and Remaining Useful Life Prediction. *Reliability Eng. Syst. Saf.* 205, 107257. doi:10.1016/j.ress.2020.107257

Shin, S. M., Choi, B. H., and Kang, H. G. (2016). Motor Health Monitoring at Standstill Through Impedance Analysis. *IEEE Trans. Ind. Electron.* 63, 4422–4431. doi:10.1109/TIE.2016.2541089

Si, L., and Baier, H. (2015). Real-time Impact Visualization Inspection of Aerospace Composite Structures with Distributed Sensors. *Sensors* 15, 16536–16556. doi:10.3390/s150716536

Si, X.-S., Wang, W., Hu, C.-H., and Zhou, D.-H. (2011). Remaining Useful Life Estimation - A Review on the Statistical Data Driven Approaches. *Eur. J. Oper. Res.* 213, 1–14. doi:10.1016/j.ejor.2010.11.018

Somol, P., Pudil, P., Novovičová, J., and Paclı́k, P. (1999). Adaptive Floating Search Methods in Feature Selection. *Pattern Recognition Lett.* 20, 1157–1163. doi:10.1016/S0167-8655(99)00083-5

Spasojevic, D., Bukvic, S., Milosevic, S., and Stanley, H. E. (1996). Barkhausen Noise: Elementary Signals, Power Laws, and Scaling Relations. *Phys. Rev. E Stat. Phys. Plasmas Fluids Relat. Interdiscip. Top.* 54, 2531–2546. doi:10.1103/physreve.54.2531

Stefanita, C.-G. (2008). *From Bulk to Nano: The Many Sides of Magnetism*, 117. Springer Berlin Heidelberg. doi:10.1007/978-3-540-70548-2

Stefatos, G., and Ben Hamza, A. (2010). Dynamic Independent Component Analysis Approach for Fault Detection and Diagnosis. *Expert Syst. Appl.* 37, 8606–8617. doi:10.1016/j.eswa.2010.06.101

Sun, B., Shengkui Zeng, S., Kang, R., and Pecht, M. (2010). "Benefits Analysis of Prognostics in Systems," in 2010 Prognostics and System Health Management Conference. Macao, China. doi:10.1109/PHM.2010.5413503

Sun, B., Jiang, X., Ye, T., and Feng, Q. (2016). A Novel Concept and Assessment Method for Trustworthiness of Prognostics. *Adv. Mech. Eng.* 8, 168781401663880–10. doi:10.1177/1687814016638807

Sutharssan, T., Stoyanov, S., Bailey, C., and Yin, C. (2015). Prognostic and Health Management for Engineering Systems: a Review of the Data-driven Approach and Algorithms. *J. Eng.* 2015, 215–222. doi:10.1049/joe.2014.0303

Tagaris, T., Ioannou, G., Sdraka, M., Alexandridis, G., and Stafylopatis, A. (2019). "Putting Together Wavelet-Based Scaleograms and Convolutional Neural Networks for Anomaly Detection in Nuclear Reactors," in ICAAI 2019: Proceedings of the 2019 3rd International Conference on Advances in Artificial Intelligence, New York, NY, USA, 237–43. doi:10.1145/3369114.3369121

Taheri, E., Kolmanovsky, I., and Gusikhin, O. (2019). Survey of Prognostics Methods for Condition-Based Maintenance in Engineering Systems. arXiv: 1912.02708.

Takahashi, T., and Matsumoto, E. (2009). Measurement and Simulation of Detection of Defects on Inner wall of Cylindrical Pipe by Piezoelectric High-Polymer Film. Proc. 6th Annu. Meet. Japan Soc. Maintenology, Sapporo. Hokkaido, Japan, 409–12.

Thrun, S., Montemerlo, M., Dahlkamp, H., Stavens, D., Aron, A., Diebel, J., et al. (2006). Stanley: The Robot that Won the DARPA Grand Challenge. *J. Field Robotics* 23, 661–692. doi:10.1002/rob.20147

Tolo, S., Tian, X., Bausch, N., Becerra, V., Santhosh, T. V., Vinod, G., et al. (2019). Robust On-Line Diagnosis Tool for the Early Accident Detection in Nuclear Power Plants. *Reliability Eng. Syst. Saf.* 186, 110–119. doi:10.1016/j.ress.2019.02.015

US DOE (2019). Infographic - Capacity Factor by Energy Source. Washington, DC: US Department of Energy, Office of Nuclear Energy. Available at: https://www.energy.gov/ne/downloads/infographic-capacity-factor-energy-source-2019.

US DOE (2020a). What's the Lifespan for a Nuclear Reactor? Much Longer Than You Might Think. Washington, DC: US Department of Energy, Office of Nuclear Energy. Available at: https://www.energy.gov/ne/articles/whats-lifespan-nuclear-reactor-much-longer-you-might-think.

US DOE (2020b). NRC Approves First US Small Modular Reactor Design. Washington, DC: US Department of Energy, Office of Nuclear Energy. Available at: https://www.energy.gov/ne/articles/nrc-approves-first-us-small-modular-reactor-design

US DOE (2020c). First US Small Modular Boiling Water Reactor Under Development. Washington, DC: US Department of Energy, Office of Nuclear Energy. Available at: https://www.energy.gov/ne/articles/first-us-small-modular-boiling-water-reactor-under-development.

US DOE (2020d). US Department of Energy Announces $160 Million in First Awards under Advanced Reactor Demonstration Program. Washington, DC: US Department of Energy, Office of Nuclear Energy. Available at: https://www.energy.gov/ne/articles/us-department-energy-announces-160-million-first-awards-under-advanced-reactor.

US EIA (2021a). Nuclear and Coal Will Account for Majority of US Generating Capacity Retirements in 2021. Washington, DC: US Energy Information Administration. Available at: https://www.eia.gov/todayinenergy/detail.php?id=46436.

US EIA (2021b). How Old Are US Nuclear Power Plants, and when Was the Newest One Built? US Energy Information Administration. Available at: https://www.eia.gov/tools/faqs/faq.php?id=228&t=21. Retrieved in January 2021.

US EIA (2021c). Nuclear Explained: US Nuclear Industry. Washington, DC: US Energy Information Administration. Available at: https://www.eia.gov/energyexplained/nuclear/us-nuclear-industry.php . Retrieved in January 2021.

US NRC (1995). Requirements for Renewal of Operating Licenses for Nuclear Power Plants. 10 CFR 54. Final Rule. Available at: https://www.nrc.gov/reading-rm/doc-collections/cfr/part054/full-text.html Accessed January 29, 2021

US NRC (2021a). Status of Initial License Renewal Applications and Industry Initiatives. Washington, DC: US Nuclear Regulatory Commission. Available at: https://www.nrc.gov/reactors/operating/licensing/renewal/applications.html. Retrieved in January 2021.

US NRC (2021b). Status of Subsequent License Renewal Applications. Washington, DC: US Nuclear Regulatory Commission. Available at: https://www.nrc.gov/

reactors/operating/licensing/renewal/subsequent-license-renewal.html. Retrieved in January 2021.

US NRC (2021c). § 50.65 Requirements for Monitoring the Effectiveness of Maintenance at Nuclear Power Plants. US Nuclear Regulatory Commission. Available at: https://www.nrc.gov/reading-rm/doc-collections/cfr/part050/part050-0065.html. Retrieved in January 2021.

US NRC (2021d). § 50.55a Codes and Standards. US Nuclear Regulatory Commission. Available at: https://www.nrc.gov/reading-rm/doc-collections/cfr/part050/part050-0055a.html. Retrieved in January 2021.

Venkatasubramanian, V. (2005). Prognostic and Diagnostic Monitoring of Complex Systems for Product Lifecycle Management: Challenges and Opportunities. *Comput. Chem. Eng.* 29, 1253–1263. doi:10.1016/j.compchemeng.2005.02.026

Verikas, A., and Bacauskiene, M. (2002). Feature Selection with Neural Networks. *Pattern Recognition Lett.* 23, 1323–1335. doi:10.1016/S0167-8655(02)00081-8

Vogl, G. W., Weiss, B. A., and Donmez, M. A. (2014). Standards for Prognostics and Health Management (PHM) Techniques within Manufacturing Operations. *Proc. Annu. Conf. Progn. Heal. Manag. Soc*. Fort Worth, TX, USA.

Vogl, G. W., Weiss, B. A., and Helu, M. (2019). A Review of Diagnostic and Prognostic Capabilities and Best Practices for Manufacturing. *J. Intell. Manuf* 30, 79–95. doi:10.1007/s10845-016-1228-8

Wadhwa, N., Peng, B., Yang, B., Zhu, S., Zhang, J., et al. (2021). A Multi-Stage Hybrid Fault Diagnosis Approach for Operating Conditions of Nuclear Power Plant. *Ann. Nucl. Energ.* 153, 108015. doi:10.1016/j.anucene.2020.108015

Wang, X., Song, T., Gong, F., and Zheng, P. (2016). On the Computational Power of Spiking Neural P Systems with Self-Organization. *Sci. Rep.* 6, 27624. doi:10.1038/srep27624

Wang, Y., Liu, Y., Khan, F., and Imtiaz, S. (2017). Semiparametric PCA and Bayesian Network Based Process Fault Diagnosis Technique. *Can. J. Chem. Eng.* 95, 1800–1816. doi:10.1002/cjce.22829

Wang, Y., Yang, H., Yuan, X., and Cao, Y. (2018). An Improved Bayesian Network Method for Fault Diagnosis. *IFAC-PapersOnLine* 51, 341–346. doi:10.1016/j.ifacol.2018.09.443

Wang, J., Peng, H., Yu, W., Ming, J., Pérez-Jiménez, M. J., Tao, C., et al. (2019). Interval-valued Fuzzy Spiking Neural P Systems for Fault Diagnosis of Power Transmission Networks. *Eng. Appl. Artif. Intelligence* 82, 102–109. doi:10.1016/j.engappai.2019.03.014

Wang, H., Peng, M.-j., Wesley Hines, J., Zheng, G.-y., Liu, Y.-k., and Upadhyaya, B. R. (2019). A Hybrid Fault Diagnosis Methodology with Support Vector Machine and Improved Particle Swarm Optimization for Nuclear Power Plants. *ISA Trans.* 95, 358–371. doi:10.1016/j.isatra.2019.05.016

Wang, B., Lei, Y., Li, N., and Yan, T. (2019). Deep Separable Convolutional Network for Remaining Useful Life Prediction of Machinery. *Mech. Syst. Signal Process.* 134, 106330. doi:10.1016/j.ymssp.2019.106330

Wang, Y., He, M., Sun, L., Wu, D., Wang, Y., and Zou, L. (2020). Improved Kalman Filtering-Based Information Fusion for Crack Monitoring Using Piezoelectric-Fiber Hybrid Sensor Network. *Front. Mater.* 7, 300. doi:10.3389/fmats.2020.00300

Wang, Y., Zhao, Y., and Addepalli, S. (2020). Remaining Useful Life Prediction Using Deep Learning Approaches: A Review. *Proced. Manufacturing* 49, 81–88. doi:10.1016/j.promfg.2020.06.015

Wang, Z., Xia, H., Peng, B., Yang, B., Zhu, S., Zhang, J., et al. (2021). A Multi-Stage Hybrid Fault Diagnosis Approach for Operating Conditions of Nuclear Power Plant. *Ann. Nucl. Energ.* 153, 108015. doi:10.1016/j.anucene.2020.108015

Wood, R. T., Upadhyaya, B. R., and Floyd, D. C. (2017). An Autonomous Control Framework for Advanced Reactors. *Nucl. Eng. Technol.* 49, 896–904. doi:10.1016/j.net.2017.07.001

Wu, Z., Qing, X. P., and Chang, F-K. (2009). Damage Detection for Composite Laminate Plates with A Distributed Hybrid PZT/FBG Sensor Network. *J. Intell. Mater. Syst. Struct.* 20, 1069–77. doi:10.1177/1045389X08101632

Wu, C., Zhu, C., and Ge, Y. (2017). A New Fault Diagnosis and Prognosis Technology for High-Power Lithium-Ion Battery. *IEEE Trans. Plasma Sci.* 45, 1533–1538. doi:10.1109/TPS.2017.2706088

Wu, G., Tong, J., Zhang, L., Zhao, Y., and Duan, Z. (2018). Framework for Fault Diagnosis with Multi-Source Sensor Nodes in Nuclear Power Plants Based on a Bayesian Network. *Ann. Nucl. Energ.* 122, 297–308. doi:10.1016/j.anucene.2018.08.050

Wu, Y., Yuan, M., Dong, S., Lin, L., and Liu, Y. (2018). Remaining Useful Life Estimation of Engineered Systems Using Vanilla LSTM Neural Networks. *Neurocomputing* 275, 167–179. doi:10.1016/j.neucom.2017.05.063

Xin, M., Jiao, W., and Da-zi, L. (2019). Fault Diagnosis of Nuclear Power Plant Based on Simplified Signed Directed Graph with Principal Component Analysis and Support Vector Machine. *Proc. 2019 Chin. Autom. Congr.*, Hangzhou, China, 3082–3087. doi:10.1109/CAC48633.2019.8997001

Xu, Z., King, I., Lyu, M. R., and Jin, R. (2010). Discriminative Semi-supervised Feature Selection via Manifold Regularization. *IEEE Trans. Neural Netw.* 21, 1033–47. doi:10.1109/TNN.2010.2047114

Xu, X., Yan, X., Sheng, C., Yuan, C., Xu, D., and Yang, J. (2017). A Belief Rule-Based Expert System for Fault Diagnosis of Marine Diesel Engines. *IEEE Trans. Syst. Man. Cybern, Syst.* 50, 1–17. doi:10.1109/TSMC.2017.2759026

Xu, B., Li, H., Pang, W., Chen, D., Tian, Y., Lei, X., et al. (2019). Bayesian Network Approach to Fault Diagnosis of a Hydroelectric Generation System. *Energy Sci Eng* 7, 1669–1677. doi:10.1002/ese3.383

Yadav, V., Agarwal, V., Gribok, A. V., and Smith, C. L. (2018). Modelling Component Failure Rates Utilizing Sensor-Based Degradation Data. Proc. 14th Probabilistic Saf. Assess. Manag. Conf. Los Angeles, CA, USA.

Yan, H., Xu, Y., Cai, F., Zhang, H., Zhao, W., and Gerada, C. (2019). PWM-VSI Fault Diagnosis for a PMSM Drive Based on the Fuzzy Logic Approach. *IEEE Trans. Power Electron.* 34, 759–768. doi:10.1109/TPEL.2018.2814615

Yang, J., and Ong, C.-J. (2011). Feature Selection Using Probabilistic Prediction of Support Vector Regression. *IEEE Trans. Neural Networks* 22, 954–62. doi:10.1109/TNN.2011.2128342

Yang, R., and Rizzoni, G. (2016). Comparison of Model Based vs. Data-Driven Methods for Fault Detection and Isolation in Engine Idle Speed Control System. *Proc. Annu. Conf. Progn. Heal. Manag. Soc.* 7, 25–33. doi:10.36001/phmconf.2016.v8i1.2502

Yang, Q. (2004). Model-based and Data Driven Fault Diagnosis Methods with Applications to Process Monitoring. Ph.D. Thesis. Cleveland, OH: Case Western Reserve University.

Ye, Z.-S., and Xie, M. (2015). Stochastic Modelling and Analysis of Degradation for Highly Reliable Products. *Appl. Stochastic Models Bus. Ind.* 31, 16–32. doi:10.1002/asmb.2063

Yildiz, B. (2003). Development of a Hybrid Intelligent System for On-Line Real-Time Monitoring of Nuclear Power Plant Operations. Ph.D. Thesis. MIT.

Yu, W., and Zhao, C. (2019). Online Fault Diagnosis for Industrial Processes With Bayesian Network-Based Probabilistic Ensemble Learning Strategy. *IEEE Trans. Automat. Sci. Eng.* 16, 1922–1932. doi:10.1109/TASE.2019.2915286

Yu, D., Chen, Z. M., Xiahou, K. S., Li, M. S., Ji, T. Y., and Wu, Q. H. (2018). A Radically Data-Driven Method for Fault Detection and Diagnosis in Wind Turbines. *Int. J. Electr. Power Energ. Syst.* 99, 577–584. doi:10.1016/j.ijepes.2018.01.009

Yu, S.-Z. (2010). Hidden Semi-Markov Models. *Artif. Intelligence* 174, 215–243. doi:10.1016/j.artint.2009.11.011

Yu, J. (2012). A Nonlinear Kernel Gaussian Mixture Model Based Inferential Monitoring Approach for Fault Detection and Diagnosis of Chemical Processes. *Chem. Eng. Sci.* 68, 506–519. doi:10.1016/j.ces.2011.10.011

Yucesan, Y. A., and Viana, F. A. C. (2020). A Physics-Informed Neural Network for Wind Turbine Main Bearing Fatigue. *Int. J. Progn Heal Manag.* 11, 1–17. doi:10.36001/ijphm.2020.v11i1.2594

Zhang, X., Wu, G., Dong, Z., and Crawford, C. (2015). Embedded Feature-Selection Support Vector Machine for Driving Pattern Recognition. *J. Franklin Inst.* 352, 669–685. doi:10.1016/j.jfranklin.2014.04.021

Zhang, X., Qiu, D., and Chen, F. (2015). Support Vector Machine with Parameter Optimization by a Novel Hybrid Method and its Application to Fault Diagnosis. *Neurocomputing* 149, 641–651. doi:10.1016/j.neucom.2014.08.010

Zhang, J., Wang, P., Yan, R., and Gao, R. X. (2018). Long Short-Term Memory for Machine Remaining Life Prediction. *J. Manufacturing Syst.* 48, 78–86. doi:10.1016/j.jmsy.2018.05.011

Zhao, X., and Golay, M. (2020). Symptom-Based Conditional Failure Probability Estimation for Selected Structures, Systems, and Components. Technical Report, MIT-ANP-TR-188. doi:10.13140/RG.2.2.26898.58569

Zhao, Y., Di Maio, F., Zio, E., Zhang, Q., Dong, C.-L., and Zhang, J.-Y. (2017). Optimization of a Dynamic Uncertain Causality Graph for Fault Diagnosis in Nuclear Power Plant. *Nucl. Sci. Tech.* 28, 34. doi:10.1007/s41365-017-0184-0

Zhao, R., Yan, R., Wang, J., and Mao, K. (2017). Learning to Monitor Machine Health with Convolutional Bi-Directional LSTM Networks. *Sensors* 17, 273. doi:10.3390/s17020273

Zhao, R., Wang, D., Yan, R., Mao, K., Shen, F., and Wang, J. (2018). Machine Health Monitoring Using Local Feature-Based Gated Recurrent Unit Networks. *IEEE Trans. Ind. Electron.* 65, 1539–1548. doi:10.1109/TIE.2017.2733438

Zhao, X., Shirvan, K., Salko, R. K., and Guo, F. (2020). On the Prediction of Critical Heat Flux Using a Physics-Informed Machine Learning-Aided Framework. *Appl. Therm. Eng.* 164, 114540. doi:10.1016/j.applthermaleng.2019.114540

Zhao, Y., Tong, J., Zhang, L., and Wu, G. (2020). Diagnosis of Operational Failures and On-Demand Failures in Nuclear Power Plants: An Approach Based on Dynamic Bayesian Networks. *Ann. Nucl. Energ.* 138, 107181. doi:10.1016/j.anucene.2019.107181

Zhou, T., Droguett, E. L., and Modarres, M. (2020). A Common Cause Failure Model for Components under Age-Related Degradation. *Reliability Eng. Syst. Saf.* 195, 106699. doi:10.1016/j.ress.2019.106699

Zhu, J., Chen, N., and Peng, W. (2019). Estimation of Bearing Remaining Useful Life Based on Multiscale Convolutional Neural Network. *IEEE Trans. Ind. Electron.* 66, 3208–3216. doi:10.1109/TIE.2018.2844856

Zio, E., Baraldi, P., and Pedroni, N. (2006). Selecting Features for Nuclear Transients Classification by Means of Genetic Algorithms. *IEEE Trans. Nucl. Sci.* 53, 1479–1493. doi:10.1109/TNS.2006.873868

Conflict of Interest: The authors declare that the research was conducted in the absence of any commercial or financial relationships that could be construed as a potential conflict of interest.

GLOSSARY

ADC analog-to-digital converter
AI artificial intelligence
ANN artificial neural network
BN Bayesian network
BWR boiling water reactor
CBM condition-based maintenance
CFR *Code of Federal Regulations*
CM condition monitoring
C-MAPSS commercial modular aero-propulsion system simulation
CNN convolutional neural network
DBN dynamic Bayesian network
DES discrete event system
DL deep learning
DOE Department of Energy (US)
DP dynamic programming
DT digital twin
ENN Elman neural network
ERM enhanced risk monitor
FBG fiber Bragg grating
FDA Fisher discriminant analysis
FFNN feed-forward neural network
FWCS feedwater and condensate system
GHG greenhouse gas
GMM Gaussian mixture model
GPR Gaussian process regression
GRU gated recurrent unit
I&C instrumentation and control
ICA independent component analysis
IEA International Energy Agency
IEEE Institute of Electrical and Electronics Engineers
ISO International Organization for Standardization
LMI laser-based mechanical impedance
LSTM long short-term memory
LTO long-term operation
LWR light water reactor
MAE magneto acoustic emission
MBN magnetic Barkhausen noise
MDP Markov decision process
ML machine learning
NAMAC nearly autonomous management and control
NEA Nuclear Energy Agency
NF neuro-fuzzy
NPP nuclear power plant
NRC Nuclear Regulatory Commission (US)
O&M operations & maintenance
OP operating procedure
PCA principal component analysis
PHM prognostics and health management
PLS partial least squares
POF probability of failure
POMDP partially observable Markov decision process
PRA probabilistic risk assessment
PWAS piezoelectric wafer active sensor
PZT piezoelectric
RBF radial basis function
RNN recurrent neural network
RPV reactor pressure vessel
RUL remaining useful life
SCS supervisory control system
SMR small modular reactor
SNN spiking neural network
SSC structure, system, and component
SVM support vector machine
US United States
V&V verification and validation

frontiers in Energy Research

ORIGINAL RESEARCH
published: 01 July 2021
doi: 10.3389/fenrg.2021.665502

Distributed Fault Diagnosis Framework for Nuclear Power Plants

*Wu Guohua[1,2], Duan Zhiyong[3], Yuan Diping[1], Yin Jiyao[1], Liu Caixue[3] and Ji Dongxu[4]**

[1] Information and Monitoring Center, Shenzhen Urban Public Safety and Technology Institute, Shenzhen, China, [2] Harbin Institute of Technology, Shenzhen, China, [3] Nuclear Power Institute of China, Chengdu, China, [4] School of Science and Engineering, Chinese University of Hong Kong, Shenzhen, China

A fault diagnosis can quickly and accurately diagnose the cause of a fault. Focusing on the characteristics of nuclear power plants (NPPs), this study proposes a distributed fault diagnosis method based on a back propagation (BP) neural network and decision tree reasoning. First, the fault diagnosis was carried out using the BP neural network and decision tree reasoning, and then a global fusion diagnosis was performed by fusing the resulting information. Second, the key technologies of the BP neural network and decision tree sample construction were studied. Finally, the simulation results show that the proposed distributed fault diagnosis system is highly reliable and has strong diagnostic ability, enabling efficient and accurate diagnoses to be realized. The distributed fault diagnosis system for NPPs provides a solid foundation for future research.

Keywords: nuclear power plants, distributed fault diagnosis, BP neural network, decision tree, information fusion

OPEN ACCESS

Edited by:
Xianping Zhong,
University of Pittsburgh, United States

Reviewed by:
Xingang Zhao,
Oak Ridge National Laboratory (DOE), United States
Zhegang Ma,
Idaho National Laboratory (DOE), United States
Jiankai Yu,
Massachusetts Institute of Technology, United States

****Correspondence:***
Ji Dongxu
jidongxu@cuhk.edu.cn

Specialty section:
This article was submitted to Nuclear Energy, a section of the journal Frontiers in Energy Research

Received: *08 February 2021*
Accepted: *16 April 2021*
Published: *01 July 2021*

Citation:
Guohua W, Zhiyong D, Diping Y, Jiyao Y, Caixue L and Dongxu J (2021) Distributed Fault Diagnosis Framework for Nuclear Power Plants. Front. Energy Res. 9:665502. doi: 10.3389/fenrg.2021.665502

INTRODUCTION

Nuclear power plants (NPPs) produce a large number of monitoring signals. For example, a typical alarm system has nearly 2,000 alarms (Mo et al., 2007). This complexity increases the difficulty of judging the current state of the NPP. With the application of digital instrumentation and control systems, this scenario becomes more obvious. This study focuses on how to improve the NPP intelligence. The operational support (Wang et al., 2016; Peng et al., 2018), fault prediction and health management (Li et al., 2018; Fan et al., 2019), and nuclear accident emergency decision-making (Zhao et al., 2015; Zhao, 2016) are the key parts of NPP intelligence. At the same time, the fault diagnosis can be used to obtain key signals from a large amount of data, allowing the current operation state of the NPP to be determined. This is the key technology for improving the NPP intelligence (see **Figure 1**) (Elnokity et al., 2012).

Many fault diagnosis methods for the NPPs have been developed, including those based on neural networks (Seker et al., 2003; Mo et al., 2007; Hadad et al., 2011), Bayesian networks (Friedman et al., 2017; Gheisari and Meybodi, 2017; Li et al., 2018), dynamic uncertainty causal graphs (Zhou and Zhang, 2017), and signed directed graphs (Liu et al., 2016). The fault diagnosis can be divided into data-driven, signal processing, and model-based methods (see **Figure 2**) (Ma and Jiang, 2011). The data-driven methods rely on a data model to obtain the fault state and often use neural networks or principal component analysis (Hines and Garvey, 2007; Li et al., 2017). The signal-based methods operate in the time domain and employ techniques such as wavelet analysis, time–frequency analysis, and spectral analysis (Ma and Jiang, 2011). There are two main approaches for the model-based fault diagnosis. One approach is based on the use of an expert knowledge, e.g., expert systems (Kramer and Palowitch, 1987; Vila-Francés et al., 2013). The other approach is based on a graph theory, i.e., the model graphically displays relationships between various parameters and faults, such as in

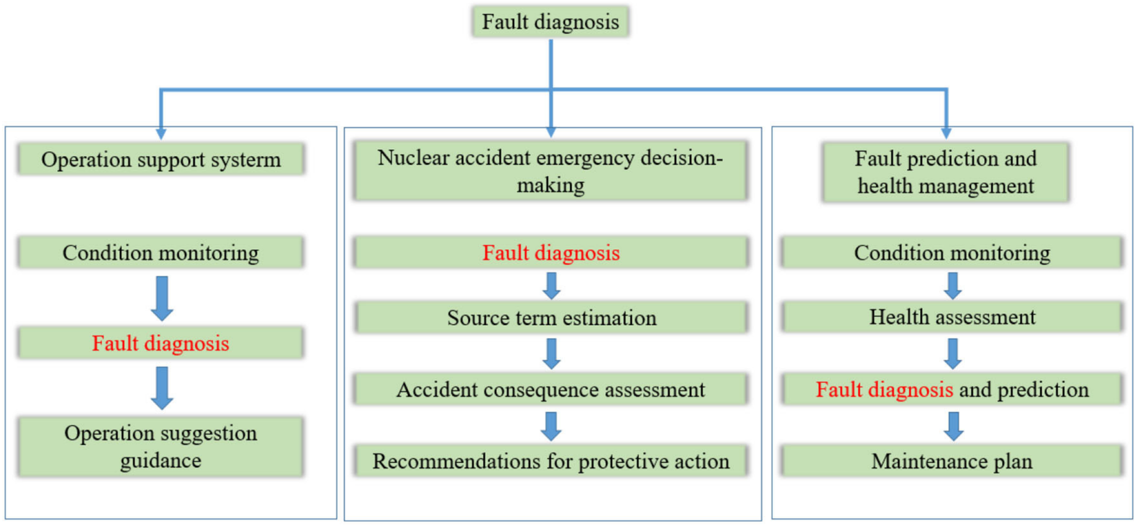

FIGURE 1 | Application of fault diagnosis in Nuclear power plants (NPPs).

a Bayesian network (Kang and Golay, 1999; Li and Ueno, 2017; Li et al., 2017; Li and Mahadevan, 2018), first principle model (Pantelides and Renfro, 2013), signed directed graph (Liu et al., 2016), and uncertain causality graph (Khakzad et al., 2011).

In the early application of fault diagnosis, the expert systems were mainly used to identify faults through the reasoning between specific parameters and the associated faults (Marseguerra et al., 2003). With the advancement in research, the data-driven methods have gradually become more popular for fault diagnosis, such as neural networks and principal component analysis (Embrechts and Benedek, 2004; Liu et al., 2014). Although the data-driven approach can quickly and accurately find the relationship between the data and fault diagnosis, it is a "black box" tool, meaning that it is difficult to determine the relationship between the system parameters and the signs of a fault (Zhu et al., 2006). Due to extensive study in the data-driven methods, the fault diagnosis has started to adopt the knowledge map approach (see **Figure 3**). However, with the application of knowledge graph, it is difficult to obtain a complex model of NPPs. Therefore, this study seeks machine learning of threshold method (less data dependence) to complete the fault diagnosis.

The NPPs are complex industrial systems in which each piece of equipment or subsystem completes the own task. Based on the function and structure of NPPs, they can be described as typical distributed systems. The various fault mechanisms of NPPs mean that the traditional methods struggle to complete fault diagnosis. The distributed diagnosis method takes into account the characteristics of the system and decomposes the complex fault diagnosis task into simple subsystems. Each subsystem uses an appropriate method and knowledge to solve the task. Finally, the diagnosis results for the subsystem were calculated by a process known as information fusion to provide the operator with a decision (Liu et al., 2016). This diagnosis strategy (as shown in **Figure 4**) has been widely used for fault diagnosis in large-scale complex systems in the aerospace and chemical industries, among many others (Liu et al., 2014).

The main problems with fault diagnosis in complex systems, such as NPPs, are as follows:

(1) The problems mainly include the complexity of the diagnosis, the limitation of the diagnosis method, and the uncertainties associated with the relevant knowledge. The existing models cannot accurately and quickly express the relationship in terms of the parameter coupling and uncertainties. This directly affects the reliability of the diagnosis results. It is difficult to construct a complete and accurate model that effectively expresses the relationships involved in the system.

In this study, the relationship between parameters is obtained by a neural network, and the complex NPP system is decomposed by a distributed neural network. The relationship between models is simplified by the distributed neural network. The proposed method then uses information fusion to improve the accuracy of fault diagnosis.

(2) The parameters involved in the accident initially change very slowly. Obtaining key information plays a very important role in fault diagnosis. The parameters of the accident change slowly in the early stages and do not exceed their thresholds. Since these weak parameter changes caused by the fault are difficult to identify, it is difficult to achieve early fault diagnosis. For example, in the early stages of accidents involving the loss of coolant, the parameters such as the containment pressure and temperature slowly rise/fall (without exceeding their thresholds), and it is difficult to identify the early signals. Thus, this study describes the generation of samples for machine learning from the trends of these parameters, which enables the speed of diagnosis to be enhanced.

Fault diagnosis, as a form of artificial intelligence (i.e., pattern recognition), is a critical and complex part of technology.

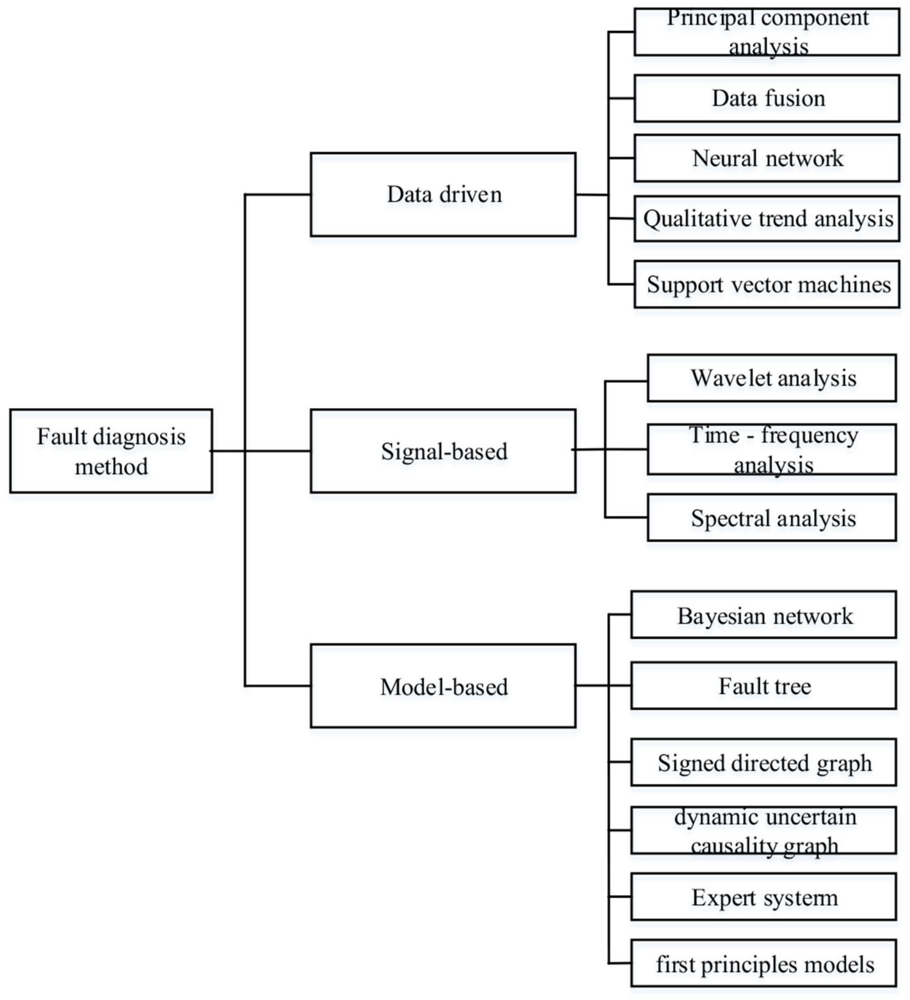

FIGURE 2 | Classification of common fault diagnosis methods.

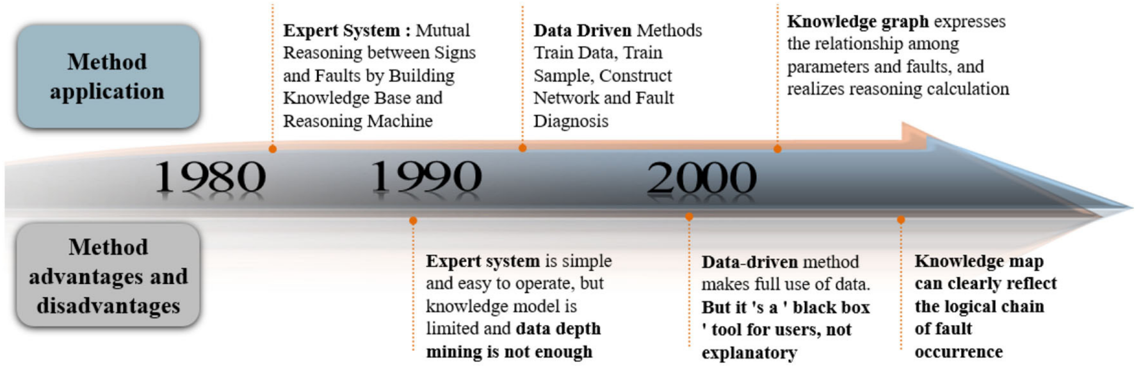

FIGURE 3 | Development history of NPP fault diagnosis methods.

This study focuses on the engineering and technical problems encountered in fault diagnosis with the aim of satisfying the real-time and accuracy requirements of diagnosis in NPPs. The method and results reported in this study will be of great significance in the further improvement of the NPP fault diagnosis.

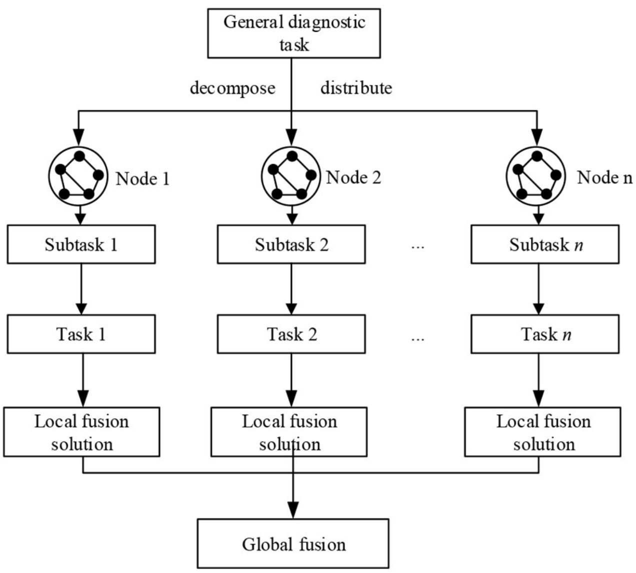

FIGURE 4 | Logic diagram of distributed fault diagnosis.

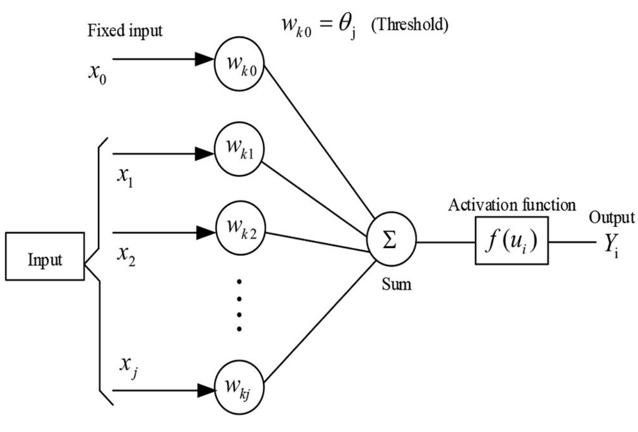

FIGURE 5 | Basic structure of a single-layer neural network.

ARTIFICIAL NEURAL NETWORK

The basic units of neural networks are called artificial neurons. The artificial neurons are models of biological nerves and are generally divided into an input, an output, and an activation function. The structure of these neurons is shown in **Figure 5** (Mo et al., 2007).

The inputs can be considered as data and they are processed by the neurons to simulate the artificial neurons. The relationship between the quantities in **Figure 5** is as follows:

$$u_i = \sum_j w_{ij} x_j + \theta_j \tag{1}$$

$$Y_i = f(u_i), \tag{2}$$

where x_j is the input signal, w is the internal structure of the neuron, u_i is the connection weight (i.e., the binding strength), θ_j is the threshold, $f(u_i)$ is an activation function, and Y_i is the output signal. The activation function acts as a linear or non-linear function. The structure of the neural network is explained in the following subsections.

Back Propagation Neural Network

Back propagation (BP) neural networks use a multi-layer feed forward structure for machine learning. The standard three-layer network structure is shown in **Figure 6** (Rohde et al., 2011).

The BP learning is divided into two parts: forward propagation and pre-propagation. The output of forward propagation in each layer is transmitted only to the neurons in the next layer. If the output layer cannot attain the desired output, it will transfer data through backpropagation and then modify the input connection weights of the neurons until the error reached the required degree of accuracy.

The principle of the BP neural network is through input and the hidden layer get output. Then the error between the actual output and the output is calculated, and the error function is used to adjust the connection weights between the layers of the network and the threshold of the neurons. When the error requirements are met, the relationship between input and output is established, so this method can be used to solve problems such as pattern recognition and classification (Liu et al., 2015).

Neural Network for Fault Diagnosis

To realize fault diagnosis in NPPs, first it is necessary to obtain data to process the samples and then apply machine learning to the samples to obtain a neural network diagnosis model. After the training model has been obtained, when the data undergo processing for input to the neural network, output is the type of fault. A diagnosis flowchart is shown in **Figure 7**.

Sample Construction Using Thresholds and Trends

The training samples are constructed according to the trend of the parameters. The trend is specified as either "rising," "declining," or "normal." This method can identify abnormalities before the parameters reach their thresholds. However, some parameters also exhibit upward or downward trends when the NPP is in normal operation. Therefore, we must consider the normal fluctuation range of the parameters.

Combined with the operation data from an NPP simulator, the changes in parameters can be analyzed. For different operating conditions, we can modify the normal values and the upper and lower bounds of the parameter fluctuations. This method not only reduces the difficulty of neural network training but also solves the problem of BP network diagnosis in different conditions.

As shown in **Figure 8**, a value of 0.75 represents the situation when a parameter rises and exceeds the upper limit of normal fluctuation, or when the parameter exceeds the upper threshold. This threshold reduces the size of the BP sample. A parameter that is decreasing and falls below the lower limit of normal fluctuation is represented by a value of 0.25. The scenario in

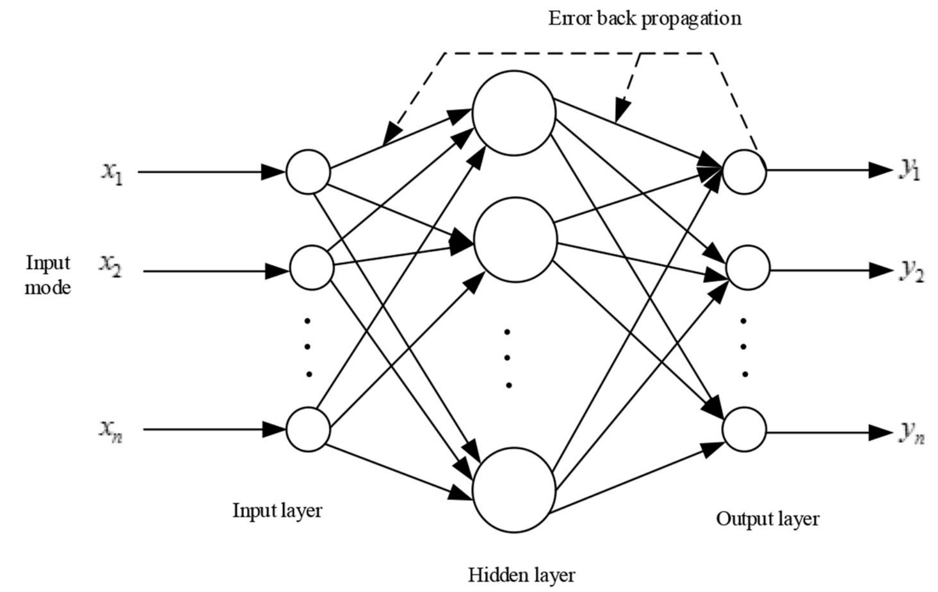

FIGURE 6 | Back propagation (BP) network model.

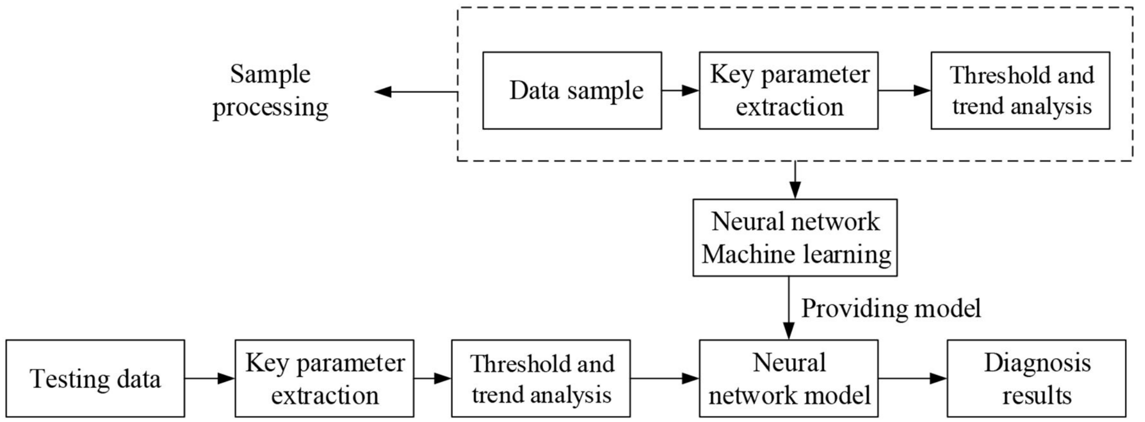

FIGURE 7 | Framework of neural network for fault diagnosis.

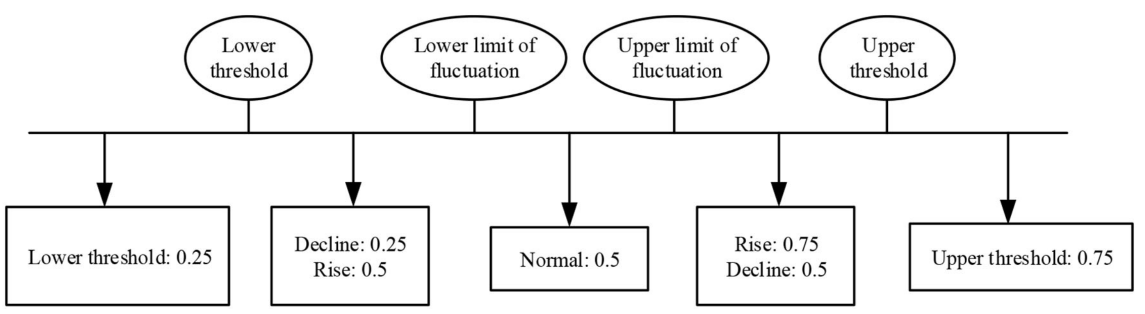

FIGURE 8 | Parameter status division and representation.

which a parameter is falling, but still exceeds the upper limit of normal fluctuation, is expressed by a value of 0.5 as shown in **Figure 8**. This can be understood as the parameter approaching the normal range. Similarly, a parameter that is below the lower limit of fluctuation but is increasing is represented by a value of 0.5, as shown in **Table 1**.

TABLE 1 | Parameter thresholds combined with trends for sample construction.

Sample input (parameters)				Sample output (fault type)		
WFWA	WFWB	LSGA	LSGB	LOFWP	FIVA	FIVB
0.5	0.5	0.5	0.5	0	0	0
0	0	0.25	0.25	1	0	0
0	0.75	0.25	0.5	0	1	0
0.75	0	0.5	0.25	0	0	1

WFWA, No. 1 steam generator feed water flow; WFWB, No. 2 steam generator feed water flow; LSGA, wide range water level of steam generator No. 1; LSGB, wide range water level of steam generator No. 2; LOFWP, loss of main feed pump, FIVA, No. 1 steam generator feed valve is wrongly closed; and FIVB, No. 2 steam generator feed valve is wrongly closed.

DECISION TREE FOR FAULT DIAGNOSIS

Theory

A decision tree is a tree structure that is used to classify data records. A leaf node of this tree represents a record set. The tree is established according to the different values of the available data. By establishing nodes and branches, a decision tree can be generated (Han and Kambr, 2001). Recently, the inductive learning of decision trees is widely used in risk assessment and fault diagnosis. The basic idea of decision trees is shown in **Figure 9**.

This classification in a tree structure is simple and easy to understand. Each path from the root node to the leaf node corresponds to an IF-THEN rule. The relationships between parameters and the outputs were clearly expressed.

Distributed Framework of Decision Tree Model

When the decision tree method is used to solve diagnosis tasks, it is necessary to establish a decision tree model. The diagnosis results of each sub-diagnosis system are comprehensively solved to obtain the final diagnosis results. This is similar to the

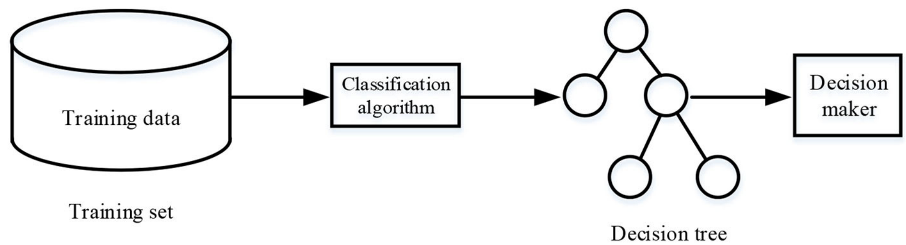

FIGURE 9 | Flowchart of decision trees.

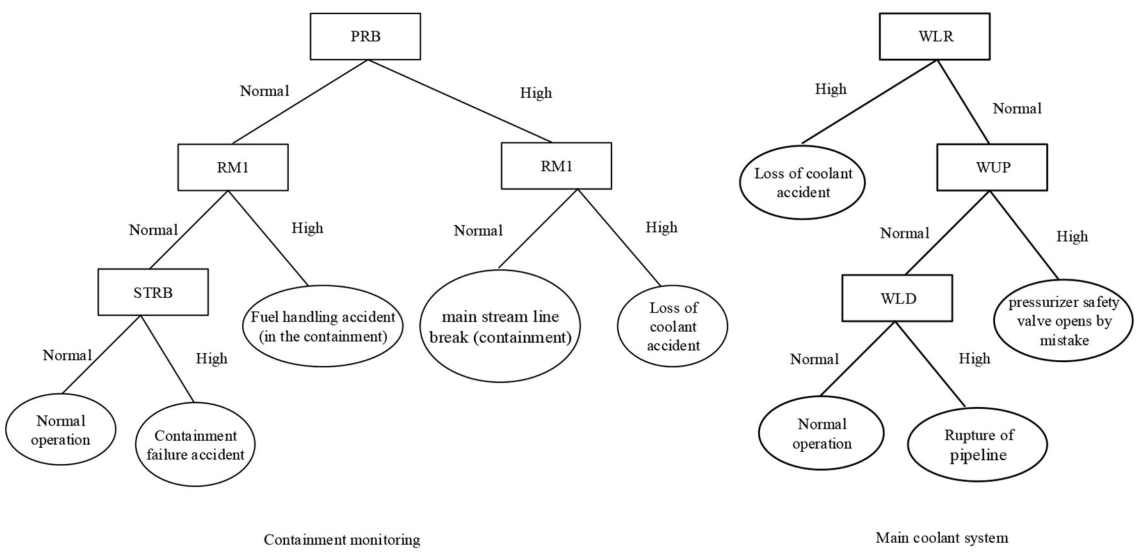

FIGURE 10 | Decision tree model of containment monitoring and the main coolant system (RM1, radioactivity level in the containment; PRB, pressure in the containment; WLR, the main coolant leakage flow rate; WUP, pressurizer safety valve flow; and WLD, lower leakage pipeline flow).

construction of BP neural network samples. The decision tree model makes up for the poor interpretability of "black box" BP neural networks. Additionally, the algorithm selects the characteristic parameters that can distinguish all kinds of faults as the root node and intermediate node of the decision tree. This greatly simplifies the rules and reduces the complexity of reasoning. The accuracy of the results can be improved by combining the decision tree method with a BP neural network. **Figure 10** shows the decision tree model for "containment monitoring" and the "main coolant system."

In **Figure 10**, each rectangle represents a monitoring parameter and each ellipse represents an accident type. Each path from root node to leaf node can be transformed into corresponding IF-THEN rules. For example:

IF (PRB = "high" and RM1 = "normal"), THEN fault type = "main stream line break (containment)"

IF (PRB = "high" and RM1 = "high"), THEN fault type = "loss of coolant accident"

IF (PRB = "normal" and RM1 = "high"), THEN fault type = "fuel handling accident (containment)."

The fault diagnosis system is divided into multiple sub-diagnosis systems, each incorporating the corresponding monitoring parameters. When a fault occurs, it may affect the parameters of multiple subsystems. Therefore, the decision tree model established for each subsystem is only preliminarily solved in the sub-task space, and rules may not be sufficient for the diagnosis. Through the reasoning between various systems, the diagnosis can be accurately completed, which is a characteristic of the distributed diagnosis method.

EVIDENCE THEORY

Based on the diagnosis results for each NPP subsystem, it is necessary to adopt an appropriate method to achieve an overall decision. An evidence theory is a kind of uncertain reasoning and decision-making method that can handle inaccurate, uncertain, and fuzzy problems. As a good decision model, the evidence theory has been widely used in multi-sensor information fusion, target recognition, and uncertain information decision-making (Uren et al., 2016).

Basic Principles of Evidence Theory

Multi-source information fusion, known as data fusion, was proposed in the 1970's (Dempster, 1967). The data fusion improves the decision-making process when the available information is uncertain, but it can give rise to ambiguous and contradictory problems. The Dempster–Shafer theory (DST) fusion model requires mutual exclusion between the elements using evidence rules. For $\Theta = \{\theta_1, \theta_2, \ldots, \theta_n\}$, evidence A and B, the basic corresponding functions m_1 and m_2, and the DST evidence combination rules are (Smarandache and Dezert, 2006):

$$m(C) = \begin{cases} \dfrac{\sum\limits_{A_i \cap B_j = C} m_1(A_i)m_2(B_j)}{1-K}, & \forall C \subset \Theta, C \neq \varnothing \\ 0, & \forall C = \varnothing \end{cases}, \tag{3}$$

$$K = \sum_{A_i \cap B_j = \varnothing} m_1(A_i)m_2(B_j) < 1, \tag{4}$$

where K is the degree of conflict between evidence A and B. A larger value of K implies that there is more conflict between evidence A and B. For multiple pieces of evidence m_i, the fusion of results given by Equation (3) can be regarded as new evidence, which is then integrated into the next piece of evidence m_i.

The DST fusion theory is based on two fusion models: the classic model (DSmC) and the hybrid model (DSmH). The fusion rule of DSmC is defined as

$$\forall A \neq \varphi \in D^{\Theta}, m_{M^f(\Theta)}(A) \triangleq [m_1 \oplus m_2 \oplus \ldots m_k](A) = \sum_{\substack{X_1,\ldots,X_k \in D^{\Theta} \\ (X_1 \cap \ldots \cap X_k) = A}} \prod_{i=1}^{k} m_i(X_i) \tag{5}$$

The fusion rule of DSmH is defined as

$$m_{M(\Theta)}(A) = \varphi(A)[S_1 + S_2 + S_3], \tag{6}$$

TABLE 2 | Basic trust distribution table.

Evidence source	Basic belief assignment	θ_1	θ_2	$\theta_1 \bigcup \theta_2$
E_1	m_1	0.2	0.7	0.1
E_2	m_2	0.6	0.2	0.2

TABLE 3 | Fusion examples.

Diagnostic system	Identification framework (diagnosable fault set)						
	θ_1	θ_2	θ_3	θ_4	θ_5	θ_6	θ_7
System 1	0.02	0.04	0.02	0.98	–	–	–
System 2	–	–	–	–	0.03	0.04	0.98
System 3	–	–	–	–	0.02	0.01	–

"–" indicates that the diagnostic system cannot diagnose the fault.

TABLE 4 | Identification framework after refinement and coarsening.

Diagnostic subsystem	New identification framework		
	θ_4	θ_7	$\widetilde{\Theta}$
Subsystem 1	0.9245	0	0.0755
Subsystem 2	0	0.9333	0.0667
Subsystem 3	0	0.9412	0.0588

TABLE 5 | Final fusion results.

	θ_4	θ_7	$\theta_4 \cap \theta_7$	$\widetilde{\Theta}$	$\theta_4 \cap \widetilde{\Theta}$	$\theta_7 \cap \widetilde{\Theta}$	$\theta_4 \cap \theta_7 \cap \widetilde{\Theta}$
Fusion results	0	0	0.8121	0.0002961	0.003579	0.07524	0.1088

where
$$S_1 = \sum_{\substack{X_1,X_2,\ldots,X_k \in D^{\Theta} \\ (X_1 \cap X_2 \cap \ldots \cap X_k) = A}} \prod_{i=1}^{k} m_i(X_i)$$

$$S_2 = \sum_{\substack{X_1,X_2,\ldots,X_k \in \varnothing \\ [u(X_1)\cup u(X_2)\cup \ldots \cup u(X_k)=A] \\ \vee [u(X_1)\cup u(X_2)\cup \ldots \cup u(X_k) \in \varnothing \wedge (A=I_i)]}} \prod_{i=1}^{k} m_i(X_i)$$

$$S_3 = \sum_{\substack{X_1,X_2,\ldots,X_k \in D^{\Theta} \\ (X_1 \cup X_2 \cup \ldots \cup X_k) = A \\ (X_1 \cap X_2 \cap \ldots \cap X_k) \in \varnothing}} \prod_{i=1}^{k} m_i(X_i)$$

Suppose that the identification framework consists of two elements, i.e., $\Theta = \{\theta_1, \theta_2\}$, and there are two independent and reliable sources of evidence, E_1 and E_2. The reliability assignment of the corresponding elements is presented in **Table 2**.

Therefore, for multiple pieces of evidence, obtaining the final consistent fusion decision results requires the support of evidence theory. The fusion results under different fusion rules are given as follows:

According to the DS fusion rules in Equations (3) and (4), the fusion results are

$$m(\theta_1) = 0.40741, m(\theta_2) = 0.55556, m(\theta_1 \bigcup \theta_2) = 0.032037$$

According to the DST classical model fusion rules in Equation (5), the fusion results are

$$m(\theta_1) = 0.22, m(\theta_2) = 0.3, m(\theta_1 \bigcup \theta_2) = 0.02,$$
$$m(\theta_1 \bigcap \theta_2) = 0.46$$

Under the distributed diagnosis strategy, the task of the system is divided into various subtask spaces. The information fusion

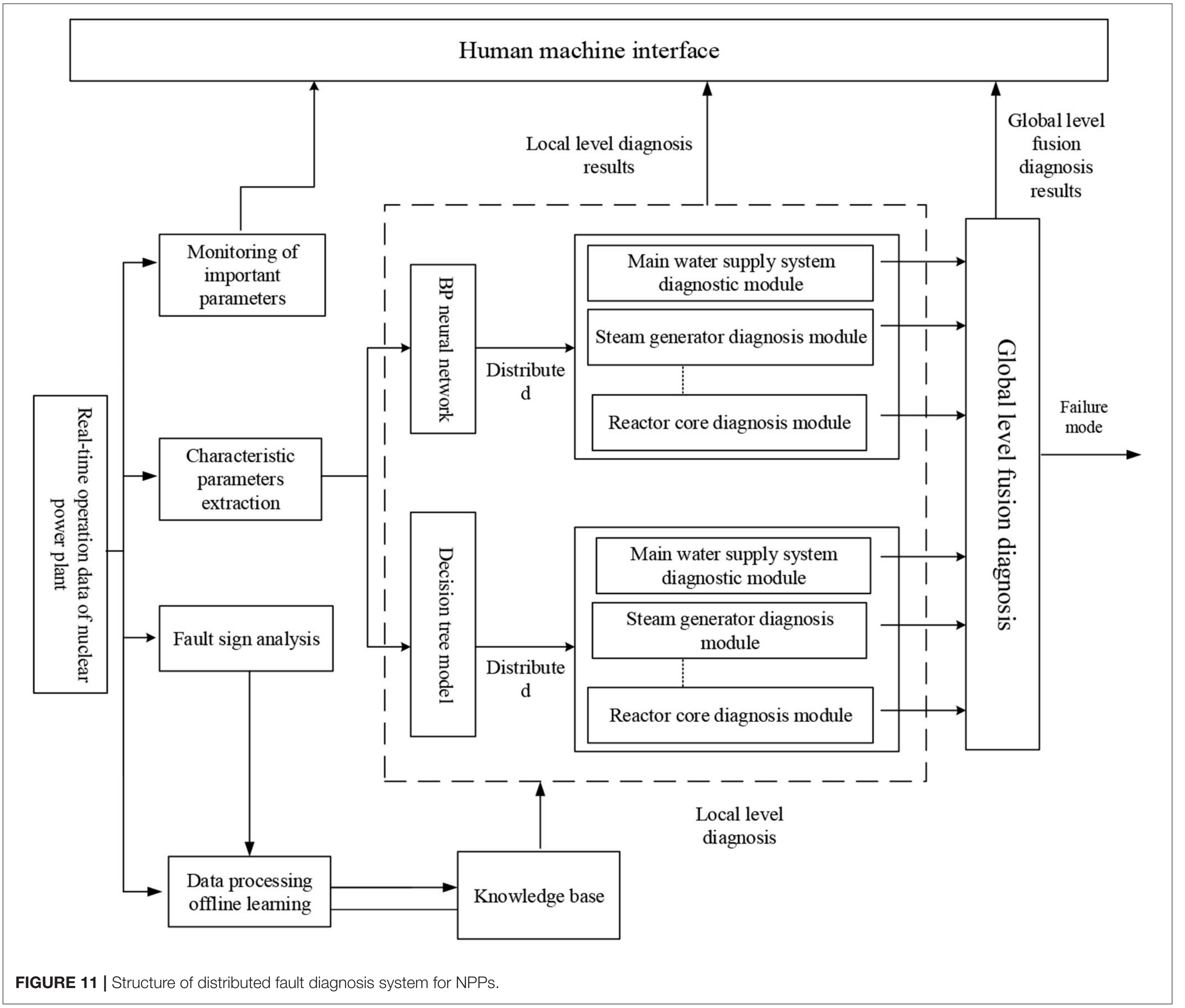

FIGURE 11 | Structure of distributed fault diagnosis system for NPPs.

is then carried out using evidence theory. Finally, the single or concurrent fault is identified.

Distributed Integration Method

Assume that the diagnostic results for a subsystem at a given time are as listed in **Table 3**, where $\theta_1 - \theta_7$ represent seven different fault types. The faults can be diagnosed by the following different diagnostic subsystems.

1. The union set of elements in the identification framework of diagnostic subsystems is the basic element of the identification framework. The refined unified identification framework is $\Theta = \{\theta_1, \theta_2, \theta_3, \theta_4, \theta_5, \theta_6, \theta_7\}$.

2. The rule based on the evidence theory produces an "explosion" when the number of elements is too large. The aim of this identification framework is to extract useful information from the evidence by setting a threshold. When the reliability value of a fault in the diagnostic subsystem exceeds the threshold, as for θ_4 and θ_7 in **Table 3**, the remaining elements $\theta_1, \theta_2, \theta_3, \theta_5$, and θ_6 are merged into one element Θ, which represents the set of elements other than θ_4 and θ_7. The reliability value of $\widetilde{\Theta}$ is the sum of the reliability values of its elements.

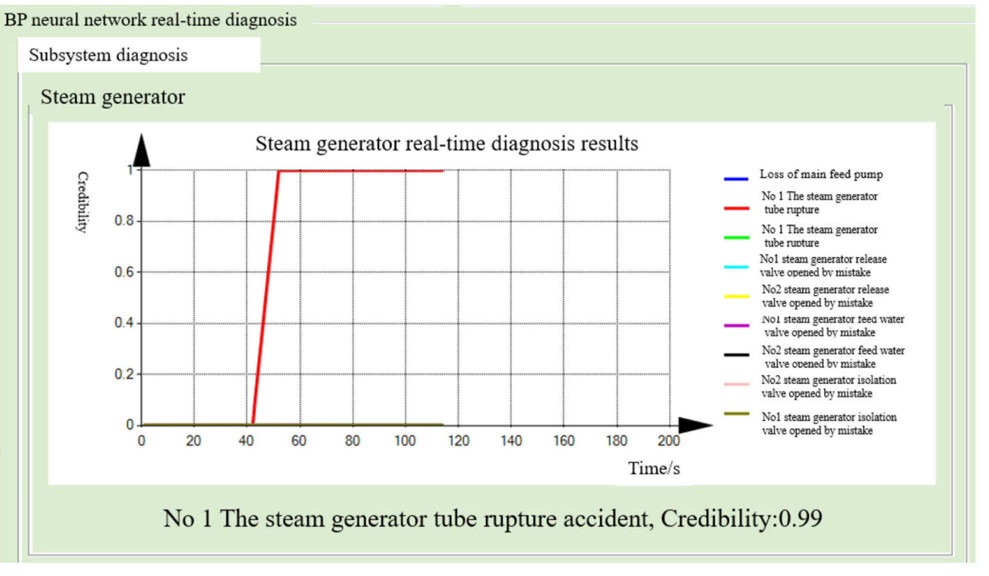

FIGURE 12 | Real-time diagnosis result of steam generator (BP neural network method).

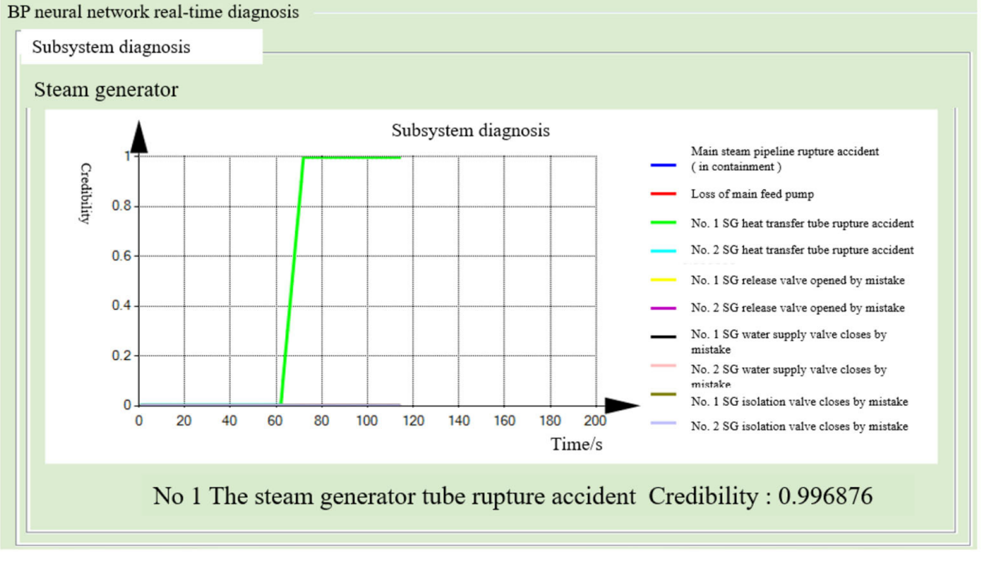

FIGURE 13 | Real-time diagnosis results of the main water supply system (BP neural network).

Finally, the reliability values of each piece of evidence under the new identification framework are normalized to obtain the results listed in **Table 4**.

The DST fusion rule can then be used with the DST rule applied for the fusion of evidence with small conflict rates. The final fusion results are presented in **Table 5**.

Framework of Distributed Fault Diagnosis

The NPP fault diagnosis system adopts a distributed frame structure. The structure is shown in **Figure 11**, and it mainly includes a knowledge base, fault diagnosis, and global-level fusion diagnosis. The knowledge base integrates the BP neural network fault-diagnosis knowledge with the decision tree model-reasoning knowledge.

CASE STUDIES

To verify the diagnostic ability of the distributed fault diagnosis system for a single fault, random faults were inserted into a

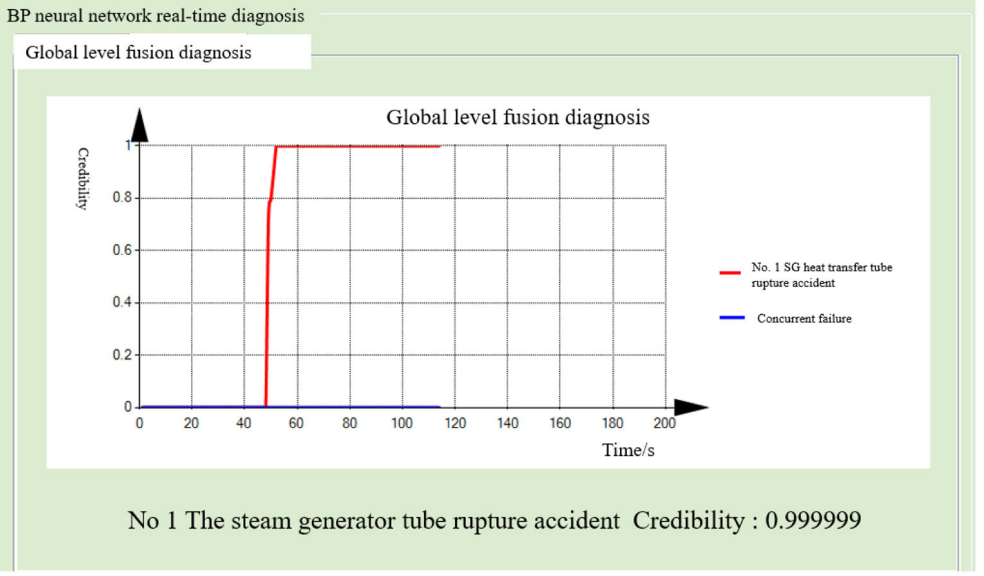

FIGURE 14 | Global-level fusion diagnosis results (BP neural network method).

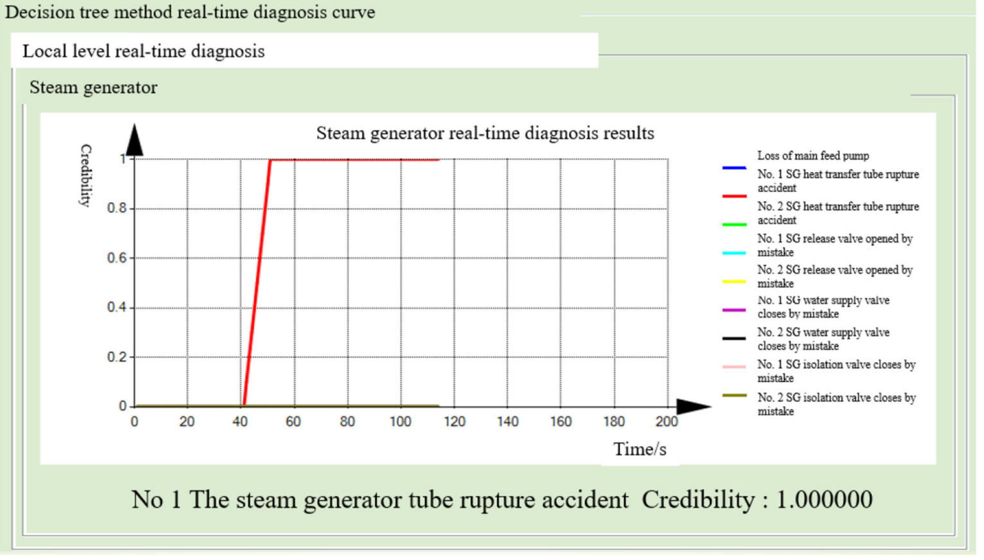

FIGURE 15 | Real-time diagnosis result of steam generator (decision tree method).

simulator. The distributed fault diagnosis system provided real-time operation data for the NPP through the operation database and then identified the fault types.

The division of systems in the distributed fault diagnosis of NPPs is based on the distributed principles. The diagnosis tasks are decomposed and assigned to each diagnosis module. The subsystem division methods are based on (1) system structure, (2) system function, and (3) time series. After considering the importance of each system of safe operation, monitoring parameters, and other factors, this study uses a method based on the combination of system structure and function to divide the subsystems. The main monitoring parameters of each subsystem are listed, and the resultants are divided into reactor core system, containment monitoring system, radiation dose monitoring system, main water supply system, steam generator, main line steam system, main coolant system, equipment-valve system, equipment-pump system.

The sample is achieved by a software PCTRAN simulator. It was taken as the data source for the present study and it is a reactor transient and accident simulation software developed

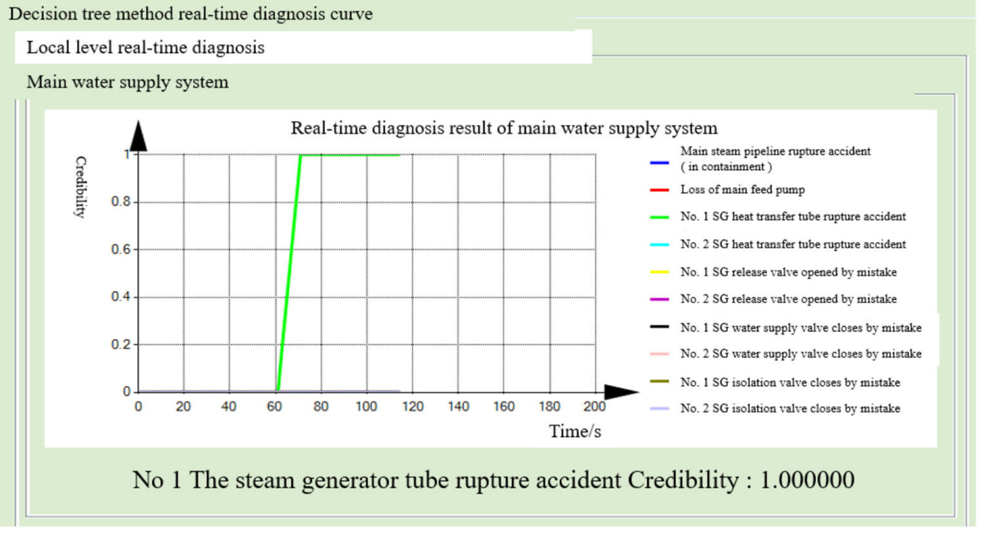

FIGURE 16 | Real-time diagnosis results of the main water supply system (decision tree method).

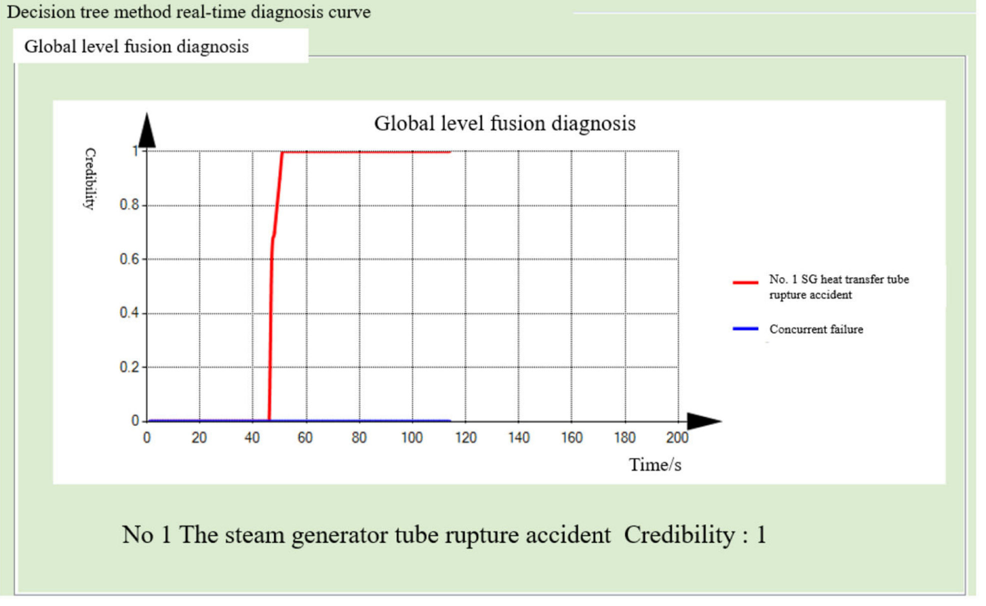

FIGURE 17 | Global-level fusion diagnosis result (decision tree method).

by the Micro-Simulation Technology Company (United States). As PCTRAN can be operated on a personal computer, it is convenient for nuclear power operation staff and researchers to study. Since its first release in 1985, the Micro-Simulation Technology Company has developed many versions of PCTRAN to suit different types of NPP (Po, 2004).

Steam Generator Tube Rupture Accident

After running the simulator under normal working conditions for 40 s, a tube rupture accident in the No. 1 steam generator, covering 100% of the cross-sectional area of the tube, was generated. The steam generator and the main water supply system successively diagnosed the tube rupture fault. The probability of the fault occurrence in the other seven diagnostic modules remained close to zero. This indicates the normal operation of the subsystem. The fusion diagnosis obtains the final fusion decision results. The diagnostic results of the BP neural network method are shown in **Figures 12–14**. The diagnostic results of the decision tree model are shown in **Figures 15–17**.

Both the BP neural network method and the decision tree model obtained the correct diagnosis results in a short time, with the steam generator module diagnosing the fault earlier

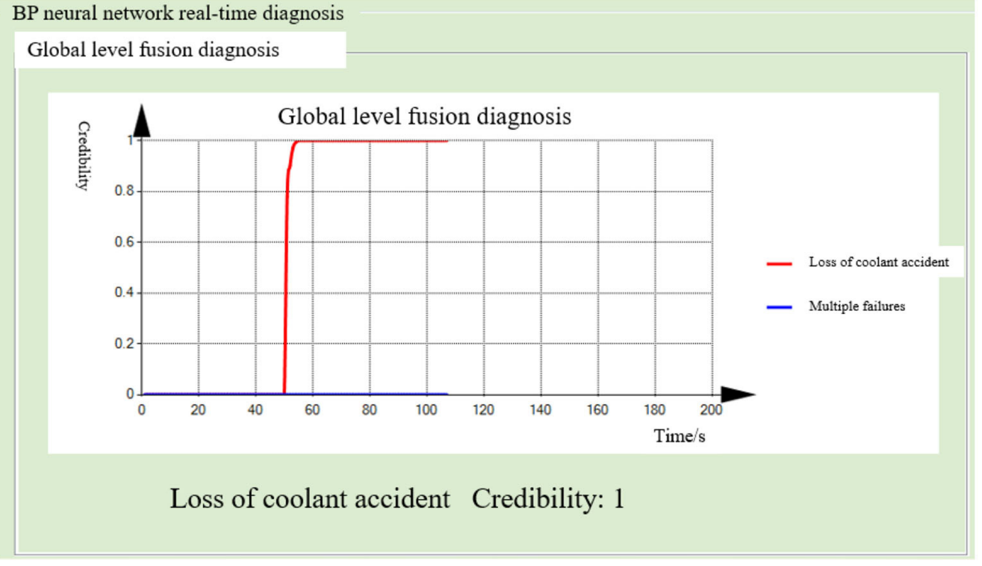

FIGURE 18 | Global-level fusion diagnosis result (BP neural network method).

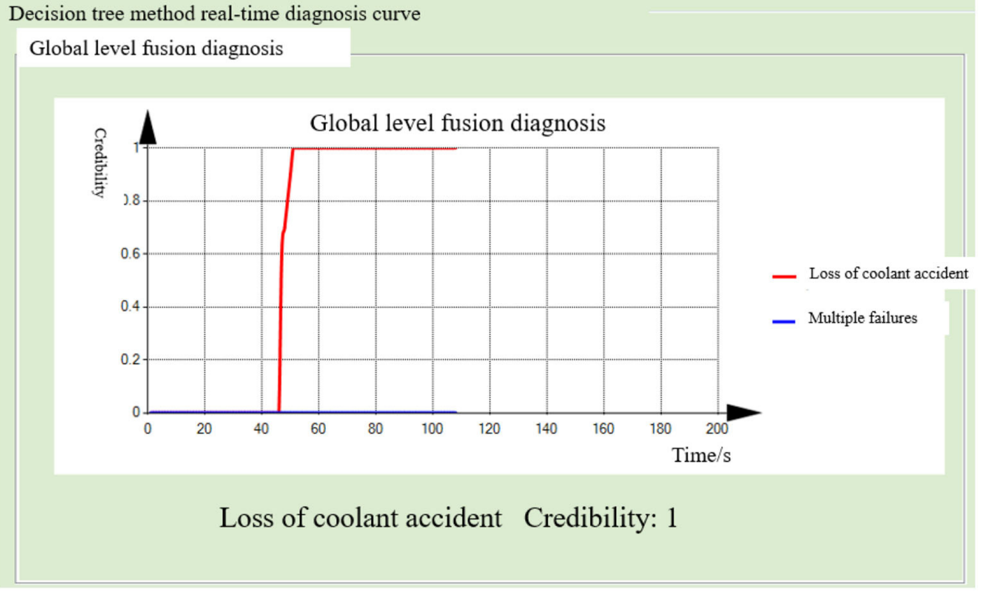

FIGURE 19 | Global-level fusion diagnosis result (decision tree method).

than the main water supply system. This is because the steam generator module can quickly diagnose such faults by monitoring the leakage flow and other parameters. When the fault occurs, the flow increases rapidly. As the main water supply system is monitoring the steam generator water level and other parameters, the symptoms are relatively slow to appear, so the fault diagnosis takes a longer time. In addition, the probability of fault-occurring results is improved by the mutual verification of both the methods.

Loss of Coolant Accident

The nuclear power simulator was operated under normal conditions for 40 s, and then a loss of coolant accident from a hole measuring 3 cm^2 was inserted. After 10 s, the probability of the coolant loss accident exceeded 90% in the main coolant system, containment monitoring, and radiation dose monitoring modules of the distributed fault diagnosis system. Three sets of evidence pointed to the coolant loss accident, while the probability of the failure in the remaining six sub-modules remained close to zero. The diagnosis results of the BP neural network method and decision tree model method are shown in **Figures 18**, **19**.

The time difference between the two methods for fault diagnosis is not obvious, because the threshold method combined with the trend of the parameters is used to monitor the operation state of each parameter, which improves the diagnosis speed. However, the decision tree reasoning method selects the characteristic parameters that have the greatest effect on fault classification as nodes, and it does not require all signs to appear. Therefore, for some faults, the decision tree method has a faster diagnosis speed.

CONCLUSION

According to the proposed distributed diagnosis method, the identification of faults in NPPs was decomposed into several subsystems. The steam generator tube rupture accident and loss of coolant accident, respectively, use BP neural network and decision tree, for fault diagnosis. Through the distributed diagnosis, the diagnosis results of different subsystems were merged. This method not only reduces the number of samples in machine learning but also increases the speed of sample learning. The threshold value of parameters was obtained to construct sample, and the speed of diagnosis was improved by obtaining the trend of parameters. Information fusion was used for the diagnosis results, thus reducing the complexity of the fusion process and improving the accuracy of the diagnosis results. The simulation results show the superiority of the method proposed in this study.

The diagnosis ability of the distributed fault diagnosis system for NPPs can be extended to different power conditions. The fault diagnosis of NPPs after the protection intervention will be the topic of future research.

DATA AVAILABILITY STATEMENT

The raw data supporting the conclusions of this article will be made available by the authors, without undue reservation.

AUTHOR CONTRIBUTIONS

All authors listed have made a substantial, direct and intellectual contribution to the work, and approved it for publication.

FUNDING

This work was supported by National Key Research and Development Program (2019YFC0810705), National Key Research and Development Program (2018YFC0810601), and R&D projects in key areas of Guangdong Province (2019B111102002).

REFERENCES

Dempster, A. P. (1967). Upper and lower probabilities induced by a multivalued mapping. *Ann. Mathemat. Statist.* 38, 325–339. doi: 10.1214/aoms/1177698950

Elnokity, O., Mahmoud, I. I., Refai, M. K., and Farahat, H. M. (2012). ANN based sensor faults detection, isolation, and reading estimates – SFDIRE: applied in a nuclear process. *Ann. Nucl. Energy* 49, 131–142. doi: 10.1016/j.anucene.2012.06.003

Embrechts, M. J., and Benedek, S. (2004). Hybrid identification of nuclear power plant transients with artificial neural networks. *IEEE T Ind. Electron*. 51, 686–693. doi: 10.1109/TIE.2004.824874

Fan, J., Fan, J., Liu, F., Qu, J., and Li, R. (2019). *A Novel Machine Learning Method Based Approach for Li-ion Battery Prognostic and Health Management*. Salt Lake City: IEEE Access. doi: 10.1109/ACCESS.2019.2947843

Friedman, J. S., Droulez, J., Bessière, P., Lobo, J., and Querlioz, D. (2017). Approximation enhancement for stochastic Bayesian inference. *Int. J. Approx. Reason.* 85, 139–158. doi: 10.1016/j.ijar.2017.03.007

Gheisari, S., and Meybodi, M. R. (2017). A New reasoning and learning model for cognitive wireless sensor networks based on bayesian networks and learning automata cooperation. *Comp. Netw.* 124, 11–26. doi: 10.1016/j.comnet.2017.05.031

Hadad, K., Pourahmadi, M., and Majidi-Maraghi, H. (2011). Fault diagnosis and classification based on wavelet transform and neural network. *Prog. Nuclear Energy* 53, 41–47. doi: 10.1016/j.pnucene.2010.09.006

Han, J., and Kambr, M. (2001). *Data Mining: Concepts and Techniques*. Beijing: Higher Education Press.

Hines, J. W., and Garvey, D. (2007). Process and equipment monitoring methodologies applied to sensor calibration monitoring. *Qual. Reliab. Eng. Int*. 23, 123–135. doi: 10.1002/qre.818

Kang, C. W., and Golay, M. W. (1999). A Bayesian belief network-based advisory system for operational availability focused diagnosis of complex nuclear power systems. *Expert Syst. App.* 17, 21–32. doi: 10.1016/S0957-4174(99)00018-4

Khakzad, N., Khan, F., and Amyotte, P. (2011). Safety analysis in process facilities: comparison of fault tree and Bayesian network approaches. *Reliabil. Eng. System Safety* 96, 925–932. doi: 10.1016/j.ress.2011.03.012

Kramer, M. A., and Palowitch, B. L. (1987). A rule-based approach to fault diagnosis using the signed directed graph. *AIChE J.* 33, 1607–1078. doi: 10.1002/aic.690330703

Li, C., and Mahadevan, S. (2018). Efficient approximate inference in Bayesian networks with continuous variables. *Reliabil. Eng. System Safety* 169, 269–280. doi: 10.1016/j.ress.2017.08.017

Li, C., and Ueno, M. (2017). A depth-first search algorithm for optimal triangulation of Bayesian network. *Int. J. Approx. Reason.* 80, 294–312. doi: 10.1016/j.ijar.2016.09.012

Li, W., Peng, M., Liu, Y., Jiang, N., Wang, H., and Duan, Z. (2018). Fault detection, identification and reconstruction of sensors in nuclear power plant with optimized PCA method. *Ann. Nucl. Energy* 113, 107–117. doi: 10.1016/j.anucene.2017.11.009

Li, W., Peng, M. J., Yang, M., Xia, G. L., Wang, H., Jiang, N., et al. (2017). Design of comprehensive diagnosis system in nuclear power plant. *Ann Nuclear Energy* 109, 92–102. doi: 10.1016/j.anucene.2017.05.024

Liu, Y. K., Wu, G. H., Xie, C. L., Duan, Z. Y., Peng, M. J., and Li, M. K. (2016). A fault diagnosis method based on signed directed graph and matrix for nuclear power plants. *Nucl. Eng. Design* 297, 166–174. doi: 10.1016/j.nucengdes.2015.11.016

Liu, Y. K., Xie, C. L., Peng, M. J., and Ling, S. H. (2014). Improvement of fault diagnosis efficiency in nuclear power plants using hybrid intelligence approach. *Prog. Nucl. Energy* 76, 122–136. doi: 10.1016/j.pnucene.2014.05.001

Liu, Y. K., Xie, F., Xie, C. L., Peng, M. J., Wu, C. H., and Xia, H. (2015). Prediction of time series of NPP operating parameters using dynamic model based on BP neural network. *Ann. Nucl. Energy* 85, 566–575. doi: 10.1016/j.anucene.2015.06.009

Ma, J., and Jiang, J. (2011). Applications of fault detection and diagnosis methods in nuclear power plants: a review. *Prog. Nucl. Energy* 53, 255–266. doi: 10.1016/j.pnucene.2010.12.001

Marseguerra, M., Zio, E., Baraldi, P., and Oldrini, A. (2003). Fuzzy logic for signal prediction in nuclear systems. *Prog. Nucl. Energy* 43, 373–380. doi: 10.1016/S0149-1970(03)00048-9

Mo, K., Lee, S. J., and Seong, P. H. (2007). A dynamic neural network aggregation model for transient diagnosis in nuclear power plants. *Prog. Nucl. Energy* 49, 262–272. doi: 10.1016/j.pnucene.2007.01.002

Pantelides, C. C., and Renfro, J. G. (2013). The online use of first-principles models in process operations: Review, current status and future needs. *Comp. Chem. Eng.* 51, 136–148. doi: 10.1016/j.compchemeng.2012.07.008

Peng, M. J., Wang, H., Chen, S. S., Xia, G. L., Liu, Y. K., Yang, X., et al. (2018). An intelligent hybrid methodology of on-line system-level fault diagnosis for nuclear power plant. *Nucl. Eng. Technol.* 50, 396–410. doi: 10.1016/j.net.2017.11.014

Po, L. C. (2004). *PCTRAN/PWR Personal Computer Transient Analyzer for a Two-Loop PWR Manual*. Micro-Simulation Technology.

Rohde, U. L., Jain, G. C., Poddar, A. K., and Ghosh, A. K. (2011). *Inverse Trigonometric Functions and Their Derivatives. Introduction to Differential Calculus: Systematic Studies with Engineering Applications for Beginners*. John Wiley & Sons, Inc. doi: 10.1002/9781118130155

Seker, S., Ayaz, E., and Türkcan, E. (2003). Elman's recurrent neural network applications to condition monitoring in nuclear power plant and rotating machinery. *Eng. Appl. Artif. Intel*. 16, 647–656. doi: 10.1016/j.engappai.2003.10.004

Smarandache, F., and Dezert, J. (2006). *Advances and Applications of DSmT for Information Fusion*. Rehoboth, DE: American Research Press.

Uren, K. R., van Schoor, G., du Rand, C. P., and Botha, A. (2016). An integrated approach to sensor FDI and signal reconstruction in HTGRs – part I: theoretical framework. *Ann. Nucl. Energy* 87, 750–760. doi: 10.1016/j.anucene.2015.06.010

Vila-Francés, J., Sanchís, J., Soria-Olivas, E., José Serrano, J., Martínez-Sober, M., Bonanad, C., et al. (2013). Expert system for predicting unstable angina based on Bayesian networks. *Exp. Syst. Appl.* 40, 5004–5010. doi: 10.1016/j.eswa.2013.03.029

Wang, H., Peng, M.-J., Wu, P., and Cheng, S. Y. (2016). Improved methods of online monitoring and prediction in condensate and feed water system of nuclear power plant. *Ann. Nucl. Energy* 90, 44–53. doi: 10.1016/j.anucene.2015.11.037

Zhao, Y. F. (2016). *Research on the Key Technologies of Nuclear Emergency Decision Making in High Temperature Gas-Cooled Reactor*. Beijing: Tsinghua University.

Zhao, Y. F., Tong, J. J., Zhang, L. G., and Zhang, Q. (2015). Pilot study of dynamic Bayesian networks approach for fault diagnostics and accident progression prediction in HTR-PM. *Nucl. Eng. Design* 291, 154–162. doi: 10.1016/j.nucengdes.2015.05.010

Zhou, Z., and Zhang, Q. (2017). Model Event/fault trees with dynamic uncertain causality graph for better probabilistic safety assessment. *IEEE Trans. Reliabil.* 99, 1–11. doi: 10.1109/TR.2017.2647845

Zhu, Y. L., Huo, L. M., and Lu, J. L. (2006). Bayesian networks-based approach for power systems fault diagnosis. *IEEE T Power Deliver*. 21, 634–639. doi: 10.1109/TPWRD.2005.858774

Conflict of Interest: The authors declare that the research was conducted in the absence of any commercial or financial relationships that could be construed as a potential conflict of interest.

Advantages of publishing in Frontiers

OPEN ACCESS
Articles are free to read for greatest visibility and readership

FAST PUBLICATION
Around 90 days from submission to decision

HIGH QUALITY PEER-REVIEW
Rigorous, collaborative, and constructive peer-review

TRANSPARENT PEER-REVIEW
Editors and reviewers acknowledged by name on published articles

Frontiers
Avenue du Tribunal-Fédéral 34
1005 Lausanne | Switzerland

Visit us: www.frontiersin.org
Contact us: frontiersin.org/about/contact

REPRODUCIBILITY OF RESEARCH
Support open data and methods to enhance research reproducibility

DIGITAL PUBLISHING
Articles designed for optimal readership across devices

FOLLOW US
@frontiersin

IMPACT METRICS
Advanced article metrics track visibility across digital media

EXTENSIVE PROMOTION
Marketing and promotion of impactful research

LOOP RESEARCH NETWORK
Our network increases your article's readership